Physiol Rev 99: 161–234, 2019
Published October 24, 2018; doi:10.1152/physrev.00041.2017

DEFINING PHYSIOLOGICAL NORMOXIA FOR IMPROVED TRANSLATION OF CELL PHYSIOLOGY TO ANIMAL MODELS AND HUMANS

Thomas P. Keeley and Giovanni E. Mann

King's British Heart Foundation Centre of Research Excellence, School of Cardiovascular Medicine and Sciences, Faculty of Life Sciences and Medicine, King's College London, London, United Kingdom

Keeley TP, Mann GE. Defining Physiological Normoxia for Improved Translation of Cell Physiology to Animal Models and Humans. *Physiol Rev* 99: 161–234, 2019. Published October 25, 2018; doi:10.1152/physrev.00041.2017.—The extensive oxygen gradient between the air we breathe (P_{O_2} ~21 kPa) and its ultimate distribution within mitochondria (as low as ~0.5–1 kPa) is testament to the efforts expended in limiting its inherent toxicity. It has long been recognized that cell culture undertaken under room air conditions falls short of replicating this protection in vitro. Despite this, difficulty in accurately determining the appropriate O_2 levels in which to culture cells, coupled with a lack of the technology to replicate and maintain a physiological O_2 environment in vitro, has hindered addressing this issue thus far. In this review, we aim to address the current understanding of tissue P_{O_2} distribution in vivo and summarize the attempts made to replicate these conditions in vitro. The state-of-the-art techniques employed to accurately determine O_2 levels, as well as the issues associated with reproducing physiological O_2 levels in vitro, are also critically reviewed. We aim to provide the framework for researchers to undertake cell culture under O_2 levels relevant to specific tissues and organs. We envisage that this review will facilitate a paradigm shift, enabling translation of findings under physiological conditions in vitro to disease pathology and the design of novel therapeutics.

I.	INTRODUCTION	161
II.	TECHNIQUES TO MEASURE OXYGEN …	162
III.	OXYGEN DELIVERY IN VIVO	165
IV.	UNDERSTANDING OXYGENATION …	168
V.	CELLULAR OXYGEN SENSING: …	175
VI.	REPLICATING NORMOXIA IN VITRO	177
VII.	CONCLUSIONS AND FUTURE …	211

I. INTRODUCTION

Although most organisms on Earth possess a carbon-based skeleton, oxygen fuels life. The conversion of a CO_2-rich atmosphere to one containing precious O_2, initially by photosynthesizing cyanobacteria, and later by plants, was the pivotal step in the evolution of multicellular life on Earth (324). However, O_2 is an inherently dangerous molecule, and hence, its utilization as a metabolic substrate is closely associated with the development of highly efficient detection [e.g., hypoxia-inducible factors (516, 630)], defense [glutathione (GSH) (195, 387) and antioxidant enzymes (261)] systems. Despite this, the damage caused by a lifetime breathing O_2 may ultimately affect lifespan (222, 324). Several excellent and comprehensive reviews have discussed the various roles played by O_2 in mammalian physiology (59, 119, 333, 565, 594, 679, 699), and thus, these will not form the primary focus of this review article. Nevertheless, a brief overview is important to inform the themes addressed herein.

The principle role of O_2 in mammalian physiology is as the terminal electron acceptor in the electron transport chain (ETC). In this capacity, a single oxygen atom is reduced to H_2O in the presence of two protons and two electrons. Such reductive/oxidative (redox) reactions are fundamental in O_2 physiology and are utilized by cytosolic enzymatic systems in addition to mitochondria. Aside from molecular O_2, oxygen strongly influences cellular physiology through the formation of reactive oxygen species (ROS). First considered merely as unwanted by-products of oxidative phosphorylation and dysfunctional enzymatic reactions (222), ROS are now considered to play functional and nonredundant roles in cell signaling in physiology as reviewed previously (119).

Our increased understanding of oxygen's role in human physiology is paralleled by the growing number of primary research publications (see **FIGURE 1**). To date, over half a million research articles reference oxygen as a keyword, and the number per year has steadily increased over the last century. Attention has shifted from initial interests in the mechanisms of cellular O_2 utilization to consequences associated with dysfunction in these processes, leading ultimately to the production of ROS **(FIGURE 1)**. Another key theme to have emerged is the concept of hypoxia, a pathological reduction in O_2 availability now accepted as a hallmark of disease conditions (522). Indeed, a significant proportion of O_2-related research still focuses on the conse-

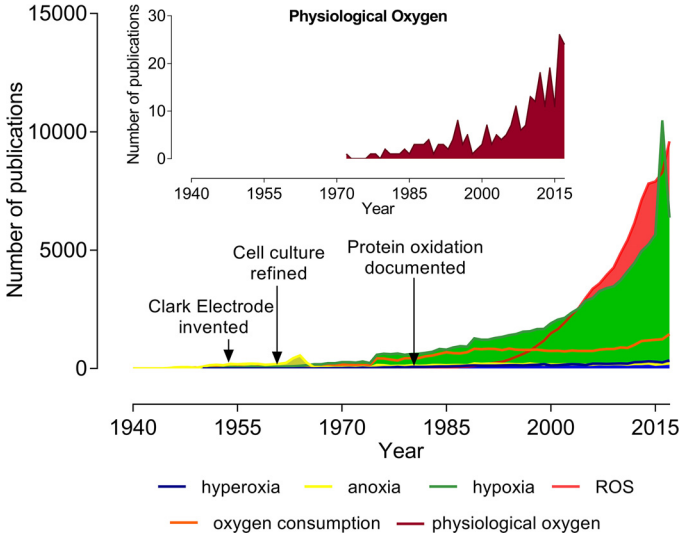

FIGURE 1. Timeline of O_2-related research publications. *Main graph*: Number of PubMed entries in which the keyword oxygen is mentioned within the title or abstract over the past 76 yr. Arrows indicate important events relevant to the scientific study of oxygen in the context of medical science. *Inset*: Distribution of PubMed entries in which "oxygen" is mentioned in either the title or abstract between January 1, 2010 and December 31, 2017. ROS, reactive oxygen species.

quences of O_2 deprivation **(FIGURE 1)**. In view of the importance of maintaining O_2 levels within a finite range at the whole organism level, we here readdress the role of O_2 in mammalian cell culture.

The invention of O_2-sensitive electrodes (87), and in recent years, phosphorescent dyes (116, 610), has enabled researchers to resolve tissue O_2 distribution in vivo. Although incredibly heterogeneous, at no point beyond the mouth is P_{O_2} equivalent to room air (20.9 kPa). Despite this, the culture of mammalian cells is routinely conducted under atmospheric O_2, conditions hyperoxic with respect to the tissue of origin. Although this discrepancy has been widely acknowledged (215, 455, 633), only in recent years have primary research publications addressed this issue directly (**FIGURE 1**, *inset*). A consensus approach to tackling this concept is still lacking, largely plagued by incorrect nomenclature and widely differing experimental conditions. This review aims to provide an insight into the current knowledge regarding tissue O_2 distribution in vivo and in doing so, to redefine the term normoxia for more appropriate use in in vitro experiments. Techniques used to monitor O_2 levels both in vivo and in vitro will be described initially, followed by an overview of experimental issues associated with varying O_2 levels in vitro. Physiological O_2 levels in numerous tissues and the existing literature concerning replication of these conditions in vitro are summarized and critically discussed. The development of cell culture techniques revolutionized medical science in the 1950s, yet maintenance of cultured cells or tissues under nonphysiological O_2 levels limits translation from bench to beside. In many fields, cell culture under atmospheric, room air O_2 levels has been assumed to reflect normoxia largely because of the complexity of conducting experiments in an oxygen-regulated workstation. This review aims to readdress the conditions in which all mammalian cells should be cultured, with the aim of more effective translation of in vitro science into potentially life-saving therapies.

II. TECHNIQUES TO MEASURE OXYGEN IN CELLS AND TISSUES

Necessity often dictates that improvements in experimental techniques frequently precede advances in scientific knowledge, and such is the case with oxygen-related physiology **(FIGURE 1)**. The study of the physiology and biochemistry of molecular O_2 was aided immensely in the 1950s by the development of O_2-sensitive electrodes, which allowed the direct quantification of O_2 levels in biological fluids (87). A number of innovative techniques have since been developed, facilitating more advanced experimental measurements with greater spatial and temporal resolution. Wire electrodes can offer excellent spatial definition over a very small sample area, whereas phosphorescence imaging techniques can offer greater stability over time and over a greater sampling size. Notably, these techniques rarely monitor O_2 concentration directly but rather P_{O_2}, which is directly proportional to concentration, or hemoglobin (Hb) saturation. The following section outlines the basic principles of the most well-established techniques currently used to monitor cellular and tissue P_{O_2}, providing a basis for discussion of data obtained using such equipment in later sections.

A. Oxygen-Sensitive Electrodes

The chemical reduction of molecular O_2 on a polarized (usually 0.6–7 V) platinum cathode generates a current proportional to the concentration of O_2 present. This concept led to the development of O_2-sensitive electrodes in the early 1950s consisting of a polarized platinum cathode and nonpolarizable silver anode (see **FIGURE 2*A***). Although effective in determining dissolved O_2, these early electrodes were not suitable for measuring tissue or blood O_2 because of the accumulation of cells/proteins on the cathode-limiting reactivity. This problem was solved by Leland Clark and colleagues who, in 1953, described the fabrication of a platinum electrode with an O_2-permeable cellophane coating (87) **(FIGURE 2*Ai*)**. The addition of a selectively permeable membrane permitted the measurement of P_{O_2}, as O_2 must now diffuse across its partial pressure gradient to react on the cathode. These electrodes, commonly referred to now as "Clark Electrodes," were greatly utilized for the measurement of liquid P_{O_2} for blood gas analysis and early mitochondrial respiration experiments (73), yet their relatively large size (<1 mm) prevented accurate measurements of tissue P_{O_2}. Efforts during the 1960s culminated in the in-

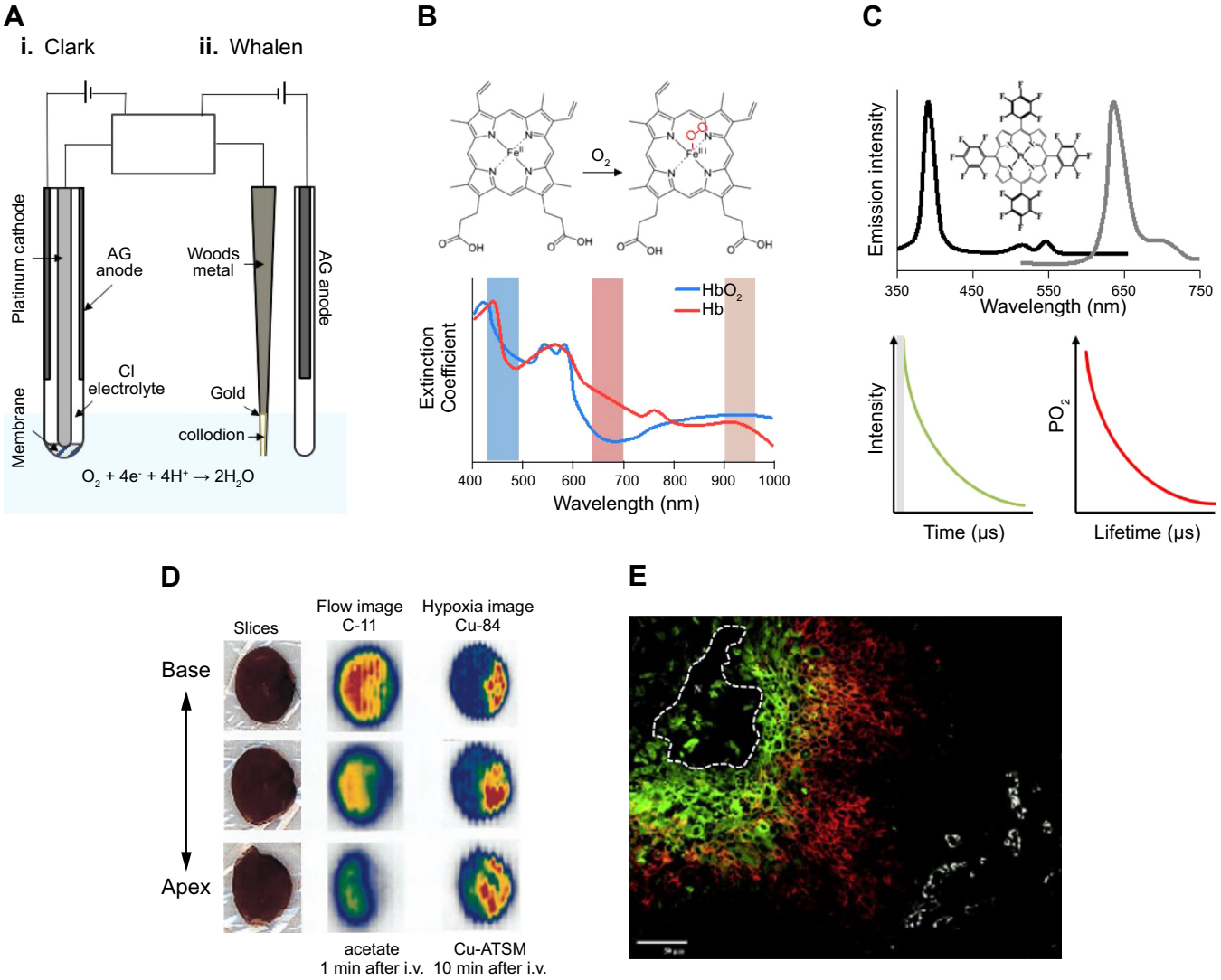

FIGURE 2. Techniques to determine tissue and cellular P_{O_2}. *A*: Diagram of the two common types of O_2-sensitive electrodes, the Clark and Whalen types. Both are connected to an external power supply and galvanometer to record changes in current due to reduction of O_2 at the cathode. *B*: The basis for hemoglobin saturation measurements. The binding of O_2 to hemoglobin is associated with a change in its spectral properties, which are measured at various wavelengths to determine the ratio of oxyhemoglobin to total hemoglobin. *C*, *Top*: the excitation (solid)/emission spectra, (dashed) spectra for Pt^{II}/porphyrin-based phosphorescent probes, with a structural schematic provided in the *inset*. Adapted from Fercher et al. (151). *Bottom*: schematics illustrating the basis for O_2 measurements by time-resolved fluorescence; *left*, after the initial excitation flash, phosphorescent emission decays at an exponential rate, with most O_2-sensitive complexes exhibiting lifetimes in the 10–1000-μs range; *right*, the relationship between calculated probe lifetime and P_{O_2}. *D*: Representative images of ^{11}C/acetate and ^{64}Cu/ATSM loaded isolated hearts subjected to left-anterior–descending artery occlusion, generating a region of ischemia identified by the absence of flow (^{11}C negative and $^{64}Cu^+$ positive). Taken with permission from Fujibayashi et al. (169). *E*: Immunohistochemical section of a squamous cell carcinoma stained to show pimonidazole (green) and carbonic anhydrase 9 (red), with blood vessels (white) and necrotic regions (enclosed in dashed white) identified. Taken with permission from Hoogsteen et al. (253).

troduction of the "Whalen"-type electrode; a recessed-tip gold alloy cathode with a diameter of 1–3 μm (644) (**FIGURE 2*Aii***). By attaching an O_2 electrode to a micromanipulator, tissue P_{O_2} histograms were easily obtainable and rapidly became the preferred method for reporting P_{O_2} (see sect. VI). In recent decades, the use of electrodes has decreased in favor of newer techniques (discussed below) because of the following disadvantages: *1*) by virtue of their chemistry, electrodes consume O_2 (proportional to their diameter) and therefore, may be considered less reliable, especially when attempting to measure very low levels of O_2, *2*) the small sampling area means measuring large areas of tissue is tedious, and *3*) many have shown that tissue penetration by electrodes produces artifactual changes in tissue P_{O_2} resulting from blood vessel rupture or cell disruption (266). The second point has been partially addressed through the de-

velopment of the multiwire platinum electrode (296), in which eight independent Clark-type electrodes are housed within a hemispherical structure of roughly ~50-μm diameter. Although greatly increasing the sampling area, these electrodes are confined to surface Po_2 measurements, and hence, their use is limited.

B. Hb/myoglobin Spectroscopy

Prior to the invention of O_2-sensitive electrodes, the only readout of blood oxygenation available was the spectrophotometric analysis of Hb, although this was only employed clinically in the late 1970s following the development of the pulse oximeter by Aoyagi and colleagues (13). This technique relies on the change in absorbance spectrum of Hb upon binding to O_2 (see **FIGURE 2*B***) characterized by a reduction in absorbance in the red region (650–700 nm) and an increase in the near-infrared (900–1000 nm) region. Isolation of the Hb-derived signal from intrinsic signals of the surrounding tissues and venous blood is achieved by only measuring the pulsatile changes in absorbance. So-called pulse oximeters are extensively used clinically to monitor peripheral arterial blood O_2 saturation, which is 95%–99% in normoxic patients. In the laboratory, a technique to measure Hb saturation in the microvasculature was developed by Pittman and Duling in 1975 (460, 461), in which the effects of light scattering by red blood cells was accounted for. A similar technique has also been used to measure myoglobin saturation in cardiac and skeletal muscle (89, 252). In the context of defining tissue Po_2, Hb saturation can be converted into approximate Po_2 based on the known Hb saturation curves for the appropriate species (594), although this conversion is subject to changes in local pH/PCO_2 and temperature and hence should be used with caution.

C. Fluorescent and Phosphorescent Probes

Optical techniques to monitor cellular and tissue Po_2 were developed by David Wilson and colleagues in the late 1980s, who introduced platinum (Pt^{II}) and palladium (Pd^{II}) porphyrin–based probes, which exhibit quenched phosphorescence in the presence of molecular O_2 (497, 610). These have been complemented by similar complexes utilizing ruthenium (Ru^{II}) (348, 366, 580) or iridium (Ir^{III}) (108), all of which can be conjugated to various macromolecular carriers or polymers to improve solubility or phosphorescence yield. A complete description of O_2-sensitive lumiphores can be found elsewhere (115). In principle, complexes are excitable in the UV range (350–410 nm) and emit in the far red (630–700 nm) region, allowing excellent resolution in biological media, with decay lifetimes in the microsecond range. Typically, measurements are taken using time-resolved phosphorescence, whereby the probe is excited, and the O_2-sensitive decay in resultant emission intensity is resolved over time (see **FIGURE 2*C***). First-generation phosphorescent complexes were hydrophilic, and hence, measurements were confined to the vasculature (535, 583), but subsequent variations have generated hydrophobic equivalents that can penetrate the cell membrane, such as Oxyphor G4 (136) or MitoXpress Intra (151). The addition of other chemical moieties to the basic metal/porphyrin structure has also alleviated issues with nonspecific protein binding that altered the spectral properties of first-generation compounds in vivo (115). With these, simultaneous measurements of blood and tissue Po_2 have been reported (9) as well as intracellular Po_2 within monolayers in culture (75, 151, 615). Ru^{II} complexes have largely been utilized in the OxyLite probe, where they are immobilized in a sensor tip (~200 μm in diameter) and excited via a fiber-optic cable, functioning in an analogous manner to a traditional electrode.

D. Magnetic, Paramagnetic, and Electron Spin Resonance

Positron emission tomography (PET), magnetic resonance imaging (MRI), and electron spin resonance (ESR) techniques have been developed to image regions of hypoxia in vivo, as reviewed elsewhere (60). Imaging using PET employs traditional biochemical markers of tissue hypoxia, such as the imidazole compounds (see below), containing the radionucleotide ^{18}F as a short-lived source of protons. These compounds accumulate within regions of hypoxia and have been useful in imaging tumor Po_2 in animal models and in the clinical setting (356). More recently, ^{64}Cu-containing bisthiosemicarbozones have been targeted as potentially useful markers of hypoxia, with ^{64}Cu-diacetyl-bis-*N*(4)-methylthiosemicarbazone (^{64}Cu/ATSM) showing high selectivity for regions of relative hypoxia in the ischemic Langendorff heart (169) and atherosclerotic lesions in rodents (426) as well as tumors in humans (602). An example of ^{64}Cu/ATSM accumulation in the myocardial ischemic core is provided in **FIGURE 2*D***. MRI oximetry emerged in the late 1980s following the discovery that rates of relaxation to perfluorocarbon (PFC) compounds were linearly related to Po_2 (572). When combined with traditional ^1H MRI anatomical imaging, MRI oximetry can provide useful spatial resolution in both animals and humans (680). In the lungs, Po_2 distribution can also be monitored by MRI using inhaled hyperpolarized ^3He, the decay of which is increased in the presence of O_2 (127) (see **FIGURE 7**). In addition to using exogenous probes, deoxyhemoglobin is a paramagnetic species itself, and its relative proportion to oxyhemoglobin can be visualized as a disturbance in the transverse relaxation time (T_2*) of the surrounding protons in water. This led to the development of blood-oxygen level–dependent MRI imaging (BOLD-MRI) (436, 577), which uses standard MRI protocols to monitor changes in Hb saturation and is widely used clinically. One major advantage of BOLD-MRI over PFC-MRI and PET is that it does not require the introduction of an exogenous probe, mitigating

fears over chemical or radioactive toxicity. Unfortunately, BOLD-MRI is not capable of determining absolute fluid P_{O_2} and hence cannot be used to monitor tissue P_{O_2}. Molecular O_2 is weakly paramagnetic itself and can be detected as a small but definitive increase in the longitudinal relaxation time (T_1) of the surrounding protons, first identified using NMR (590) and later confirmed using MRI (267, 432, 656). Notably, changes in T_1 rates occur under conditions in which very limited increases in Hb saturation (and therefore T_2* rates) were detected (656). Although this technique has been used to determine absolute increases in O_2 content (ml/L blood) following hyperoxic inspiration, it has had limited application to determine absolute physiological tissue O_2 concentration. Varying T_1 times were reported in the liver, kidney, and muscle of rabbits, which, when combined with simultaneous measurements of T_2* rates, may be indicative of tissue P_{O_2} (432, 656).

Much like PET and PFC-MRI, ESR oximetry relies on the interaction between a probe and molecular O_2. The most commonly used probes to measure P_{O_2} using ESR are lithium-based cyanines and India ink (8), which are biocompatible particulate probes and have been used to report tissue P_{O_2} in liver (275), heart (487), lungs (487), digestive tract (228), and bone (360). The presence of O_2 in close proximity to the ESR probe causes a broadening of the probe spectrum, measurable in the line width, which is directly proportional to P_{O_2}. Hence, unlike PET and MRI, ESR permits the direct quantification of tissue P_{O_2} and can be used for long periods of time because of the inert and stable nature of the spin probes (8). Unfortunately, the complex and costly equipment required to detect spin resonance limits the application of ESR to specialized facilities.

E. Immunohistochemical Methods

The techniques discussed so far have been developed to monitor relative or absolute tissue P_{O_2}. Complimentary to these has been the immunohistochemical identification of hypoxic areas using exogenous dyes like pimonidazole or EF5 (357, 474) or antibodies raised against known hypoxia-inducible target proteins such as hypoxic-induced factor (HIF) or CA9, which rely on the cellular response to lowered O_2 levels rather than the absolute P_{O_2}. Pimonidazole and EF5 are 2-nitroimidazole derivatives containing a NO_2 group attached to an imidazole ring, which undergoes rapid reduction to produce a highly reactive intermediate species that will react with any macromolecule in the vicinity. At a P_{O_2} more than ~1.5 kPa O_2, this reduction is prevented, and thus 2-nitroimidazole staining is selective for regions of severe hypoxia. When sections of hypoxic tissue are costained with pimonidazole and a hypoxia-inducible protein such as HIF-1α or CA9, distinct and mildly overlapping regions are observed (see **FIGURE 2*E***), suggesting that the two probes are marking areas of differing severity of hypoxia (253, 545). Although the nature of pimonidazole O_2 sensitivity has been considered reasonably binary (staining is either present or absent), gradients in intensity corresponding to measurable gradients in P_{O_2} have been reported across the intestinal wall (294). This tissue is reported to be severely hypoxic (see sect. VI*F2*), and hence, it is possible that differences in staining intensity may be resolved within the reported range (P_{O_2} 0–1.5 kPa). A disadvantage in the use of 2-nitroimidazole compounds to identify hypoxic tissue is that staining requires live cells; thus, the dye must be injected before samples being collected. This limits its use in retrospectively identifying hypoxic areas in tissue specimens already collected or in patient samples. A caveat to the use of immunostaining members of the HIF pathway as a marker of tissue hypoxia is the well-described potential of HIF-1α to be stabilized under oxygenated conditions, most notably during inflammation because of cross-talk with NFκB and direct effects of ROS (44, 607). Hence, results obtained using HIF-based immunostaining should always be confirmed with an alternative method.

III. OXYGEN DELIVERY IN VIVO

A basic understanding of the delivery of O_2 from the atmosphere to the cytosol is fundamental for interpreting specific tissue O_2 distribution. Moreover, insights into O_2 transport in vivo provide a useful perspective for some of the challenges associated with oxygenation of cell monolayers in vitro. A point worth clarifying before any detailed further discussion is the difference between the terms saturation, concentration, and content as commonly used throughout physiology and partial pressure used universally. In mammals, O_2 is transported in two forms: bound to Hb and dissolved in blood. Saturation refers to the percentage of total number of Hb bindings sites saturated with O_2 (4 mol of O_2 bind to 1 mol of Hb), noting that Hb saturation occurs in continuum until all molecules are saturated. This unit does not strictly measure the concentration of O_2 present (although this can be inferred) but is a good measurement of total blood O_2 content. Although convention is to express components of a chemical reaction as a concentration (in moles per liter, for example), O_2 should be reported as partial pressure (in mmHg, Torr, or kPa, **FIGURE 5*A***) in physiology, noting the final dissolved gaseous concentration in a liquid is proportional to its partial pressure within the corresponding gas phase [Henry's Law (235), taking into account changes in temperature and solubility; sect. IV*B*]. This is because the chemical potential of physiological gases is determined by their partial pressure, and as such, they will diffuse down pressure, not concentration, gradients. Content refers to the total amount of O_2, in ml/100 ml, that blood can carry, combining that bound to Hb with that dissolved in plasma according to the following equation:

$$cO_2 = ([O_2]_{max} \times [Hb] \times SO_2 \times 0.01) + (H \times P_{O_2}) \quad (1)$$

in which the maximal O_2-carrying capacity of blood ($[O_2]_{max}$) is 1.31–1.36 ml O_2/g Hb, otherwise known as

Hüfner's constant (110, 194), and *H* is the Henry's Law constant for O_2 (0.023 ml/kPa/100 ml of blood). Human blood contains, on average, 14–15 g Hb per 100 ml (194, 604), and therefore the O_2 content (cO_2) of fully O_2-saturated (SO_2 ~100%) arterial blood = (1.34 × 15 × 100 × 0.01) + (0.023 × 13) = 20.4 ml/100 ml blood. Note that O_2 content is also expressed in units of concentration (ml/100 ml), but differs from the traditional use of O_2 concentration, which typically refers to only dissolved O_2 in solution.

With these three terms defined, the disparity between O_2 delivery in vivo and in vitro becomes readily apparent. In the absence of Hb in vitro, O_2 delivery to the cell monolayer is defined largely by the P_{O_2} of the culture medium directly adjacent, and therefore, the total available O_2 is considerably lower (e.g., cO_2 = 0.48 ml/100 ml medium under standard atmospheric conditions). The issue of O_2 delivery in vitro will be discussed in more detail in sect. IV. As cells cannot access O_2 bound to Hb, total O_2 content is not a particularly useful unit to use when comparing in vivo and in vitro O_2 conditions at the cellular level. Ideally, [O_2] should be defined in units of partial pressure (mmHg or kPa) in compliance with Henry's Law (235). However, the majority of biologists prefer to express gas concentrations in vitro as a percentage of atmospheric composition (i.e., cultured in a standard 37°C, 5% CO_2 incubator). As O_2 expressed as a percentage of ≈kPa at sea level (see **FIGURE 5A**), we have standardized the expression of [O_2] in kPa units in this review.

A. From Air to Blood

Even before entering the circulation, humidification of incoming air within the trachea reduces P_{O_2}, and the introduction of CO_2 (~5 kPa) within the alveoli reduces this further **(FIGURE 3)**. Hence, the gradient between atmosphere and alveoli can be described according to the following equations:

$$P_{O_{2(\text{trachea})}} = (P_{\text{atm}} - P_{H2O}) \times Fi_{O_2} \quad (2)$$

$$P_{O_{2(\text{alveoli})}} = P_{O_{2(\text{trachea})}} - (P_{CO_2}/RQ) \quad (3)$$

in which atmospheric pressure (P_{atm}) is 101.325 kPa at sea level, normal water vapor partial pressure (P_{H2O}) is ~6.2 kPa, and the fraction of O_2 in inspired air (Fi_{O_2}) is 0.209. Thus, $P_{O_{2(\text{trachea})}}$ is normally ~19.9 kPa. As this inspired air mixes with expired air containing CO_2 (P_{CO_2} ~5 kPa) when respiring with mixed carbohydrate/fat fuel (RQ, respiratory quotient 0.8), the P_{O_2} is reduced further to ~13.3 kPa. A proportion of venous (deoxygenated) blood from the microvasculature supplying the larger airway and lung adventitia drains into the pulmonary vein rather than the bronchial vein (19, 76). Because of this nuance in lung perfusion, known as pulmonary venous admixture or shunt, a small gradient exists between the alveoli and arterial P_{O_2} (usually <1.3 kPa in healthy adults), spoiling an otherwise remarkably efficient exchange. Taken together, the passage of O_2 from air to the blood results in a gradient of ~9 kPa, the largest such gradient in mammalian physiology.

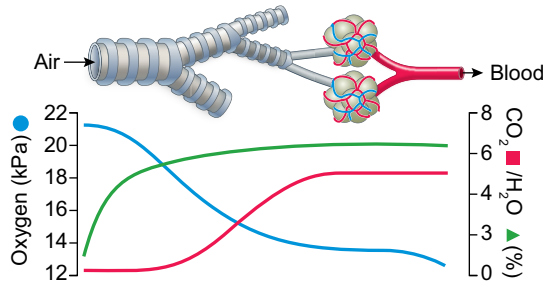

FIGURE 3. Oxygen gradients in the respiratory system. Concentrations, in kPa, of O_2 (●, *left axis*), CO_2 (■, *right axis*), and H_2O (▲, *right axis*) from dry atmosphere to the pulmonary venous circulation. Increases in PH_2O and P_{CO_2} in the respiratory tract reduce P_{O_2} proportionally, and venous admixture within the pulmonary vein reduces P_{O_2} further.

B. From Blood to Cytosol

1. Longitudinal gradients within the vasculature

The subject of intravascular O_2 gradients has been reviewed elegantly by Tsai et al. (2003), and as such, it will only be described briefly in this review. Duling and Berne (1970) were the first to demonstrate experimentally a significant loss of oxygen from the arteriolar circulation. They and many others subsequently established that *1*) there is a significant decrease in O_2 between the systemic arterial circulation and arteriolar vessels (43, 123, 124, 263, 325, 459), which is proportional to luminal diameter (124, 500) and inversely proportional to red blood cell velocity/blood flow (295, 584); *2*) the difference between terminal arteriolar and postcapillary venular O_2 is minimal (325, 534), as is the gradient between capillary and tissue O_2 (43, 325); *3*) the next largest tissue compartment outside the lungs in which a significant O_2 gradient is observed is the vascular wall of arterioles (99, 124, 428, 507, 532, 591), which is proportional to the thickness of the arteriolar wall (124); and *4*) a postcapillary diffusional shunt occurs in most microvascular beds, in which a portion of O_2 from saturated arterioles diffuses into venules running parallel (131, 534). Furthermore, measurements of O_2 saturation in red blood cells by absorption at 555 nm (460, 461) confirm that Hb saturation falls proportionally with dissolved O_2 (457). Based on these observations, the arteriolar network appears to plays more of a role in the delivery of O_2 to the tissue than previously considered (500), and there may even be a role for postcapillary venules in homogenizing tissue P_{O_2} (328). This was first noted following the observation that the re-

lationship between venular diameter and luminal P_{O_2} was opposite to that described for arteriolar vessels. In other words, blood P_{O_2} increases between postcapillary and collecting venules (43, 131, 295, 325, 532, 534, 622). However, it must be noted that blood entering the arteriolar network has a P_{O_2} above the steepest part of the O_2 dissociation curve of Hb (see **FIGURE 4*B***), and therefore, it is hard to reconcile how so much O_2 is transferred to the surrounding tissues from these vessels unless only the transfer of dissolved O_2 is being measured. Moreover, one must also weigh up the influence of the magnitude of the vascular wall P_{O_2} gradient (the argument in favor of arteriolar O_2 delivery) against the raw number of vessels (capillaries vastly outnumber arterioles) when concluding the relative contribution of each type of vessel to tissue O_2 delivery.

2. Radial gradients across and within the vascular wall

The evidence for longitudinal O_2 gradients within the vasculature is complimented by the finding of significant radial, or transmural, gradients across the vascular wall. Radial gradients have been reported in the rabbit aortic wall (99, 428, 508), cat pial vessels (124), dog carotid arteries (507), dog femoral arteries (410), rat mesenteric arterioles (591), and rat cortical microvessels (622). Elegant work by Niinikoski et al. (428) and Santilli et al. (507, 508) using electrode penetration of the vascular wall demonstrated the existence of a substantial drop in O_2 between the lumen and a very thin tissue layer directly adjacent, attributed by the authors to the endothelium, although the magnitude of this drop has been questioned subsequently (see sect. VI*B1*). Nevertheless, a mismatch between intimal and luminal P_{O_2} would suggest inefficient transfer of O_2 from blood to cell. A physical barrier at the tissue level seems highly unlikely because a high O_2 diffusion resistance of the vascular wall would result in higher downstream P_{O_2} than observed (591), and O_2 is freely soluble in the plasma membrane (562).

The transfer of O_2 between the lumen and the endothelial cell initially involves the dissociation of O_2 from Hb. Considering the well-characterized O_2 dissociation curve for Hb **(FIGURE 4*B*)**, it is clear that arterial blood exists at a sufficiently high P_{O_2} to prevent substantial O_2 dissociation from Hb, as intended in such conduit vessels. Although this relationship can vary with changes in local pH/CO_2 (the Bohr Shift), it is unlikely that such changes would lead to large dissociations at such a high blood P_{O_2} (see **FIGURE 4*B***). Moreover, measurements of luminal P_{O_2}, as referenced above, reflect dissolved P_{O_2} rather than that stored in Hb (total O_2 content). Thus, the large drop in P_{O_2} between lumen and endothelial cell cannot be explained by limited dissociation from Hb. The relative contribution of vascular wall/tissue O_2 consumption to this large decline is not fully agreed upon, as reviewed elegantly elsewhere (456, 594, 603). There is general disagreement as to whether the vascular wall can consume enough O_2 to account for the large radial gradient detected, with large differences between cultured cells, tissue segments, and in vivo measurements clouding any consensus [summarized elegantly by Vadapalli and colleagues (603)]. Differences in experimental technique and interpretation can certainly account for some of this variation (see sect. VI*B1* for a more detailed discussion), leading to the conclusion that many reported measurements of vascular wall O_2 consumption may be overes-

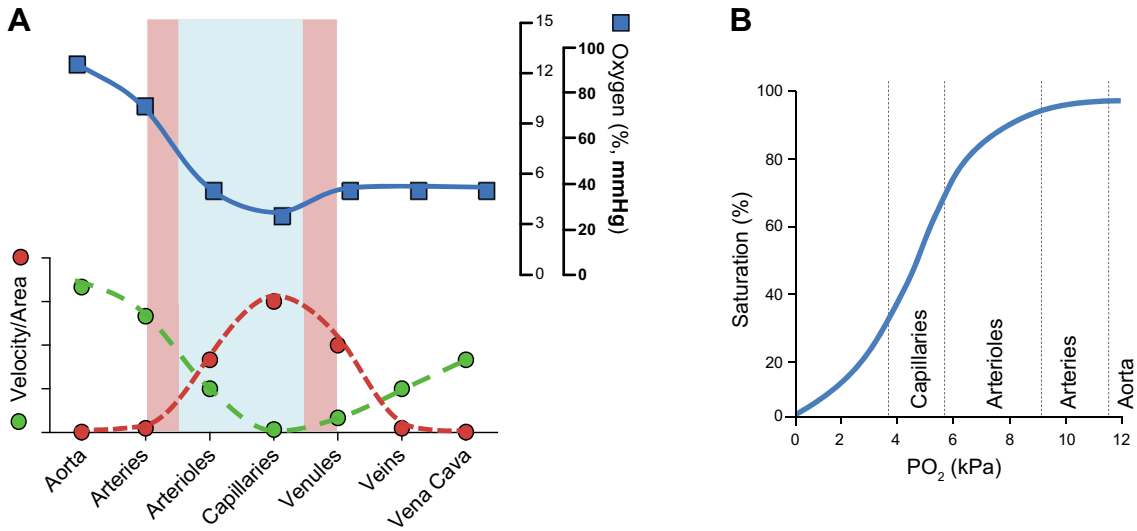

FIGURE 4. Oxygen gradients in the vascular system. *A*: The relationship between P_{O_2} (*right axis*), area and velocity throughout the vasculature. Highlighted are the generally perceived vessels in which gaseous (red) and nutrient (blue) exchange takes place. Velocity and area are arbitrarily defined in this review, and average P_{O_2} is adapted from Tsai et al. (594). *B*: A standard oxyhemoglobin saturation curve, with the average P_{O_2} values within relevant blood vessels annotated.

timated (456, 603). It therefore seems unlikely that this alone is sufficient to drive the large radial gradients alone. Recent evidence indicates that the major barrier to the transfer of O_2 from the lumen to tissue may in fact be the plasma phase of blood. This was first proposed by Hellums (231), who hypothesized that plasma (in which O_2 is poorly soluble) represents a significant barrier between the red blood cell and endothelium. In this model, dissolved O_2 fluctuates as a function of hematocrit, with so-called erythrocyte-associated transients increasing P_{O_2} near red blood cells and gradients extending in between. Such theories were corroborated by others (148, 405) and later demonstrated experimentally (22, 184, 328). In large vessels with wall thickness large enough to prevent efficient oxygenation of the vascular cells by diffusion alone, O_2 is supplied via the vasa vasorum as opposed to directly from the lumen (58, 230, 410), as discussed in detail in sect. VI*B1*.

3. From vessel to cytosol

The largest O_2 gradient in the vascular network is across the arteriolar wall, implicating these vessels as primary sites for O_2 delivery. However, the smaller overall area of arteriolar networks compared with capillaries dictates that large heterogeneity should therefore exist in tissue P_{O_2}, with large gradients extending between arteriolar vessels. O_2 transport between the capillary and tissue was first addressed by Krogh (316), in his now seminal description of the cylinder model. These relatively simple models tend to oversimplify, because microvascular networks are rarely uniformly distributed (except perhaps in skeletal muscle), but rather display a more disorganized network. Moreover, Krogh's model assumed that longitudinal gradients occur along the length of capillaries, which we now know is not necessarily the case. The presence of both longitudinal and radial gradients in the vasculature, and diffusional transfer of O_2 between neighboring arterioles, capillaries, and venules, results in a reasonably narrow Gaussian tissue P_{O_2} distribution (593). The lack of substantial intratissue P_{O_2} heterogeneity is of physiological significance, because an implication of Krogh's model of tissue O_2 distribution is that tissue close to the venular end of the microvascular network would be at a distinct disadvantage in terms of P_{O_2}. Of course, this viewpoint is still oversimplified as neither tissue perfusion (i.e., the number of microvascular vessels per cm^3 tissue), nor is cellular O_2 demand generally homogeneous, and thus, tissue P_{O_2} gradients can still form, especially in larger organs and under uncontrolled tumor growth (as will be discussed in sect. VI). P_{O_2} distribution in different organs/tissues will be discussed in later sections.

IV. UNDERSTANDING OXYGENATION IN VITRO

A reoccurring theme throughout this review will be the complex nature of cellular oxygenation in vitro. The combined effects of a static layer of medium above an O_2-consuming monolayer of cells, and poor solubility of O_2 leads to the formation of a gradient between the atmosphere and intracellular environment (10, 75, 420). In some cases, this gradient can be substantial enough to significantly reduce intracellular P_{O_2} below ambient, used herein analogously to headspace to refer to the gas phase immediately adjacent to the medium. Thus, intracellular oxygenation, and not ambient P_{O_2}, is the key parameter to consider when designing research under low O_2 environments. This section will address some of the nuances associated with achieving the desired intracellular O_2 level in vitro to recapitulate levels in vivo.

A. What Is the P_{O_2} in Room Air?

The often-quoted 20.9 kPa refers strictly to standard dry atmospheric air (see **FIGURE 5*B***). However, most cell culture is conducted within a controlled atmosphere of 95% air: 5% CO_2. Moreover, incubators are normally run at 75% humidity (compared with ~50% at room air) to prevent excessive evaporation of medium. Considering this, the actual P_{O_2} within a standard cell culture incubator is ~18.5 kPa (at sea level; **FIGURE 5**) (377, 420). This value is even lower at high altitude, as the water vapor and CO_2 components are a constant ~47/35 mmHg even under reduced atmospheric pressure. Most atmosphere-regulated cell culture chambers used to perform research under O_2 conditions different from atmospheric alter the P_{O_2} at the expense of nitrogen, thereby maintaining atmospheric pressure. Moreover, many are engineered to run at slightly higher atmospheric pressure at sea level (101.33–101.78 kPa) to obviate fluctuations in P_{O_2} due to changes in altitude.

B. Achieving the Appropriate Dissolved O_2 Level In Vitro

Modulating the gaseous atmosphere with respect to O_2 is straightforward, yet cells do not exist in contact with O_2 in the gas phase, with the possible exception of lung epithelial cells (see sect. VI*A*). The evolution of red cells as an intricate and highly efficient O_2 transporter bears testament to the poor solubility of this gas in solution. In contrast to CO_2, which reaches equilibrium in solution within minutes, O_2 dissolves too slowly to be overlooked in experimental protocols.

1. Factors affecting O_2 solubility

Efforts to determine O_2 solubility are spearheaded by oceanography and hydrometallurgy communities, with O_2 in solution used for numerous industrial processes. Initially defined by Henry's Law (235) (see sect. III*A*), the solubility of a gas in pure water is related to the temperature of water and the gaseous pressure. Such relationships have been confirmed more recently, both experimentally and computa-

A

	%	kPa	mmHg	μM
%	-	1.02	7.65	13.5
kPa	0.98	-	7.5	13.2
mmHg	0.13	0.132	-	1.76
μM	0.074	0.076	0.57	-

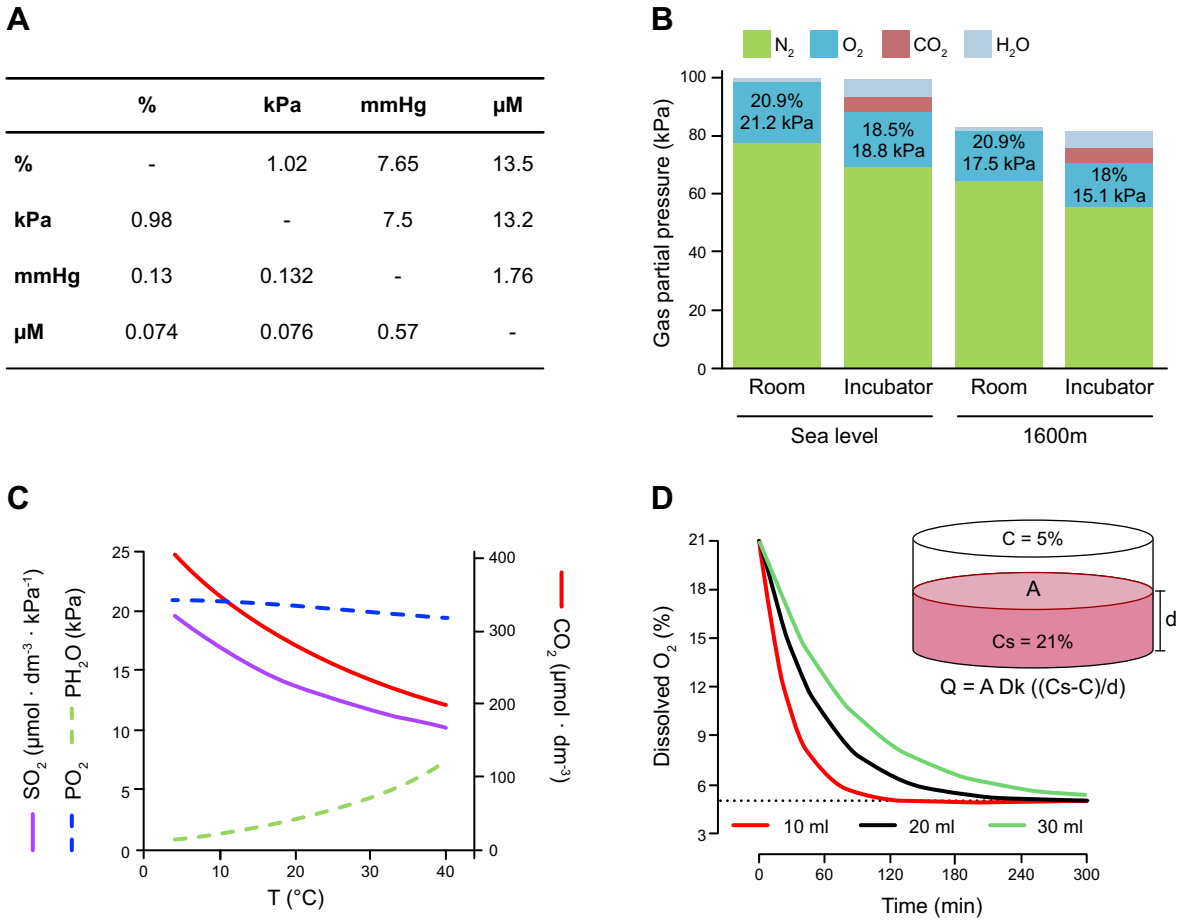

FIGURE 5. Parameters of atmospheric O_2 levels within the cell culture environment. *A*: An approximate O_2 unit conversion table with the multiplication factor required to convert current unit (row) into desired unit (column). *B*: The atmospheric composition at sea level, at 1,600 m above sea level, and within a standard culture incubator (5% CO_2, 75% humidity). *C*: The P_{H2O} and Po_2 in pure water are plotted across a range of temperatures, and the concentration (cO_2) and solubility (S) of O_2 calculated based on the equations of Benson and Krause (32), as summarized by Forstner and Gnaiger (159). *D*: An application of Fick's second law of diffusion to describe the time required for culture medium to equilibrate following exposure to an atmosphere of different O_2 content. A, liquid surface area; C, new concentration; Cs, saturating concentration; D, diffusivity of O_2 in liquid; d, liquid depth; k, solubility of O_2 in liquid; Q, rate of diffusion.

tionally [see Battino (1981) (25) and Ming and Zhenhao (2010) (399) for a review], and are illustrated in **FIGURE 5*C***. The relationship between temperature, pressure, and O_2 solubility is further defined by the Bunsen adsorption coefficient (α, measured in $dm^3 \cdot dm^{-3} \cdot kPa^{-1}$). From α, the solubility of O_2 (So_2) is defined here in $\mu mol \cdot dm^{-3} \cdot kPa^{-1}$ by:

$$So_2 = \alpha / (\text{molar volume} \times 101.325) \quad [O_2 \text{ molar volume} = 22.393] \qquad (4)$$

$$So_2 = \alpha / 2269.9$$

This initial equation was refined further by Benson and Krause (32, 33) in their proposal of units of standard concentration (c*), defined as the concentration of dissolved O_2 per volume of solution. As such, cO_2* in pure water under standard atmospheric conditions is defined as:

$$cO_2^* = So_2 \times (P_{atm} - P_{H_2O}) \times FO_2 \qquad (5)$$

Temperature also strongly impacts the P_{H_2O} of a given atmosphere, with higher temperature increasing evaporation and thus increasing P_{H_2O} at the expense of O_2. The salinity of a solution also impacts O_2 solubility, as demonstrated in pioneering work from Sechenov (524) and tabulated for convenience elsewhere (399). With relevance to physiology, the vast majority of experimental work is conducted in solutions of a reasonably similar salinity, and thus, this factor can be assumed constant. As shown in **FIGURE 5*C***, the solubility of O_2 in pure water at 37°C is ~77% than at 20°C, resulting in ~30% less O_2 in solution. This merits consideration when comparing experimental data derived at room temperature with that at 37°C. Moreover, with relevance to sect. IV*B2*, the equilibration of culture medium from room air to physiological O_2 levels is significantly more time efficient when the solutions are cooled to 4°C.

Table 1. *Permeability of commonly used plastic culture surfaces*

Surface	D (10^{-5} cm^2 s^{-1})	k (10^{-9} mol cm^{-3} mmHg^{-1})	Reference
Medium	3.3	1.2	(371, 389)
	2	1.2	(671)
	2.8	1.3	(112, 466)
Polystyrene	0.01	8.6	(466)
PDMS	2.2	12.2	(466)
Teflon	0.03	5.1	(311)

D, O_2 diffusivity; k, O_2 solubility coefficient; PDMS, polydimethylsiloxane; Teflon, polytetrafluoroethylene.

2. Equilibration in solution

Mass diffusion was first described by Fick in 1855 in a seminal piece of work from which we now derive Fick's laws of diffusion (153). In the absence of cells, O_2 equilibration between atmosphere and medium follows Fick's second law and can therefore be estimated using a one-dimension, single-compartment diffusion model. This is described by the equation $Q = AK[(Cs\text{-}C)/d]$ (458), in which Q is the rate of O_2 diffusion (μM min^{-1}), A is the surface area (cm^2), K is Krogh's constant (derived from the diffusivity and solubility of O_2), Cs and C are the saturating and desired P_{O_2} (kPa), respectively, and d is the depth of the medium (cm). To frame this scenario in the context of in vitro cell culture, imagine a 90-mm petri dish filled with 20 ml of medium and placed within a sealed chamber at a P_{O_2} of 5 kPa. Using Fick's laws, we can estimate that this medium will take ~2 h to equilibrate to 5 kPa, as shown in **FIGURE 5*D***, in agreement with experimentally derived values (10, 420). This rate can be increased by dividing the 20 ml into two 90-mm petri dishes, thereby doubling the effective surface area for diffusion. Dissolved O_2 levels achieved in culture medium are a critical and often underestimated factor in conducting experiments under low O_2 conditions aimed at recapitulating O_2 levels in vivo. Thus, addition of poorly equilibrated, overly oxygenated medium to cells preadapted to low O_2 conditions may generate a reaction akin to the reoxygenation phenomena observed during stroke and myocardial infarction.

3. Accounting for plastic leaching

The equations described above assume that the only path by which O_2 equilibrates in solution is through the gas/liquid interface. Although by far the most important source, plastic is not completely impermeable to O_2, and hence, O_2 can diffuse through the sides and bottom of culture dishes to varying degrees. This is largely deemed negligible by most researchers based on the extremely low diffusivity and solubility coefficients of standard polystyrene cultureware (see **TABLE 1**). The effect of substrate O_2 permeability on pericellular P_{O_2}, specifically comparing impermeable polystyrene with permeably substrates such as silicone rubber or Teflon membranes, has been demonstrated mathematically (274, 466) and experimentally (659, 690). Notably, Powers et al. (466) incorporated substrate permeability into the most widely adopted mathematical model to determine pericellular P_{O_2} (671), accounting for the surface area in contact with cells and substrate O_2 diffusivity and solubility. This was intentionally left out in **TABLE 2** for greater clarity, but essentially involves an additional α value for the substrate. When monolayer O_2 consumption substantially outweighs O_2 diffusion capacity, using a gas-permeable culture substrate can be an effective way to minimize unintentionally hypoxic conditions. On a separate note, plasticware left at room air (P_{O_2} 20 kPa) will accumulate a significant amount of O_2, and this will eventually leach out when placed in an environment of lower P_{O_2}, thus acting as a O_2 source (558). When plastic equilibrated to 20 kPa was placed within an anoxic water solution, dissolved P_{O_2} reached ~12 kPa after 60 h (558). Although specific rates of leaching will depend on the plastic composition and its mass/surface, it is highly advised that when working with cells preadapted to a specific low P_{O_2}, all plasticware (pipette tips, stripettes, petri dishes, and culture flasks) be preequilibrated at the appropriate P_{O_2} before use. This is of particular importance when working with near anoxic con-

Table 2. *Equations used to predict pericellular P_{O_2} in vitro*

Equation	Reference
$h = k\,[(P_S - P)/V]$	(559)
$-DdP/dx = VpP/[k(K_m+P)]$	(671)
$Solved$: $\theta = 0.5\,[1-\alpha-\beta_M+[(1+\alpha+\beta_M)^2-4\alpha]^{0.5}$	
$P = P_s-(Vp/60D)(760/k)(h/A)$	(389)
$-DdP/dx = -Dk(P_x - P_s)/h$	(371)
$1-\theta = [F_V+(1-F_V)(\theta/\beta_V+\theta)](\theta/\beta_M+\theta)\alpha^*$ $(Solved)$	(466)
$P = [(P-P_s)DA]/Vh$	(596)

α, dVp/DkP_s; $\beta_M = K_m/P_s$; $\beta_V = K_V/P_S$ (where K_V is a fitted constant describing dV/dP_s; θ, P/P_s; A, surface area; D, O_2 diffusivity in liquid; d, fluid height; F_V, $V_{max,O}/V_{max,\infty}$; k, O_2 solubility in liquid; K_m, P_{O_2} when O_2 consumption is 0.5max; P, cell density; P, pericellular P_{O_2}; P_s, P_{O_2} at gas/liquid interface; V = O_2 consumption rate (V_{max}).

ditions, in which even small amounts of O_2 leaching can severely compromise experiments, and we would always recommend measuring Po_2 in the medium/monolayer under such conditions to be confident a sufficiently low Po_2 is achieved and maintained.

C. Accommodating O_2 Diffusion and Monolayer Consumption

One of the most common, and incorrect, assumptions made during in vitro research is that intracellular Po_2 and ambient Po_2 are synonymous. The consumption of O_2 by cells, coupled to the poor solubility of O_2 in solution, generates a gradient between the headspace and monolayer proportional to the rate of monolayer O_2 consumption (389). Without compensation, cell cultures may inadvertently experience culture-induced hypoxia by consuming O_2 faster than it can diffuse, as discussed in sect. IV-D. Under these conditions, it may become difficult to differentiate the cellular response to physiological and hypoxic O_2 levels, resulting in incorrect interpretations. Compounding this problem has been the lack of technology to accurately monitor intracellular O_2 levels in living cells (see sect. II). In lieu of physical measurements, many have relied on an derivation of Fick's second law to predict pericellular Po_2 in monolayers cultured under static conditions (26, 199, 371, 384, 389, 421, 466, 559, 596, 659, 671). By considering oxygen diffusion within a culture dish as a one-dimensional diffusion/reaction, cell boundary O_2 levels can be predicted and, given that O_2 can freely diffuse across the plasma membrane (562), this approximately equates to generalized intracellular O_2 levels **(FIGURE 6*A*)**. Although exact equations differ between studies (summarized in **TABLE 2**), the common critical variables in determining pericellular Po_2 were always, as expected, ambient Po_2, cell density, cellular O_2 consumption, and medium height. The most comprehensive equation to date has been put forward by Powers et al. (466), in which the equation by Yarmush and colleagues (671) was adapted to reflect the change in cellular O_2 consumption as a function of ambient Po_2. Common to a number of such studies was the conclusion that hepatocyte monolayers [rabbit (559), human (671), and HepG2/3B cell lines (389)] are most likely severely hypoxic even when cultured under room air, which has subsequently been demonstrated experimentally (see sect. VI*E*).

These theoretical observations have been corroborated using electrode and fluorescence-based probes to experimentally determine pericellular Po_2 in monolayer cultures. Increased cell density has been shown to decrease pericellular Po_2 in monolayers of rat hepatocytes (250, 421), human dermal fibroblasts (581), T-47D breast cancer cells (453), and peripheral blood mononuclear cells (PBMC) (63). Notably, comparisons between cell types (389) revealed the importance of considering cell type–specific differences in density at confluence in addition to O_2 consumption rate per cell. Although mesangial cells had similar O_2 consumption rates to Hep3B cells (~9 nmol/min/mg protein), vastly different pericellular Po_2 (14.6 versus ~0 kPa at room air) results from differences in monolayer protein content, reflecting morphological differences in cell types (389). The other significant variable, fluid height, has also been confirmed experimentally (77, 371, 389, 421, 581) and is likely the most easily controlled to maintain the appropriate pericellular Po_2. Using the equation first described by Stevens in

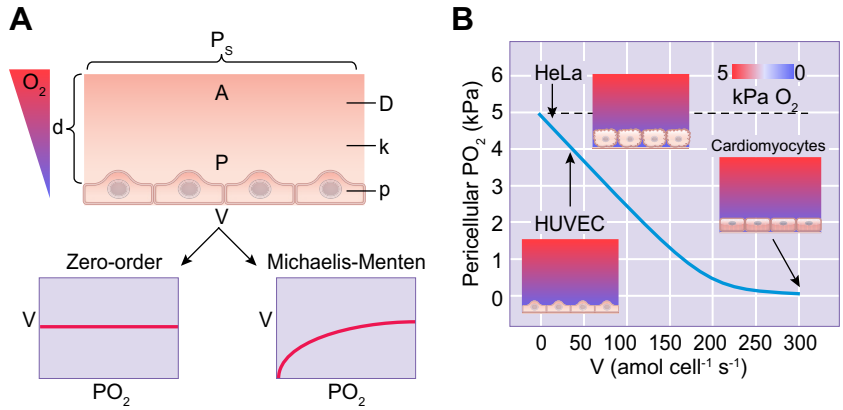

FIGURE 6. Predicting pericellular Po_2 in cell monolayers. *A*: Parameters critical in predicting pericellular Po_2 in cultured cells. The value of *V* (O_2 consumption rate) can be simplified by considering a zero-order relationship between *V* and Po_2, as described by Yarmush et al. (671) or modeled using Michaelis–Menton kinetics as described by Powers et al. (466). As we know, O_2 consumption is affected by O_2 availability, predictions will have more accuracy if *V* is modeled using the latter. *B*: Illustration of the relationship between pericellular Po_2 and cellular O_2 consumption, with commonly used cell types annotated according to published values. Cell types with high O_2 consumption such as cardiomyocytes or hepatocytes can initiate a self-inflicted hypoxia when ambient Po_2 is low. *A*, surface area at gas/liquid interface; *D*, O_2 diffusivity in liquid; *d*, fluid height; *k* = O_2 solubility in liquid; *P*, cell density; *P*, pericellular Po_2; P_s, Po_2 at gas/liquid interface; *V*, O_2 consumption rate (V_{max}).

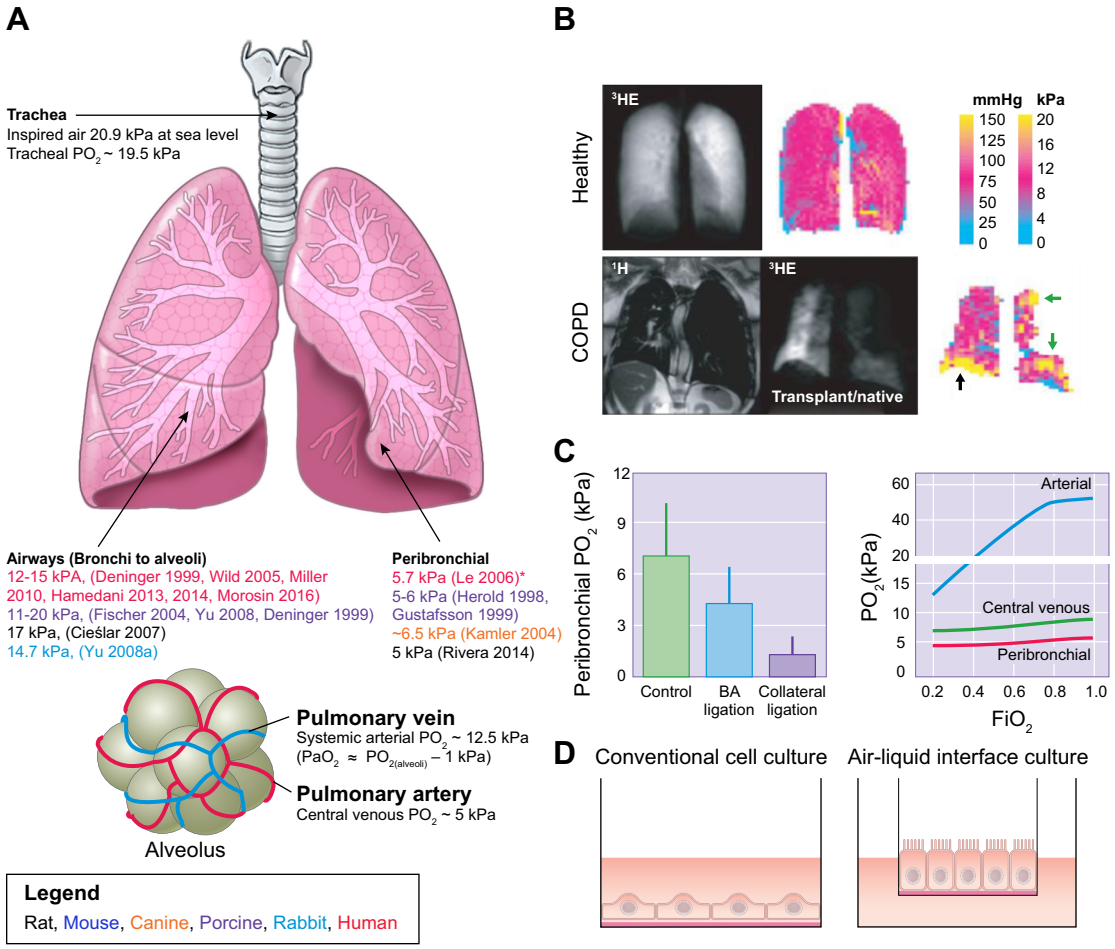

FIGURE 7. Oxygen distribution in the lung. *A*: An illustration depicting the known distribution of Po_2 in the mammalian lung, combining experimentally derived values with theoretical values derived from established physiology. Pulmonary arterial Po_2 (Pao_2) is usually slightly lower than alveoli Po_2 as outlined in the equation $Pao_2 = Po_2$(alveoli) – 1 kPa and discussed in Section III*A*. *B*: Whole lung Po_2 mapping using ^{3}He-based magnetic resonance imaging (MRI) scanning in healthy volunteers and in patients with chronic obstructive pulmonary disease (COPD). Taken with permission from Miller et al. (396). *C*: Peribronchial Po_2 values determined using microelectrode penetration upon (*left*) ligation of the bronchial artery (BA) or bronchial collaterals in dog [adapted with permission from Kamler et al. (282)], and (*right*) increases in forced inspiratory Po_2 (FiO_2), [adapted from Herold et al. (236)]. Both examples illustrate the dependence of peribronchial Po_2 on bronchial artery perfusion rather than the bronchi themselves. *D*: Comparison between conventional cell culture, in which the monolayer is completely submerged in medium, and air/liquid interface culture used to maintain differentiated primary epithelial cells. Transwell chambers are used to elevate the monolayer, exposing the apical surface to the atmosphere while maintaining basolateral access to medium through a microporous membrane.

1965 (559), one can calculate the required medium height to achieve the desired pericellular Po_2 as recently reviewed (462). Other methods to control pericellular Po_2 include varying the permeability of the base substrate (466, 659) to bypass the need for O_2 to diffuse through the medium and increasing ambient Po_2 to compensate for monolayer consumption and poor diffusivity (75).

As illustrated in **FIGURE 6*B***, cellular O_2 consumption rates vary considerably between cell types: from 4×10^{-5}-0.02 amol O_2 cell^{-1} s^{-1} in red blood cells (179, 510), to as high as 200–500 amol O_2 cell^{-1}s^{-1} in cardiomyocytes and hepatocytes (20, 165, 199, 478). These differences between cell types most likely arise from differences in metabolic activity and mitochondrial content/density. As monolayer O_2 consumption is a major determinant of O_2 diffusion, and ultimately pericellular Po_2, low consuming cell types are likely to experience much greater intracellular Po_2 than those that consume O_2 more rapidly when placed in the same environment. Sekine and colleagues (521) illustrate this concept by comparing pericellular Po_2 values and oxygen consumption rates in monolayers of human induced pluripotent stem cell cardiomyocytes, rat cardiomyocytes, human aortic smooth muscle cells, and cardiac fibroblasts. Cardiomyocyte monolayers consume significantly more O_2 than the noncardiomyocyte cell types, and this is reflected in a much steeper gradient between ambient and pericellular Po_2 (see **FIGURE 6*B***). Similar results were obtained when comparing medium

P_{O_2} in monolayers of human umbilical vein endothelial cells (HUVEC; low consuming, large size) and human embryonic stem cells (hESC; high consuming, small size) (2). If cellular O_2 consumption significantly outweighs O_2 diffusion capacity, a condition of self-inflicted hypoxia may arise at sufficiently low ambient P_{O_2} (77, 421) **(FIGURE 6*B*)**. In reality, because cellular O_2 consumption decreases with ambient P_{O_2} (88, 211, 441, 443), the accuracy of many of the predictions (which assume a constant rate of O_2 consumption) are limited under extreme hypoxia. It is more likely that under these conditions, intracellular O_2 levels in high-consuming cell types range around a value more conducive to viability under the control of negative feedback mechanisms orchestrated by HIF (178). In support of this, rat hepatocytes cultured at a P_{O_2} of 4 kPa stain strongly with the hypoxic marker Hypoxyprobe (indicating cytosolic P_{O_2} below 1 kPa) but retain reasonable viability, suggesting a sufficient supply of O_2 to maintain function (421).

One technique used extensively to alleviate problems associated with poor oxygenation in vitro has been the use of bioreactor-type culture conditions in which medium is continuously stirred. Under these conditions, cellular oxygenation can occur through convection in addition to diffusion, greatly increasing O_2 supply (172). Medium agitation also forms a critical component of a successful microbial culture system, in which bacterial or fungal cells are cultured in suspension at very high densities and therefore require additional oxygenation. Such conditions are not generally appropriate for the majority of adherent cell lines without prior immobilization [see bioartificial livers, for an example (579)], although some success has been obtained using roller bottle technology, in which adherent cells are cultured on the side of a cylindrical device placed horizontally on an orbital shaker (175, 462). Furthermore, microfluidic perfusion has received increasing attention in recent years and also solves several problems associated with monolayer oxygenation, especially when constructed using plastic with a high O_2 permeability coefficient. Many of these techniques can create adequate monolayer oxygenation, even though more effort and expense is required, and thereby provide more accessible means of altering existing culture conditions to improve oxygenation.

D. Evidence for Compromised Oxygen Delivery In Vitro

As eluded to above, the concept of self-inflicted hypoxia is not restricted to theory. Confluent HepG2 cultures rapidly (within 1 h) deplete medium P_{O_2} to <0.1 kPa even at an ambient P_{O_2} of ~20 kPa. In these studies, an hypoxic status was confirmed by continuous secretion of the HIF target protein erythropoietin (EPO) and an increase in lactate production, indicative of a switch from oxidative phosphorylation to glycolysis (659). Similar observations were made by Metzen et al. (389) and Bhatia et al. (421) in HepG2 and rat hepatocytes, respectively. Compromised O_2 delivery in vitro is not confined to hepatocyte cultures, because large culture O_2 gradients have been reported using a number of different cell types under standard culture conditions and low ambient P_{O_2} (see **TABLE 3**). Traditional micromanipulator-mounted electrode methodologies have largely been superseded by fluorescence- and phosphorescence-based techniques, which can provide a more accurate determination of pericellular P_{O_2} in culture dishes. Using immobilized luminescent dyes (see sect. IIC), large culture gradients have been demonstrated in cultures of hESC (2, 320) and Caco-2 intestinal epithelial cells (690). Meanwhile, cell-permeable phosphorescent nanoparticles have been used to monitor intracellular (cytosolic) P_{O_2} in mouse embryonic fibroblasts (151), cortical neurons (114), and in HUVEC (75). Hence, intracellular or pericellular P_{O_2} provides a more accurate parameter when translating in vitro experiments to an in vivo setting.

E. Maintaining the Appropriate Environment for the Duration of Culture

Culture of mammalian cells under reduced O_2 environments has generally been undertaken using three types of equipment: *1*) an airtight, gassed chamber placed within a standard CO_2 incubator, *2*) a tri-gas incubator, or *3*) a dedicated O_2-regulated workstation, with cost and infrastructure requirements increasing accordingly. The former is most widely used because of the relatively low price and ease with which it can be accommodated into existing culture infrastructure, although dedicated chambers generally have limited multiuser space and accessibility. Tri-gas incubators are variations of standard CO_2-regulated cell culture incubators in which an additional N_2 gas input is provided, with which the P_{O_2} can be manipulated to a required level. tri-gas incubators offer increased capacity for multiusers, especially units equipped with independent, modular compartments. However, both these types of equipment suffer from an important disadvantage when used for long-term culture of cells under defined low O_2 conditions. Cells need to be removed from the chamber or tri-gas incubator to feed, monitor, and perform any required subculture or experimental treatments. Thus, cells are re-exposed to hyperoxic atmospheric levels of O_2. Such fluctuations in the resultant pericellular P_{O_2} induce a phenotype distinct from that of cells maintained long term under a defined level of O_2 (289, 437, 640). Indeed, direct comparisons between culture in tri-gas incubators and dedicated O_2-regulated workstations demonstrate that repeated re-exposure to atmospheric O_2 levels during culture is detrimental to human mesenchymal stem cell (MSC) growth (289). Medium and pericellular P_{O_2} require hours to re-equilibrate to a required P_{O_2} level even when only transiently exposed (~5 min) to atmospheric levels (320, 404, 690). Such technical problems associated with in vitro cell culture mimic reperfusion injury, commonly following restoration of cerebral or myo-

Table 3. *Pericellular Po_2 levels under standard culture conditions*

Cell Type	Method	Po_2 (kPa)		Reference
		Ambient*	Pericellular	
Rat hepatocytes	electrode	18	8	(250)
		13	5.8	
		4	1.5	
HepG2/3B	electrode	18	<0.1	(659)
HepG2/3B	electrode	18	<0.1	(389)
			<0.1	
BAEC	electrode	18	10.4	(389)
HUVEC hEPC	Fiber-optic probe	21	19–20	(2)
		5	3.4	
		1	0.7	
HASMC	ESR	21	18.9	(442)
HUVEC	MitoXpress	18.5	~17	(75)
		5	3.5	
hiPSC-CM	electrode	21	10.4	(521)
HASMC			16.4	
HCF			18.6	
HMVEC			17.9	
Rat-CM			14.9	
mESC	Fiber-optic probe	2	2	(404)
hESC	Fiber-optic probe	21	4–5	(2)
iPSC		5	1.5	
		1	0.4	
MEF	MitoXpress	21	8.1	(151)
		10	3.8	
hESC	Fiber-optic probe	21	15	(320)
		5	≤1	
Rat mesangial LLC-PK_1	electrode	18	14.7	(389)
			<0.1	
Type II alveolar	electrode	18	13.3	(371)
Dermal fibroblasts	electrode	18	12	(581)
		2	0	
T-47D	electrode	21	1–18	(453)
MIN6 (β cells) PANC-1	Pimonidazole HIF-1α	20	–	(511)
		10	–	
		7	+	
		5	++	
		3	++	
		0	+++	
Trophoblast	electrode	21	<1	(77)
hESC	Fiber-optic probe	21	15	(320)
		5	≤1	
PMN	Oxodish	21	0–14	(63)
		4	<1	
RAW 264.7	Patch probe	20	~8	(690)
		5	~1.5	

Continued

Table 3.—*Continued*

Cell Type	Method	P_{O_2} (kPa) Ambient*	P_{O_2} (kPa) Pericellular	Reference
Caco-2	Patch probe	19	~4–5	(114)
		1	<0.1	
Cortical neurons	MitoXpress	18–20	14–16	(250)

*Unless clearly defined, ambient P_{O_2} was determined to be either 21 or 18 kPa based on the inclusion/absence of 5% CO_2 and humidification. BAEC, bovine aortic endothelial cell; ESR, electron spin resonance; hESC, human embryonic stem cell; HASMC, human aortic smooth muscle cell; HCF, human cardiac fibroblast; hEPC, human endothelial progenitor cell; hiPSC-CM, human induced pluripotent stem cell–cardiomyocyte differentiated; HMVEC, human cardiac microvascular endothelial cell; hPSC, human pluripotent stem cell; HUVEC, human umbilical vein endothelial cell; iPSC, induced pluripotent stem cell; MEF, mouse embryonic fibroblast; mESC, mouse embryonic stem cell; PMN, peripheral blood mononuclear cells; Rat-CM, rat cardiomyocytes.

cardial blood after infarction. Re-exposure to atmospheric P_{O_2} can be avoided completely by using a dedicated O_2-regulated workstation, where access to cells for subculture and treatment is permitted through gas-tight glove ports and transfer chambers. It is for this reason that we strongly recommend that any work investigating the effects of prolonged culture under well-defined low P_{O_2} be conducted using a dedicated O_2-regulated workstation.

V. CELLULAR OXYGEN SENSING: WHEN IS LOW O_2 HYPOXIC?

Having established the difficulties in accurately predicting and controlling monolayer oxygenation in vitro, a consideration for how cells sense the difference between normoxic and hypoxic P_{O_2} is now relevant. The question posed relates to the understanding that physiological oxygenation varies by so much in vivo that the use of terminology like hyperoxia, normoxia, and hypoxia should be used contextually rather than absolutely and should always be defined quantitatively for better interpretation. Each cell type has unique responses to a reduction in available O_2. For example, endothelial cells release vascular endothelium–derived growth factor (VEGF) and nitric oxide (NO) to initiate vasodilation and angiogenesis in an attempt to increase local blood flow, thereby normalizing tissue O_2 distribution (351, 536, 630). A more generalized hypoxic response is orchestrated predominantly by HIFs, with additional contributions from less well-defined pathways. The relevance of these mechanisms in the context of in vitro normoxia remains to be defined fully, because they have evolved to respond to acute reductions in P_{O_2} within (patho)physiological levels, and not the substantial reductions imposed in the majority of studies in vitro (room air to 1–3 kPa). Thus, the study of cellular phenotypes under low O_2 generally requires culturing cells for a sufficient period to allow adaptation to the new baseline [O_2]. Several excellent articles have reviewed the general and state-of-the-art literature concerning how cells sense O_2 (476, 516, 522, 575), and as such, only the most well-established cellular O_2 sensors will be covered here. Particular emphasis will be placed on their relevance under physiological O_2 levels in terms of the P_{O_2} at which they have been shown to be active. This will be followed by a brief discussion of how the duration of exposure to low O_2 can influence the interpretation of experimental data.

A. Cellular Oxygen Sensors

1. HIFs

Several excellent reviews have been published on the physiology and biochemistry of HIFs (472, 504, 516, 522), and therefore HIFs will only be briefly discussed. HIFs are evolutionarily conserved transcription factors expressed in all eukaryotic organisms as three α isoforms (HIF1–3) and a β subunit. The vast majority of research to date has focused on HIF-1, which regulates the acute and reactive phase of the hypoxic response in most cell types (257, 549). Although the β subunit is constitutively expressed and not actively degraded, the α subunit is posttranslationally modified through O_2-dependent hydroxylation at prolyl resides [by prolyl hydroxylases (PHD)], which targets the subunit for degradation (35, 134), or at asparagine residues by factor inhibiting HIF-1, which interferes with its binding to transcriptional coactivators (238, 322, 323). Thus, when intracellular O_2 availability decreases, these enzymes are no longer able to hydroxylate HIFα subunits, resulting in the formation of a transcriptionally competent stable α/β dimer. This can then translocate to the nucleus where it binds hypoxia-response elements, initiating the transcription of hypoxia-sensitive genes. Such genes encode proteins such as VEGF (162, 536), EPO (630), and glucose transporter 1 (128), which function collectively to either increase O_2 delivery or reduce cellular O_2 consumption. It was traditionally considered that a large degree of redundancy exists between HIF-1α and -2α (549, 667), which itself has fewer selective targets (120, 193, 257, 444, 569, 599, 634). However, recent pangenomic screens (503, 514, 515) have identified a large number of HIF response element (HRE) binding sites with distinct isoform binding affinities, despite an identical core recognition sequence (RCGTG). Such

variance may represent different topographical chromatin binding locations, affinity for HIF-β binding partner, and/or the involvement of other transcription factors, most notably AP-1 (321, 503). Comparatively little is known about HIF-3α, but it is thought to act as a negative regulator of HIF-1 and -2 (219).

The K_m for O_2 of the reaction catalyzed by PHD ranges between 140 and 250 μM (~10–20 kPa) (243, 517), and thus, O_2 may be a rate-limiting substrate under atmospheric O_2 conditions. Despite this, HIFs are not constitutively stabilized in cells at physiologically normoxic levels (on average 5 kPa), otherwise organisms would have no reactive response to further reductions during genuine hypoxia. Persistent stabilization is prevented by HIF-dependent negative feedback mechanisms including specific interactions with microRNA 210 (631) and ROS (254), upregulation of PHD 2 and 3 (36, 106, 178, 372), and the global impact of HIF-induced proteins to increase intracellular O_2 levels. Thus, any reduction in O_2 availability is addressed by transient stabilization of HIF-1α, and the upregulation of associated regulated proteins, followed by pathway normalization at a new baseline reflecting the altered O_2 levels. A question that remains unsolved in HIF hydroxylation is the concept of range finding; oxygen-dependent regulation of HIF is observed in a variety of tissues existing across a huge variety of O_2 levels (476). The high K_m of PHD enzymes for O_2 has led many to conclude that absolute O_2 levels are perhaps of secondary importance in the mechanism by which cells sense O_2 and that complimentary signals may further modulate hydroxylase activity. To date, alternative signals include ROS (74, 378), intracellular [Fe^{2+}] (306), and competing hydroxylase substrates (91). Inclusion of these additional parameters in the mechanism of HIF O_2 sensing creates an increasingly complex model which may offer insight into the range-finding capabilities of the system (476), a concept critical for defining physiological normoxia.

2. Mitochondria and/or superoxide

Given their central role in O_2 homeostasis and intracellular signaling, mitochondria are prime candidates for intracellular O_2 sensors. Mechanisms by which these organelles are thought to transduce changes in O_2 levels revolve around changes in either intracellular redox or energy states (or both) (74, 633). Limitations in O_2 supply would logically lead to reductions in mitochondrial ATP generation, which subsequently activates AMP-dependent protein kinase, a cellular energy sensor (220, 556), although some have argued this occurs because of ROS generation and not changes in ADP/ATP (132). AMP-dependent protein kinase, in turn, targets several transcription factors to repress fatty acid biosynthesis and upregulate proteins involved in glycolysis, resulting in a metabolic shift away from O_2-consuming oxidative phosphorylation (221). Pharmacological inhibition of the ETC can mimic hypoxic responses (121, 392), although others report an abolition in O_2 sensing following ETC inhibition (635). One major limitation to the energy state hypothesis of mitochondrial O_2 sensing is that the P50 of cytochrome *c* oxidase for O_2 is ~0.07 kPa (181), and thus, ATP production would not be expected to decrease until cytosolic P_{O_2} falls very low. However, some have suggested that the affinity of cytochrome *c* oxidase for O_2 is modified substantially by cellular reducing agents [GSH and NAD(P)H], suggesting that O_2 may become rate limiting at much higher levels than previously predicted (633, 653). The generation of superoxide anions by the ETC has formed the basis of intense debate in the context of mitochondrial O_2 sensing, with both decreases and increases in mitochondrial superoxide ($O_2^{\cdot -}$) generation reported to mediate O_2 sensing. On one side, reductions in O_2 availability would logically result in reductions in $O_2^{\cdot -}$ production, which in turn, would cause the cytosolic environment to become more reduced, affecting many redox-sensitive pathways (15, 480, 641). Conversely, others have reported a paradoxical increase in superoxide generation in mitochondria during hypoxia (74, 206, 207, 373, 450, 609, 636), resulting from enhanced electron leak within the ETC.

Mitochondria are not the only source of ROS within the cytosol, and indeed, other enzymatic sources have been implicated as O_2 sensors. Because NAD(P)H oxidases (NOX) function to generate ROS with a reported P50 for O_2 of ~1.7 kPa (31), it is tempting to speculate that NOX serve as a key cytosolic O_2 sensors (633). Indeed, mice lacking an essential subunit of the NOX2 isoform ($gp91^{phox}$) exhibit impaired O_2 sensing (168), although this remains controversial (14, 633). Both increases (229, 375) and decreases (100) in NOX-derived ROS generation have been reported during hypoxia.

3. Gaseous messengers

A new O_2-sensing mechanism has emerged in recent years focusing on the interplay between two physiological gaseous messenger molecules, carbon monoxide (CO) and hydrogen sulfide (H_2S) (468). The effects of CO on hypoxia-induced ventilation have been well known for 50 yr (352), yet the finding that it is produced endogenously highlighted its possible involvement in O_2 sensing. CO is produced by heme oxygenases, of which there are two principle isoforms: inducible (HO-1) and constitutively expressed (HO-2) (369, 542). Importantly, production of CO is O_2 dependent (652) with a P50 of 8.7 kPa (683), placing this potential sensor within the physiological range. CO was found to inhibit the activity of cystathionine-γ-lyase, the enzyme responsible for H_2S synthesis, and hence, H_2S production is increased when HO-2 becomes substrate limited during hypoxia (683). In archetypical O_2-sensing cells (e.g., type I cells of the carotid body), it is proposed that H_2S initiates depolarization through inhibition of Ca^{2+}-activated K^+ channels (340) and increasing Ca^{2+} influx (56).

Less is known about the role this CO/H_2S-sensing system functions in nonexcitable, nonspecialized cell types.

B. Exposure or Adaptation: Does Timing Matter?

With the exception of the HIFs, the above O_2-sensing mechanisms have been described in the context of whole body physiological reactions to hypoxia, and therefore have an implied negative feedback loop whereby a plethora of actions instigated by the sensing of hypoxia act in conjunction to increase tissue P_{O_2} to alleviate input stimuli. There is little information on how these mechanisms function in chronically hypoxic environments. The general consensus is that HIF-1α actions peak after 12–16 h of exposure to low O_2 and then normalize by 24 h to a new set point (62, 178, 249, 630). In contrast, any stabilization of HIF-2α has been shown to require considerably longer (>72 h) (249, 355). Because these transient responses to reduced O_2 availability are unavoidable during transfer from room air to physiological normoxia, it is critical that experiments aimed at recapitulating physiological conditions enable cells to adapt long term. Importantly, this should include the time required for the expression of any induced protein to also normalize. A global analysis of protein half-life reveals a mean half-life of 46 h (520), and thus, the adaptation time required to circumvent these initial responses to reduced O_2 can be estimated. We have observed that at least 5 days are required for a phenotype to stabilize in human endothelial cells when transferred from room air to a P_{O_2} of 5 kPa during culture (75, 290), with culture beyond this period inducing no further alterations in cell phenotype (75). To avoid misinterpretation of experimental data, we suggest that cells are cultured for as long as possible (at least 5 days) under physiological normoxic conditions.

VI. REPLICATING NORMOXIA IN VITRO

Significant efforts have been undertaken to better recapitulate a physiological milieu in vitro, with particular focus on the physical environment in which cells are cultured. For example, numerous studies have characterized the phenotype of endothelial cells exposed to laminar flow (80), or vascular smooth muscle cells (481) and renal mesangial cells (198) exposed to cyclic biaxial stretch, or dermal fibroblasts in three-dimensional (3D) extracellular matrix culture (197). However, few studies have carefully considered the gaseous composition of the culture environment. The following sections provide an overview of current understanding of P_{O_2} in specific tissues in vivo and summarize the key studies aimed at replicating these conditions in vitro. We focus specifically on investigations in mammalian cells under quasi-physiological P_{O_2} (not hypoxia) and long-term culture conditions (2–12 kPa, >24 h) to avoid confusing physiological phenotypes with those associated with relatively rapid adaptive responses to reduced O_2 availability. However, it is worth noting that when reviewing this literature, in most cases, only ambient P_{O_2} is considered and therefore many observations may not describe the ideal physiologically normoxic phenotype. Furthermore, tissue P_{O_2} distribution is considerably heterogeneous in both space (regional differences in perfusion or consumption) and time (changes in metabolic activity). The data quoted in this review therefore often represent one observation across a range of potential values and should be interpreted accordingly. All measurements of tissue P_{O_2} discussed in this review have, to the best of our knowledge, been performed on intact preparations kept in situ to maintain the endogenous blood supply and minimize interference from the atmosphere.

A. Lungs

In the airways, P_{O_2} in the gaseous phase can be predicted accurately, and thus, concentrations within the respiratory tract are known with high certainty (see sect. III*A* and **FIGURE 3**). Consistent with the large area occupied by the bronchi, bronchioles, and alveoli, whole-organ P_{O_2} maps (see **FIGURE 7*B***) conducted with MRI scanning using ^{3}He polarization (3) reveal average P_{O_2} values of 14.5 (107), 13.4 (649), 13.6 (396), 14 (216), ~12.7 (217), and 13.5 kPa (407) in human subjects, largely reflecting inspired air P_{O_2}. Whole-lung P_{O_2} is lower in chronic smokers (216) but does not differ in patients with heart failure, although the alveolar/arterial gradient (see sect. III*A*) is significantly higher in these patients, suggesting a less efficient gaseous transfer (407). These values closely reflect values obtained in experimental animal models, in which mean P_{O_2} values of 11 (156), 14.7 (682), and 19.6 kPa (107) have been reported in porcine lung, 17.1 kPa in rat lung (85), and 14.7 kPa in rabbit lung (681). Regional heterogeneity in P_{O_2} measurements throughout the lung was common in all the above studies, consistent with the known variability in lung perfusion and gas exchange. This, coupled with a small image acquisition field of view, can lead to lung P_{O_2} values skewed by sampling in highly or poorly perfused regions. Encouragingly, lung or alveolar P_{O_2} values determined by ^{3}He MRI correlate very well with traditional methods used to determine alveolar P_{O_2}, in which P_{O_2} in the expired gas is related to arterial P_{O_2} and P_{CO_2} using *Eqns 2*/3 (see section III*A*) (217, 407).

The need to transition into the aqueous phase within the airway surface liquid (ASL) for bioavailability make estimates of how a gaseous P_{O_2} of 13–18 kPa translates into cytosolic P_{O_2} within airway epithelial cells ambiguous. The average ASL depth in healthy human bronchi is 15–80 μm (273) and is therefore unlikely to present a significant barrier to O_2 diffusion. To our knowledge, no measurements of ASL P_{O_2} in healthy bronchi have been reported, and thus, we are left to interpolate lung epithelial P_{O_2} based on ASL

depth. Worlitzsch et al. (664) elegantly demonstrated that increased ASL depth (up to 800 μm) in patients with cystic fibrosis resulted in a mean mucosal P_{O_2} of 2.5 mmHg (0.3 kPa). Such hypoxic conditions were associated not only with increased ASL, but also with increased epithelial cell O_2 consumption and facilitated the early pathogenesis of anaerobic *Pseudomonas aeruginosa* infections (664).

Beyond the epithelia, the lung connective tissue largely consists of fibroblasts whose role it is to maintain the structural integrity of the organ. Intriguingly, adventitial P_{O_2} has been reported significantly lower than the average lung P_{O_2} (13–14 kPa) as measured by ^{3}He inhalation. Using microelectrode penetration, peribronchial P_{O_2} values of 5.7 kPa were recorded in patients inspiring >50% FiO_2 (326). Similar values have been described in porcine [5.1 kPa (236), 5.8 kPa (205)], canine [~6.5 kPa (282)], and rat [5.1 kPa (487)] experimental models. In the latter study (487), an implantable electron paramagnetic resonance (EPR) resonator was used in conjunction with O_2-sensitive EPR probes to monitor deep tissue P_{O_2} in real time, confirming measurements using microelectrodes. Anatomically, the site most often sampled by microelectrode penetration lies ~1 cm distal to the tracheal bifurcation, near to the peribronchial lymph node. Kamler and colleagues (282) demonstrated that ligation of the aortic stem of the bronchial artery dramatically reduces peribronchial P_{O_2} in this region, even when breathing was maintained (**FIGURE 7*C***). This, coupled with the observation that peribronchial P_{O_2} does not increase proportionally with FiO_2 (unlike arterial P_{O_2}) (236), suggests that lung adventitial P_{O_2} is critically dependent on blood perfusion from the bronchial artery and does not receive O_2 supply directly from the airways. How representative this highly sampled region is of nonairway lung tissue as a whole remains to be established, although it has been used as a measure of overall tissue oxygenation following lung transplant and correlates well with improved outcomes (282, 425, 431).

Unlike most other cell types, lung epithelial cells experience a high P_{O_2} physiologically and are only separated from gaseous O_2 by a thin layer of ASL. These conditions have been recapitulated in vitro in the form of air/liquid interface culture, as illustrated in **FIGURE 7*D***. First introduced in the late 1980s by Wu, Kim, and colleagues (6, 7, 645), this technique has been shown to be essential in maintaining primary cultures of tracheal and bronchial epithelial cells in a differentiated state in vitro. Principally, the pseudostratified phenotype observed in vivo can be recapitulated in vitro after ~7 days culture at the air/liquid interface (5, 645), with cells typically differentiating into ciliated and granulated mucus-secreting epithelial cells. Other responses to culture at the air/liquid interface include increased Na^+ transport via short-circuit current (278), restoration of epithelial barrier function (190), and a transcriptional profile more comparative with fresh tracheal/bronchial epithelial cells in vivo (126, 454), even in response to cigarette smoke inhalation (381). More recently, culture at the air/liquid interface has been used as a tool to differentiate inducible pluripotent stem cells into mature airway epithelial cells (470, 662). This method of culture clearly has profound impact on the phenotype of airway epithelial cells, very accurately recapitulating that observed in vivo. However, we could not identify a publication employing air/liquid interface culture in which the P_{O_2} was implicitly defined. When the immortalized epithelial A549 cell line was cultured long term at a P_{O_2} of 13 kPa, an increased sensitivity to copper oxide nanoparticles was observed paralleled by a decrease in cellular antioxidant defenses (317). Although pericellular P_{O_2} may be lower than 13 kPa in this model, thus poorly representing physiological normoxia, this study provides important insight into the potential of employing culture under physiological normoxia to evaluate environmental toxicity in models of airway damage. Standard incubator conditions (~18.5 kPa, 5 kPa CO_2) reasonably reflect upper tracheal P_{O_2}, but bronchiolar P_{O_2} can drop as low as 13 kPa. Thus, careful control of ambient P_{O_2} during air/liquid interface culture may yield interesting insights into phenotypic differences related to P_{O_2} between epithelial cells along the length of the respiratory tract.

B. The Vasculature

The mechanics of O_2 distribution in the vasculature have already been covered in section III*B*, and this section aims to further discuss the absolute P_{O_2} values measured in the vascular network. In estimating P_{O_2} values experienced by different cell types in the vascular wall (endothelial, smooth muscle, and fibroblasts), it is critical to assess the level of O_2 within the wall tissue itself. An excellent review by Tsai, Johnson, and Intaglietta (594) summarizes the distribution and gradients of O_2 in the microvasculature, and we have in this review, integrated their summaries and conclusions with recent research findings. Current understanding of the P_{O_2} levels in vessels related to specific tissues will be discussed in the context of the relevant tissue.

1. The macrovascular wall

Section III*B2* introduced the concept of radial gradients across the vascular wall, which are particularly prominent in larger arteries such as the aorta and carotid arteries. O_2 supply to the endothelial layer occurs largely by diffusion from the lumen (containing oxygenated blood P_{O_2} ~12 kPa), noting that the thickness of the walls of such vessels can severely limit adequate delivery. As such, vessel wall P_{O_2} decreases significantly between the luminal and medial layers, as first reported nearly 50 yr ago (410, 428). By advancing a tissue-penetrating Clark-type electrode perpendicular to the vessel wall, as illustrated in **FIGURE 8*B***, a pattern of wall oxygenation in large arterial vessels such as the aorta, femoral, and carotid arteries is clearly evident.

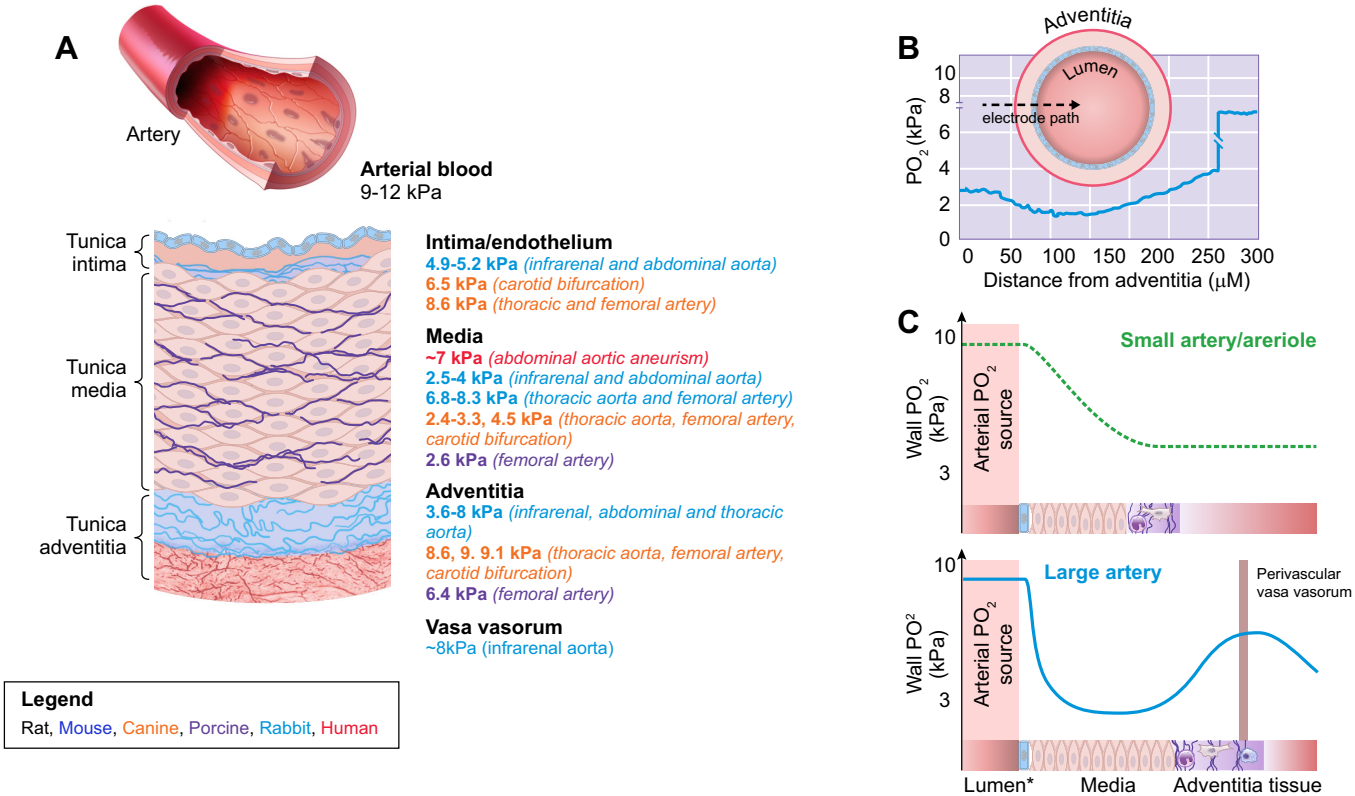

FIGURE 8. Oxygen distribution in the arterial wall. *A*: Illustration of known distribution of P_{O_2} in the wall of large arteries such as the aorta and carotid and femoral arteries, combining experimentally derived values with theoretical values obtained from established physiology. *B*: Representative trace obtained when a microelectrode is advanced in 5-μm increments through the wall of the rabbit thoracic aorta. Redrawn with permission from Niinikoski et al. (428). *C*: Graphical P_{O_2} profiles through the walls of small (*top*) and large (*bottom*) arteries, illustrating the effect that the vasa vasorum has on adventitial P_{O_2}. *Endothelium.

Penetrating the intimal layer was associated with a prominent, rapid reduction in P_{O_2} in the rabbit infrarenal aorta (237, 330, 428, 509) and abdominal aorta (505, 506, 508), pigeon abdominal aorta (214), and dog carotid artery (507). In such studies, P_{O_2} in the intimal layer reached an average of 3–5 kPa, representing a drop of 5–7 kPa from the lumen. Others reported no such sudden drop in similarly sized vessels and preparations (23, 57, 97, 99, 279, 691), instead reporting gradual declines in P_{O_2} across the inner third of the wall, reaching a similar nadir within the medial layer. Such discrepancies have been attributed largely to differences in methodology, including *1*) the nature of vessel preparation and maintenance, with contrasting P_{O_2} profiles observed when the vessel is left in situ (237) versus. superfused with physiological solution at a controlled P_{O_2} (97) and 2) the method of electrode advancing, with many using vibration-mounting apparatus to minimize tissue distortion. Some (509) have postulated that the resonance created by such devices can interfere with the laminar flow patterns close to the vessel wall, considered critical in forming the aforementioned O_2 diffusion barrier. In contrast, others (98) have suggested that the sharp decline in P_{O_2} at the intimal layer is an artifact resulting from the use of large-diameter electrodes. Whether sharp or gradual, experimental evidence is clear that vessel wall P_{O_2} declines proportional to distance from the lumen (in vessels devoid of vasa vasorum, see below).

Aside from this discrepancy, remarkable conformity exists in the reported minimal vessel wall P_{O_2}. The nadir within the medial layer shown in **FIGURE 8*B–C*** occurs at 50%–70% of the wall thickness away from the adventitia (~200 μm in a rabbit thoracic aorta) and reaches a P_{O_2} of 3–4 kPa (23, 237, 279, 330, 428, 505–509). This value has been shown to correlate negatively with total wall thickness (97, 279), and hence, conditions in which vessel wall hyperplasia occurs can result in significant reductions in medial P_{O_2}, as observed in alloxan-induced diabetes (505), atherosclerosis (279), hypertension (99, 506), after insertion of vascular grafts (330, 509) or stents (508), and after balloon de-endothelialization (691). Reduced medial P_{O_2} in such conditions has been attributed to an altered bioenergetic profile in resident (and migrating) cells (330) as well as biophysical considerations such as increased wall stress (508) and compression of the vasa vasorum (57, 508). Medial hypoxia has been demonstrated in vivo in rabbits with late-stage atherosclerotic plaques in the aortic arch and thoracic aorta using the biochemical hypoxia marker 7-(4'-(2-nitroimidazol-1-yl)-butyl)-theophylline (41). In this study, plaques >400 μm in diameter exhibited hypoxic regions

~200 μm in diameter and 200–300 μm from the endothelial/intimal surface, with an estimated P_{O_2} of 0.5 kPa. Using similar probes ([^{18}F]EF5 and [^{64}Cu]ATSM), hypoxic regions have been visualized within the media of athero-susceptible transgenic mice (427, 537) and rabbits (426). Atherosclerotic plaques occur preferentially in regions of the vasculature that experience oscillatory blood flow, such as the inner curvature of the aortic arch and carotid bifurcation (370), and lower medial P_{O_2} has been measured in such regions using microelectrodes (507). It is therefore possible that medial hypoxia precedes and facilitates atherogenesis in such regions rather than occurring subsequent to plaque development and wall thickening.

Limited data are available on P_{O_2} profiles in large arteries in humans, as measurements are invasive and difficult to perform in humans. However, Vorp and colleagues (620, 621) performed microelectrode measurements of P_{O_2} within the abdominal aortic wall of patients with aneurysms. Although reported measurements were normalized to luminal P_{O_2}, interpolation based on an average aortic luminal P_{O_2} of ~11 kPa suggests that the aortic aneurysm wall P_{O_2} was ~7 kPa in the absence of intraluminal thrombi, falling to ~2.5 kPa when a thick thrombus was evident (620). Although the exact topographical location of the P_{O_2} sampling point was not reported, an aortic wall P_{O_2} of ~7 kPa is similar to values measured in animal models (279, 505, 506, 508).

The walls of large blood vessels can be thick enough in diameter to merit their own blood supply, and in arteries, these vessels are termed the vasa vasorum. The extent and nature of such vessels is critically dependent on the wall thickness. Peri-adventitial vasa can exist in moderately sized arteries such as the femoral or carotid, whereas vasa penetrating into the media are thought only to occur beyond a critical threshold diameter (>500 μm or 29 lamellar units, irrespective of species or vessel characteristics) (661). In the context of vessel wall P_{O_2} distribution, the presence of vasa vasorum is critical in defining adventitial P_{O_2}, as outlined in **FIGURE 8*C***. An upward inflection beyond the medial nadir in the P_{O_2} profile of a vessel wall is characteristic of a second source of O_2 diffusion from the outer layers. Arteries confirmed histologically to be devoid of adventitial vasa demonstrate a continuous decline in P_{O_2} between the lumen and adventitia (97, 99, 279), and experimental disruption of vasa vasorum patency (surgical or resulting from increased wall stress secondary to increased blood pressure) in those vessels possessing peri-adventitial vasa results in a significant reduction in adventitial P_{O_2} (23, 57, 330, 508, 509, 691). Moreover, increases in aortic tissue P_{O_2} in response to vasodilatory compounds (adenosine and epinephrine) applied to the adventitia have been attributed to vasa vasorum vasodilation (58). Notably, adventitial and medial neovascularization often occurs in response to vessel injury (413), and Lee et al. (330) showed that decreased adventitial P_{O_2} following insertion of an anastomotic graft can resolve over time in conjunction with the histological appearance of new medial vasa.

2. The microvasculature

The vascular network between an artery and vein, encompassing arterioles, capillaries, and venules is the prime region for O_2 exchange, as evidenced by the significant difference in blood P_{O_2} between an artery and vein (~6–7 kPa). This longitudinal gradient was first highlighted in section III*B1* and is the focus of previous reviews (456, 594). As such, only an overview of blood P_{O_2} within the microvascular network will be included in this review. Microvascular networks are present in all organs, and we provide an overview of blood P_{O_2} in an idealized microvascular network comprised of *1*) a feeding artery, *2*) first-, second-, and third-order arterioles, *3*) a capillary bed, *4*) first-, second-, and third-order venules, and *5*) a collecting vein **(FIGURE 9*A*)**. The majority of studies of microvascular P_{O_2} distribution have focused on three experimental preparations: the hamster skinfold/cheek window, rat cremaster/spinotrapezius muscle, and rat pial/cortical microvasculature. Their minimally invasive nature and the ability to monitor intravascular P_{O_2} in live animals are major advantages of such models. A summary of studies for each experimental model is provided in **FIGURE 9*B***. Blood enters the microvascular network at an average P_{O_2} of ~9 kPa and rapidly declines along the arterioles to reach a capillary P_{O_2} ~5 kPa. As described by Tsai et al. (594), such a finding suggests that arterioles, and not capillaries, are the major source of O_2 delivery in most microvascular beds. This may be true for hamster cheek pouch and rat muscle preparations, but reports in rat pial microvessels indicate that intravascular P_{O_2} in precapillary arterioles is still ~7–9 kPa, and only falls substantially once it has entered the capillary networks (622). However, recent evidence using two-photon time resolved phosphorescence (500) has refuted such claims, demonstrating that arterioles in the mouse cerebral cortex are responsible for ~50% of O_2 delivered to the underlying parenchyma. These authors postulated that the expansive capillary network may act as a reserve mechanism for O_2 delivery during times of increased activity (500).

Unlike large vessels, the presence of radial gradients and their contribution to tissue P_{O_2} in arterioles is less well defined. Many studies report differences between intravascular and periarteriolar P_{O_2} (260, 531, 585, 591), which appear proportional to the blood P_{O_2} and luminal diameter (594). Such differences are in the order of 2.5–3.5 kPa in large (A1) arterioles (531, 591) and ~1.5 kPa in moderately sized (~40-μm diameter) arterioles (260, 531, 585). In contrast, others have observed an arteriolar wall O_2 gradient of only a few of millimeters mercury [1.4 mmHg/0.2 kPa per micrometer (122, 123); 1.2 mmHg/0.16 kPa per micrometer (527, 623)]. Pittman (456) proposed a possible explanation for this discrepancy, citing misinterpretation of phos-

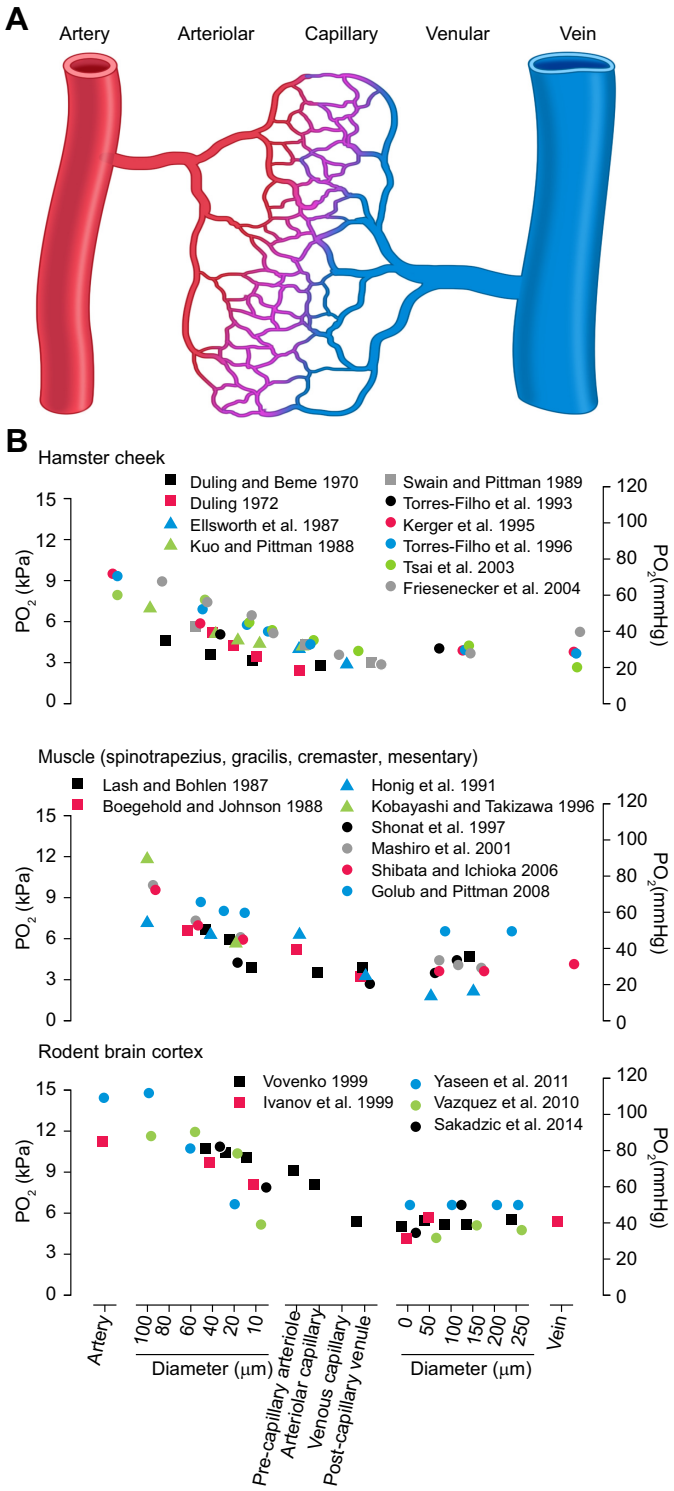

FIGURE 9. Oxygen distribution in the microvasculature. *A*: An idealized microvascular network. *B*: Reported P_{O_2} values plotted against the vessel diameter in microvascular experimental preparations. Results are separated according to tissue and coded according to the measurement technique employed: □, microelectrode penetration; △, derived from measurements of hemoglobin saturation, in which P_{O_2} was interpolated based on known species hemoglobin (Hb) dissociation curves; and ○, phosphorescence-quenching microscopy. Adapted from Tsai et al. (594).

phorescence quenching data due to O_2 consumption by the probe itself. Attempts to remedy these differences have subsequently been made by adapting the methodology (182, 183, 185). Unusually high vascular wall consumption, the reasoning put forward to explain large radial arteriolar gradients (594), was also refuted by Vadapalli et al. (603). With relevance to estimating physiological normoxia for cells resident within the microvascular wall, we believe that intravascular (blood) P_{O_2} most appropriately represents this value.

3. The human umbilical vein

One of the most well-studied and widely utilized vascular cell type in vitro are HUVEC. However, its unique physiology (fetal, venous tissue carrying oxygenated blood at a low flow rate) means it does not reflect normal artery/vein, macro/microvascular characteristics. Unlike many other tissues in the human body, the umbilical cord can be accessed relatively easily/noninvasively for blood collection and gas analysis, albeit ex vivo. It is therefore fortunate that endothelial cells isolated from these vessels have been used extensively in vascular biology in vitro, allowing for an accurate and well-characterized transition to physiologically normoxic cell culture. A meta-analysis of data extracted from a number of studies reporting umbilical blood P_{O_2} (102, 109, 298, 313, 347, 376, 465, 486, 576, 605, 675) reveals a mean blood P_{O_2} of 3.8 and 2.4 kPa within umbilical veins and arteries, respectively. Although collected ex vivo under room air, this has been shown not to increase measured O_2 levels in umbilical blood (382). Interestingly, umbilical vein P_{O_2} decreases throughout gestation from ~6 kPa at 20 wk to ~4 kPa at 36 wk (639), and final P_{O_2} at birth is significantly affected by the method of delivery (spontaneous vaginal versus caesarean) (109, 313) and position of the fetus (breech) (102). The human umbilical vein is a macrovessel of 2–3-mm diameter with an average wall thickness of 430 μm and a moderate adventitial layer (344). Although not studied, based on these dimensions, it seems likely that a significant radial gradient would be apparent across the length of the wall (section III*B2*), and thus, physiological normoxia in smooth muscle cells in these vessels may be lower than that measured in the endothelium [~3.5 kPa (75)].

4. Endothelial cells

The physiological response to hypoxic tissue O_2 levels is an initial vasodilation followed by the induction of angiogenesis, with both responses increasing O_2 delivery and thereby alleviating the harmful effects of hypoxia (536, 571). Given the primary role of endothelial cells in orchestrating such responses, it is no surprise this cell type has received considerable attention in the context of low O_2 physiology (393, 472, 523), as summarized in **TABLE 4**. We recently described a well-defined model to recapitulate physiological

Table 4. *The effects of culture at physiological normoxia on endothelial cell physiology*

Species	Cell Type	Po_2 (kPa)	Time (days)	Summary*	Reference
Human	HUVEC	5 (12 shear)	3	↑ Growth (BrdU)	(695)
				↑ Expression of membrane and ECM proteins CD105, CD31, fibronectin, laminin, and type VI collagen.	
				Different morphology after 24 h shear stress (20 dyne/cm^2) (more spindle-like, elongated).	
				↑ NO and PGI_2 production with shear stress, ↔ with 20% versus 12% O_2	
	EPC	5, 1	3	Dissolved medium O_2 level much lower in ESC, iPSC, and EPC cultures than HUVEC.	(2)
	HUVEC			↑ Traditional hypoxia-sensitive genes (VEGF, Glut1, and EPO).	
	HUVEC	3	up to 25	↑ FGF and VEGF stimulated growth and migration.	(276, 277)
	HUAEC			Putting nonadapted cells in 3% O_2 for 1 day ↑ effects of FGF and VEGF and putting adapted cells in 21% O_2 did not reverse the effect of adaptation of growth.	
				↓ Cell surface area compared with nonadapted once adhered.	
				Microarray analysis showed 41–74 upregulated and 21–86 downregulated genes (all HIF regulated), (HUVEC/HUAEC).	
	HUVEC	5 (5 shear)	3	↔ Protein/mRNA expression following shear between 5% and 20% O_2.	(1)
				↓ Apoptosis gene expression (Bcl), no additive effect of 5-FU.	
				↑ Permeability with 5-FU, reversed by resveratrol.	
	HUVEC	5	1, >5	Culture at 5 kPa ambient Po_2 results in intracellular Po_2 of ~3.5 kPa in HUVEC monolayers.	(75)
				↓ Induction of antioxidant defense proteins (HO-1 and NQO1) by electrophilic agents.	
				↔ Induction of glutathione-related proteins (GCLC, GCLM, and xCT) but no change in $[GSH]_i$.	
				↑ Bach1 protein and siRNA-mediated knockdown rescued HO-1 induction at 5 kPa O_2.	
				↓ Proliferation	
	HUVEC	5, 1	>5	IC_{50} for HIF-1α stabilization is 2.3 kPa O_2 when plotted against intracellular Po_2.	(290)
				↑ PP2A-C protein and colocalization with eNOS-mediated rapid dephosphorylation in response to Ca^{2+}-dependent stimuli, but not laminar shear stress.	
				PP2A-C protein levels show bell-shaped relationship with ambient Po_2, peaking at 5 kPa.	
				NO bioavailability inversely proportional to Po_2.	
				Culture at physiological normoxia-induced phenotype distinct from that under hyperoxic (room air) and hypoxic (1 kPa O_2) conditions.	

Continued

Table 4.—*Continued*

Species	Cell Type	Po_2 (kPa)	Time (days)	Summary*	Reference
	HUVEC	5	>5	↓ Plateau phase $[Ca^{2+}]_i$ in cells at 5 kPa O_2, rescued by cotreatment with SERCA-inhibitor CPA. Cells at 5 kPa O_2 more resistant to Ca^{2+} overload due to mitochondrial sparing by increased SERCA activity.	(291)
	HPMVEC	5	12	Confluent monolayers contained 30% fewer cells, but formed a tighter barrier as measured by TER.	(547)
	ST1.6R			↑ Cortical actin levels.	
	HDMVEC	5	14	↑ Basal and stimulated growth (PMA and IL-1β). ↑ ECM proteins (type VI collagen).	(697)
Bovine	Corneal EC	6	4	↑ [^{3}H]thymidine incorporation and cell count.	(684)
	BRMVEC	95, 40, 20, 105	4	Endothelial cells more sensitive to effects of oxygen compared with pericytes and fibroblasts from same vessel.	(490)
Rat	Liver sinusoidal EC	5	5	↓ Basal apoptosis (MTT and Annexin V/PI). ↔ Morphology of confluent monolayer or fenestrated characteristics. ↓ Endocytotic capacity during culture significantly less at 5%. ↓ ICAM-1 and IL-6 expression/production (proinflammatory) and ↑ IL-10 production (anti-inflammatory) (only measured after 48 h). ↑ H_2O_2 basal production (DCF), treatment with catalase reverses effects on apoptosis. ↔ NO release (Griess reaction).	(377)

BRMVEC, bovine retinal microvascular endothelial cells; CPA, cyclopiazonic acid; DCF, dichlorofluoroscein; ECM, extracellular matrix; EPC, endothelial progenitor cell; EPO, erythropoietin; ESC, embryonic stem cell; FGF, fibroblast growth factor; 5-FU, 5-fluorouracil; GCLC, glutamate-cysteine ligase catalytic; GCLCM, glutamate-cysteine ligase catalytic modulatory subunit; Glut1, glucose transporter 1; GSH, glutathione; HDMVEC, human dermal microvascular endothelial cell; HO-1, heme-oxygenase 1; HPMVEC, human pulmonary microvascular endothelial cell; HUAEC, human umbilical artery endothelial cell; HUVEC, human umbilical vein endothelial cell; ICAM-1, intracellular adhesion molecule 1; IL-1β, interleukin-1β; iPSC, inducible pluripotent stem cell; MTT, 3-(4,5-dimethylthiazol-2-yl)-2,5-diphenyltetrazolium bromide; NO, nitric oxide; PGI_2, prostacyclin; PI, propidium; iodide PMA, phorbol 12-myristate 13-acetate; PP2A-C, protein phosphatase 2A catalytic subunit; SERCA, sarco/endoplasmic reticulum Ca^{2+}-ATPase; TER, transendothelial resistance; VEGF, vascular endothelial growth factor; xCT, cystine-glutamate antiporter system X; EC, endothelial cells, eNOS, endothelial nitric oxide synthase.

normoxia in cultured human venous and arterial endothelial cells (75, 290, 291). Using a phosphorescent nanoparticle probe to monitor intracellular Po_2 in living cells **(FIGURE 10*A*)**, we established that culture at a Po_2 of 5 kPa was required to compensate for monolayer O_2 consumption and recapitulate a physiologically normoxic intracellular environment of 3.5–4 kPa (measured in umbilical venous blood, see above). To maintain such conditions in different culture apparatus (6-, 24-, or 96-well plates) with various surface area, volume was adjusted to achieve similar surface area: medium-depth ratios. For example, 100 μl in a 96-well plate has roughly the same surface area: medium-depth as 500 μl in a 24-well plate.

The importance of distinguishing between ambient and intracellular Po_2 was further highlighted by the different absolute P_{50} (akin to EC_{50}/IC_{50}) (633) values for HIF-1α stabilization when plotted against each O_2 parameter **(FIGURE 10*C*)** (290). When ambient Po_2 is used, the resulting P_{50} value (4.3 kPa) is not consistent with the known Po_2 distribution in the majority of the microvasculature nor in tissues, where a Po_2 4–5 kPa would be considered normoxic, and hence, minimal HIF-1α stabilization should be apparent. In contrast, use of intracellular O_2 levels results in a P_{50} value of 2.3 kPa, a level more consistent with what one may expect to observe in the hypoxic vasculature in vivo. Under these defined conditions, we have shown that the induction of nuclear factor E2-regulated factor 2–regulated antioxidant gene expression in response to oxidative stress was markedly attenuated in HUVEC **(FIGURE 10*D*)**. Similar findings have been reported in RAW 264.7 macrophages cultured at 5 kPa (208), and in human diploid fibroblasts upon re-exposure to atmospheric Po_2 following long-term culture at 3 kPa (21). Notably, this phenotype was only

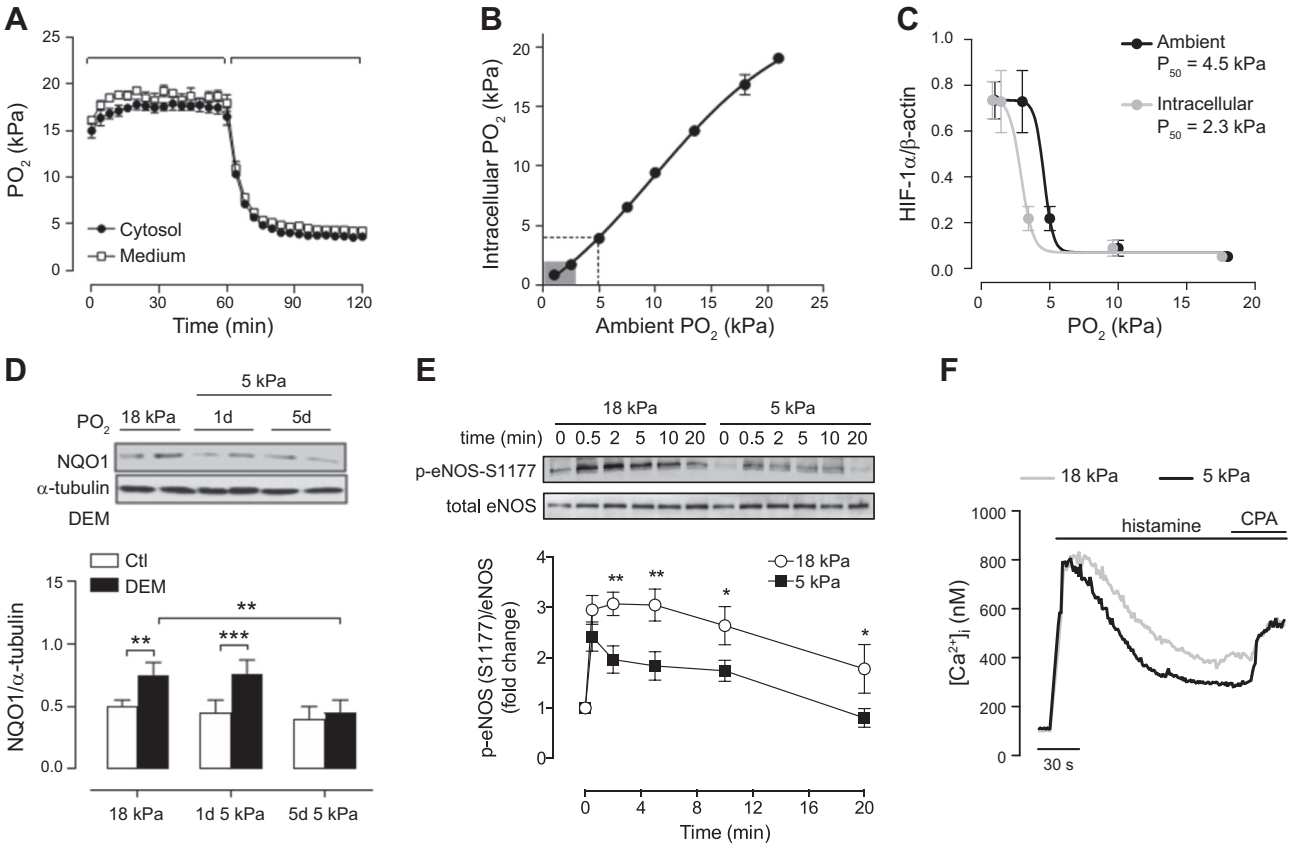

FIGURE 10. Effects of physiological normoxia on human endothelial cells. Experimental data describing the careful definition of cellular oxygenation in vitro and the subsequent characterization of cellular function and phenotype during long-term culture under these conditions. *A*: Intracellular Po_2 in human umbilical vein endothelial cell (HUVEC) monolayers cultured in 96-well plates (100-μl volume) at a Po_2 of 18 kPa and then exposed acutely to 5 kPa, measured using MitoXpress Intra in an O_2-regulated plate reader. This illustrates that the Po_2 in the medium is only moderately higher than cytosolic, and both parameters rapidly change upon changes in ambient Po_2. *B*: Intracellular Po_2 in HUVEC monolayers as a function of the ambient Po_2, defined by a four-parameter sigmoidal fit. Dashed lines indicate the conditions in which HUVEC were subsequently cultured. *C*: HIF-1α protein levels in HUVEC were cultured for 5 days at the indicated Po_2 in an O_2-regulated workstation and corrected for the resulting intracellular Po_2 determined in *B*. Plotting against intracellular Po_2 results in P_{50} values more likely to be observed in the vasculature in vivo. *D*: Expression of a Nrf2 regulated antioxidant defense protein, NAD(P)H-quinone oxidoreductase 1 (NQO1), in HUVEC cultured at a Po_2 of 18 or 5 kPa for 1–5 days and then challenged with the electrophile diethyl maleate (DEM; 100 μM for 24 h). These data illustrate the difference between cellular phenotypes when cells are exposed acutely (24 h) or chronically (5 days) to lower O_2. *E*: Phosphorylation of endothelial nitric oxide synthase (eNOS) in response to histamine (10 μM, 2 min) stimulation in HUVEC cultured at a Po_2 of 18 or 5 kPa for 5 days, demonstrating a more rapid decline in phosphorylation over time in cells cultured under physiological normoxia. *F*: Intracellular Ca^{2+} mobilization in response to histamine, measured using Fura-2AM. Lower plateau $[Ca^{2+}]_i$ at physiological normoxia are reversed by treatment with the sarco/endoplasmic reticulum Ca^{2+}-ATPase inhibitor cyclopiazonic acid (CPA). *A*, *B*, and *D* are replotted from Chapple et al. (75); *C* and *E* are taken from Keeley et al. (290); and *F* is taken from Keeley et al. (291).

observed following long-term adaptation (>5 days) to physiological normoxia (75). GSH-based defense systems remained intact, and this alone conferred sufficient protection to maintain cell viability (69). In line with this, basal levels of apoptosis are lower in HUVEC (1) and rat liver sinusoidal endothelial cells (377) cultured at 5 kPa for 3 and 5 days, respectively. We have recently shown that HUVEC cultured at a Po_2 of 5 kPa exhibited significantly less sensitivity to Ca^{2+} overload–induced cell death (291), which we attributed this enhanced sarco/endoplasmic reticulum Ca^{2+}-ATPase activity, sparing the mitochondria from Ca^{2+} overload **(FIGURE 10*F*)**.

There are conflicting reports on the effects of physiological O_2 levels on endothelial cell proliferation in vitro. In the context of angiogenesis, the consensus is that a higher proliferative rates occur in endothelial cells cultured under physiological O_2 levels, and indeed, this has been demonstrated in HUVEC (2, 276, 277, 695) and human dermal microvascular endothelial cells (697). However, we ob-

served a significant reduction in HUVEC proliferation following culture at 5 kPa for more than 5 days (75), in line with the quiescent nature of endothelial cells in vivo (133, 244). Moreover, production of extracellular matrix proteins type IV collagen (49, 697), fibronectin, CD105, CD31, and laminin (695) is significantly higher in human dermal microvascular endothelial cells and HUVEC cultured at 5 kPa levels. Differentiating between endothelial cell responses to physiological and hypoxic O_2 levels is especially relevant given their unique and highly regulated response to pathological hypoxia. For example, different HUVEC phenotypes are observed when cultured at a Po_2 of 3 (277) and 5 kPa (2, 75), largely due to increased stabilization of HIF-1α under the lower O_2 level. We have recently demonstrated that the synthesis of nitric oxide (NO) is significantly altered when endothelial cells are cultured at 5 kPa **(FIGURE 10*E*)** (290). Importantly, these processes were still functional, yet under more strict regulatory control by protein phosphatase 2A. This is in stark contrast to the phenotype observed in hypoxic (1 kPa) cells, in which stimulation of NO synthesis is largely abolished. In many respects, cells cultured at hypoxic O_2 levels more closely resemble those maintained at room air than those cultured at physiological O_2 levels, further highlighting the importance of this distinction.

5. Circulating and immune cells

As for endothelial and smooth muscle cells, no single O_2 level can be described as normoxic for circulating cells. This does not preclude the study of circulating cells under physiologically relevant O_2 levels in vitro, because even the highest O_2 levels encountered in vivo (~13 kPa within the pulmonary circulation) are still much lower than atmospheric. Although circulating cells are exposed to the full dynamic range of blood physiological O_2 (~5–13 kPa) over a relatively short period of time, the majority of blood at any given time resides in the venous and microvascular compartments (~60%–75%) (24, 47), in which Po_2 averages 5 kPa (594). Moreover, most monocytes reside within the spleen at rest (564), where Po_2 ranges from 2 to 5 kPa in rodents (48, 61, 67, 266) and swine (573), and 7–8 kPa in rabbits (613, 614). Such variance likely reflects the heterogeneous perfusion of the spleen, with pronounced gradients extending away from the splenic artery in mice (61).

Several studies have investigated the effects of isolation and culture of human PBMC under physiological O_2 (as summarized in **TABLE 5**). Basal proliferation of human $CD4^+$/$CD8^+$ PBMC (16, 17, 315) and murine $CD4^+$ T cells (259) was largely unchanged during culture at a Po_2 of 5 kPa, whereas proliferation stimulated by concanavalin A or CD3/CD28 cross-linking was markedly lower (16, 17). Interestingly, growth stimulated by another lectin, phytohemagglutinin, was unaffected by culture at 5 kPa (16, 17, 315). Another common observation during culture at 5 kPa is enhanced T cell differentiation and activation, with increased early expression of the activated lymphocyte marker CD69 on PBMC (17, 210, 315), activation of PBMC-matured human dendritic cells (171), and murine splenocyte–differentiated T cell CD4:CD8 maturation (61). Indeed, a transcriptional array of human PBMC samples cultured at 5 kPa for 15 days revealed significant upregulation of genes important for lymphocyte biology, whereas expansion at room air highlighted upregulation of gene clusters associated with stress responses, cell death, and repair mechanisms (210). Expansion of human PBMC under atmospheric conditions reduces intracellular GSH levels because of oxidative stress associated with prolonged hyperoxia. This artifact can be reduced by expansion of PMBC expanded at a Po_2 of 5 kPa (146). Associated with atmospheric culture–induced GSH depletion is the induction of antioxidant and defense proteins such as superoxide dismutase (SOD), catalase, and GSH peroxidase-1 (146), resulting in lower basal cytosolic ROS (146, 315). One potentially significant consequence of the altered human PBMC phenotype at a Po_2 of 5 kPa was reported by Sahaf and colleagues (499). The HIV transactivator of transcription protein, previously understood to induce apoptosis in ex vivo T cell preparations, caused rapid proliferation and primed cells for subsequent infection more rapidly than phytohemagglutinin (499). This novel finding highlights the possibility of drawing misinformed conclusions based on in vitro experiments performed under hyperoxic conditions. In summary, culture of PBMC and similar cells under physiological Po_2 conditions has significant consequences on cell proliferation, redox status, and differentiation capacity. It remains to be investigated whether changes in Po_2 within the physiological range (2–5 kPa) (e.g., as would occur when monocytes enter the systemic circulation from the spleen), have functional consequences on their physiology.

Human peripheral blood neutrophils undergo rapid (within 24 h) and constitutive apoptosis after isolation and culture under standard culture conditions (Po_2 18–20 kPa). This can be reduced significantly by isolation in a low Po_2 (0–3 kPa) environment (218) and with inhibitors of HIF-1α hydroxylation (628). Moreover, hyperoxia-induced apoptosis was also reduced in peripheral neutrophils isolated from patients with von Hippel–Lindau syndrome (627), although this was further reduced by hypoxic incubation, suggesting a role for both HIF-1α–dependent and independent pathways. Despite enhanced survival, neutrophils maintained at a Po_2 of 3 kPa exhibited defective respiratory burst activity and hence killing ability against *Staphylococcus aureus* infection, seemingly through the limitation of molecular O_2 as a substrate for the generation of ROS (383). This may result from suboptimal O_2 diffusion/supply capacity in vitro, as elegantly demonstrated recently (63), rather than true substrate limitation. The effects of low Po_2 culture on neutrophils has been summarized elsewhere (354, 574) and so will not be discussed in further detail in this review. Although a Po_2 of 3 kPa may be considered

Table 5. *The effects of culture at physiological normoxia on circulating cell physiology*

Species	Cell Type	Po_2 (kPa)	Time (days)	Summary	Reference
Human	PBMC	5	1–5	↑ Unstimulated and Con A–stimulated proliferation; no effect on PHA stimulation. ↑ Early expression of lymphocyte marker CD69. ↓ Basal and H_2O_2-induced ROS production (DCF). Altered released cytokine profile following stimulation with Con A or LPS.	(315)
	PBMC	5	15	Gene expression array revealed higher expression of genes important for lymphocyte biology, immune function and cell-cycle progression. ↓ Expression of genes involved in stress response, cell death, and cellular repair.	(210)
	PBMC	5	5	Proliferation stimulated by antigen CD8/CD28 cross-linking, or Con A, was ↑ at 5%, but no effect on phytohemagglutinin-stimulated proliferation. Unstimulated cell viability unaffected by adaptation to 5%.	(16)
	Negatively enriched T cells	5	3	↓ GSH and GSH:GSSG following culture (versus fresh), less reduction at 5%.	(17)
	PBMC			↓ Proliferation ↑ CD8/CD28-stimulated NO and ROS production. ↑ Lymphocyte marker CD69.	
	PBMC	5	>6	Tat protein induces apoptosis at 20%, but proliferation at 5% O_2 Tat can be used to prime cells for HIV infection as well as other methods, only at 5% O_2.	(499)
	PBMC	5	7	In vitro culture ↑ SOD1–3, CAT, and GPx mRNA. At 5% O_2, ↓ CAT and GPx mRNA versus room air. ↑ GPx activity, no change in CAT or SOD activity. ↑ Intracellular GSH, although overall decrease during culture. ↓ Superoxide and hydrogen peroxide.	(146)
	PBMC-matured dendritic cells	5	duration of culture	↔ Total cell yield. ↓ Endocytosis of dextran/FITC. ↑ LPS-induced IL-12 (p70) and T cell activation during coculture.	(171)
Mouse	$CD4^+$ T cells	5, 1	36 h	↑ Th17-specific differentiation at 5%; ↓ all subset differentiation at 1%. No effect of 5% on proliferation, 1%. ↓ Increased mTORC1 activity at 5% O_2.	(259)
	Primary splenocytes	2.5	6	↑ CD4:CD8, but dramatically higher killing (lytic) potential of $CD8^+$ cells at 5%, with ↑ density of CD25 surface antigen.	(61)
	Splenocyte-differentiated T cells			↓ Cell death	

Continued

Table 5.—*Continued*

Species	Cell Type	Po_2 (kPa)	Time (days)	Summary	Reference
	macrophage line J774	6	24 h	↓ *Leishmania amazonensis* (intracellular parasite) infection at 5%. ↔ NO or ROS production.	(105)

CAT, catalase; Con A, concanavalin A; DCF, dichlorofluoroscein; LPS, lipopolysaccharide; FITC, fluorescein isothiocyanate; GPx, glutathione peroxidase; GSH, glutathione (reduced); GSSG, glutathione (oxidised); HIV, human immunodeficiency virus; IL-12, interleukin-12; mTORC, mammalian target of rapamycin; NO, nitric oxide; PBMC, peripheral blood mononuclear cell; PHA, phytohaemagglutinin; ROS, reactive oxygen species; SOD, superoxide dismutase; Tat, HIV transactivator of transcription.

subphysiological in the general context of this article, one must consider that inflammation can produce localized areas of profound tissue hypoxia (63, 189, 331, 367, 538, 588), and therefore it may be more appropriate to study neutrophil physiology under such conditions, especially if these cells cannot survive at higher Po_2 for more than a few hours. Active neutrophils consume high amounts of O_2 and can actually create or exacerbate a hypoxic environment in vivo and in vitro (63), which can accelerate the resolution of tissue inflammation.

C. Heart

The heart is second only to the lungs in terms of exposure to O_2, yet in contrast to the lungs, it is a highly metabolically active tissue with a large O_2 requirement. Although the coronary artery branches directly from the ascending aorta in which blood is at its most oxygenated, measurements of cardioplegic solution Po_2 sampled from numerous coronary artery branches in patients undergoing revascularization or aortic valve replacement surgery reveal levels of 5 kPa (202). We could not find any measurements of coronary artery Po_2 in healthy humans or experimental animal models, and thus, whether these measurements reflect normal physiology or are lower as a result of disease remains unclear. Interestingly, Po_2 values not much lower than these are reported within the coronary sinus in humans [2.7–4.4 kPa (385, 624, 646)], canine [2.9 kPa (69)], and in the great cardiac vein of patients undergoing coronary artery bypass surgery [3.5 kPa (651)]. Using a blood-borne phosphorescent probe, Rumsy and colleagues (496) measured the Po_2 distribution in the epicardial microvasculature of the porcine heart before and during infarction. An average Po_2 of 2.2 kPa was recorded in noninfarcted tissue, with a gradient observed toward the ischemic core. The coronary microvasculature penetrates the myocardium superficially, and compression of microvessels during systole means perfusion of the deep myocardial tissue is intermittent. As a result, a gradient of Po_2 has been observed between the superficial epicardium, the deep myocardium, and individual myocytes, as illustrated in **FIGURE 11**. Such levels range from 4.1 to 6.1 kPa at the epicardial surface (245, 543) to 3.4 kPa in the subepicardium (3-mm depth in the canine heart) (654) and 2–3 kPa in the myocardial tissue (11, 40, 72, 150, 297, 358, 487, 648, 654). Hence, coronary microvascular Po_2 [2.2 kPa (496)] closely matches the average adjacent tissue Po_2, supporting the concept that a significant portion of O_2 diffusion must occur upstream of the capillary bed.

The increase in O_2 between the endocardium and coronary sinus reflects the increasingly acknowledged arteriolar/venular shunting hypothesis of O_2 distribution (328, 594). Generally, excellent corroboration exists in cardiac Po_2 measurements using a variety of techniques including the use of implantable EPR probes, which can be used to monitor cardiac Po_2 with impressive temporal resolution (72, 339, 487) and are stable for at least 112 days in situ (297), although these typically do not offer great spatial resolution. Anatomical complexity in O_2 delivery is compounded by the extremely high O_2 consumption rate of cardiomyocytes (see section IVC), resulting in very low intracellular Po_2 [1–1.6 kPa (84, 252)], although this low O_2 does not limit aerobic respiration in these cells (84). Myoglobin, present within the cytosol of skeletal and cardiomyocytes, has a greater affinity for O_2 than Hb [P50 of ~0.3 versus ~3.5 kPa (12)] and is thought to facilitate O_2 delivery to respiring mitochondria (567, 568). It may do this simply by providing a store of O_2 within the cell that can be made available during periods of increased activity or, perhaps, by removing dissolved O_2 from the cytosol, thereby increasing the concentration gradient from the blood to cell in a process of facilitated diffusion (90, 234, 281, 657, 658). Hence, actual O_2 content within a cardiomyocyte in vitro will be higher than the detected dissolved Po_2, complicating interpretations of relative monolayer oxygenation.

Stem cells derived from human myocardial biopsies cultured at a Po_2 of 5 kPa exhibit greater chromosomal stability and fewer karyotypic defects over 1–2 mo of culture than their room air counterparts (343). Moreover, a greater yield was achieved per biopsy, with a higher reparative capacity when subsequently transplanted into a mouse infarcted heart (342). Interestingly, Puente et al. (471) recently demonstrated that the dramatic rise in cardiac tissue Po_2 in the fetal heart at birth induces growth arrest through oxidative damage. This elegant study may explain the en-

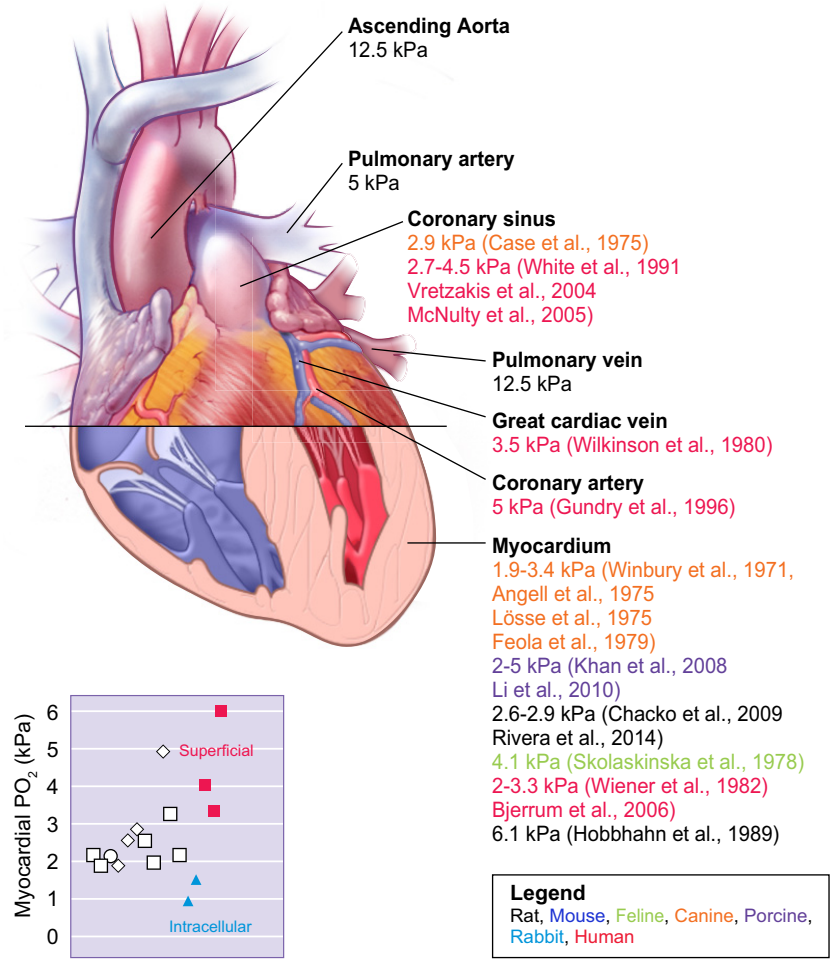

FIGURE 11. Oxygen distribution in the adult heart. Illustration depicting the P_{O_2} within the heart, summarizing published studies for different species with known values established in physiology. Individual myocardial P_{O_2} values are further summarized in the adjacent graph, separated according to technique used: □, microelectrode penetration; △, derived from measurements of myohemoglobin saturation, in which P_{O_2} was interpolated based on known species Hb dissociation curves; ○, phosphorescence quenching microscopy; and ◇, implanted electron paramagnetic resonance (EPR) probes. Values are color-coded to highlight those taken at superficial sites (red) or single-cell intracellular measurements (blue).

hanced proliferative and reparative potential of cardiac stem cells under physiological O_2 levels, especially when one considers that the true intracellular O_2 level in these cells may be considerably lower than 5 kPa.

Murine cardiac fibroblasts cultured at a P_{O_2} of 3 kPa were also found to proliferate more rapidly, which was attributed to reduced expression of p21 and a less oxidized environment (494). However, because intracellular P_{O_2} in these cells are likely to be considerably lower than the ambient (and physiological) 3 kPa, these results more accurately represent a hypoxic phenotype acknowledged by the authors. In line with this, human cardiac fibroblasts cultured under perfused conditions at a P_{O_2} of 5 kPa exhibit decreased growth relatively to room air and hypoxic (1 kPa) cultures (600), suggesting hypoxia and hyperoxia, but not physiological normoxia, are potent triggers for fibroblast proliferation in vitro. In this recent study, a clear delineation between the cellular response to normoxia (5 kPa) and hypoxia (1 kPa) is demonstrated, with hypoxia strongly associated with markers of pathological cardiac remodeling (600). However, cells were subjected to altered ambient P_{O_2} for only 24 h in this study and hence may not represent truly adapted cells. Rat neonatal cardiomyocytes isolated and maintained at a P_{O_2} of 5 kPa release higher concentrations of adenosine but rapidly release the vasoconstrictive angiotensin II when exposed to higher O_2 levels (655). Although limited, these studies collectively demonstrate that culture of cardiac-derived cells under physiological O_2 levels robustly alters their phenotype with significant therapeutic implications.

D. Brain

The brain receives blood from mainly the common carotid artery and, to a lesser extent, the vertebral artery, both of which branch directly from the ascending aortic arch. In line with microvascular O_2 distribution outlined above, oxygen levels of ~8 kPa have been measured in rat (70, 527) and mouse (501) pial arterioles. Moreover, a P_{O_2} of ~3.5 kPa in the pial parenchyma (at depth of ~50 μm) (390, 527) indicates a significant loss of O_2 across the pial arteriolar wall (527). Similar to other major organs, the cerebral vasculature extends superficially throughout the brain, with fewer vessels penetrating the inner layers of the cortex. Accordingly, P_{O_2} within the cortex decrease proportional to the depth: from ~5 kPa the superficial cortex (70, 111, 247,

248, 351, 688) to ~3 kPa in the deep white matter (70, 111, 390, 501, 544), as illustrated in **FIGURE 12**. This gradient further extends into the deeper regions associated with central nervous system function (hypothalamus, hippocampus, and midbrain). Surprisingly, Po_2 levels within these regions have been measured as low as 0.5 kPa [0.5–1 kPa midbrain (70), 0.4 kPa pons (70), 1.5–2 kPa hypothalamus (70), and 0.8–3.5 kPa caudate nucleus (525)]. However, Lyons and colleagues (364) have challenged this concept recently. Using two-photon phosphorescence quenching method (section IIC), they observed no change in intravascular Po_2 in either arterioles or venules of the somatosensory cortex with increasing depth from the surface (364). These authors proposed that anesthesia and associated stressful handling during the experiment setup may artificially alter brain activity and hence tissue Po_2 (364). Prior measurements were made using the surgical insertion of a microelectrode, and therefore revisiting brain tissue Po_2 levels using two-photon light microscopy could provide further insights (501, 502). Indeed, Lecoq and colleagues (328) were able to measure neuronal Po_2 in the mouse olfactory bulb during odor stimulation, in which average microvascular Po_2 increased from ~6 kPa to 7.5 kPa, simultaneous with similar increases in red blood cell velocity and intracellular Ca^{2+} (328). Notably, neuropil Po_2 was substantially lower than the surrounding microvasculature (~3 kPa), yet still increased upon odor stimulation. In subsequent studies, a mean interstitial Po_2 of 3–4 kPa was found in the murine olfactory bulb and somatosensory cortex (364, 445), consistent with previous studies using implanted ESR probes (125, 350, 439). Changes in brain oxygenation during stimulation or disease have become the focus of increased experimental and clinical studies, the former spurred on by the development of BOLD-MRI (see section II*D*). Although blood-oxygen level–dependent functional MRI imaging has established clinically that changes in blood saturation correlate with changes in neuronal activity within the predicted area [as reviewed (164)], this technique cannot be used to quantify absolute changes in Po_2 in the brain. However, several recent studies using microelectrode and phosphorescence-quenching techniques have demonstrated quantitative changes in brain tissue Po_2 (either in the microvasculature or surrounding neurons) upon sensory stimulation (256, 328, 445, 692). In these studies, stimulation of neuronal activity was associated with a transient reduction in tissue Po_2, likely representing localized increases in O_2 consumption, followed by increases in local blood Po_2 and flow, confirming similar observations using fMRI.

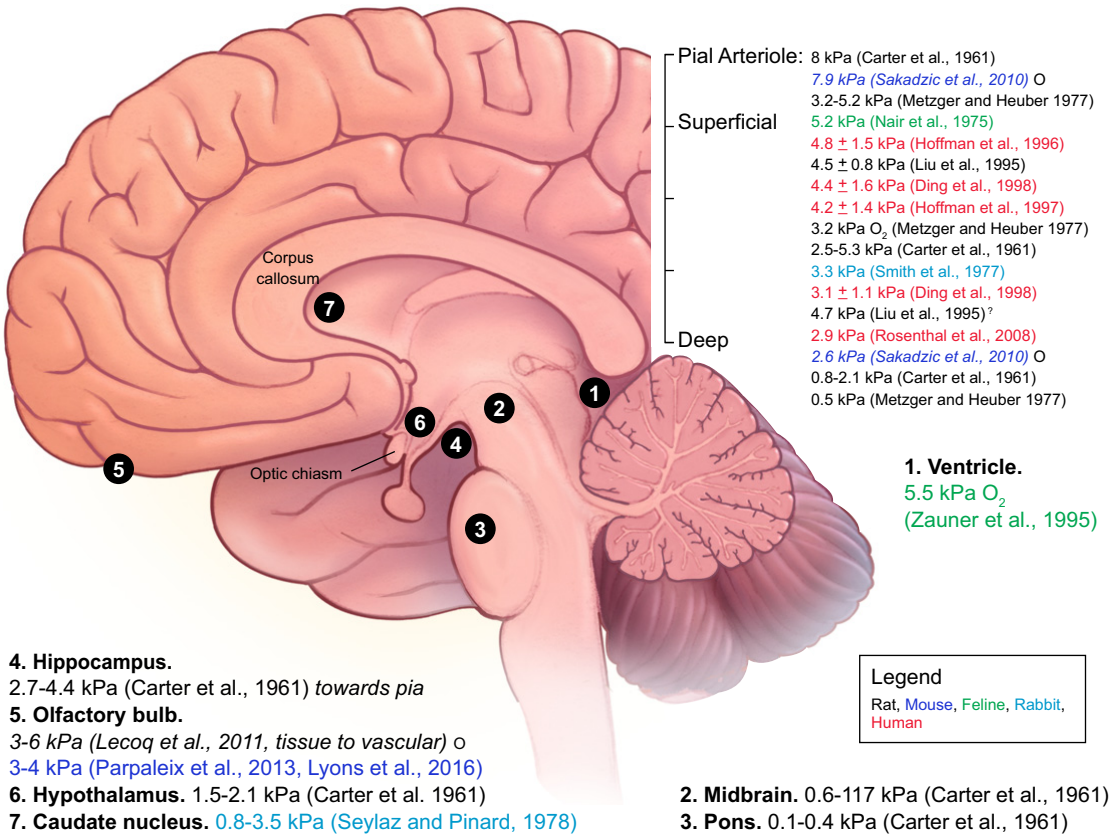

FIGURE 12. O_2 distribution in the brain. Illustration depicting the reported Po_2 distribution within the brain, with Po_2 values concerning microvascular or gray matter arranged according to reported depth of measurement. In some cases, depth was estimated based on the methodological description. Studies marked with a ○ were conducted using two-photon phosphorescence quenching method (PQM).

Neurons isolated from rat striatum (578) and cortex (698), human fetal neurons and the neuronal cell line SH-SY5Y (617), as well as mouse astrocytes (95), have all been studied under physiological normoxia (defined by authors as an ambient P_{O_2} of 3–5 kPa). A common phenotypic change was observed in all these cell types following normoxic culture, characterized by a hyperpolarized mitochondrial membrane potential, reduced ROS generation and greater survival during prolonged culture. The latter two features may result from enhanced activity of manganese SOD under low O_2 (617). The most significant impact to be uncovered following culture under normoxia is on neuronal mitochondria. In addition to mitochondrial hyperpolarization (578, 698), more dense mitochondrial networks have been observed (578). Moreover, a proteomic screen of SH-SY5Y cells maintained at a P_{O_2} of 5 kPa revealed significant induction of mitochondrial complex I proteins, most notably NADH:ubiquinone oxidoreductase subunit 3, which was associated with greater sensitivity to the complex I inhibitor rotenone (617).

Neuronal stem cells (NSC), otherwise known as neuronal precursor cells, are adult stem cells which differentiate into neurons, astrocytes, and glial within the central nervous system. Neurogenesis generally occurs in regions of the inner brain, such as the hippocampus and dentate gyrus (135), and as such, occurs within a physiological P_{O_2} range of 0.5–3 kPa (see **FIGURE 12**). NSC from the embryo (554), sciatic nerve (409), cortex (553), midbrain (561), and ganglionic eminence (255, 258) all exhibit higher proliferation, survival, and differentiation potential when cultured at 3 kPa. These effects were associated with enhanced HIF-2α stabilization and downstream protein expression (258, 554), resulting in an increased transplantation potential following in vitro expansion (553, 554). NSC from whole mouse brain homogenates cultured at 5 kPa also exhibit a higher differentiation potential associated with greater mitochondrial oxidative phosphorylation and reduced production of ROS (563). Although informative, this latter study makes no justification for the level of O_2 used, instead opting for the arbitrary use of 5 kPa as physiological normoxia. Although not necessarily incorrect, the numerous studies listed above suggest that NSC may rarely experience a P_{O_2} of 5 kPa. Nonetheless, these and other studies have led many to propose a causal relationship between O_2 concentration and stem cell differentiation potential (625), with numerous cell types displaying enhanced differentiation potential under lower O_2 levels. This is corroborated by the anatomical topology of neurogenesis, which occurs predominantly in the brain regions containing lower O_2 **(FIGURE 12)**.

E. Liver

The liver is a highly vascularized and metabolically active tissue and as such is relatively well oxygenated as illustrated in **FIGURE 13**. Blood entering the hepatic artery is fully saturated and rich in O_2 [human 12.2 kPa (526)]. Processed blood exiting the hepatic vein reportedly has a P_{O_2} between 4 and 6.5 kPa (526, 598, 660), whereas blood entering through the portal vein is at ~6.5 kPa (526, 598, 660). This dramatic gradient likely reflects the mixing of hepatic arterial blood with venous portal vein blood (at a ratio of 1:3) before entering the hepatic triad, as well as a high metabolic demand of the underlying tissue. Indeed, blood P_{O_2} within the portal triad is already reduced compared with that of the hepatic artery (8.7 kPa) (660). This level is further reduced within the liver parenchyma, where a P_{O_2} of between 4 and 7 kPa has been reported (54, 55, 103, 312, 327, 546, 608). Using the oxygen-sensitive EPR probes India ink and lithium phthalocyanine, Jiang et al. (275) were able to measure P_{O_2} localized to Kupffer cells and whole liver P_{O_2}, respectively, and demonstrated that Kupffer cells experience a lower P_{O_2} than the average liver parenchyma (2 versus 3.2 kPa). These values are lower than expected within the liver, possibly reflecting differences in experimental technique. The gradient between the portal triad and vein creates a functional polarization of the underlying hepatocytes, wherein nitrogen metabolism and albumin secretion are proportional to cell surface O_2 level (37). This allows a similar effluent composition under conditions of flow reversal. Clearly, although a significant loss of O_2 occurs during passage through the liver, this organ is still extremely well oxygenated in relation to other similarly active tissues such as the heart or brain (377).

Studies in vitro have provided some explanation for the abnormally high oxygen levels in liver tissue. In contrast to the majority of cell types, hepatocytes isolated from rat livers and maintained under low O_2 (4–10 kPa) for the duration of culture (3–9 days) responded adversely. This included reduced viability (37, 345, 669) and diminished liver-specific gene expression (299, 345) and functions such as nitrogen metabolism and albumin excretion (37, 669). Moreover, several reports have highlighted the enhanced infectivity of liver-associated pathogens such as hepatitis C and *Plasmodium berghei* (during liver-stage malaria) in hepatocytes under low O_2 conditions in vitro (421, 612). Interestingly, acetaminophen toxicity was less pronounced in mouse hepatocytes cultured at a P_{O_2} of 5 kPa relative to room air (668), although significantly higher basal lactate dehydrogenase release was observed in these cells. Part of this adverse response can be attributed to the very high O_2 consumption rate of primary hepatocytes, which, during static cell culture in vitro, can create an extensive O_2 gradient between air and cytosol (see section IVC) (75, 671). In this context, culture under previously regarded physiological P_{O_2} (4–10 kPa) may actually expose the cell monolayer to a P_{O_2} as low as 0.5 kPa (421). In corroboration, exposure to relatively high (but still lower than ambient) P_{O_2} (13–17 kPa) proved beneficial for cell yield (345, 368) and the response to phenobarbital challenge (299). HepG3 and

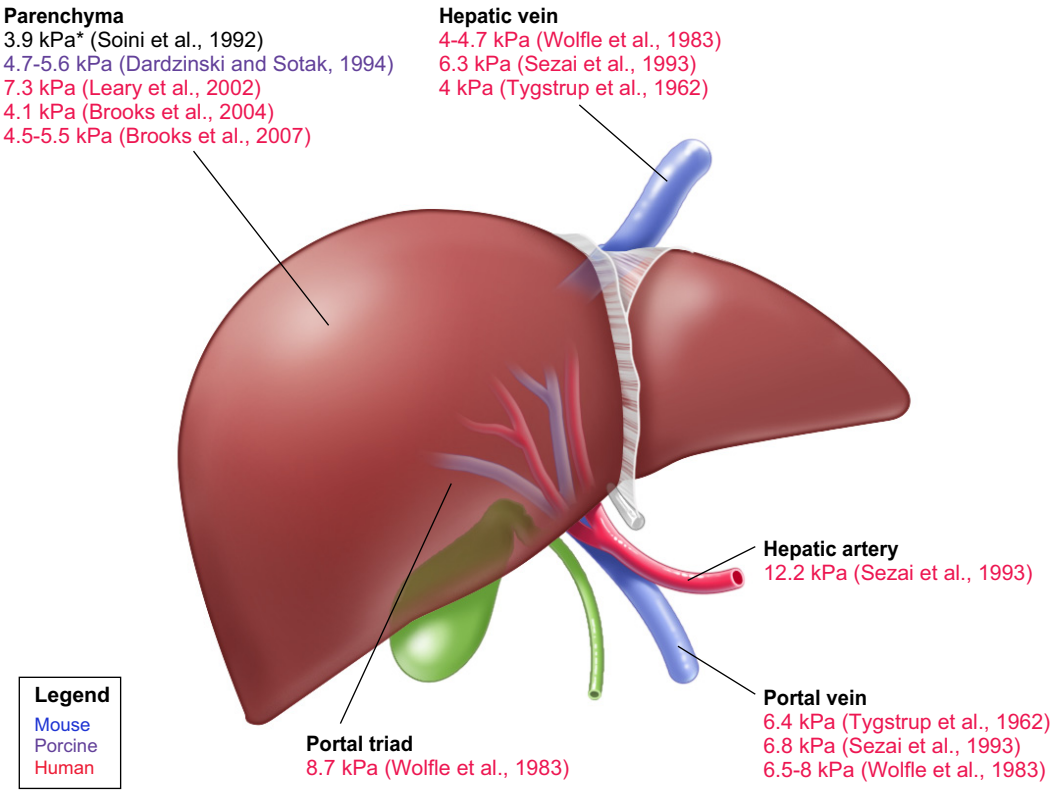

FIGURE 13. O_2 distribution in the liver. Illustration of the reported P_{O_2} distribution in the liver. Note, blood entering the sinusoids is a 3:1 mixture of portal venous and hepatic arterial blood, thus sinusoidal O_2 concentrations can be estimated based on known values for the source vessels (P_{O_2} ~8 kPa).

Hep3B cells cultured at 8 kPa for up to 30 days had higher intracellular, but not mitochondrial, ROS generation with severely reduced intracellular GSH levels (587). Despite this, SOD activity and expression were significantly higher in these cells, and they exhibited greater resistance to oxidative challenge. These studies in hepatocytes emphasize the need to understand monolayer oxygenation more closely. Ambient P_{O_2} during in vitro culture must be accurately tailored to the cell type to avoid exposing high O_2-demanding cells to cellular hypoxia (204).

F. Kidneys

The kidneys comprise only 1% of total body mass, yet filter ~20% of cardiac output (4.2 ml/min/g tissue) and as such are disproportionately perfused compared with the other organs. Indeed, renal cortical blood flow is the highest recorded per gram of tissue within the body (386), and the metabolic requirements are relatively low under normal conditions, yet increase linearly with glomerular filtration rate, renal blood flow, and Na^+ transport (479, 642). Considering such hyperperfusion, renal tissue should be extremely well oxygenated as with other well-perfused organs such as the liver (see above). Counterintuitively, however, renal cortical P_{O_2} has been measured at 4.7 kPa in the dog (28), 5–7 kPa in the rat (50, 51, 203, 334, 349, 362, 519, 642), 6 kPa in the pig, and 4–9.5 kPa in human (411, 541).

When the measuring electrode is advanced beyond ~3 mm (in the rat kidney), a sharp reduction in tissue P_{O_2} is observed corresponding to entry into the medulla (see **FIGURE 14**), where O_2 levels are between 1 kPa in the dog (28), 1.3–4.2 kPa in the rat (50, 51, 203, 334, 349, 362, 519, 642), 3.3 kPa in the pig (693), and 2 kPa in human (693). In elegant work by Lübbers and Baumgärtl, a large heterogeneity in cortical P_{O_2} was observed whereby some regions experienced near-arterial P_{O_2} values (~11 kPa) (334, 362). Such heterogeneity was not apparent within the medulla, prompting these authors to conclude that the highly vascularized anatomy of the cortex results in the formation of large intrarenal P_{O_2} gradients. Using ultramicroelectrodes (diameter 3–5 μm), Welch and colleagues achieved measurements of P_{O_2} in the nephrons of rats (642). In line with previous data, a significant drop in P_{O_2} was reported between the renal artery and efferent arterioles (10.7–6 kPa), and tubular P_{O_2} remained around 6 kPa before increasing within the renal vein to 6.7 kPa (see **FIGURE 14**). Kidney P_{O_2} values determined by Clark electrode penetration were corroborated by recent measurements using BOLD-MRI (395, 451, 693), confirming the validity of both techniques. Notably, measurement of kidney P_{O_2} using a dual laser Doppler blood flow/O_2 electrode technique consistently demonstrated lower cortical P_{O_2} values than the corresponding single O_2 electrode [1.3 (434) and 2.1 (463) versus 5.3–6.7 kPa]. This disparity was attributed to the larger diameter

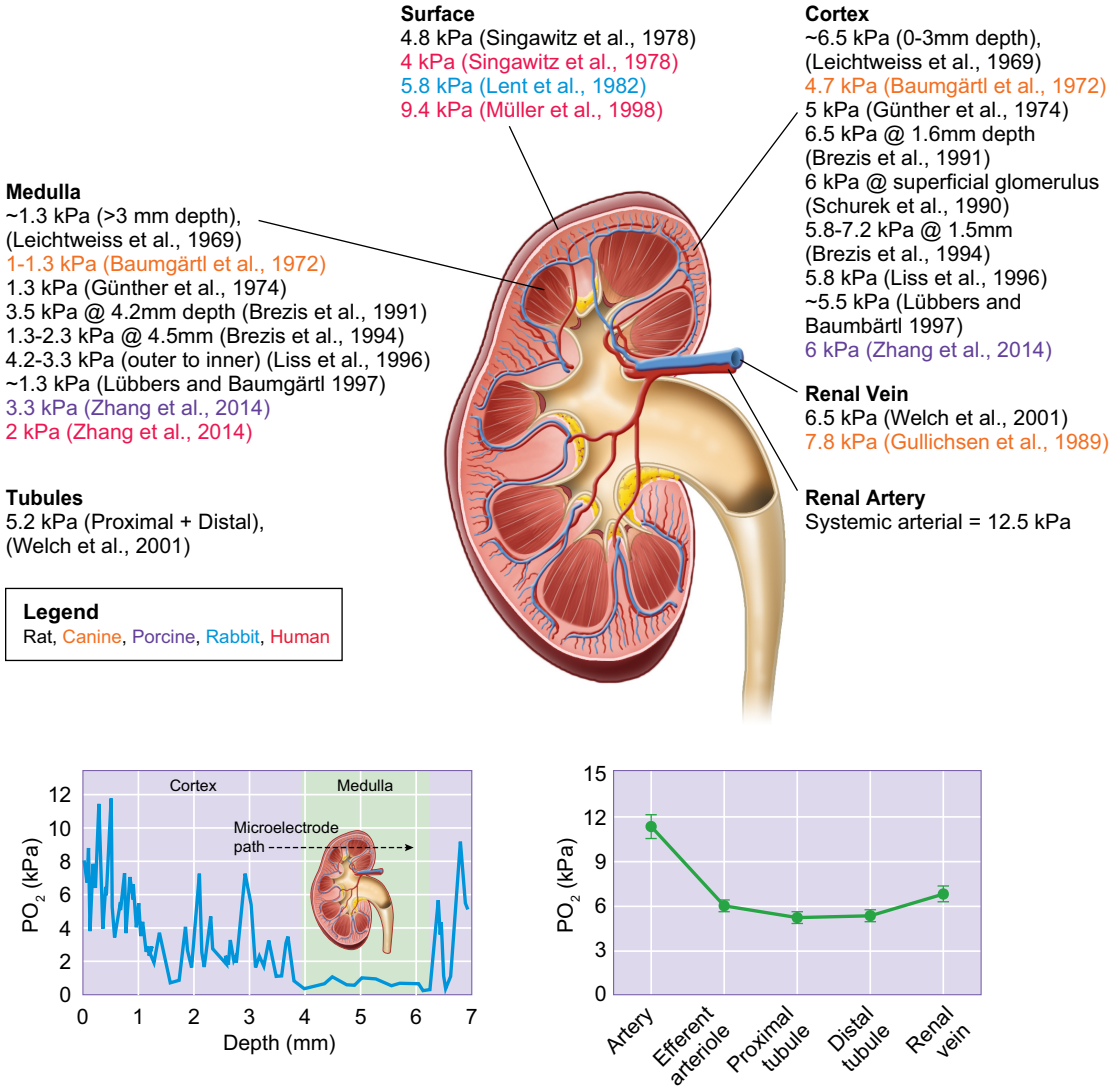

FIGURE 14. O_2 distribution in the kidney. Anatomical illustration of known P_{O_2} values in the kidney, derived from a number of different experimental models, species, and techniques. *Bottom left*: a representative trace obtained from invading an O_2-sensitive microelectrode into the rat kidney following the illustrated path. Depths corresponding to the cortex and medulla are highlighted. Adapted with permission from Lübbers and Baumgärtl (362). *Bottom right*: P_{O_2} values within an individual rat nephron. Adapted with permission from Welch et al. (642).

O_2 electrode required in the dual electrode array compared with that used in tissue penetration studies (350–500 μm versus <20 μm), potentially resulting in damage to the delicate kidney architecture (434).

The substantial drop in P_{O_2} between the renal artery and cortical tissue prompted many to postulate the existence of a preglomerular O_2 shunt (28, 334, 338). This was confirmed by Schurek and colleagues, who demonstrated that inspiration of gas at 100 kPa P_{O_2} led to minimal changes in glomerular P_{O_2} (5.6–9 kPa) despite a robust increase in systemic P_{O_2} (12–74.6 kPa) (519). The close anatomical relationship between interlobular arteries and veins, and the absence of surrounding capillaries (141, 422), is thought to be responsible for such a shunt in line with the arteriovenous O_2 transfer theory proposed by Duling and Berne (123). Indeed, renal vein P_{O_2} is unusually high compared with systemic venous P_{O_2} (measured at 6.5 and 7.8 kPa in the rat (642) and dog (201), respectively, versus ~5 kPa), further corroborating renal arteriovenous O_2 transfer. Moreover, although whole kidney O_2 consumption is second only to the heart (10 versus 15 ml/min/g), renal blood flow far exceeds myocardial blood flow (750 versus 250 ml/min), and thus, renal O_2 extraction is only ~10% versus 55% in the heart (452, 479, 485, 687). Taken together, these observations led O'Connor and colleagues to hypothesize that renal tissue is maintained at a low P_{O_2} level relative to blood flow to prevent overoxygenation and excessive oxidative stress (433). Unfortunately, the side effect of this proposed adaptation is that segments of the papillae within the medulla (in particular the S3 proximal tubule and medullary thick ascending limb) are exquisitely sensi-

tivity to reductions in blood flow and are the first sites damaged during acute renal ischemia (46, 130).

Considering the prominent role of HIF signaling in the kidney (209) and its sensitivity to low oxygen (167, 398), relatively little has been published on the long-term culture of kidney-derived cells under physiological normoxia. This may, in part, be complicated by the significant differences in what may constitute normoxia in this tissue, with medullary P_{O_2} values often 4–5 kPa O_2 lower than corresponding cortical tissue (see above). Much like the gastrointestinal tract (see section VI*G*), parts of the renal medulla may exist in a state of physiological hypoxia. In intestinal epithelia, cellular phenotypes characterized at a P_{O_2} of 1 kPa appear a better reflection of their in vivo counterparts than those cultured under room air. However, exposure of renal tubular epithelial cells to hypoxia (1–3 kPa) results in robust HIF downstream target protein (VEGF and EPO) induction (129, 209, 337, 417), phenotypes not observed in their counterparts in vivo (491). This discrepancy may reflect the artifactual baseline cellular P_{O_2} before hypoxic exposure (room air, P_{O_2} ~18 kPa), potentially exacerbating the subsequent hypoxic response. It would be interesting to explore whether small reductions in cellular P_{O_2} around physiological normoxic values (from 1.5/2 to 1 kPa) can elicit more physiologically relevant responses in these cells. Such experiments may identify additional, more subtle roles for the HIF in renal cells and in doing so, shed further light on the renal cell specificity of von Hippel–Lindau syndrome (29, 419, 503).

G. The Digestive System

The discovery of anaerobic bacterium resident within the intestinal lumen led to the concept of physiological hypoxia within the adjacent intestinal tissue (696), with important implications for our understanding of host/microbiome interactions (292). This section aims to review the literature, with an overview of digestive system P_{O_2} and discussion of the importance of considering the O_2 environment during culture of cells derived from the digestive tract in vitro. The digestive tract is characterized by an adventitial (serosa) layer, a muscular middle layer, and an epithelial (mucosal) layer. Large arterioles run longitudinally along the serosa and the microvasculature (mesentery), penetrating toward the mucosal layer. Although the digestive tract receives a high proportion of blood flow, only 25% of this perfuses the mucosal and muscular layers at rest (81, 191). Measurements of digestive tract P_{O_2} have been divided into luminal, mucosal, and serosal tissue, and the gradient between these values discussed when evident.

1. Stomach

The stomach, similar to the lungs and skin, can come into direct contact with atmospheric levels of O_2. As a result, P_{O_2} measurements at the submucosal aspect of the gastric fundus–using microelectrodes are in the range of 6–10.2 kPa in humans undergoing esophagectomy (94, 264, 265, 529) and 7.6 kPa in experimental canine models (318), with similar values (8.4 kPa) reported in canine serosa (353). Using activated charcoal as an EPR probe (see section II*D*), He and colleagues (228) determined a luminal P_{O_2} of 7.7 kPa at the level of the fundus/pylorus. Because P_{O_2} values are roughly equal across the gastric wall (lumen> mucosa>serosa; **FIGURE 15*A***), and such a level is not dissimilar from what might be expected in the arteriolar circulation (see section VI*B2* and **FIGURE 9**), we might conclude neither the contents of the stomach or the cells of the gastric

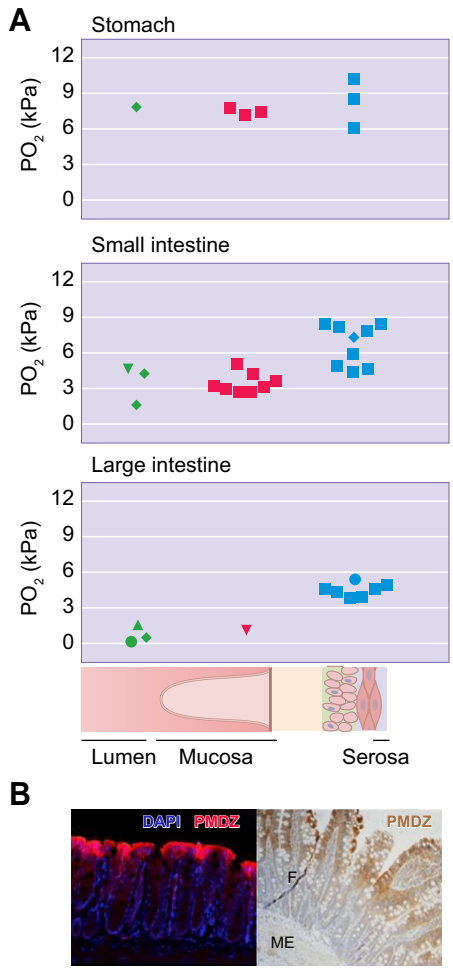

FIGURE 15. O_2 distribution in the gastrointestinal tract. *A*: Data from a number of studies (see text for more discussion and references) investigating P_{O_2} distribution in the gastrointestinal tract. Values are separated into those taken from the stomach and small and large intestines and further divided according to anatomical/cellular location (lumen, mucosa, or serosa). Symbols are coded according to technique employed: □, microelectrode; △, approximate based on pimonidazole staining; ▽, suffusion; ○, phosphorescence quenching microscopy; and ◇, electron paramagnetic resonance (EPR). *B*: Immunohistochemical images of the colon wall stained with the hypoxia-specific probe pimonidazole. Images are taken using either fluorescence (*left*) or bright-field (*right*) microscopes. Taken with permission from Kelly et al. (294) and Fisher et al. (157), respectively.

wall represent a significant source of O_2 consumption, at least under basal conditions.

2. Intestines

As illustrated in **FIGURE 15A**, a longitudinal gradient in luminal P_{O_2} is observed during passage along the gastrointestinal tract. From a luminal P_{O_2} of 7.7 kPa in the stomach (228), luminal P_{O_2} in the small intestine decreases to between 4.2 and 4.6 kPa (312), and decreases even further to 0.4–1.5 kPa in the large intestine (9, 228, 294, 346). Importantly, the techniques used to obtain such data, including EPR and two-photon phosphorescent quenching, are noninvasive and therefore avoid contaminating the bowel environment with atmospheric air and preserve the integrity of the bowel wall. A similar longitudinal gradient is observed in mucosal P_{O_2} **(FIGURE 15A)**; from 6 to 10 kPa in the stomach to values of 3.5 kPa [rat (42)], 5.8 kPa [dog (353)], 2.6–5 kPa [pig (212, 213, 305, 429, 540, 611)], and 4.5–4.8 kPa [humans (529)] in the small intestine and values less than 1 kPa in the colon (9, 294). A similar longitudinal gradient is present, albeit fewer pronounced, at the serosal aspect **(FIGURE 15A)**. Small intestine serosal P_{O_2} is 5.6 kPa [rabbit (163)], 7.2–8.4 kPa [pig (157, 213, 429, 540)], and 8.1 kPa in humans (570). In the large intestine, P_{O_2} at the serosal layer is reported at 4.6 kPa [rabbit (163)], 3.7–4.5 kPa [pig, corrected for Fi_{O_2} 0.21 (301, 388)], 5.3 kPa [mouse (9)], and 3.9–5.5 kPa [human (412, 529, 530)].

From such data, it is clear that O_2 levels show a general decline along the length of the gastrointestinal tract, being highest in the stomach and lowest in the colon. It is perhaps of more interest to note that the radial gradient across the intestinal wall (lumen to serosa) does not behave proportionally. No detectable difference is observed between the lumen and serosa of the stomach, whereas the lumen of the large intestine is ~5 kPa lower than the serosal layer **(FIGURE 15A)**. This radial gradient has been demonstrated directly in the small intestine using the penetrating microelectrode technique (42, 212, 429), by two-photon phosphorescence quenching method (540), and by pimonidazole staining (157), and also in the colon (294) (representative immunohistochemical images from the latter studies are shown in **FIGURE 15B**). Data from the study by Bohlen indicate a difference of as much as 2.3 kPa O_2 between the apex and base of a villus (42), whereas a difference of 4.6–9 kPa is reported between the mucosa and serosa (212, 429, 540). This is corroborated by a gradient in pimonidazole staining along the villus length (157, 294). It was originally proposed that this gradient occurs because of an arteriolar/venular O_2 shunt at the base of the villus, where vessels reside in close proximity to each other (42). However, the finding that this gradient is abolished by antibiotic treatment and is absent in germ-free mice (294) would suggest the O_2 consumption by the gut microbiome is wholly responsible. Upon reflection, this is logical given that the bacterial population increases along the gastrointestinal tract, whereas there is no evidence to suggest the proposed arteriolar/venular shunt shows similar topographical changes.

The extremely low physiological P_{O_2} experienced by intestinal epithelium in vivo creates an interesting scenario whereby there is probably no real distinction between hypoxia and normoxia, but rather a state of physiological hypoxia exists in the intestinal mucosa (92, 696). Hence, those pathways traditionally important in coordinating a cellular response to pathological hypoxia, such as the HIFs (see section V*A1*), may have more importance in defining the phenotype of intestinal epithelia in vivo. Indeed, a healthy gut epithelium respiring on their preferred substrate butyrate exhibits profound HRE/luciferase activity and HIF-1α stabilization (63, 294), indicating a persistent activation of the pathway. This constitutive activity was found to be essential for the production of defensins, key endogenous antimicrobial peptides secreted by the intestinal epithelium and accumulated within the mucus layer (293), which itself is regulated by HIF-1α at a number of levels (170, 359). Moreover, expression of the multidrug-resistance protein 1 (P-glycoprotein) was also found to be dependent on constitutive HIF-1α activity in the intestine (93). HIF activity is also crucial in maintaining intestinal barrier integrity, with key junctional proteins such as claudin-1 and creatine kinases M and B regulated by HIF-1 and HIF-2, respectively (180, 498). Notably, a key role for constitutive HIF-2α activity in maintaining iron absorption has also been identified in the mouse duodenum, the epithelium of which also exhibits strong basal pimonidazole staining (379). Hence, the state of physiological hypoxia is important in maintaining host defense, barrier integrity, and iron absorption throughout the gastrointestinal tract.

Importantly, in the context of replicating normoxia in vitro, experiments in which intestinal epithelial cell lines (Caco-2 and T84) are exposed to physiological normoxia (P_{O_2} 1–2 kPa) generally corroborate such observations (see **TABLE 6** for summary). Notably, although few studies have extended the period of normoxic culture beyond 24 h, a number did demonstrate a stable phenotype after up to 4 days of normoxia (93, 566). A point worth discussing is the apparent discrepancy between the effects of low O_2 exposure on transepithelial resistance (TER) in vitro and in vivo. Exposure of Caco-2 and T84 cells to a P_{O_2} of 1–2 kPa induces no change or increases in TER in vitro (170, 284, 566), a characteristic unique to intestinal epithelial cells (170). In contrast, intestinal permeability is consistently decreased in mice breathing low O_2 (8 kPa) (170, 284, 408, 566). Aside from technical differences, there are two possible explanations for these observations. First, hypoxic exposure does not alter TER in vitro relative to room air cultured cells, a condition wholly artificial in the context of physiology. Moreover, if mucosal P_{O_2} is normally physiologically hypoxic (see above), then a reduction in inspiratory P_{O_2} (from 20.9 to 8 kPa) may create a genuinely pathologically hypox-

Table 6. *The effects of culture at physiological normoxia on intestinal cell physiology*

Cell Type	Po_2 (kPa)	Time (h)	Summary	Reference
T84	2.6	0–48	Intestinal epithelial cells maintain barrier resistance under hypoxia, whereas oral epithelia and endothelial cells increase permeability.	(170)
Caco-2 B			↑ ITF mRNA by 4 h, maintained at protein level for 48 h, and is HIF-1 dependent.	
			Anti-ITF antibody attenuates hypoxia-induced ↑ resistance in Caco-2 cells. Addition of ITF to endothelial cells ↑ resistance during hypoxia.	
			ITF is induced in vivo by hypoxia (8% O_2, 4 h).	
			Hypoxia in vivo associated with increased permeability relative to normoxic controls. Possibly under pathological hypoxia in vivo.	
Caco-2	2.6	0–96	↑ MRD1 mRNA (18 h) and protein (maintained at 96 h, peak at 48 h) in hypoxia, dependent on HIF-1.	(93)
			Increase in protein translated to increased surface expression and function (drug efflux).	
T84	2.6	0–96	↑ CD79 and CD339 mRNA (18 h) and protein (maintained at 96 h, peak at 48 h) in hypoxia, dependent on HIF-1.	(566)
Caco-2			Both proteins are ecto-5′-nucleases responsible for metabolizing 5′-AMP to adenosine, which activates A2B receptors and ↑ barrier integrity.	
T84	2.6	0–48	↑ MUC3 selectively by hypoxia: mRNA (maintained by 24 h) and protein (peaked at 24 h and declined afterwards). Probably HIF-1 mediated.	(359)
ModeK			MUC3 interacts with ITF at the apical surface of epithelial cells.	
T84	2	0–48	Hypoxia ↓ adenosine uptake.	(408)
Caco-2			↓ ENT1 and 2 mRNA and protein during hypoxia, maintained at 48 h and HIF-1–dependent	
			siRNA against ENT2 decreased adenosine uptake, therefore explaining first observation.	
			Hypoxia in vivo associated with increased permeability relative to normoxic controls. Possibly under pathological hypoxia in vivo.	
T84	2	0–48	Time-dependent increased Netrin-1 protein during hypoxia, dependent on HIF-1 activity.	(492)
Caco-2			Endogenous netrin-1 reduces monocyte transepithelial migration via activation of the adenosine A2B receptor on the monocyte. This reduces inflammatory activation and therefore protects the epithelial barrier during inflammation.	
T84	1	0–24	HIF-1 conditional KO reduced expression of DEFB1 in mouse intestine and Caco-2 cells.	(293)
Caco-2			Exposure to hypoxia ↑ HIF-1, although basal levels were observed.	
			No change in DEFB1 protein during hypoxia, despite ↑ HIF and dependence on it.	
			HIF-1 siRNA reduces hBD-1 soluble protein excreted, which would ↑ bacterial load in intestine	
			In human bowel scrapings (epithelial-enriched), expression of DEFB1 mRNA correlated linearly with GLUT1 (HIF target), and hBD-1 staining was most prominent at apical edge of colonic mucosa.	

Continued

Table 6.—*Continued*

Cell Type	Po_2 (kPa)	Time (h)	Summary	Reference
Caco-2	1	0–48	Enzymes involved in creatine metabolism regulated specifically by HIF-2 during hypoxia.	(180)
T84			Induction of CKM and CKB maintained at 48 h (protein) and abolished with HIF-2 siRNA	
			CKM and CKB enzymes are localized to the apical surface of polarized epithelium and enriched at the adherens junction.	
			HIF-2–dependent CK induction maintains barrier integrity and protects against inflammation.	
			Inhibition of CK strongly decreases resistance under hypoxic conditions.	
Caco-2	1	0–144	Measurements of medium Po_2 using optical sensor spots immobilized onto standard 24WPs, gas-permeable 24WP, and Transwell inserts.	(690)
			Medium Po_2 reached 4 kPa after 6 days postconfluence in standard 24WP, whereas it was only ~15 kPa in gas-permeable plates and in inserts.	
			Despite low O_2 levels, no HIF-1 stabilization was observed under standard conditions in normal plates.	
			Medium volume was 1 ml: very high for 24-well plate, large depth would lead to O_2 depletion.	
Caco-2	1	24	Hypoxic preincubation significantly reduced bacterial internalization.	(689)
			This was dependent on β-1 integrin, the protein levels of which were decreased by hypoxic exposure in correlation with increased HIF-1, although no definitive siRNA experiment was performed.	
			Hypoxia reduces bacterial infection by downregulating β1 integrin.	

CK, creatine kinase; CKB, creatine kinase B; CKM, creatine kinase M; DEFB1, β defensin gene; ENT, equilibrative nucleoside transporter; GLUT1, glucose transporter 1; hBD-1, human β-defensin; HIF, hypoxia-inducible factor; ITF, intestinal trefoil factor; MRD1, multidrug resistance protein 1; MUC, mucin; 24WP, 24-well plate.

ic/near anoxic environment within the mucosal intestinal epithelium. Similar conditions are observed during inflammatory bowel disease and ulcerative colitis (63, 284), conditions associated with increased intestinal permeability. Thus, fundamental differences in the context and degree of hypoxia under these experimental conditions make comparisons difficult to interpret. Second, whole body hypoxia undoubtedly has effects beyond the intestines, and it is therefore difficult to isolate the actions of any paracrine mediators released by other tissues also responding to reduced systemic arterial Po_2. Notably, work by Zeitouni and colleagues (689, 690), using O_2-sensitive chips immobilized on the bottom of standard culture plates, indicates that exposure of Caco-2 cells to an ambient Po_2 of ~1 kPa results in a near anoxic medium Po_2 after 6 days (690). However, it should be noted that the authors used 1 mL of medium in a 24-well plate, double the recommended volume for such dishes. Using the example discussed in a previous section (section IVC), these conditions would generate a value for d double that commonly used (0.2 mm), facilitating self-inflicted hypoxia in this scenario. Ideally, the correct in vitro experiment to accompany in vivo hypoxia models would be exposure of intestinal epithelial cells to very low (Po_2 ~0–0.5 kPa) O_2 from a baseline of 1–3 kPa to more accurately reflect conditions generated in vivo.

3. The pancreas

Interest in pancreatic Po_2 distribution arose largely out of the need to understand the oxygenation of endogenous islets to match this when implanted elsewhere. Using a microelectrode, Harper and colleagues (226) reported a Po_2 of 3.3 kPa in the acinar/exocrine region of the exteriorized rat pancreas. This was corroborated by more detailed measurements by Carlsson and colleagues (66, 67), who reported a gradient from 4.6 to 2.7 kPa O_2 between the surface and interior of the exocrine pancreas. Kinnala and colleagues used a technique termed suffusion tonometry to monitor whole organ Po_2 in the porcine pancreas. Briefly, a silicone tube is implanted into the tissue and equilibrated with anoxic saline. After a subsequent period of equilibration with the tissue, fluid is extracted from the tube and Po_2 deter-

mined using a standard electrode. Using this technique, they reported pancreatic P_{O_2} values of 5.3 (302) and 5.6 (303), thus reasonably matching reported values using microelectrode techniques. The islets of Langerhans are important anatomical features of the pancreas wherein insulin and glucagon are synthesized and secreted. These tiny collections of cells constitute only 1%–2% of total pancreatic tissue, yet receive 10%–15% of organ blood flow (268). This extensive perfusion is reflected in a P_{O_2} level considerably higher than the surrounding parenchyma, between 5 and 6 kPa in the rat (66, 67).

The high rates of O_2 consumption in pancreatic β cells has presented a unique problem during their isolation, culture, and implantation. Isolated β cells typically exist in culture as suspended spheroids, and pimonidazole staining illustrates that such conditions produced severe hypoxia (113, 438), which is proportional to medium P_{O_2} and islet size (310). This also extends to monolayer cultures of the pancreatic cell line MIN6, in which intracellular P_{O_2} (based on pimonidazole staining) was far below ambient (511). Moreover, exogenously implanted islets rapidly develop hypoxia regardless of their anatomical location (66, 67), reflecting an inability of neovascularization to counteract islet O_2 consumption. Attempts to address this problem have included the use of permeably culture supports such as silicone membranes (18, 304), PFC-based culture dishes (166), or O_2-leaching materials (96) as well as culture under hyperoxic ambient P_{O_2} (50 kPa) (309). Using a PFC/polydimethylsiloxane construct, Fraker and colleagues elegantly demonstrated that the combination of high substrate solubility and lower ambient P_{O_2} (~12.6 kPa) produced the greatest volume of physiologically oxygenated (predicted pericellular P_{O_2} of ~5.5 kPa) β cells and almost no anoxic cells compared with culture under room air on traditional plasticware (166). This translated into greater β cell viability and function following isolation and a trend toward greater in vivo survivability once transplanted.

H. Bone and Cartilage

1. Bone and bone marrow

Typical bone consists of an outer cortical/compact layer, a spongy/cancellous inner layer, and the medulla containing the bone marrow **(FIGURE 16*A*)**. The outer mineralized layers are sparsely populated with cells and are effectively avascular, and the only vessels found within this layer are the superficial periosteal arteries and penetrating nutrient arteries perfusing the bone marrow. As such, mineralized bone tissue exists at relatively low P_{O_2}. In the only known publication measuring bone extravascular P_{O_2}, Brighton and Heppenstall reported a steep gradient in P_{O_2} between the diaphyseal and metaphyseal regions (14.5 to 2.6 kPa) of the rabbit proximal tibial epiphyses (52). Because the reported P_{O_2} in the diaphyseal region is beyond the physiological arterial range (12–13 kPa), the accuracy of these values necessitates further study. The concept of a steep gradient between regions of mineralized bone has been predicted mathematically (685). More recently, measurement of P_{O_2} distribution in the mouse tibia was partially accomplished using implantable lithium phthalocyanine crystal EPR probes (see section II*D*) (360, 361). P_{O_2} at the periosteum of normal tibia was 6 kPa (360), whereas localized P_{O_2} within the bone upon fracturing decreased significantly to ~1.5 kPa immediately after injury (361). Subsequent angiogenesis and healing resulted in a robust increase in bone P_{O_2} (from 1.5 to ~7 kPa), indicating that neovascularization of damaged bone can restore normal O_2 distribution (361). Notably, periosteal P_{O_2} values reported by Lu and colleagues match closely the intravascular P_{O_2} values in microvessels of the periosteum [6.6 kPa (552)], suggesting a limited radial gradient in this tissue, which is consistent with the sparsely populated nature of mineralized bone.

The isolation and maintenance of human stem cells under low O_2 has generated promising advances in their clinical application. Although effects of culture under physiological O_2 levels on partially differentiated precursor stem cells have already been discussed under the auspice of their respective tissue origin, bone marrow is a primary source of adult pluripotent stem cells. Furthermore, this tissue is also the source of hemopoietic stem cells, which give rise to all circulating blood cells. As such, a detailed understanding of their physiological environment is of clinical relevance. P_{O_2} has been determined in human sternum [5.4 kPa (192)] and iliac crest marrow [6.8 (262), 7.2 (227), and 6.1 kPa (154)], canine femoral medulla [6.4 kPa (308)], and mouse femoral marrow [~4 kPa (71)]. These measurements were largely obtained from blood gas analysis following the aspiration of marrow. Recently, detailed in situ measurements of marrow O_2 levels in living mice have been obtained using the more advanced two photon light microscopy method (see section VIC) (552), with impressive resolution. Spencer and colleagues (502) reported an intravascular P_{O_2} gradient between vessels in the periosteum (6.6 kPa), cortical bone (4.2 kPa), and marrow (3 kPa). By comparing intravascular and extravascular P_{O_2} within the bone marrow, these authors identified a significant radial gradient (~1.5 kPa) in these vessels, which could be abolished by sublethal irradiation or chemotherapy. Indeed, localized bone marrow hypoxia was associated with large clusters of cells within the marrow, indicating that O_2 consumption maintains a low P_{O_2} environment in the bone marrow.

Although elegant and informative, the study by Spencer and colleagues reports bone marrow P_{O_2} values considerably lower than values reported by numerous other laboratories (~2 versus ~5 kPa). Tissue trauma associated with bone marrow aspiration or microelectrode penetration may lead to artificially high marrow O_2 level estimations, and hence, the noninvasive measurements by Spencer et al. may be

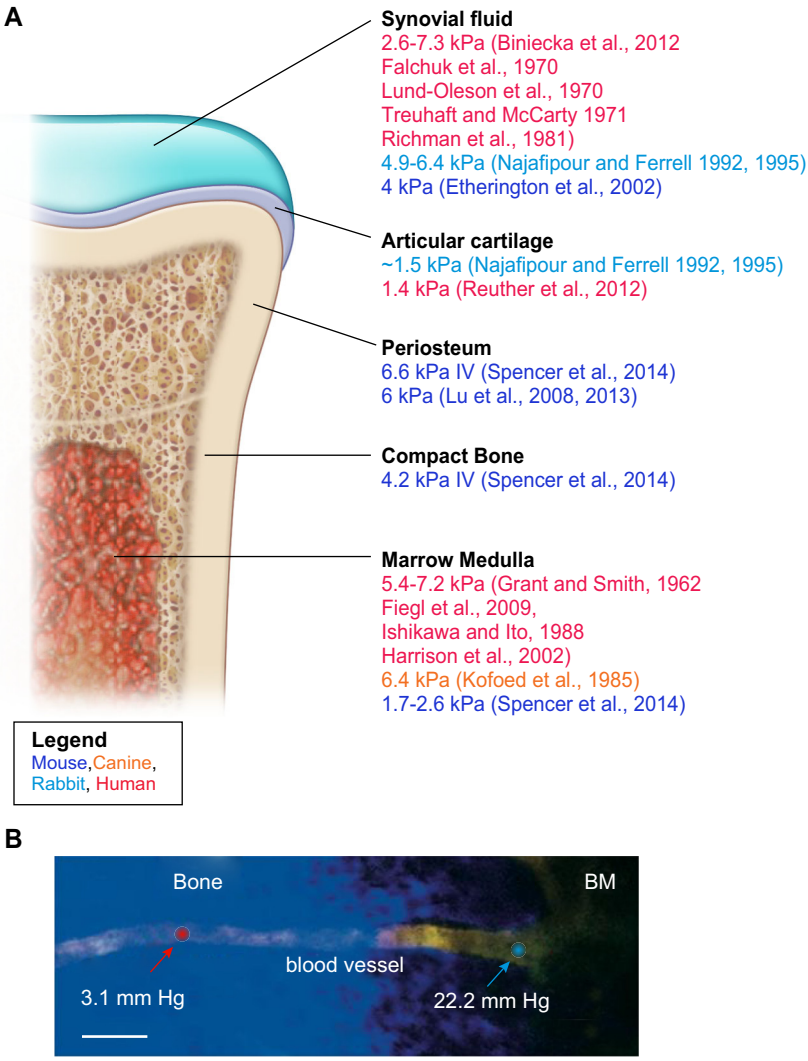

FIGURE 16. Oxygen distribution in bone and cartilage. *A*: Distribution of O_2 within a typical synovial joint. *B*: Representative image highlighting the passage of a microvessel (yellow) from the outer bone (blue) into the marrow (black). Intravascular P_{O_2} was determined at two different points: within the bone (red arrow and dot) and within the marrow (green arrow and dot). Adapted with permission from Spencer et al. (552). IV, intravascular.

physiologically representative. Species differences are an unlikely explanation, because Ceradini et al. (71) reported a bone marrow P_{O_2} of ~4 kPa in the mouse femoral marrow. Instead, regional differences in bone P_{O_2} may provide some clarification, with Spencer et al. opting to study the calvaria (skull cap) in contrast to the femur, sternum, or iliac crest. Similarly, P_{O_2} distribution in the brain microvasculature differs subtly from other microvascular beds **(FIGURE 9)**.

2. Cartilage and synovial fluid

Many bones are connected via a synovial joint consisting of a fluid-filled synovial cavity and articular cartilage lining the epiphyses of the bone **(FIGURE 16*A*)**. In addition to providing mechanical support during movement, synovial fluid is also crucial in supplying nutrients, including O_2, to the articular cartilage, which itself is completely avascular. Chondrocyte physiology is strongly influenced by O_2 tension, during development and in adult life (513), and increases in O_2 consumption are observed during rheumatoid arthritis–associated inflammation (331). For these reasons, understanding P_{O_2} distribution within the synovial joint is of great interest. Of the studies reporting synovial P_{O_2} values, only two investigated synovial fluid P_{O_2} in healthy tissue. Ferrell and Najafipour (1992) reported a mean P_{O_2} of 6.4 kPa in the rabbit knee (152). Using microelectrode penetration, these authors also demonstrated a gradient in P_{O_2} between the superficial synovial membrane and articular cartilage, at which point, mean P_{O_2} reached ~1.5 kPa, a value corroborated in human septal cartilage more recently (482). Although such P_{O_2} distribution traces are commonly reported in numerous tissues, the study of a synovial joint under immobile anesthetized conditions may create an artifactual gradient which would not otherwise be present in a mobile joint (152). Indeed, Etherington and colleagues (137) reported a transient increase in knee synovial P_{O_2} upon mobilization of the joint. A number of studies have reported synovial fluid P_{O_2} in the human arthritic knee, with values ranging from 2.6 (38), 3.5 (363), 3.7 (143), 4.1 (588), and 5.7 (363) to 7.3 kPa (484). Inflammatory arthritis was also associated with a decline in knee synovial P_{O_2} in rabbits (416) and mice (137). In general, synovial P_{O_2} cor-

related negatively with the severity of inflammation (588), with relationships to blood flow (416) and white blood cell count (484) observed. Furthermore, patients with osteoarthritis had significantly higher synovial fluid Po_2 than those with rheumatoid arthritis (363). Hence, it is likely that the inflamed nature of the arthritic joint produces a pathophysiologically hypoxic environment relative to the normal joint, and thus, Po_2 values derived from the study of such joints likely underestimate physiological normoxia.

3. Resident bone cells

As described in sections VIG*1* and VIG*2*, the avascular nature of mineralized bone and cartilage creates a physiological milieu containing relatively little O_2 (~1.5 kPa in deep cortical bone and articular cartilage) for resident cells. **TABLE 7** provides an overview of studies conducted to investigate the effects of culture at physiological normoxia on bone cell physiology. Long-term culture (>72 h) of osteoblasts at the lower end of this physiological range (Po_2 2 kPa) is associated with a significant reduction in mineralization (Ca^{2+} deposition as measured by Alizarin red staining) and alkaline phosphatase activity compared with room air cultures (329, 423, 435, 601, 686). This was reportedly due to a delayed (601) or reduced (423) expression of the osteocyte markers osteocalcin and procollagen lysine dioxygenase and was associated with a reduced ability to synthesize and deposit collagen (435). Indeed, microarray analysis of human osteoblastic cells (SV40-transformed Human Fetal Osteoblastic cells) cultured at 2 kPa for up to 3 wk revealed the greatest impact of low O_2 on the mineralization phase of differentiation (424). However, culture under an ambient Po_2 of 2 kPa would result in a much lower intracellular Po_2, and hence, this phenotype is likely representative of a reactive, hypoxic cell rather than the physiological norm. This hypothesis is corroborated by the observation that preosteoblastic cell lines (MC3T3-E1 and MLOA5) cultured long term at a Po_2 of 2 kPa exhibit marked HIF-1α stabilization (686), pimonidazole staining, and HRE luciferase activity (329), indicating a classical hypoxic phenotype. In contrast, paired cultures maintained at a Po_2 of 5 kPa showed no such HIF-1α activity (329), consistent with our findings in human endothelial cells maintained >5 days under similar conditions (see **FIGURE 10**). Under this more physiologically relevant Po_2 (accommodating for monolayer consumption), MC3T3-E1 cells exhibited earlier and more robust mineralization and alkaline phosphatase activity, which was associated with increased expression of the osteocytic markers osteocalcin, Dmp1, Mepe, and Fgf23 (241). Similar findings were reported in murine calvarial organ cultures maintained under 5 kPa O_2 (241). These findings suggest that higher O_2 levels may stimulate osteocyte maturation and mineral bone formation in vivo, supported by the knowledge that the highest intraosseal Po_2 values (6–7 kPa) recorded are in the periosteal layers of diaphyseal bone (52, 552). Thus, the appropriate intracellular O_2 level in vitro should be defined based on the differentiation state to be studied.

4. Chondrocytes

Grimshaw and Mason (2000) (196) attributed the unusual ability of chondrocytes to withstand severe hypoxia to a very low mitochondrial mass in vivo (53) and low O_2 consumption rates in vivo and in vitro (240). As chondrocytes experience very low O_2 levels in vivo (~1.5 kPa, see **FIGURE 16*A***), O_2 conservation may be necessary. There are numerous studies of chondrocytes during culture under normoxic conditions in vitro, as summarized in **TABLE 8**. Such studies have largely focused on culture techniques to reverse the dedifferentiation of primary chondrocytes that occurs following isolation and monolayer culture in vitro. Dedifferentiation is characterized by a switch in collagen production from type II to type I (34), with concomitant downregulation of key chondrocyte markers aggregan and SOX9. Although very low O_2 (<1.5 kPa) levels exist in deep articular cartilage, new cartilage is formed at the superficial layer adjacent to the synovial fluid where Po_2 values are closer to 5 kPa (see **FIGURE 16*A***). When cultured on alginate beads at a Po_2 of 5 kPa for 2–4 wk, the phenomenon of redifferentiation is accelerated and enhanced in human (287, 414, 518), bovine (117, 118, 239, 415), mouse (242), and rabbit (233) chondrocytes. In addition to the expression of *Col2a1*, *Aggregan*, and *SOX9*, increased deposition of collagen and glycosaminoglycan was frequently observed in alginate 3D bead cultures (518). Furthermore, enlarged matrix area was noted in E14.5 murine forelimbs cultured ex vivo at 5 kPa (242), indicating this effect is not confined to isolated cells.

Culture in 3D alginate beads presents a particular problem concerning O_2 diffusion, and ultimately, intracellular Po_2. Li et al. (341) addressed this question using a combination of experimentally determined O_2 consumption rates and Po_2 distribution modeling in scaffold-free aggregate cultures seeded at various densities. They reported a critical threshold of ~8 kPa, at which point cells no longer synthesized collagen and preferentially produced proteoglycans. How this relates to previous studies is unclear given that the majority of the studies cited above use cells cultured in pellet or alginate 3D conditions at 5 kPa and report increased collagen deposition relative to room air cultures. Based on the Po_2 profiles published by Li et al., average pellet Po_2 may be closer to 8 kPa when cultured at room air (~18.5 kPa) than under 5 kPa, and therefore, one might expect increased collagen deposition in these pellets. Despite this, gradients in collagen deposition have been observed in alginate beads under 5 kPa, with the highest collagen-associated staining apparent at the periphery (117). Thus, the concept of a critical threshold for collagen deposition may have some merit, but discrepancies in the actual Po_2 value are expected given differences in O_2 diffusion between scaffold-free and alginate cultures.

Table 7. *The effects of culture at physiological normoxia on bone cell physiology*

Species	Cell Type	Po_2 (kPa)	Time	Comments	Reference
Human	SV-HFO (human osteoblastic cell line)	2	3 wk	↓ Mineralization due to less differentiation and maturation of extracellular matrix components (collagen). ↓ ROS (mitoSOX and DCF) and lower expression of SOD1/2 and CAT.	(423)
		2	3 wk	Microarray of cells cultured at 2 kPa for various phases of differentiation. Impact most prominent during early phase when mineralization begins to occur.	(424)
Mouse	MC3T3-E1 preosteoblast Calvarial organ culture	5	35 d	Earlier and greater Ca^{2+} mineralization. ↑ ALP staining and earlier. ↑ Osteocalcin expression initially, but declined by 35 d. ↑ Cx43 expression at cell/cell junctions and whole cell lysates. ↑ Osteocyte markers (Dmp1, Mepe, and Fgf23). ↑ Osteocyte population (cells expressing Dmp1 and Mepe) in organoid cultures.	(241)
	MC3T3-E1 preosteoblast	2,5	72 h	Two kPa strongly associated with HIF stabilization (PMZD staining and HRE luciferase), not observed at 5 kPa. ↑ PGE_2 production and EP1 receptor expression at 2 kPa.	(329)
	MLOA5 (preosteoblast) MLOY4 (osteocyte)	2,5	7 d	↓ Po_2 associated with ↓ ALP activity and mineral deposition. No change in viability. ↑ HIF stabilization at 2 kPa preserves cell function under hypoxia.	(686)
Rat	Calvarial osteoblasts	10	7 d	Compared with hyperoxia (90% O_2), ↑ proliferation. No change in ALP activity.	(595)
	Primary osteoblasts	0.2–20	18 d	↓ Bone module formation with ↓ Po_2. At 2 kPa O_2, ↓ proliferation, but no change in apoptosis. Delayed osteoblast differentiation markers (osteocalcin and PLOD) and ↓ collagen production.	(601)
Rabbit	Periosteal organ culture	1–90	6 wk	Highest growth and chondrogenesis at 15 kPa. ↓ Collagen synthesis at very high and very low O_2 levels. Culture in a "sealed jar" apparatus.	(435)

ALP, alkaline phosphatase; CAT, catalase; Cx43, connexin 43; DCF, dichlorofluorescein; Dmp1, dentin matrix protein 1; EP1, prostaglandin E receptor 1; Fgf23, fibroblast growth factor 23; HIF, hypoxia-inducible factor; HRE, hypoxia-responsive element; Mepe, matrix extracellular phosphoglycoprotein; PGE_2, prostaglandin E_2; PLOD, procollagen lysine, 2-oxoglutarate, 5-dioxygenase; PMZD, pimonidazole; ROS, reactive oxygen species; SOD, superoxide dismutase; SV-HFO, SV40-transformed human fetal osteoblastic cell.

5. Marrow-derived stem cells

The concept of a stem cell niche within the bone marrow and its influence on mesenchymal and hematopoietic stem cell (HSC) fate are front and center in our understanding of the physiology of these cells. Elegant imaging-based investigations have demonstrated that HSC preferentially localize to small arterioles within the endosteal marrow (319), and that variations from this niche induce a proliferative and hypoxic phenotype (319, 430). Given our knowledge that the steepest O_2 gradients outside the lungs exist across the walls of arterioles (section III*B* and **FIGURE 9**), it is likely that steep gradients in Po_2 also exist in between arterioles within the bone marrow. Such heterogeneity in marrow Po_2 may be confounded by regional heterogeneity in cell populations, with various degrees of cellular activity and thus O_2 consumption (552). Measurements of marrow Po_2 range from 1.7 to 7.2 kPa (**FIGURE 16*B***), yet no study has directly

Table 8. *The effects of culture at physiological normoxia on chondrocyte physiology*

Species	Cell Type	Po_2 (kPa)	Time	Comments	Reference
Human	Chondrocytes	5	4 wk	↑ Collagen II, aggregan, and SOX9 mRNA in 3D culture. ↑ Proliferation and GAG synthesis. No change in pH or glucose consumption. Redifferenatiated phenotype only achieved when 5 kPa O_2 and 3D culture combined.	(414)
	Meniscus cells Chondrocytes	5	2 wk	No change in collagen I mRNA. ↑ Collagen II and SOX9 mRNA in meniscus cells, but not chondrocytes.	(4)
		5	3 wk	↑ GAG and hyaline cartilage–like matrix deposition. ↑ Collagen II, aggregan, and SOX9 protein expression.	(287)
		5	5 d	No change in aggregan or Col I mRNA expression or in DNA content, lactate production, or glucose consumption. ↑ VEGF production and mRNA levels at pH 7.4 and 5 kPa O_2.	(104)
		5	4 wk	No change in growth or DNA content. ↑ CD44 and CD105 expression. ↑ Pellet volume and GAG content. No change in col1/2 mRNA expression, but ↑ aggregan mRNA.	(518)
		20	N/A	Modeling O_2 consumption and Po_2 profiles in 3D alginate chondrocyte cultures. Po_2 <8 kPa makes chondrocytes favor proteoglycan synthesis over collagen.	(341)
Bovine	Chondrocytes	3–60	6 d	↓ DNA content with ↓ Po_2. ↓ Sulfate incorporation, as indicative of GAG synthesis, with ↓ Po_2. ↑ Proteoglycan aggregation with ↓ Po_2.	(86)
		0.1, 5, 10, 20	7 d	No change in viability or proliferation, which didn't actually occur. No change in aggregan expression. ↑ Pellet volume peaking at 10 kPa O_2, indicative of ↑ collagen synthesis. No change in pH until 0.1 kPa. ↓ rRNA yield at 0.1 kPa. Suggested that chondrocytes are particularly robust in withstanding hypoxia relative to other cell types.	(196)

Continued

Table 8.—*Continued*

Species	Cell Type	Po_2 (kPa)	Time	Comments	Reference
		5	4 wk	No change in growth, viability, or pH. No change in collagen I mRNA. ↑ Collagen II and aggregan mRNA. ↑ Matrix collagen and GAG content during 3D culture. Culture at 5 kPa exacerbated redifferentiation during 3D culture. All culture performed on orbital shakers so pericellular Po_2 was also ~5 kPa.	(415)
Bovine		5	3 wk	↓ Collagen I mRNA during redifferentiation. ↑ Collagen II and XI and aggregan mRNA during redifferentiation. ↑ Collagen staining in 3D beads, especially toward the periphery in which Po_2 would be highest.	(117)
		5	3 wk	↓ Collagen I and ↑ collagen II/aggregan mRNA and staining during redifferentiation. ↑ Sulfate and proline incorporation, indicative of GAG and proteoglycan synthesis.	(118)
		2, 5	14 d	↓ Proliferation at both O_2 levels, but no change in protein content. ↑ O_2 consumption during monolayer culture, which was proportional to Po_2. ↑ ROS at 20 kPa. Differences in cellular phenotype between 2 and 5 kPa.	(240)
		2, 5	9 d	↑ Mitochondrial mass during culture, more pronounced at 20 kPa than 2. Associated with ↑ oxidative phosphorylation. ↑ ROS and O_2 consumption at 20 kPa, which could be restored to fresh/2 kPa values, but treatment with NAC. ↑ GAG accumulation in 3D culture at 5 kPa.	(239)
Mouse	C3H10T1/2 E14.5 murine forearm limb	5	7 d	↑ BMP-2 induced GAG synthesis with concomitant ↓ ALP activity and alizarin red staining, indicating less osteoblastic differentiation. No change in adipocyte differentiation. No change in proliferation. ↑ Col2a1 mRNA expression and ↓ Col10a1 mRNA expression, mediated by ↑ p-p38 and HDAC4 activity. Enlarged matrix area in forelimbs cultured at 5 kPa O_2. 5 kPa O_2 promotes chondrogenic differentiation, but not terminally.	(242)

Continued

Table 8.—*Continued*

Species	Cell Type	Po_2 (kPa)	Time	Comments	Reference
Rabbit	Chondrocyte	5	3 wk	↑ Proliferation ↑ Collagen II mRNA but no change in aggregan or collagen I. ↑ Aggregation with more collagen and GAG deposition. Culture at 5 kPa O_2 during the expansion phase more pronounced than during the 3D phase.	(233)

ALP, alkaline phosphatase; BMP-2, bone morphogenic protein 2; ColX, collagen X; 3D, three-dimensional; GAG, glycosaminoglycan; HDAC4, histone deacetylase 4; NAC, *N*-acetyl cysteine; ROS, reactive oxygen species; VEGF, vascular endothelial growth factor.

addressed the concept of localized regions of lower Po_2. Moreover, MSC and HSC may originate from the bone marrow, but their sites of action extend throughout the body. Indeed, many have postulated that changes in Po_2 as cells exit the marrow into the systemic bloodstream serve as a key trigger for terminal differentiation (402). In light of this, defining physiological normoxia for marrow-derived stem cells is difficult. In this review, we will consider 3–5 kPa as normoxia but will discuss select studies in which cells were cultured under 2 kPa for comparative purposes. A full summary of papers meeting these criteria is provided in **TABLE 9**.

Expansion at a Po_2 of 3–5 kPa has repeatedly demonstrated greater colony formation or proliferation of MSC isolated from human (149, 528, 616) and sheep (700) bone marrow, although conflicting evidence has also been reported (449). A number of studies have identified an enhanced chondrogenic differentiation potential in MSC colonies expanded at 5 kPa (336, 374, 391, 528, 700), as characterized by the expression of *Col2a1* (see above) and quantitative analysis of glycosaminoglycan deposition. One study of human MSC cultured at 5 kPa reported no change in chondrogenic or osteogenic differentiation (449). This could be related to the source of cells used, as the latter study sourced human MSC from a commercial supplier, whereas the majority of studies obtain cells directly from donors. A common observation reported by Pattappa et al. and others (149, 700) is a reduced level of cellular senescence after long-term expansion at 5 kPa. This finding may be related to the increased level of stemness or differentiation potential in these cells and supports the notion of a more physiologically relevant phenotype under physiological Po_2 in vitro. Fewer studies have focused on HSC ($CD44^+$) within the marrow. Reykdal et al. observed less nitrite accumulation in cultures of human $CD34^+$ HSC isolated and expanded at 5 kPa for 7 days. These authors attributed this to reduced induction of the inducible isoform of nitric oxide synthase, although they did not investigate the contributions of other isoforms. Similar to MSC, HSC proliferate more rapidly under 5 kPa and form larger colonies (483).

I. Skin

The measurement of transcutaneous Po_2 using noninvasive techniques has long been used experimentally and clinically as a readout of peripheral perfusion/oxygenation. This procedure involves placing a housed electrode onto the skin surface heated to 41°C–44°C to encourage microvascular vasodilation, thus increasing local blood supply, which creates a local excess of O_2 delivered by the arteriolar circulation **(FIGURE 17*A*)**. Transcutaneous Po_2 is directly proportional to cutaneous blood flow (647) and is inversely proportional to epidermal thickness (144). Heating the skin from 37°C to 45°C increases blood flow 3- to 4-fold (269); thus, temperature intimately influences the reported Po_2 value. For example, transcutaneous Po_2 in the human forearm was recorded as 9.3 kPa at 44°C by Falstie-Jensen et al., yet only 5.1 kPa at 41°C by Spence et al. (550). Although a useful readout of arterial oxygenation clinically, such artifactual conditions result in relatively poor correlation with bone fide measurements of skin Po_2 (see **FIGURE 17*B***). Using penetrating electrodes, Po_2 has been determined in the human abdominal, forearm, thigh, and fingernail cuticular dermis as well as in rat abdomen. At a generalized subcutaneous level, Po_2 has been reported to range between 3 (266), 4.1 (626), 5 (551), 5.3 (632), 6.3 (637), and 8 kPa (138). More detailed investigations by Evans and Naylor (140), Baumgärtl et al. (27), and Wang et al. recorded Po_2 profiles at various dermal depths (see **FIGURE 17*C***). Evans and Naylor reported Po_2 values of 6.1, 6.2 and 7.4 kPa at depths of 1–2, 3, and 5 mm, respectively, and similar profiles are also reported at equivalent depths in other areas of skin (27, 632). Clearly, the skin has two distinct sources of O_2 diffusion, the atmosphere and microvasculature, and a nadir exists in which cells receive little O_2 from either. One apparent pitfall in skin Po_2 measurements using penetrating electrodes is the potential for overestimated values resulting from damage to the dense microvasculature. Jamieson and Brenk demonstrated that larger electrodes (330-μm versus 60-μm diameter) produced higher average subcutaneous Po_2 values in the rat abdomen (alongside similar measure-

Table 9. *The effects of culture at physiological normoxia on marrow-derived stem cells*

Species	Cell Type	Po_2 (kPa)	Time	Comments	References
Human	MSC	1	1–3 wk	↓ Proliferation ↓ Adipogenic and chondrogenic differentiation.	(251)
	MSC in pellet culture	2	14 d	↑ Sulfated GAG, collagen, and proteoglycan formation, with more homogeneous surface distribution. More chondrogenic.	(374)
	Hemopoietic	5	10 d	↑ $CD34^+CD38^-$ expansion due to ↑ proliferation, not ↓ apoptosis. ↑ Myeloid-committed cells ($CD33^+CD14^+$) with ↑ colony-forming potential. ↑ Subsequent cell engraftment in irradiated mice.	(495)
	MSC	5, 2	thawing and duration of culture	↓ Colony numbers and cell yield at 5% specifically, but ↓ colony and individual cell size at 2%. ↑ Bone-marrow specific markers (CD44, 73, and 105) at both 5 and 2 kPa. ↓ Cellular senescence at 5% and 2%. ↓ O_2 consumption (microelectrode) and ↑ lactate production, with ↓ proportion of ATP generated by oxidative phosphorylation (azide sensitive). ↑ Chondrogenic differentiation at 5% specifically.	(449)
	Hemopoietic ($CD44^+$ progenitor)	5	>7 d	↓ NO production (Griess). ↑ Proliferation and colony formation, with ↑ progenitor cell production and proliferation.	(483)
	Mesenchymal	3	up to 100 d	↑ Colony formation following isolation at 3 kPa ↔ Hypoxia–associated genes, but 2313 differentially expressed genes related mostly to aging (↓) and bone-marrow specific markers (↑). ↓ Senescence over 100 d, with high population doubling times. ↓ AGE accumulation and SA-β-gal^+ cells, markers of senescence,	(149)
	MIAMI	3	15 d	highest proliferation at 3 kPa. ↑ Embryonic and stem genes OCT4, REX-1, and hTeRT. ↓ Osteoblast marker genes Runx and OCN. ↓ ALP activity, mineral deposition, and ECM-associated Ca^{2+} content. MIAMI cells less differentiation/mature than MSC.	(101)

Continued

Table 9.—*Continued*

Species	Cell Type	Po_2 (kPa)	Time	Comments	References
	Marrow nucleated cells	1,5,10	6 d	Largest colonies formed with the highest density of cells at 5 kPa. Similar colonies formed between 1 and 20 kPa.	(616)
Porcine	MSC	5	42 d	Agarose constructs contained increased GAG deposition, particularly within the core. ↑ Col2a1 and ↓ Col1a1 relative to room air	(391)
	MSC	5	expd/dif/both	Expansion at 5% results in larger colony formation and thus higher cell yield. Differentiation at 5%, even when following expansion at 20%, enhances the chondrogenic potential of MSC; more stable pellet/hydrogel with ↑ Ca^{2+} content and ↓ collagen X	(528)
Rat	MSC	5	up to 21 d	Enhanced calcium content and mineralization at 5 kPa O_2 suggests cells more likely differentiate in response to stimulation at 5 kPa O_2.	(336)
Sheep	Mesenchymal	5	up to 14 d	↑ Colony size and number, ↑ proliferation. ↓ Senescence ↑ Chondrogenic differentiation	(700)

AGE, advanced glycosylation end products; ALP, alkaline phosphatase; ColX, collagen X; ECM, extracellular matrix; GAG, glycosaminoglycan; hTeRT, human telomerase reverse transcriptase; MIAMI, marrow-isolated adult multilineage inducible cells; MSC, mesenchymal stem cell; NO, nitric oxide; OCN, osteocalcin; OCT4, octamer-binding transcription factor 4; Runx; Runt-related transcription factor 1; SA-β-gal, senescence associated β-galatosidase.

ments in liver, kidney, and splenic tissue), with evidence of macroscopic tissue damage.

More recently, significant efforts have been made to develop techniques to noninvasively monitor cutaneous Po_2 using phosphorescence quenching. Unlike the methods discussed in section IIC, in which a synthetic porphyrin-type dye is administered exogenously as an O_2-sensitive probe, a technique developed by Mik and colleagues (223) employs 5-aminolevulinic acid, a precursor to the endogenously produced protoporphyrin IX. 5-Aminolevulinic acid cream is administered topically to the skin and results in accumulation of protoporphyrin IX in the mitochondria of epidermal cells within ~3 h (224). Using this technique, a Po_2 of between 6.3 and 8 kPa was reported in cutaneous mitochondria of the rat abdomen (223, 225, 637), which correlates well with similar measurements using microelectrodes (138, 139). By coinjection of the hydrophilic Oxyphor G4 dye, simultaneous measurement of mitochondrial and microvascular Po_2 was possible (223). A gradient of ~2.7 kPa between blood and mitochondria was reported in the rat abdominal cutis, which was abolished by topical application of cyanide. Notably, a microvascular Po_2 of 10 kPa measured in this study is well within the range of reported transcutaneous Po_2 values [9.3–11.2 kPa (144, 560, 647)], confirming that transcutaneous measurements accurately reflect microvascular Po_2. In a more recent study, mitochondrial Po_2 was found to be a very sensitive indicator of the limit of hemodilution in pigs (489). However, the average baseline mitochondrial Po_2 value reported in this study (2.7 kPa) is far lower than that recorded in rats in previous investigations [7.3–8 kPa (223, 225)], a discrepancy that remains unexplained.

Fibroblasts isolated from mouse embryos and tail and human dermis have all been cultured at 3–5 kPa **(TABLE 10)**. Common to many of these independent reports is the observation that cells maintained at low O_2 exhibit markedly less chromosomal instability/breakage (78, 283, 446) and senescence (78, 446). This was particularly apparent in mouse-derived fibroblasts (446), which appear highly sensitive to the damaging effects of atmospheric conditions. Mouse embryonic fibroblasts cultured at 3 kPa had higher and persistent expression of the p53-related proteins $p19^{ARF}$ and p16, yet senescence could be rapidly induced by re-exposure to 20 kPa (446). Notably, this sensitivity ap-

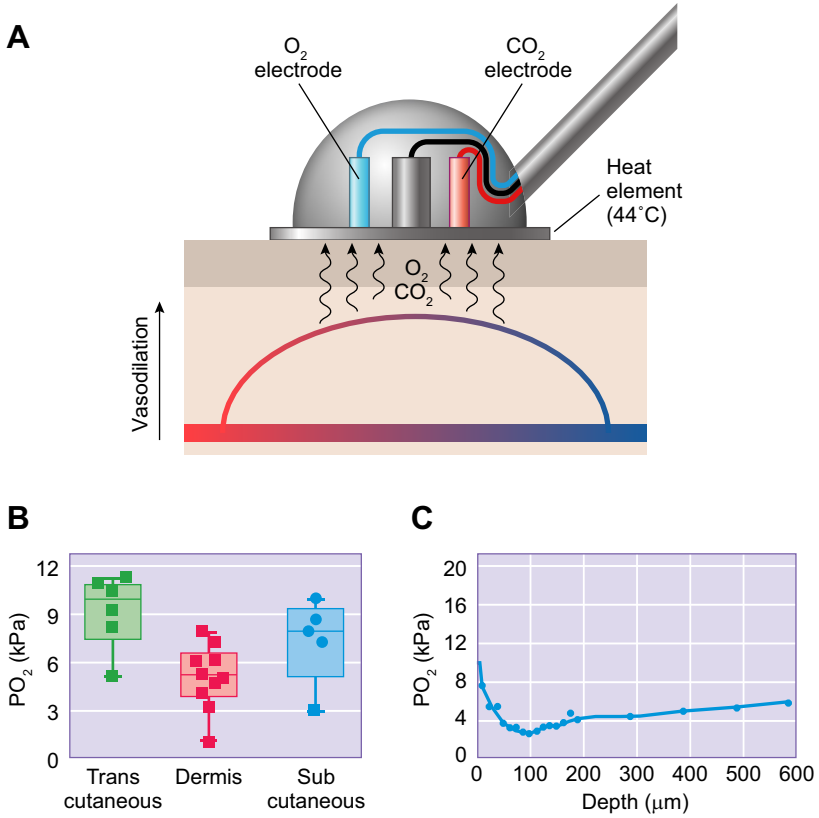

FIGURE 17. Oxygen distribution in the skin. *A*: Concept of transcutaneous measurement of blood gas concentrations. Heating the skin causes vasodilation and enhances O_2 delivery to the epidermis, where it diffuses toward the measurement electrodes. *B*: Distribution of published P_{O_2} values in the dermis and subcutaneous tissues as well as transcutaneous measurements. Symbols are coded according to technique used: □, microelectrode; and ○, phosphorescence-quenching microscopy. *C*: An example of a P_{O_2} profile generating by electrode penetration of the skin. Adapted with permission from Baumgärtl et al. (27).

pears specific to laboratory rodent strains and is not observed in wild animals of the same species (448). This could reflect the longer telomeres observed in laboratory species (232) that are thought to occur in the absence of evolutionary selection for short telomeres in the wild. In human keratinocytes, isolation and culture at 4 kPa O_2 results in enhanced migration rates associated with reduced superoxide generation compared with cells cultured under 20 kPa (493).

Carrera et al. (68) reported increased HIF-1α activity in primary keratinocyte populations cultured at a P_{O_2} of 5 kPa for up to 4 days. This was reduced by inhibition of the MAPK cascade and with certain DNA-damaging compounds, such doxorubicin, with minimal effects on proliferation. It is likely that these observations can be attributed to the phenomenon of self-inflicted hypoxia (see section IV*D*) based on the following observations: *1*) HIF-1α protein levels were still minimal at 5 kPa compared with those observed at 1 kPa. Because monolayer oxygenation decreases with cell density (see section IV*C*), HIF-1α protein may only be stabilized at confluency and may therefore only affect proliferation in its latter stages; *2*) prominent HIF-1α protein expression and HRE-luciferase were observed in monolayers of the colon cancerous cell line HCT116 under the same conditions. Oxygen consumption rates are reportedly higher in these cells compared with primary human keratinocytes [25 versus 8 amol/min/cell (147, 619, 638)] and thus would have a lower intracellular P_{O_2} and hence higher HIF-1α activity; and finally, *3*) inhibition of HIF-1α stabilization was observed when cellular activity was reduced by MAPK inhibitors or by DNA damaging agents. A reduction in cellular activity may result in decreased O_2 consumption rates, thereby increasing intracellular P_{O_2}. As discussed in section IV*D*, an understanding of O_2 dynamics in monolayer cultures is critical in interpreting experimental data and should be considered when designing a model of in vitro normoxia.

J. Adipose Tissue

Interest in P_{O_2} distribution in adipose tissue has increased in the last two decades (246) based on the observations that tissue from obese patients or animals can be hypoxic, although this is not fully accepted (188). In lean mice, P_{O_2} values have been reported between 6.4 and 7.7 kPa in epididymal fat pads (673, 676) and 5.6 kPa in the perigonadal white adipose tissue (477). Parallel measurements in the *ob/ob* transgenic obese mouse revealed a consistently lower adipose tissue P_{O_2} (2–4.6 kPa, decreasing with age), with strong histochemical evidence for tissue hypoxia through pimonidazole staining (477, 673, 676). In humans, subcutaneous adipose tissue P_{O_2} was measured at 7.6 kPa in the arm (280) and 7.3–7.9 kPa in in abdomen (187, 447) of lean patients. In contrast to rodent models of obesity, adipose tissue P_{O_2} in obese patients has been shown to be both higher (187, 618) and lower (280, 447) compared with

Table 10. *The effects of culture at physiological normoxia on skin cell physiology*

Species	Cell Type	Po_2 (kPa)	Time (days)	Comments	Reference
Human	82–6 and Bj (HCA2) MEF	3	60 (from isolation)	MEF cultures did not undergo senescence at 3 kPa, but it could be induced by exposure to 20 kPa at early time points. At 3 kPa, MEFs behaved more like human fibroblasts. Changes in expression patterns of p53 regulatory proteins $p19^{ARF}$ and p16 at 3 kPa. ↑ Chromosomal breakage at 20 kPa in MEFs. MEF are particularly sensitive to oxygen metabolism damage, but at 3 kPa are just as robust as human fibroblasts.	(446)
	Keratinocyte	4	From isolation	Comparison between cells from young and old donors. ↑ Migration (scratch) in young, but not old, cells. No change in proliferation. ↓ ROS (DHE) independent of age. Scratching induces ROS production at leading edge, dissipation of which related to migration rate.	(493)
	Dermal Fibroblasts	2	>3	No change in metabolic activity or morphology. ↓ Inhibition of metabolic activity by blue light (450 nm) at 2 kPa, whereas near infra-red light (850 nm) stimulated metabolism only at 2 kPa.	(394)
	HCT116 Keratinocytes	5	4	↑ HIF protein at 5 kPa in HCT116, much less in keratinocytes (barely visible), accompanied by HRE/Luc activity and GLUT1 mRNA increases in HCT116 cells. Inhibition of MAPK cascade with UO126-reduced HIF1 protein, as did treatment with doxorubicin. ↑ Proliferation in HCT116 cells at 5 kPa, barely effected by HIF1 knock out. All observations consistent with self-inflicted hypoxia due to O_2 consumption. Inhibition of MAPK- or DNA-damaging agents would reduce cellular activity (O_2 consumption), thereby increasing pericellular.	(68)
Mouse	Tail fibroblasts MEF	3	7.5	Spontaneous chromosomal breaks at 20 kPa reduced at 3 kPa in cells with compromised chromosome stability ($Ku86^{-/-}$). No change in cell proliferation. Some level of spontaneous instability even at 3 kPa, probably due to other sources of ROS.	(78, 283)
Rodent	Fibroblasts	3	30	Fibroblasts from laboratory mouse strains are the only rodent cells to exhibit marked sensitivity to O_2.	(448)

DHE, dihydroethidium; GLUT1, glucose transporter 1; HRE-Luc, luciferase conjugated hypoxia-responsive element; MAPK, mitogen-activated protein kinase; MEF, mouse embryonic fibroblast; ROS, reactive oxygen species.

matched lean patients. Pasarica and colleagues (447) were able to demonstrate that adipose tissue P_{O_2} correlated negatively with percentage fat composition and the expression of the inflammatory marker CD68 while correlating positively with capillary density. Based on these correlative relationships and the known histological characteristics of adipose tissue from obese patients (582), a lower P_{O_2} in tissue from obese patients seems logical. The work by Goossens and colleagues (39, 187, 618) reports a higher fasting adipose tissue P_{O_2} in obese patients compared with matched lean (~9 versus ~6 kPa) subjects (187) and that weight loss in obese patients is associated with a significant reduction in mean adipose P_{O_2} (6.8 to 5.5 kPa) (618). It was demonstrated that increasing and decreasing adipose tissue blood flow (using isoprenaline and angiotensin II infusion, respectively) leads to corresponding changes in tissue P_{O_2}, corroborating claims by Pasarica et al. (447) concerning the relationship between adipose tissue P_{O_2} and perfusion/vascularization. As adipose tissue blood flow is reduced in obese patients (187), one would expect a lower P_{O_2}. These discrepancies could be due to either differences in technique used to monitor P_{O_2}, with Goossens and colleagues using a custom-designed microdialysis technique as opposed to the more commonly used electrode/fiberoptic probe or physiological state in which measurements were made [fasting (187) versus normal (280, 447)].

As discussed and reviewed in by Trayhurn (586), a large body of work exists examining the effects of hypoxia (P_{O_2} of 1–2 kPa) on adipocyte function in vitro to better understand the pathophysiology of obesity. However, as highlighted by Trayhurn, culture at 20 kPa followed by a dramatic drop to 1–2 kPa has limited physiological significance, as neither the starting P_{O_2} nor hypoxic value are physiological for adipocytes. It is far more likely that adipocytes experience a P_{O_2} of around 6–7 kPa in vivo, and to date, two studies have attempted to address this issue. The first by Wood and colleagues (663) exposed primary human adipocytes to P_{O_2} values of 1, 3, 5, 10, 15, and 20 kPa for 24 h and measured expression and release of the key adipokines leptin and adiponectin as well as IL-6 and VEGF. A strong negative correlation was observed between leptin, VEGF, and IL-6 mRNA expression, and P_{O_2}, whereas the opposite was observed for adiponectin and glucose uptake (663). Notably, the steepest part of the O_2 concentration response curve was between 3 and 10 kPa, the physiological/pathophysiological range of P_{O_2} in adipose tissue (see above). However, adipocytes were only exposed to different P_{O_2} environments for 24 h, which may induce a response more representative of a response to low O_2 and less indicative of their physiology in vivo. This problem was addressed in a subsequent study in which Famulla and colleagues (145) cultured adipocytes at 5 and 10 kPa for 14 days before measuring key adipocyte functions. Corroborating observations by Wood et al. (663), leptin expression and secretion were decreased at lower O_2 and associated with increased triglyceride content and glycerol release. Interestingly, peak responses were observed at a P_{O_2} of 10 kPa (145), conditions in which intracellular P_{O_2} is likely to be ~7 kPa based on known O_2 consumption rates of cultured adipocytes (694).

In addition to adipocytes and vascular cells, adipose tissue also contains a population of multipotent stem cells known as stromal cells (177). A number of studies have investigated the effects of long-term culture of these adipose-derived multipotent stem cells at low O_2 levels, as summarized in **TABLE 11**. Similar to other types of stem cells (see section VI, *H5* and *K3*), culture at either 2 (606) or 5 (464, 512, 533) kPa for the duration of culture/differentiation resulted in increased adipogenic (512, 606) and/or osteogenic/chondrogenic (464, 606) differentiation in vitro. Notably, enhanced differentiation potential in vitro did not translate into increased chondrogenesis when explanted in vivo (464). Although informative, the rationale behind culturing adipose derived stem cells at 2–5 kPa is unclear in light of the known distribution of P_{O_2} in such tissue in vivo (mean tissue P_{O_2} ~7 kPa). It is possible that populations of stem cells exist in localized regions of lower P_{O_2} within the tissue, although no evidence for this has been put forward to date. It seems more likely that 2 or 5 kPa O_2 was chosen as a "best guess" based on similar publications in cells of different origin. Although the matter may appear trivial, the work of Wood et al. (663) discussed above illustrates a steep relationship between ambient P_{O_2} and adipocyte function between 3 and 10 kPa, and thus, selecting the most appropriate ambient P_{O_2} at which to culture such cells is absolutely critical.

K. Uterus and Embryo

1. Uterus and oviduct

The uterus is a highly dynamic organ that experiences gross changes in physiology and function throughout the menstrual cycle, with surges in hormone secretion closely linked to contractile function and blood flow. In seminal work during the late 1960s, Mitchell and Yochim described periodic fluctuations in luminal (intrauterine) P_{O_2} that were rhythmic from hour to hour (401), and also changed dramatically according to stage of the menstrual cycle (400). During estrous, intrauterine P_{O_2} has been reported at between 3 (677) and 3.4 kPa (288, 400, 401) in the rat, 2.7 kPa in the guinea pig (174), 4.9 kPa in hamster (155), 5.7 kPa in rabbit, 1.7 kPa in rhesus monkeys (155), and between 2 (674) and 2.4–2.5 kPa in humans (440, 488). In experimental rodent models, intrauterine P_{O_2} peaked during the diestrous-1 period (288) and was strongly associated with similar increases in blood flow (174, 400). Such changes were not observed in primates (155). Upon conception, intrauterine P_{O_2} rises dramatically in rats (677) and

Table 11. *The effects of culture at physiological normoxia on adipose tissue–resident cells*

Species	Cell Type	Po_2 (kPa)	Time (days)	Comments	Reference
Human	Adipocytes	15, 10, 5, 3, 1	1	Leptin, VEGF, and IL-6 mRNA and secretion inversely proportional to Po_2. Adiponectin mRNA and secretion proportional to Po_2. Steepest part of sigmoid curves between 3 and 10 kPa, with 10 kPa often not different from room air. Glucose uptake and GLUT transporter expression increased proportional to Po_2 and corresponds to increased lactate secretion.	(663)
	Adipocytes	10, 5	14	No change in differentiation (Oil Red O staining), but decreased lipid droplet size proportional to Po_2. Increased triglyceride content at 10 kPa. Increased expression and secretion of adiponectin, IL-6, and DPP4, with concomitant decreases in leptin secretion (adipokine secretion). Increased glycerol release and hormone sensitive lipase expression at 10 kPa (lipolysis). Conditioned medium from 10 kPa cells induced the lowest SMC proliferation.	(145)
	Adipose MSC	5	duration of induction	A combination of kinase chemical inhibitors and 5% O_2 is optimal for the induction of iPSCs from adipose-derived stem cells.	(533)
	Adipose MSC	2	duration of culture	↑ Proliferation ↑ Viability ↑ Adipogenic and osteogenic differentiation potential following preadaptation to low O_2.	(606)
	Adipose MSC	5	21	↓ Fatty acid binding protein 4 expression. ↓ Glycerol-3-phosphate dehydrogenase activity and triglyceride content, markers of adipogenic differentiation. Effects of low O_2 abolished by cytoskeletal inhibitors cytochalasin D and blebbistatin.	(512)
Human, rabbit	Adipose stromal cells	5	21	Culture at 5 kPa increases chondrogenic differentiation of stromal cells in vitro but does not increase subsequent chondrogenesis in vivo.	(464)

DPP4, dipeptidyl peptidase-4; GLUT, glucose transporter; IL-6, interleukin-6; iPSC, inducible pluripotent stem cell; MSC, mesenchymal stem cell; SMC, smooth muscle cell; VEGF, vascular endothelial growth factor.

rabbits (155), simultaneous with increases in progestin and decreases in estrogen secretion (677). Indeed, ovariectomy to mimic estrogen depletion also caused large increases in intrauterine Po_2 in rats (from 3.4 to 8.2 kPa), which were reversed by concomitant estrogen treatment (401). Unfortunately, no data exist to our knowledge concerning intrauterine Po_2 across the menstrual cycle in humans, nor are there direct measurements before and after conception. Endometrial Po_2 was measured by Rodesch and colleagues (488) in patients undergoing elective termination procedures at 8–10 wk and in those at 12–13 wk. These authors report an increase from a mean Po_2 of 5.3 kPa in the early termination to 6.2 kPa at 12–13 wk. Similarly, Jauniaux and colleagues (271) measured Po_2 in coelomic/amniotic fluid and in the decidual lining in pregnancies between 7 and 10 wk and 11–16 wk. Although intrauterine fluid Po_2 was similar [2.5 kPa, similar to that reported by Ottosen et al. (440) and Yedwab et al. (674)], Po_2 in the decidual lining was significantly higher in late pregnancies (8.6 versus 9.8 kPa) (271). Thus, intrauterine Po_2 is relatively low before pregnancy and during estrous, especially in primates and humans, but rises rapidly within the uterine wall (myome-

trium/decidua) upon conception or during diestrus in line with increases in blood flow.

In the fallopian tubes, a dichotomy exists between mammalian species according to whether ovulation is cyclic or initiated by copulation. In rodent species (noncycling), Po_2 within the fallopian tubes/oviducts remains constant and is relatively high, ranging from 6.8 to 8 kPa in rabbits (155, 380) and 5.6 kPa in hamsters (155). In contrast, Po_2 in the oviduct of rhesus monkeys is incredibly low when ovulation is not occurring (<1 kPa O_2) but increases dramatically during ovulation to between 7 and 10 kPa (155, 365). During passage to the uterus, the oocyte receives nutrients and O_2 directly from the fallopian tube lumen, and thus, it is postulated that rodent oviduct Po_2 is maintained at a high level to ensure it can accommodate an oocyte at any point (365).

2. In vitro fertilization

One of the earliest adoptions of in vitro culture under physiological normoxia was in the field of in vitro fertilization (IVF), in which the first successful culture of a human embryo to the blastocyst stage was achieved only under 5 kPa (557). Since then, working under a reduced ambient Po_2 (usually 5 kPa) has become reasonably common both in research and clinical IVF (45, 186, 285, 314, 418). Given the demand for improved clinical outcomes with IVF procedures, a large number of clinical trials have been performed to investigate whether culturing early-stage embryos at 5 kPa is beneficial. These have been reviewed extensively in several meta-analyses (45, 186, 418), and as such, this topic will not be discussed in detail. In two reviews published in 2011 (45, 186), conflicting conclusions were drawn. Bontekoe and colleagues (45) reported a statistically significant improvement in live birth rate when embryos were cultured at 5–6 kPa O_2, which equated to an increase in success rate from 30% to between 32% and 43%. In contrast, Gomes-Sobrinho and colleagues (186) were unable to conclude that culture at low O_2 improved outcomes, although they did state that many results seemed promising. Notably, seven studies were retrieved in both reviews based on their respective selection criteria, yet these were not the same seven studies. Differences in selection criteria, with those applied by Bontekoe et al. (45) appearing stricter, are likely to explain the discrepancy in outcomes. In a later review by Nastri and colleagues (418), a small (5%), but significant, improvement was detected in live birth rates when embryos were cultured at 5–6 kPa, corroborating the findings of Bontekoe et al. (45). Common to all reviews was the criticism of study quality, especially related to investigator bias and differences in equipment/technique.

More recently, some have challenged the dogma that 5 kPa represents the ideal physiological Po_2 at which IVF should be conducted (286, 406, 670). This is based on the observation that Po_2 drops substantially between the oviduct and uterine lining from ~6 to 2–3 kPa (see **FIGURE 18**), and thus, the early blastocyst may experience a decrease in ambient Po_2 during implantation. To model this in vitro, embryos have been cultured at room air (670) or 5 kPa (286) until day 3, at which point ambient Po_2 was reduced to 2 kPa and blastocyst yield and quantity assessed at day 5. Cell yield increased 2-fold when embryos were cultured at 2 kPa between days 3 and 5 only when they were previously cultured at 5 kPa (286) with no significant effect detected if the embryo was previously kept at room air (670). In light of the significant effort and expense invested in improving IVF outcomes by utilizing the concept of physiological normoxia, these more intricate efforts to better match physiological conditions are a logical progression.

3. Embryonic stem cells

Embryonic stem cells (ESC) are pluripotent stem cells derived from the inner cell mass of the early blastocyst, preimplantation into the uterine wall, and receive nutrients and O_2 from the fallopian tube/uterine fluid. As such, they propagate in an environment containing low O_2, ranging between 2 and 5 kPa depending on the species (see above). Much like in IVF procedures, the derivation of ESC from the early blastocyst has long been conducted under low O_2 conditions [see (397) and (539) for reviews, and **TABLE 12** for an up-to-date summary]. This has largely been driven by enhanced proliferation or colony/embryonic body formation, consistently observed in both mouse and human ESC expanded at a Po_2 of 2–5 kPa (30, 142, 161, 173, 176, 300, 403, 467, 469, 473, 475, 629). A second advantage is a higher degree of pluripotency and less spontaneous differentiation; whether determined by expression of the OCT4/NANOG/SOX2 triad or downstream targets (643, 678), by

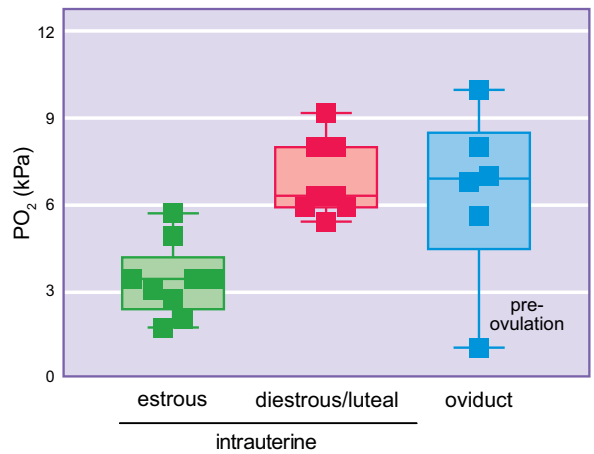

FIGURE 18. Oxygen distribution in the oviduct and uterus. Reported values for intrauterine and oviduct Po_2 across mammalian species. Intrauterine values are separated according to menstrual cycle stage. In rhesus monkeys, ovulation is associated with large fluctuations in oviduct Po_2 (365); hence, the preovulation value is labeled appropriately.

SSEA-1 expression (142, 469), or by morphological analysis (161, 469). Interestingly, although maintained in an undifferentiated state, ESC at low O_2 can also more readily differentiate, and to a higher degree, when stimulated. More efficient differentiation into cardiomyocyte (30), vascular (320, 473), pulmonary (173), chondrocyte (307), and, most often, neuronal (300, 403, 404, 666) lineages has been reported. Differentiation into neural precursor cells appears to occur preferentially at very low P_{O_2} (2–3.5 kPa) under the control of HIF-1/2 (666).

Genomic stability has often been assessed in ESC cultured at low O_2 and compared with those exposed to room air. Forsyth et al. (161) showed that hESC exhibited greater spontaneous chromosomal aberrations after 20 passages at room air compared with those maintained for the equivalent time at 2 kPa, which had very few additional aberrations. Lengner et al. (335) subsequently demonstrated that culture at room air is responsible for the premature and irreversible inactivation of an X chromosome frequently observed during hESC culture, through demethylation of the *XIST* gene promoter region. Similarly, hypermethylation of the DLK1/DIO3 cluster at room air results in silencing of this gene region which can be prevented by maintenance at physiological P_{O_2} levels (5 kPa) **(TABLE 12)**.

ESC are known to be highly metabolically active, preferring glycolysis as their source of ATP generation (79). This phenotype appears accentuated when ESC are cultured at low O_2, with higher rates of glucose consumption and lactate production frequency observed (83, 158, 596). In their most recent paper, Christensen and colleagues (83) propose that increased glycolysis is facilitated by enhanced expression of GLUT3, which correlated positively with OCT4 mRNA expression, thus relating glycolytic activity to pluripotency. ESC are also known to consume a large amount of O_2, which creates a concern regarding self-inflicted hypoxia during culture (see section IV). It has been demonstrated on a number of occasions that O_2 can be severely limited in monolayer cultures of ESC, especially at low ambient P_{O_2} (320, 466, 467, 596). Hence, as proposed by Turner et al. (596), confluent cultures kept at a P_{O_2} of 2 kPa [and even perhaps at 5 kPa (2, 320)] are inevitably encroaching on anoxia. This issue, although acknowledged, is yet to be satisfactorily addressed and thus calls into question the physiological validity of using very low (2–5 kPa) ambient P_{O_2} in ESC culture, with an intracellular P_{O_2} ~2–5 kPa being the actual desired outcome. Limited studies have been conducted with ESC cultured at higher (6–10 kPa) O_2 levels, which may counteract O_2 consumption to produce a more physiological intracellular P_{O_2}. In mouse ESC, similar levels of proliferation and pluripotency (OCT4/NANOG/SOX2 mRNA) (467) and VEGF production (473) were observed between ~4–10 kPa ambient P_{O_2}. However, human ESC differentiated to a higher degree during colony growth at 10 versus 5 kPa ambient P_{O_2} (469). Thus, there may well be physiological consequences to the self-inflicted hypoxia occurring following culture at 2–5 kPa, although this needs further investigation.

4. Placental tissue and trophoblasts

Placental development, and subsequently the health, of the tissue and fetus are closely linked to changes in P_{O_2} (270, 597, 650). During embryogenesis, rapid proliferation of trophoblastic tissue creates thick villus membranes, which result in reduced diffusion of O_2 from the maternal arterial blood to the surrounding tissue. As such, intervillous P_{O_2} is reportedly as low as 2–3 kPa in human placenta at 8–10 wk gestation (271, 272, 488), which has been shown to modulate the proliferative and angiogenic trophoblastic phenotype required to establish a patent intervillous circulation (65, 270, 597). Once adequate perfusion is established (>12-wk gestation), a rapid rise in villous/placental tissue P_{O_2} is observed, reaching 7–8 kPa (271, 272, 488, 548), in which placental tissue P_{O_2} remains largely stable for the duration of gestation (597).

The issue of oxygenation in vitro has long been considered important in the culture of trophoblasts and placental tissue explants, and a large amount of the literature has already been elegantly reviewed by Tuuli and colleagues (597). Numerous studies have attempted to understand the impact of changes in P_{O_2} on trophoblast phenotype, largely through comparative studies on cultures maintained at ambient P_{O_2} values ranging from 20 to <1 kPa. However, measurement of pericellular P_{O_2} in primary human trophoblast cultures using a microelectrode revealed that cells were experiencing near anoxic (P_{O_2} of 0.1–0.6 kPa) conditions even when cultured under ambient (20 kPa) P_{O_2} (77). This gradient was medium-depth–dependent and abolished by methanol fixation of the cells, confirming evidence discussed previously (section IVC). Although not confirmed by others to date, these data clearly call into question the validity of using standard culture conditions to study primary trophoblasts in vitro.

VII. CONCLUSIONS AND FUTURE PROSPECTS

The concept that oxygen is critical for normal cellular function is unanimously accepted. However, for scientists, O_2 may represent more of a double-edged sword in view of the numerous damaging effects associated with reactive species produced from O_2. Despite this, traditional methods used extensively in the culture of mammalian cells result in the exposure to undefined, uncontrolled O_2 levels, which are often at either extreme of the quasi-physiological range (i.e., either hyperoxic or hypoxic with respect to the physiological milieu). In this review, we have provided an up-to-date assessment of the current understanding of P_{O_2} distribution in tissues and organs in vivo and discussed some examples

Table 12. *The effects of physiological normoxia on embryonic stem cell physiology*

Species	Cell Type	Po_2 (kPa)	Time (days)	Comments	Reference
Human	ESC (H1)	5	12–15	hESC differentiation in culture was inversely proportional to Po_2: little differentiation apparent when cultured at 1–4 kPa O_2. Greater embryonic body formation under low O_2. Phenomenon is not reversible, exposure to room air after low O_2 does not induce much more differentiation.	(142)
	ESC (H1, RH1 and H9)	2	14	Clonal recovery was 4- to 12-fold higher at 2 kPa, and cells were less differentiated. Switching back to room air reduced colony formation. Less spontaneous chromosomal alterations and perhaps longer telomeres.	(161)
	ESC (H1, RH1 and H9)	2	10 passages	Genetic screen of cells cultured for 10 passages at 2 or 18 kPa O_2. Between passage 0 and 10, no change in genome at room air, but robust genomic changes at 2 kPa.	(160)
	H1 and H9	4	7 (after multiple passages)	Cultures at 4 kPa displayed less heterogeneity in their transcriptome. No change in the expression of pluripotency after culture at 20 kPa for 7 days, although a number of genes under the OCT4/NANOG/SOX2 triad are expressed much less.	(643)
	CLS1/2	1, 5, 10, 15	Up to 8 wk	Colony formation as inversely proportional to Po_2. After 4 wk, re-exposure to room air rapidly induced proliferation and differentiation, even in cultures kept at 5 kPa for 18 mo. Colonies at 5 kPa O_2 homogeneous and undifferentiated. Inhibition of notch signaling–normalized differentiation.	(469)
	Blastocyst-derived	5	From thawing	Cells thawed at 5 kPa O_2 and then exposed to room air for >3 days. No gross changes in genome after chronic culture at room air. Spontaneous differentiation reduced after exposure to room air. Exposure to room air induces irreversible X chromosome inactivation.	(335)
	H9	5	6–12	At room air, dissolved Po_2 ~15 kPa, and near 1 kPa at 5 kPa ambient. Decreased O_2 consumption at 5 kPa. Early vascular markers (CD42, KDR, and CD56) increased at 5 kPa, with morphological evidence for increased endothelial differentiation. When differentiation was split into two parts; culture at 5 kPa was only required for the first 6 days. Culture at 5 kPa increases ROS formation (DCF) and inhibition with DPI abolished this and the increased EC differentiation.	(320)

Continued

Table 12.—*Continued*

Species	Cell Type	Po_2 (kPa)	Time (days)	Comments	Reference
	MEL-2 ESC	2	Up to 5	No significant change in proliferation. ↑ Lactate and glucose consumption and ↓ ammonia consumption. ↑ Production of alanine and ↑ consumption of aspartate, asparagine, and glycine. ↓ Consumption of glutamine. Good information on O_2 diffusion and limitations in vitro. Intracellular Po_2 most certainly close to 0 kPa at 2 kPa ambient in ESC cultures.	(596)
Human	Shef3 and Hues-7	5	Minimum of 3 passages	No large change in amino acid utilization or production. ↑ Glycine consumption ↓ Serine uptake	(82)
	hESC and hiPSC	2	>5	Genomic screen suggested culture at 2 kPa shifted cells toward neuronal lineages (expression of SOX1, HES5, and FOXG1), specifically toward glial differentiation versus neuronal. Effect was abolished by HIF-2 siRNA and HIF-a inhibition. HIF regulates MYC, and thus LIN28/let-7, a key neuronal lineage regulator.	(666)
	Blastocyst-derived	5	From derivation/thawing	Imprinted region DLK1-DIO3 frequently silenced during culture because of hypermethylation. When lines were derived and maintained at 5 kPa, gene products from these regions (MEG3 and SNORD114–3) were still highly expressed. Re-exposure to room air caused rapid downregulation of these gene products and methylation of their promoters. Greater genomic stability when cultured and maintained at 5 kPa O_2.	(665)
	Shef3 and Hues-7	5	Minimum of 3 passages	↑ GLUT3 expression and membrane localization. GLUT3 mRNA positively correlates with OCT4 mRNA. Changes in GLUT3 expression may underlie changes in lactate/glucose consumption.	(83)
Mouse	D3	4	9	mESC cultured at 4 kPa for 9 days and then back to room air for 5 more. Early culture at 4 kPa O_2 increased differentiated cardiomyocyte yield.	(30)
	Stem cell (fresh)	5	28	More outgrowths from blastocysts and increased proliferation with more alkaline phosphatase activity in outgrowths.	(176)
	Stem cell (fresh)	5	From blastocyst isolation	↑ Overall cellular yield. ↓ ROS production (measured using DCF fluorescence). Combination of low O_2 and physiological levels of glucose (100 mg/dl) optimum for yield.	(629)

Continued

Table 12.—*Continued*

Species	Cell Type	Po_2 (kPa)	Time (days)	Comments	Reference
	CCE and D3 mESC	0, 1, 5, 20 and 40	Up to 25	Mathematical modeling of Po_2 at the cell layer. ↑ Proliferation at 5 kPa versus room air. Very low O_2 levels (<1 kPa), ↓ pluripotency genes (Oct4, Nanog, and Sox2) and at 40 kPa.	(467)
	D3 mESC	3.5	12	Greater degree of differentiation into dopaminergic neuronal precursor cells at low O_2 and with greater yield.	(300)
Mouse	iPSC (MEF)	5	Up to 30	↑ Efficiency of pluripotency induction and ↑ yield. Observed with both viral and nonviral transfection methods. No change in proliferation. ↑ 57.2% ESC-specific genes, ↓ 67.5% fibroblast-specific genes. Demonstrates efficiency in differentiation.	(678)
	R1	1, 2, 4, 8	7	Production and secretion of Flt-1 and VEGF change temporally over 7 days and at low O_2, driving ESC into either hematopoietic or endothelial lineages at different time points. Colony formation greatest at 2–4 kPa O_2 and lowest at 1 and 20 kPa.	(473)
	E14Tg2a mESC	2	8	Increased viability during 8 days of differentiation. ↑ Neuronal stem cell differentiation. Valuable data on dissolved Po_2 in culture.	(404)
	E14Tg2a mESC	2	8	Highest number and diameter of neural bodies (rosettes) between 4 and 10 kPa O_2, with the greatest number of viable cells. Greatest number of neuronal precursor cells observed at 4 kPa O_2. Increases from 2 to 4/6 kPa O_2 associated with ↑ total yield.	(403)
	R1 129/Sv (ESC) MAR B6D2 F1 (ESC)	5	3	↑ Apoptosis ↑ Proliferation ↑ ROS generation (measured using DCF fluorescence). ↓ Cardiomyocyte differentiation	(475)
	E14Tg2A (ESC) iPSwt4F (iPSC)	5	Up to 12	↑ Embryonic body formation ↑ Expression of NKx2.1 and FOXA2, markers of endodermal and early lung epithelial lineages. ↑ Differentiation into early pulmonary lineages following stimulated differentiation.	(173)

DCF, dichlorofluoroscein; DLK1-DIO3, delta-like homolog 1-type III iodothyronine deiodinase gene cluster; DPI, diphenyleneiodonium; EC, endothelial cell; ESC, embryonic stem cell; Flt-1, vascular endothelial growth factor receptor 1; FOXA4, forkhead box protein A2; FOXG1, forkhead box protein G1; GLUT, glucose transporter; HES5, Hes family BHLH transcription factor 5; hESC, human embryonic stem cell; HIF, hypoxia-inducible factor; hiPSC, human induced pluripotent stem cell; iPSC, inducible pluripotent stem cell; KDR, kinase insert domain receptor/vascular endothelial growth factor receptor 2; MEF, mouse embryonic fibroblast; MYC, v-Myc avian myelocytomatosis viral oncogene homolog; NKx2.1, NK2 Homeobox 1; OCT4, octamer-binding transcription factor 4; ROS, reactive oxygen species; VEGF, vascular endothelium–derived growth factor; mESC, mouse embryonic stem cells.

of in which this knowledge has been implemented to enhance the physiological relevance of cell culture conditions in vitro. In collating and critically discussing this information, we hope to provide a reference source for future research aimed at designing novel and physiologically relevant experiments to address ever-more complex scientific questions.

As highlighted throughout this review, accurately recapitulating physiological normoxia in vitro is far more complex than simply adjusting the ambient headspace Po_2. An understanding of the physical conditions in which cells are cultured (i.e., plastic permeability, volume of medium used, and rates of O_2 equilibration in solution) should underpin the choice of the final desired pericellular Po_2 determined using mathematical models and/or experimental data to predict pericellular versus ambient Po_2. Such careful experimental design informed by our review of the literature should provide researchers with the closest representation of likely tissue Po_2 levels in vivo. Differences in experimental conditions and protocols for cell culture, when sufficient detail is reported, and concerns about the definition of physiological normoxia have may limit collective advances for translational research.

Powerful tools are now available to better predict and measure Po_2 in culture, with accumulating studies highlighting their necessity. We thus hope that the contents of this review will help unify experimental approaches used by basic and clinical researchers. In this context, we propose the following guidelines for researchers who wish to culture their cells under defined physiological normoxia in vitro:

1. **Define the conditions appropriately.** Oxygen levels should be measured and defined in terms of Po_2 whenever possible. Often reported as room air or 20% O_2, most cell culture experiments are conducted in incubators in which the ambient Po_2 is closer to 18.5 kPa, and sometimes below.
2. **Start the experiment properly.** Always pre-equilibrate all culture media and solutions for a minimum of 2 h, and considerably longer for large volumes, at the appropriate ambient Po_2 before use on cells. It is advisable to store all culture plasticware at the desired Po_2 to avoid O_2 leaching.
3. **Controlling monolayer oxygenation.** We have highlighted throughout this review that appropriately controlling monolayer oxygenation is a consistent problem. There are several parameters that can be easily altered to maintain control over monolayer oxygenation, listed according to relative ease:
   - *i. Use of O_2-permeable plastic*: this creates a new and much more efficient way in which O_2 can be delivered to the monolayer, alleviating problems due to static medium.
   - *ii. Various medium height: surface area:* by minimizing the ratio between medium height and culture surface area, one reduces the distance for O_2 diffusion and thereby maximizes delivery. Simply reducing the volume of medium can achieve this.
   - *iii. Various ambient Po_2:* if medium volume cannot be reduced, one can increase the ambient Po_2 to compensate for monolayer O_2 consumption.
   - *iv. Continuous perfusion:* to completely alleviate issues associated with O_2 delivery, continuous perfusion of well-oxygenated medium is an elegant way to control intracellular O_2 precisely, even in response to large increases in O_2 consumption.

   Results should always be interpreted in the context of pericellular or intracellular Po_2 rather than ambient Po_2. Mathematical models have proved a useful tool to predict such values, and recent advances in experimental techniques have allowed the direct monitoring of intracellular Po_2.
4. **Consider a range of Po_2 values.** Oxygenation in vivo is heterogeneous in both space and time, and thus, no single value can be described as normoxia for a given cell type. Moreover, the expression and activity of many proteins are not linearly related to the intracellular Po_2. It is for these reasons that we find it far more informative to conduct preliminary studies under a range of physiological O_2 levels (2–10 kPa, for example), which offer a far more relevant comparison than 21 versus 1 kPa.

Can culture under physiological normoxia improve the translation of cell physiology to animal models and the clinic? There are several excellent studies (342, 499, 553, 578) that have already provided convincing evidence in favor of this hypothesis, and the concept is already implemented clinically in IVF clinics around the world. Despite this, we believe there is still significant scope to demonstrate that culturing cells under their respective physiologically normoxic conditions genuinely recapitulates their native phenotype and improves outcomes of clinical relevance. Moving forward, we believe it is critical for this field of research to avoid isolated phenotypic comparisons between cells at room air and those at normoxia, instead focusing on whether culture under physiological conditions can reveal novel insights into disease pathology or pharmacodynamics and kinetics of existing and novel therapeutics. Moreover, it is perhaps overly simplistic to consider only one normoxic value within a given tissue when there is clearly considerably complexity in tissue oxygenation. Thus, the oxygen-sensitivity of a pathway of interest may be more accurately assessed over a small range of normoxic values, such as that between the renal medulla and cortex (section VI*F*) or from the inner bone marrow to the associated vasculature (Section VI*H*). Furthermore, although critically important, O_2 represents just one component of the physiological milieu that is altered during standard culture practice, with other factors such as biomechanics, 3D coculture, and substrate matrix contributing equally to the cellular phenotype. Mov-

ing forward, it is essential to better model all these factors together to truly begin recapitulating the physiological environment in vitro.

ACKNOWLEDGMENTS

We thank Professor Sir Peter Ratcliffe, FRS (The Francis Crick Institute, London, U.K. and University of Oxford, U.K.) for helpful comments and discussion of this article.

Address for reprint request and other correspondence: G. E. Mann or T. P. Keeley, King's BHF Centre of Research Excellence, School of Cardiovascular Medicine and Sciences, King's College London, 150 Stamford St., London SE1 9NH, UK (e-mail: giovanni.mann@kcl.ac.uk or thomas.keeley@ndm.ox.ac.uk).

GRANTS

This work was supported by research grants from the British Heart Foundation (FS/13/66/30445, PG/13/1/29801) and Heart Research UK (Novel Emerging Technologies RG2633).

DISCLOSURES

No conflicts of interest, financial or otherwise, are declared by the author(s).

REFERENCES

1. Abaci HE, Shen Y-I, Tan S, Gerecht S. Recapitulating physiological and pathological shear stress and oxygen to model vasculature in health and disease. *Sci Rep* 4: 4951, 2014. doi:10.1038/srep04951.

2. Abaci HE, Truitt R, Luong E, Drazer G, Gerecht S. Adaptation to oxygen deprivation in cultures of human pluripotent stem cells, endothelial progenitor cells, and umbilical vein endothelial cells. *Am J Physiol Cell Physiol* 298: C1527–C1537, 2010. doi:10.1152/ajpcell.00484.2009.

3. Adamson EB, Ludwig KD, Mummy DG, Fain SB. Magnetic resonance imaging with hyperpolarized agents: methods and applications. *Phys Med Biol* 62: R81–R123, 2017. doi:10.1088/1361-6560/aa6be8.

4. Adesida AB, Grady LM, Khan WS, Millward-Sadler SJ, Salter DM, and Hardingham TE. Human meniscus cells express hypoxia inducible factor-1α and increased SOX9 in response to low oxygen tension in cell aggregate culture. *Arthritis research & therapy* 9: R69, 2007.

5. Adler KB, Cheng P-W, Kim KC. Characterization of guinea pig tracheal epithelial cells maintained in biphasic organotypic culture: cellular composition and biochemical analysis of released glycoconjugates. *Am J Respir Cell Mol Biol* 2: 145–154, 1990. doi:10.1165/ajrcmb/2.2.145.

6. Adler KB, Khosla J, Kim KC. Morphometric and biochemical characterization ofa chamber system for maintaining differentiated guinea pig respiratory mucosal cells between air and liquid phases. *Am Rev Respir Dis* 137: 14, 1988.

7. Adler KB, Schwarz JE, Whitcutt MJ, Wu R. A new chamber system for maintaining differentiated guinea pig respiratory epithelial cells between air and liquid phases. *Biotechniques* 5: 462–466, 1987.

8. Ahmad R, Kuppusamy P. Theory, instrumentation, and applications of electron paramagnetic resonance oximetry. *Chem Rev* 110: 3212–3236, 2010. doi:10.1021/cr900396q.

9. Albenberg L, Esipova TV, Judge CP, Bittinger K, Chen J, Laughlin A, Grunberg S, Baldassano RN, Lewis JD, Li H, Thom SR, Bushman FD, Vinogradov SA, Wu GD. Correlation between intraluminal oxygen gradient and radial partitioning of intestinal microbiota. *Gastroenterology* 147: 1055–63.e8, 2014. doi:10.1053/j.gastro.2014.07.020.

10. Allen CB, Schneider BK, White CW. Limitations to oxygen diffusion and equilibration in in vitro cell exposure systems in hyperoxia and hypoxia. *Am J Physiol Lung Cell Mol Physiol* 281: L1021–L1027, 2001. doi:10.1152/ajplung.2001.281.4.L1021.

11. Angell CS, Lakatta EG, Weisfeldt ML, Shock NW. Relationship of intramyocardial oxygen tension and epicardial ST segment changes following acute coronary artery ligation: effects of coronary perfusion pressure. *Cardiovasc Res* 9: 12–18, 1975. doi:10.1093/cvr/9.1.12.

12. Antonini E, Brunori M. *Hemoglobin and myoglobin in their reactions with ligands*. New York: North-Holland Pub. Co, 1971.

13. Aoyagi T, Kishi M, Yamaguchi K, Watanabe S. Improvement of the earpiece oximeter. *Japan Soc Med Electr Biol Engin* 974: 90–91, 1974.

14. Archer SL, Reeve HL, Michelakis E, Puttagunta L, Waite R, Nelson DP, Dinauer MC, Weir EK. O2 sensing is preserved in mice lacking the gp91 phox subunit of NADPH oxidase. *Proc Natl Acad Sci USA* 96: 7944–7949, 1999. doi:10.1073/pnas.96.14.7944.

15. Archer SL, Will JA, Weir EK. Redox status in the control of pulmonary vascular tone. *Herz* 11: 127–141, 1986.

16. Atkuri KR, Herzenberg LA, Herzenberg LA. Culturing at atmospheric oxygen levels impacts lymphocyte function. *Proc Natl Acad Sci USA* 102: 3756–3759, 2005. doi:10.1073/pnas.0409910102.

17. Atkuri KR, Herzenberg LA, Niemi A-K, Cowan T, Herzenberg LA. Importance of culturing primary lymphocytes at physiological oxygen levels. *Proc Natl Acad Sci USA* 104: 4547–4552, 2007. doi:10.1073/pnas.0611732104.

18. Avgoustiniatos ES, Hering BJ, Rozak PR, Wilson JR, Tempelman LA, Balamurugan AN, Welch DP, Weegman BP, Suszynski TM, Papas KK. Commercially available gas-permeable cell culture bags may not prevent anoxia in cultured or shipped islets. *Transplant Proc* 40: 395–400, 2008. doi:10.1016/j.transproceed.2008.01.059.

19. Aviado DM, Daly MD, Lee CY, Schmidt CF. The contribution of the bronchial circulation to the venous admixture in pulmonary venous blood. *J Physiol* 155: 602–622, 1961. doi:10.1113/jphysiol.1961.sp006650.

20. Balis UJ, Behnia K, Dwarakanath B, Bhatia SN, Sullivan SJ, Yarmush ML, Toner M. Oxygen consumption characteristics of porcine hepatocytes. *Metab Eng* 1: 49–62, 1999. doi:10.1006/mben.1998.0105.

21. Bannai S, Sato H, Ishii T, Sugita Y. Induction of cystine transport activity in human fibroblasts by oxygen. *J Biol Chem* 264: 18480–18484, 1989.

22. Barker MC, Golub AS, Pittman RN. Erythrocyte-associated transients in capillary P_{O_2}: an isovolemic hemodilution study in the rat spinotrapezius muscle. *Am J Physiol Heart Circ Physiol* 292: H2540–H2549, 2007. doi:10.1152/ajpheart.00915.2006.

23. Barker SG, Talbert A, Cottam S, Baskerville PA, Martin JF. Arterial intimal hyperplasia after occlusion of the adventitial vasa vasorum in the pig. *Arterioscler Thromb* 13: 70–77, 1993. doi:10.1161/01.ATV.13.1.70.

24. Barrett KE, Barman SM, Boitano S. *Ganong's review of medical physiology*. New Delhi: McGraw Hill, 2010.

25. Battino R. *Oxygen and ozone. IUPAC solubility data series*. Oxford, UK: Pergamon Press, 1981, vol 7.

26. Baumgardner JE, Otto CM. In vitro intermittent hypoxia: challenges for creating hypoxia in cell culture. *Respir Physiol Neurobiol* 136: 131–139, 2003. doi:10.1016/S1569-9048(03)00077-6.

27. Baumgärtl H, Ehrly AM, Saeger-Lorenz K, Lübbers DW (editors). *Clinical Oxygen Pressure Measurement*. New York: Springer, 1987, p. 121–128. doi:10.1007/978-3-642-71226-5_15

28. Baumgärtl H, Leichtweiss HP, Lübbers DW, Weiss C, Huland H. The oxygen supply of the dog kidney: measurements of intrarenal pO 2. *Microvasc Res* 4: 247–257, 1972. doi:10.1016/0026-2862(72)90036-2.

29. Bausch B, Jilg C, Gläsker S, Vortmeyer A, Lützen N, Anton A, Eng C, Neumann HP. Renal cancer in von Hippel-Lindau disease and related syndromes. *Nat Rev Nephrol* 9: 529–538, 2013. doi:10.1038/nrneph.2013.144.

30. Bauwens C, Yin T, Dang S, Peerani R, Zandstra PW. Development of a perfusion fed bioreactor for embryonic stem cell-derived cardiomyocyte generation: oxygen-mediated enhancement of cardiomyocyte output. *Biotechnol Bioeng* 90: 452–461, 2005. doi:10.1002/bit.20445.

31. Bedard K, Krause K-H. The NOX family of ROS-generating NADPH oxidases: physiology and pathophysiology. *Physiol Rev* 87: 245–313, 2007. doi:10.1152/physrev.00044.2005.

32. Benson BB, Krause D Jr. The concentration and isotopic fractionation of gases dissolved in freshwater in equilibrium with the atmosphere. 1. Oxygen. *Limnol Oceanogr* 25: 662–671, 1980. doi:10.4319/lo.1980.25.4.0662.

33. Benson BB, Krause D Jr, Peterson MA. The solubility and isotopic fractionation of gases in dilute aqueous solution. I. Oxygen. *J Solution Chem* 8: 655–690, 1979. doi:10.1007/BF01033696.

34. Benya PD, Padilla SR, Nimni ME. Independent regulation of collagen types by chondrocytes during the loss of differentiated function in culture. *Cell* 15: 1313–1321, 1978. doi:10.1016/0092-8674(78)90056-9.

35. Berra E, Benizri E, Ginouvès A, Volmat V, Roux D, Pouysségur J. HIF prolyl-hydroxylase 2 is the key oxygen sensor setting low steady-state levels of HIF-1alpha in normoxia. *EMBO J* 22: 4082–4090, 2003. doi:10.1093/emboj/cdg392.

36. Berra E, Richard DE, Gothié E, Pouysségur J. HIF-1-dependent transcriptional activity is required for oxygen-mediated HIF-1α degradation. *FEBS Lett* 491: 85–90, 2001. doi:10.1016/S0014-5793(01)02159-7.

37. Bhatia SN, Toner M, Foy BD, Rotem A, O'Neil KM, Tompkins RG, Yarmush ML. Zonal liver cell heterogeneity: effects of oxygen on metabolic functions of hepatocytes. *J Cell Eng* 1: 125–135, 1996.

38. Biniecka M, Kennedy A, Fearon U, Ng CT, Veale DJ, O'Sullivan JN. Oxidative damage in synovial tissue is associated with in vivo hypoxic status in the arthritic joint. *Ann Rheum Dis* 69: 1172–1178, 2010. doi:10.1136/ard.2009.111211.

39. Bizzarri A, Koehler H, Cajlakovic M, Pasic A, Schaupp L, Klimant I, Ribitsch V. Continuous oxygen monitoring in subcutaneous adipose tissue using microdialysis. *Anal Chim Acta* 573-574: 48–56, 2006. doi:10.1016/j.aca.2006.03.101.

40. Bjerrum JT, Perko MJ, Beck B. Myocardial oxygen tension during surgical revascularization. A clinical comparison between blood cardioplegia and crystalloid cardioplegia. *Eur J Cardiothorac Surg* 29: 181–185, 2006. doi:10.1016/j.ejcts.2005.11.024.

41. Björnheden T, Levin M, Evaldsson M, Wiklund O. Evidence of hypoxic areas within the arterial wall in vivo. *Arterioscler Thromb Vasc Biol* 19: 870–876, 1999. doi:10.1161/01.ATV.19.4.870.

42. Bohlen HG. Intestinal tissue Po_2 and microvascular responses during glucose exposure. *Am J Physiol* 238: H164–H171, 1980.

43. Bohlen HG. Tissue Po_2 in the intestinal muscle layer of rats during chronic diabetes. *Circ Res* 52: 677–682, 1983. doi:10.1161/01.RES.52.6.677.

44. Bonello S, Zähringer C, BelAiba RS, Djordjevic T, Hess J, Michiels C, Kietzmann T, Görlach A. Reactive oxygen species activate the HIF-1alpha promoter via a functional NFkappaB site. *Arterioscler Thromb Vasc Biol* 27: 755–761, 2007. doi:10.1161/01.ATV.0000258979.92828.bc.

45. Bontekoe S, Mantikou E, van Wely M, Seshadri S, Repping S, Mastenbroek S. Low oxygen concentrations for embryo culture in assisted reproductive technologies. *Cochrane Database Syst Rev* 7, 2011.

46. Bonventre JV, Zuk A. Ischemic acute renal failure: an inflammatory disease? *Kidney Int* 66: 480–485, 2004. doi:10.1111/j.1523-1755.2004.761_2.x.

47. Brandis K. *The Physiology Viva*. Southport: Australia Print and Copy, 2002.

48. Braun RD, Lanzen JL, Snyder SA, Dewhirst MW. Comparison of tumor and normal tissue oxygen tension measurements using OxyLite or microelectrodes in rodents. *Am J Physiol Heart Circ Physiol* 280: H2533–H2544, 2001. doi:10.1152/ajpheart.2001.280.6.H2533.

49. Brevig T, Røhrmann JH, Riemann H. Oxygen reduces accumulation of type IV collagen in endothelial cell subcellular matrix via oxidative stress. *Artif Organs* 30: 915–921, 2006. doi:10.1111/j.1525-1594.2006.00324.x.

50. Brezis M, Heyman SN, Dinour D, Epstein FH, Rosen S. Role of nitric oxide in renal medullary oxygenation. Studies in isolated and intact rat kidneys. *J Clin Invest* 88: 390–395, 1991. doi:10.1172/JCI115316.

51. Brezis M, Heyman SN, Epstein FH. Determinants of intrarenal oxygenation. II. Hemodynamic effects. *Am J Physiol* 267: F1063–F1068, 1994.

52. Brighton CT, Heppenstall RB. Oxygen tension in zones of the epiphyseal plate, the metaphysis and diaphysis. An in vitro and in vivo study in rats and rabbits. *J Bone Joint Surg Am* 53: 719–728, 1971. doi:10.2106/00004623-197153040-00011.

53. Brighton CT, Kitajima T, Hunt RM. Zonal analysis of cytoplasmic components of articular cartilage chondrocytes. *Arthritis Rheum* 27: 1290–1299, 1984. doi:10.1002/art.1780271112.

54. Brooks AJ, Eastwood J, Beckingham IJ, Girling KJ. Liver tissue partial pressure of oxygen and carbon dioxide during partial hepatectomy. *Br J Anaesth* 92: 735–737, 2004. doi:10.1093/bja/aeh112.

55. Brooks AJ, Hammond JS, Girling K, Beckingham IJ. The effect of hepatic vascular inflow occlusion on liver tissue pH, carbon dioxide, and oxygen partial pressures: defining the optimal clamp/release regime for intermittent portal clamping. *J Surg Res* 141: 247–251, 2007. doi:10.1016/j.jss.2006.10.054.

56. Buckler KJ. Effects of exogenous hydrogen sulphide on calcium signalling, background (TASK) K channel activity and mitochondrial function in chemoreceptor cells. *Pflugers Arch* 463: 743–754, 2012. doi:10.1007/s00424-012-1089-8.

57. Buerk DG, Goldstick TK. Arterial wall oxygen consumption rate varies spatially. *Am J Physiol* 243: H948–H958, 1982.

58. Buerk DG, Goldstick TK. Oxygen tension changes in the outer vascular wall supplied by vasa vasorum following adenosine and epinephrine. *Blood Vessels* 23: 9–21, 1986.

59. Bunn HF, Poyton RO. Oxygen sensing and molecular adaptation to hypoxia. *Physiol Rev* 76: 839–885, 1996. doi:10.1152/physrev.1996.76.3.839.

60. Gaertner FC, Souvatzoglou M, Brix G, Beer AJ. Imaging of hypoxia using PET and MRI. *Curr Pharm Biotechnol* 13: 552–570, 2012. doi:10.2174/138920112799436267.

61. Caldwell CC, Kojima H, Lukashev D, Armstrong J, Farber M, Apasov SG, Sitkovsky MV. Differential effects of physiologically relevant hypoxic conditions on T lymphocyte development and effector functions. *J Immunol* 167: 6140–6149, 2001. doi:10.4049/jimmunol.167.11.6140.

62. Calvani M, Rapisarda A, Uranchimeg B, Shoemaker RH, Melillo G. Hypoxic induction of an HIF-1alpha-dependent bFGF autocrine loop drives angiogenesis in human endothelial cells. *Blood* 107: 2705–2712, 2006. doi:10.1182/blood-2005-09-3541.

63. Campbell EL, Bruyninckx WJ, Kelly CJ, Glover LE, McNamee EN, Bowers BE, Bayless AJ, Scully M, Saeedi BJ, Golden-Mason L, Ehrentraut SF, Curtis VF, Burgess A, Garvey JF, Sorensen A, Nemenoff R, Jedlicka P, Taylor CT, Kominsky DJ, Colgan SP. Transmigrating neutrophils shape the mucosal microenvironment through localized oxygen depletion to influence resolution of inflammation. *Immunity* 40: 66–77, 2014. doi:10.1016/j.immuni.2013.11.020.

65. Caniggia I, Winter J, Lye SJ, Post M. Oxygen and placental development during the first trimester: implications for the pathophysiology of pre-eclampsia. *Placenta* 21, Suppl A: S25–S30, 2000. doi:10.1053/plac.1999.0522.

66. Carlsson PO, Liss P, Andersson A, Jansson L. Measurements of oxygen tension in native and transplanted rat pancreatic islets. *Diabetes* 47: 1027–1032, 1998. doi:10.2337/diabetes.47.7.1027.

67. Carlsson PO, Palm F, Andersson A, Liss P. Markedly decreased oxygen tension in transplanted rat pancreatic islets irrespective of the implantation site. *Diabetes* 50: 489–495, 2001. doi:10.2337/diabetes.50.3.489.

68. Carrera S, Senra J, Acosta MI, Althubiti M, Hammond EM, de Verdier PJ, Macip S. The role of the HIF-1α transcription factor in increased cell division at physiological oxygen tensions. *PLoS One* 9: e97938, 2014. doi:10.1371/journal.pone.0097938.

69. Case RB, Greenberg H, Moskowitz R. Alterations in coronary sinus pO2 and O2 saturation resulting from pCO2 changes. *Cardiovasc Res* 9: 167–177, 1975. doi:10.1093/cvr/9.2.167.

70. Cater DB, Garattini S, Marina F, Silver IA. Changes of oxygen tension in brain and somatic tissues induced by vasodilator and vasoconstrictor drugs. *Proc R Soc Lond B Biol Sci* 155: 136–158, 1961. doi:10.1098/rspb.1961.0061.

71. Ceradini DJ, Kulkarni AR, Callaghan MJ, Tepper OM, Bastidas N, Kleinman ME, Capla JM, Galiano RD, Levine JP, Gurtner GC. Progenitor cell trafficking is regulated by hypoxic gradients through HIF-1 induction of SDF-1. *Nat Med* 10: 858–864, 2004. doi:10.1038/nm1075.

72. Chacko SM, Khan M, Kuppusamy ML, Pandian RP, Varadharaj S, Selvendiran K, Bratasz A, Rivera BK, Kuppusamy P. Myocardial oxygenation and functional recovery in infarct rat hearts transplanted with mesenchymal stem cells. *Am J Physiol Heart Circ Physiol* 296: H1263–H1273, 2009. doi:10.1152/ajpheart.01311.2008.

73. Chance B. The energy-linked reaction of calcium with mitochondria. *J Biol Chem* 240: 2729–2748, 1965.

74. Chandel NS, Maltepe E, Goldwasser E, Mathieu CE, Simon MC, Schumacker PT. Mitochondrial reactive oxygen species trigger hypoxia-induced transcription. *Proc Natl Acad Sci USA* 95: 11715–11720, 1998. doi:10.1073/pnas.95.20.11715.

75. Chapple SJ, Keeley TP, Mastronicola D, Arno M, Vizcay-Barrena G, Fleck R, Siow RCM, Mann GE. Bach1 differentially regulates distinct Nrf2-dependent genes in human venous and coronary artery endothelial cells adapted to physiological oxygen levels. *Free Radic Biol Med* 92: 152–162, 2016. doi:10.1016/j.freeradbiomed.2015.12.013.

76. Charan NB, Thompson WH, Carvalho P. Functional anatomy of bronchial veins. *Pulm Pharmacol Ther* 20: 100–103, 2007. doi:10.1016/j.pupt.2006.03.004.

77. Chen B, Longtine MS, Nelson DM. Pericellular oxygen concentration of cultured primary human trophoblasts. *Placenta* 34: 106–109, 2013. doi:10.1016/j.placenta.2012.11.011.

78. Chen Q, Fischer A, Reagan JD, Yan L-J, Ames BN. Oxidative DNA damage and senescence of human diploid fibroblast cells. *Proc Natl Acad Sci USA* 92: 4337–4341, 1995. doi:10.1073/pnas.92.10.4337.

79. Chen X, Chen A, Woo TL, Choo AB, Reuveny S, Oh SK. Investigations into the metabolism of two-dimensional colony and suspended microcarrier cultures of human embryonic stem cells in serum-free media. *Stem Cells Dev* 19: 1781–1792, 2010. doi:10.1089/scd.2010.0077.

80. Chiu J-J, Chien S. Effects of disturbed flow on vascular endothelium: pathophysiological basis and clinical perspectives. *Physiol Rev* 91: 327–387, 2011. doi:10.1152/physrev.00047.2009.

81. Chou CC, Coatney RW. Nutrient-induced changes in intestinal blood flow in the dog. *Br Vet J* 150: 423–437, 1994. doi:10.1016/S0007-1935(05)80192-7.

82. Christensen DR, Calder PC, Houghton FD. Effect of oxygen tension on the amino acid utilisation of human embryonic stem cells. *Cell Physiol Biochem* 33: 237–246, 2014. doi:10.1159/000356665.

83. Christensen DR, Calder PC, Houghton FD. GLUT3 and PKM2 regulate OCT4 expression and support the hypoxic culture of human embryonic stem cells. *Sci Rep* 5: 17500, 2015. doi:10.1038/srep17500.

84. Chung Y. Myocardial Po2 does not limit aerobic metabolism in the postischemic heart. *Am J Physiol Heart Circ Physiol* 310: H226–H238, 2016. doi:10.1152/ajpheart.00335.2015.

85. Cieślar K, Stupar V, Canet-Soulas E, Gaillard S, Crémillieux Y. Alveolar oxygen partial pressure and oxygen depletion rate mapping in rats using 3He ventilation imaging. *Magn Reson Med* 57: 423–430, 2007. doi:10.1002/mrm.21110.

86. Clark CC, Tolin BS, Brighton CT. The effect of oxygen tension on proteoglycan synthesis and aggregation in mammalian growth plate chondrocytes. *J Orthop Res* 9: 477–484, 1991. doi:10.1002/jor.1100090403.

87. Clark LC Jr, Wolf R, Granger D, Taylor Z. Continuous recording of blood oxygen tensions by polarography. *J Appl Physiol* 6: 189–193, 1953. doi:10.1152/jappl.1953.6.3.189.

88. Clementi E, Brown GC, Foxwell N, Moncada S. On the mechanism by which vascular endothelial cells regulate their oxygen consumption. *Proc Natl Acad Sci USA* 96: 1559–1562, 1999. doi:10.1073/pnas.96.4.1559.

89. Coburn RF, Ploegmakers F, Gondrie P, Abboud R. Myocardial myoglobin oxygen tension. *Am J Physiol* 224: 870–876, 1973.

90. Cole RP, Sukanek PC, Wittenberg JB, Wittenberg BA. Mitochondrial function in the presence of myoglobin. *J Appl Physiol Respir Environ Exerc Physiol* 53: 1116–1124, 1982.

91. Coleman ML, McDonough MA, Hewitson KS, Coles C, Mecinovic J, Edelmann M, Cook KM, Cockman ME, Lancaster DE, Kessler BM, Oldham NJ, Ratcliffe PJ, Schofield CJ. Asparaginyl hydroxylation of the Notch ankyrin repeat domain by factor inhibiting hypoxia-inducible factor. *J Biol Chem* 282: 24027–24038, 2007. doi:10.1074/jbc.M704102200.

92. Colgan SP, Taylor CT. Hypoxia: an alarm signal during intestinal inflammation. *Nat Rev Gastroenterol Hepatol* 7: 281–287, 2010. doi:10.1038/nrgastro.2010.39.

93. Comerford KM, Wallace TJ, Karhausen J, Louis NA, Montalto MC, Colgan SP. Hypoxia-inducible factor-1-dependent regulation of the multidrug resistance (MDR1) gene. *Cancer Res* 62: 3387–3394, 2002.

94. Cooper GJ, Sherry KM, Thorpe JA. Changes in gastric tissue oxygenation during mobilisation for oesophageal replacement. *Eur J Cardiothorac Surg* 9: 158–160, 1995. doi:10.1016/S1010-7940(05)80065-X.

95. Copin JC, Gasche Y, Li Y, Chan PH. Prolonged hypoxia during cell development protects mature manganese superoxide dismutase-deficient astrocytes from damage by oxidative stress. *FASEB J* 15: 525–534, 2001. doi:10.1096/fj.00-0330com.

96. Coronel MM, Geusz R, Stabler CL. Mitigating hypoxic stress on pancreatic islets via in situ oxygen generating biomaterial. *Biomaterials* 129: 139–151, 2017. doi:10.1016/j.biomaterials.2017.03.018.

97. Crawford DW, Back LH, Cole MA. In vivo oxygen transport in the normal rabbit femoral arterial wall. *J Clin Invest* 65: 1498–1508, 1980. doi:10.1172/JCI109815.

98. Crawford DW, Blankenhorn DH. Arterial wall oxygenation, oxyradicals, and atherosclerosis. *Atherosclerosis* 89: 97–108, 1991. doi:10.1016/0021-9150(91)90049-9.

99. Crawford DW, Kramsch DM. The oxygen environment of the arterial media in early rabbit hypertension. *Exp Mol Pathol* 49: 215–233, 1988. doi:10.1016/0014-4800(88)90035-4.

100. Cross AR, Henderson L, Jones OT, Delpiano MA, Hentschel J, Acker H. Involvement of an NAD(P)H oxidase as a pO2 sensor protein in the rat carotid body. *Biochem J* 272: 743–747, 1990. doi:10.1042/bj2720743.

101. D'Ippolito G, Diabira S, Howard GA, Roos BA, Schiller PC. Low oxygen tension inhibits osteogenic differentiation and enhances stemness of human MIAMI cells. *Bone* 39: 513–522, 2006. doi:10.1016/j.bone.2006.02.061.

102. Daniel Y, Fait G, Lessing JB, Jaffa A, Gull I, Shenav M, Peyser MR, Kupferminc MJ. Umbilical cord blood acid-base values in uncomplicated term vaginal breech deliveries. *Acta Obstet Gynecol Scand* 77: 182–185, 1998. doi:10.1080/j.1600-0412.1998.770210.x.

103. Dardzinski BJ, Sotak CH. Rapid tissue oxygen tension mapping using 19F inversion-recovery echo-planar imaging of perfluoro-15-crown-5-ether. *Magn Reson Med* 32: 88–97, 1994. doi:10.1002/mrm.1910320112.

104. Das RHJ, van Osch GJVM, Kreukniet M, Oostra J, Weinans H, Jahr H. Effects of individual control of pH and hypoxia in chondrocyte culture. *J Orthop Res* 28: 537–545, 2010.

105. Degrossoli A, Arrais-Silva WW, Colhone MC, Gadelha FR, Joazeiro PP, Giorgio S. The influence of low oxygen on macrophage response to Leishmania infection. *Scand J Immunol* 74: 165–175, 2011. doi:10.1111/j.1365-3083.2011.02566.x.

106. del Peso L, Castellanos MC, Temes E, Martín-Puig S, Cuevas Y, Olmos G, Landázuri MO. The von Hippel Lindau/hypoxia-inducible factor (HIF) pathway regulates the transcription of the HIF-proline hydroxylase genes in response to low oxygen. *J Biol Chem* 278: 48690–48695, 2003. doi:10.1074/jbc.M308862200.

107. Deninger AJ, Eberle B, Ebert M, Grossmann T, Heil W, Kauczor H, Lauer L, Markstaller K, Otten E, Schmiedeskamp J, Schreiber W, Surkau R, Thelen M, Weiler N. Quantification of regional intrapulmonary oxygen partial pressure evolution during apnea by (3)He MRI. *J Magn Reson* 141: 207–216, 1999. doi:10.1006/jmre.1999.1902.

108. Di Marco G, Lanza M, Pieruccini M, Campagna S. A luminescent iridium (III) cyclometallated complex immobilized in a polymeric matrix as a solid-state oxygen sensor. *Adv Mater* 8: 576–580, 1996. doi:10.1002/adma.19960080709.

109. Dickinson JE, Eriksen NL, Meyer BA, Parisi VM. The effect of preterm birth on umbilical cord blood gases. *Obstet Gynecol* 79: 575–578, 1992.

110. Dijkhuizen P, Buursma A, Fongers TME, Gerding AM, Oeseburg B, Zijlstra WG. The oxygen binding capacity of human haemoglobin. Hüfner's factor redetermined. *Pflugers Arch* 369: 223–231, 1977. doi:10.1007/BF00582188.

111. Dings J, Meixensberger J, Jäger A, Roosen K. Clinical experience with 118 brain tissue oxygen partial pressure catheter probes. *Neurosurgery* 43: 1082–1095, 1998. doi:10.1097/00006123-199811000-00045.

112. Dionne KE. Oxygen transport to respiring myocytes. *J Biol Chem* 265: 15400–15402, 1990.

113. Dionne KE, Colton CK, Yarmush ML. Effect of oxygen on isolated pancreatic tissue. *ASAIO Trans* 35: 739–741, 1989. doi:10.1097/00002480-198907000-00185.

114. Dmitriev RI, Borisov SM, Kondrashina AV, Pakan JMP, Anilkumar U, Prehn JHM, Zhdanov AV, McDermott KW, Klimant I, Papkovsky DB. Imaging oxygen in neural cell and tissue models by means of anionic cell-permeable phosphorescent nanoparticles. *Cell Mol Life Sci* 72: 367–381, 2015. doi:10.1007/s00018-014-1673-5.

115. Dmitriev RI, Papkovsky DB. Optical probes and techniques for O2 measurement in live cells and tissue. *Cell Mol Life Sci* 69: 2025–2039, 2012. doi:10.1007/s00018-011-0914-0.

116. Dmitriev RI, Zhdanov AV, Jasionek G, Papkovsky DB. Assessment of cellular oxygen gradients with a panel of phosphorescent oxygen-sensitive probes. *Anal Chem* 84: 2930–2938, 2012. doi:10.1021/ac3000144.

117. Domm C, Schünke M, Christesen K, Kurz B. Redifferentiation of dedifferentiated bovine articular chondrocytes in alginate culture under low oxygen tension. *Osteoarthritis Cartilage* 10: 13–22, 2002. doi:10.1053/joca.2001.0477.

118. Domm C, Schünke M, Steinhagen J, Freitag S, Kurz B. Influence of various alginate brands on the redifferentiation of dedifferentiated bovine articular chondrocytes in alginate bead culture under high and low oxygen tension. *Tissue Eng* 10: 1796–1805, 2004. doi:10.1089/ten.2004.10.1796.

119. Dröge W. Free radicals in the physiological control of cell function. *Physiol Rev* 82: 47–95, 2002. doi:10.1152/physrev.00018.2001.

120. Duan L-J, Zhang-Benoit Y, Fong G-H. Endothelium-intrinsic requirement for Hif-2alpha during vascular development. *Circulation* 111: 2227–2232, 2005. doi:10.1161/01.CIR.0000163580.98098.A3.

121. Duchen MR, Biscoe TJ. Relative mitochondrial membrane potential and [Ca2+]i in type I cells isolated from the rabbit carotid body. *J Physiol* 450: 33–61, 1992. doi:10.1113/jphysiol.1992.sp019115.

122. Duling BR. Microvascular responses to alterations in oxygen tension. *Circ Res* 31: 481–489, 1972. doi:10.1161/01.RES.31.4.481.

123. Duling BR, Berne RM. Longitudinal gradients in periarteriolar oxygen tension. A possible mechanism for the participation of oxygen in local regulation of blood flow. *Circ Res* 27: 669–678, 1970. doi:10.1161/01.RES.27.5.669.

124. Duling BR, Kuschinsky W, Wahl M. Measurements of the perivascular Po_2 in the vicinity of the pial vessels of the cat. *Pflugers Arch* 383: 29–34, 1979. doi:10.1007/BF00584471.

125. Dunn JF, Grinberg O, Roche M, Nwaigwe CI, Hou HG, Swartz HM. Noninvasive assessment of cerebral oxygenation during acclimation to hypobaric hypoxia. *J Cereb Blood Flow Metab* 20: 1632–1635, 2000. doi:10.1097/00004647-200012000-00002.

126. Dvorak A, Tilley AE, Shaykhiev R, Wang R, Crystal RG. Do airway epithelium air-liquid cultures represent the in vivo airway epithelium transcriptome? *Am J Respir Cell Mol Biol* 44: 465–473, 2011. doi:10.1165/rcmb.2009-0453OC.

127. Eberle B, Weiler N, Markstaller K, Kauczor H, Deninger A, Ebert M, Grossmann T, Heil W, Lauer LO, Roberts TPL, Schreiber WG, Surkau R, Dick WF, Otten EW, Thelen M. Analysis of intrapulmonary O(2) concentration by MR imaging of inhaled hyperpolarized helium-3. *J Appl Physiol (1985)* 87: 2043–2052, 1999. doi:10.1152/jappl.1999.87.6.2043.

128. Ebert BL, Firth JD, Ratcliffe PJ. Hypoxia and mitochondrial inhibitors regulate expression of glucose transporter-1 via distinct Cis-acting sequences. *J Biol Chem* 270: 29083–29089, 1995. doi:10.1074/jbc.270.49.29083.

129. El Awad B, Kreft B, Wolber EM, Hellwig-Bürgel T, Metzen E, Fandrey J, Jelkmann W. Hypoxia and interleukin-1beta stimulate vascular endothelial growth factor production in human proximal tubular cells. *Kidney Int* 58: 43–50, 2000. doi:10.1046/j.1523-1755.2000.00139.x.

130. El Sabbahy M, Vaidya VS. Ischemic kidney injury and mechanisms of tissue repair. *Wiley Interdiscip Rev Syst Biol Med* 3: 606–618, 2011. doi:10.1002/wsbm.133.

131. Ellsworth ML, Pittman RN. Arterioles supply oxygen to capillaries by diffusion as well as by convection. *Am J Physiol* 258: H1240–H1243, 1990.

132. Emerling BM, Weinberg F, Snyder C, Burgess Z, Mutlu GM, Viollet B, Budinger GRS, Chandel NS. Hypoxic activation of AMPK is dependent on mitochondrial ROS but independent of an increase in AMP/ATP ratio. *Free Radic Biol Med* 46: 1386–1391, 2009. doi:10.1016/j.freeradbiomed.2009.02.019.

133. Engerman RL, Pfaffenbach D, Davis MD. Cell turnover of capillaries. *Lab Invest* 17: 738–743, 1967.

134. Epstein AC, Gleadle JM, McNeill LA, Hewitson KS, O'Rourke J, Mole DR, Mukherji M, Metzen E, Wilson MI, Dhanda A, Tian YM, Masson N, Hamilton DL, Jaakkola P, Barstead R, Hodgkin J, Maxwell PH, Pugh CW, Schofield CJ, Ratcliffe PJ. C. elegans EGL-9 and mammalian homologs define a family of dioxygenases that regulate HIF by prolyl hydroxylation. *Cell* 107: 43–54, 2001. doi:10.1016/S0092-8674(01)00507-4.

135. Ernst A, Alkass K, Bernard S, Salehpour M, Perl S, Tisdale J, Possnert G, Druid H, Frisén J. Neurogenesis in the striatum of the adult human brain. *Cell* 156: 1072–1083, 2014. doi:10.1016/j.cell.2014.01.044.

136. Esipova TV, Karagodov A, Miller J, Wilson DF, Busch TM, Vinogradov SA. Two new "protected" oxyphors for biological oximetry: properties and application in tumor imaging. *Anal Chem* 83: 8756–8765, 2011. doi:10.1021/ac2022234.

137. Etherington PJ, Winlove P, Taylor P, Paleolog E, Miotla JM. VEGF release is associated with reduced oxygen tensions in experimental inflammatory arthritis. *Clin Exp Rheumatol* 20: 799–805, 2002.

138. Evans NT, Naylor PF. The dynamics of changes in dermal oxygen tension. *Respir Physiol* 2: 61–72, 1966. doi:10.1016/0034-5687(66)90038-7.

139. Evans NT, Naylor PF. The oxygen tension gradient across human epidermis. *Respir Physiol* 3: 38–42, 1967. doi:10.1016/0034-5687(67)90021-7.

140. Evans NT, Naylor PF. Steady states of oxygen tension in human dermis. *Respir Physiol* 2: 46–60, 1966. doi:10.1016/0034-5687(66)90037-5.

141. Evans RG, Smith DW, Khan Z, Ngo JP, Gardiner BS. Letter to the editor: "The plausibility of arterial-to-venous oxygen shunting in the kidney: it all depends on radial geometry". *Am J Physiol Renal Physiol* 309: F179–F180, 2015. doi:10.1152/ajprenal.00094.2015.

142. Ezashi T, Das P, Roberts RM. Low O2 tensions and the prevention of differentiation of hES cells. *Proc Natl Acad Sci USA* 102: 4783–4788, 2005. doi:10.1073/pnas.0501283102.

143. Falchuk KH, Goetzl EJ, Kulka JP. Respiratory gases of synovial fluids. An approach to synovial tissue circulatory-metabolic imbalance in rheumatoid arthritis. *Am J Med* 49: 223–231, 1970. doi:10.1016/S0002-9343(70)80078-X.

144. Falstie-Jensen N, Spaun E, Brøchner-Mortensen J, Falstie-Jensen S. The influence of epidermal thickness on transcutaneous oxygen pressure measurements in normal persons. *Scand J Clin Lab Invest* 48: 519–523, 1988. doi:10.3109/00365518809085767.

145. Famulla S, Schlich R, Sell H, Eckel J. Differentiation of human adipocytes at physiological oxygen levels results in increased adiponectin secretion and isoproterenol-stimulated lipolysis. *Adipocyte* 1: 132–181, 2012. doi:10.4161/adip.19962.

146. Fan J, Cai H, Yang S, Yan L, Tan W. Comparison between the effects of normoxia and hypoxia on antioxidant enzymes and glutathione redox state in ex vivo culture of CD34(+) cells. *Comp Biochem Physiol B Biochem Mol Biol* 151: 153–158, 2008. doi:10.1016/j.cbpb.2008.06.008.

147. Faubert B, Boily G, Izreig S, Griss T, Samborska B, Dong Z, Dupuy F, Chambers C, Fuerth BJ, Viollet B, Mamer OA, Avizonis D, DeBerardinis RJ, Siegel PM, Jones RG. AMPK is a negative regulator of the Warburg effect and suppresses tumor growth in vivo. *Cell Metab* 17: 113–124, 2013. doi:10.1016/j.cmet.2012.12.001.

148. Federspiel WJ, Popel AS. A theoretical analysis of the effect of the particulate nature of blood on oxygen release in capillaries. *Microvasc Res* 32: 164–189, 1986. doi:10.1016/0026-2862(86)90052-X.

149. Fehrer C, Brunauer R, Laschober G, Unterluggauer H, Reitinger S, Kloss F, Gülly C, Gassner R, Lepperdinger G. Reduced oxygen tension attenuates differentiation ca-

pacity of human mesenchymal stem cells and prolongs their lifespan. *Aging Cell* 6: 745–757, 2007. doi:10.1111/j.1474-9726.2007.00336.x.

150. Feola M, Azar D, Wiener L. Improved oxygenation of ischemic myocardium by hemodilution with stroma-free hemoglobin solution. *Chest* 75: 369–375, 1979. doi:10.1378/chest.75.3.369.

151. Fercher A, Borisov SM, Zhdanov AV, Klimant I, Papkovsky DB. Intracellular O2 sensing probe based on cell-penetrating phosphorescent nanoparticles. *ACS Nano* 5: 5499–5508, 2011. doi:10.1021/nn200807g.

152. Ferrell WR, Najafipour H. Changes in synovial Po_2 and blood flow in the rabbit knee joint due to stimulation of the posterior articular nerve. *J Physiol* 449: 607–617, 1992. doi:10.1113/jphysiol.1992.sp019104.

153. Fick AV. On liquid diffusion. *Lond Edinb Dublin Philos Mag J Sci* 10: 30–39, 1855. doi:10.1080/14786445508641925.

154. Fiegl M, Samudio I, Clise-Dwyer K, Burks JK, Mnjoyan Z, Andreeff M. CXCR4 expression and biologic activity in acute myeloid leukemia are dependent on oxygen partial pressure. *Blood* 113: 1504–1512, 2009. doi:10.1182/blood-2008-06-161539.

155. Fischer B, Bavister BD. Oxygen tension in the oviduct and uterus of rhesus monkeys, hamsters and rabbits. *J Reprod Fertil* 99: 673–679, 1993. doi:10.1530/jrf.0.0990673.

156. Fischer MC, Spector ZZ, Ishii M, Yu J, Emami K, Itkin M, Rizi R. Single-acquisition sequence for the measurement of oxygen partial pressure by hyperpolarized gas MRI. *Magn Reson Med* 52: 766–773, 2004. doi:10.1002/mrm.20239.

157. Fisher EM, Khan M, Salisbury R, Kuppusamy P. Noninvasive monitoring of small intestinal oxygen in a rat model of chronic mesenteric ischemia. *Cell Biochem Biophys* 67: 451–459, 2013. doi:10.1007/s12013-013-9611-y.

158. Forristal CE, Christensen DR, Chinnery FE, Petruzzelli R, Parry KL, Sanchez-Elsner T, Houghton FD. Environmental oxygen tension regulates the energy metabolism and self-renewal of human embryonic stem cells. *PLoS One* 8: e62507, 2013. doi:10.1371/journal.pone.0062507.

159. Forstner H, Gnaiger E (editors). *Polarographic Oxygen Sensors*. New York: Springer, 1983, p. 321–333. doi:10.1007/978-3-642-81863-9_28

160. Forsyth NR, Kay A, Hampson K, Downing A, Talbot R, McWhir J. Transcriptome alterations due to physiological normoxic (2% O2) culture of human embryonic stem cells. *Regen Med* 3: 817–833, 2008. doi:10.2217/17460751.3.6.817.

161. Forsyth NR, Musio A, Vezzoni P, Simpson AHRW, Noble BS, McWhir J. Physiologic oxygen enhances human embryonic stem cell clonal recovery and reduces chromosomal abnormalities. *Cloning Stem Cells* 8: 16–23, 2006. doi:10.1089/clo.2006.8.16.

162. Forsythe JA, Jiang B-H, Iyer NV, Agani F, Leung SW, Koos RD, Semenza GL. Activation of vascular endothelial growth factor gene transcription by hypoxia-inducible factor 1. *Mol Cell Biol* 16: 4604–4613, 1996. doi:10.1128/MCB.16.9.4604.

163. Foster ME, Laycock JRD, Silver IA, Leaper DJ. Hypovolaemia and healing in colonic anastomoses. *Br J Surg* 72: 831–834, 1985. doi:10.1002/bjs.1800721019.

164. Fox MD, Raichle ME. Spontaneous fluctuations in brain activity observed with functional magnetic resonance imaging. *Nat Rev Neurosci* 8: 700–711, 2007. doi:10.1038/nrn2201.

165. Foy BD, Rotem A, Toner M, Tompkins RG, Yarmush ML. A device to measure the oxygen uptake rate of attached cells: importance in bioartificial organ design. *Cell Transplant* 3: 515–527, 1994. doi:10.1177/096368979400300609.

166. Fraker CA, Cechin S, Álvarez-Cubela S, Echeverri F, Bernal A, Poo R, Ricordi C, Inverardi L, Domínguez-Bendala J. A physiological pattern of oxygenation using perfluorocarbon-based culture devices maximizes pancreatic islet viability and enhances β-cell function. *Cell Transplant* 22: 1723–1733, 2013. doi:10.3727/096368912X657873.

167. Fu Q, Colgan SP, Shelley CS. Hypoxia: The Force that Drives Chronic Kidney Disease. *Clin Med Res* 14: 15–39, 2016. doi:10.3121/cmr.2015.1282.

168. Fu XW, Wang D, Nurse CA, Dinauer MC, Cutz E. NADPH oxidase is an O2 sensor in airway chemoreceptors: evidence from K+ current modulation in wild-type and oxidase-deficient mice. *Proc Natl Acad Sci USA* 97: 4374–4379, 2000. doi:10.1073/pnas.97.8.4374.

169. Fujibayashi Y, Cutler CS, Anderson CJ, McCarthy DW, Jones LA, Sharp T, Yonekura Y, Welch MJ. Comparative studies of Cu-64-ATSM and C-11-acetate in an acute myocardial infarction model: ex vivo imaging of hypoxia in rats. *Nucl Med Biol* 26: 117–121, 1999. doi:10.1016/S0969-8051(98)00049-3.

170. Furuta GT, Turner JR, Taylor CT, Hershberg RM, Comerford K, Narravula S, Podolsky DK, Colgan SP. Hypoxia-inducible factor 1-dependent induction of intestinal trefoil factor protects barrier function during hypoxia. *J Exp Med* 193: 1027–1034, 2001. doi:10.1084/jem.193.9.1027.

171. Futalan D, Huang C-T, Schmidt-Wolf IGH, Larsson M, Messmer D. Effect of oxygen levels on the physiology of dendritic cells: implications for adoptive cell therapy. *Mol Med* 17: 910–916, 2011. doi:10.2119/molmed.2011.00031.

172. Garcia-Ochoa F, Gomez E. Bioreactor scale-up and oxygen transfer rate in microbial processes: an overview. *Biotechnol Adv* 27: 153–176, 2009. doi:10.1016/j.biotechadv.2008.10.006.

173. Garreta E, Melo E, Navajas D, Farré R. Low oxygen tension enhances the generation of lung progenitor cells from mouse embryonic and induced pluripotent stem cells. *Physiol Rep* 2: e12075, 2014. doi:10.14814/phy2.12075.

174. Garris DR, Mitchell JA. Intrauterine oxygen tension during the estrous cycle in the guinea pig: its relation to uterine blood volume and plasma estrogen and progesterone levels. *Biol Reprod* 21: 149–159, 1979. doi:10.1095/biolreprod21.1.149.

175. Gey GO. An Improved Technic for Massive Tissue Culture. *Am J Cancer* 17: 752–756, 1933.

176. Gibbons J, Hewitt E, Gardner DK. Effects of oxygen tension on the establishment and lactate dehydrogenase activity of murine embryonic stem cells. *Cloning Stem Cells* 8: 117–122, 2006. doi:10.1089/clo.2006.8.117.

177. Gimble JM, Bunnell BA, Frazier T, Rowan B, Shah F, Thomas-Porch C, Wu X. Adipose-derived stromal/stem cells: a primer. *Organogenesis* 9: 3–10, 2013. doi:10.4161/org.24279.

178. Ginouvès A, Ilc K, Macías N, Pouysségur J, Berra E. PHDs overactivation during chronic hypoxia "desensitizes" HIFalpha and protects cells from necrosis. *Proc Natl Acad Sci USA* 105: 4745–4750, 2008. doi:10.1073/pnas.0705680105.

179. Giulivi C, Hochstein P, Davies KJ. Hydrogen peroxide production by red blood cells. *Free Radic Biol Med* 16: 123–129, 1994. doi:10.1016/0891-5849(94)90249-6.

180. Glover LE, Bowers BE, Saeedi B, Ehrentraut SF, Campbell EL, Bayless AJ, Dobrinskikh E, Kendrick AA, Kelly CJ, Burgess A, Miller L, Kominsky DJ, Jedlicka P, Colgan SP. Control of creatine metabolism by HIF is an endogenous mechanism of barrier regulation in colitis. *Proc Natl Acad Sci USA* 110: 19820–19825, 2013. doi:10.1073/pnas.1302840110.

181. Gnaiger E, Lassnig B, Kuznetsov A, Rieger G, Margreiter R. Mitochondrial oxygen affinity, respiratory flux control and excess capacity of cytochrome c oxidase. *J Exp Biol* 201: 1129–1139, 1998.

182. Golub AS, Barker MC, Pittman RN. Microvascular oxygen tension in the rat mesentery. *Am J Physiol Heart Circ Physiol* 294: H21–H28, 2008. doi:10.1152/ajpheart.00861.2007.

183. Golub AS, Barker MC, Pittman RN. Po_2 profiles near arterioles and tissue oxygen consumption in rat mesentery. *Am J Physiol Heart Circ Physiol* 293: H1097–H1106, 2007. doi:10.1152/ajpheart.00077.2007.

184. Golub AS, Pittman RN. Erythrocyte-associated transients in Po_2 revealed in capillaries of rat mesentery. *Am J Physiol Heart Circ Physiol* 288: H2735–H2743, 2005. doi:10.1152/ajpheart.00711.2004.

185. Golub AS, Pittman RN. Po_2 measurements in the microcirculation using phosphorescence quenching microscopy at high magnification. *Am J Physiol Heart Circ Physiol* 294: H2905–H2916, 2008. doi:10.1152/ajpheart.01347.2007.

186. Gomes Sobrinho DB, Oliveira JBA, Petersen CG, Mauri AL, Silva LFI, Massaro FC, Baruffi RLR, Cavagna M, Franco JG Jr. IVF/ICSI outcomes after culture of human embryos at low oxygen tension: a meta-analysis. *Reprod Biol Endocrinol* 9: 143, 2011. doi:10.1186/1477-7827-9-143.

187. Goossens GH, Bizzarri A, Venteclef N, Essers Y, Cleutjens JP, Konings E, Jocken JWE, Cajlakovic M, Ribitsch V, Clément K, Blaak EE. Increased adipose tissue oxygen tension in obese compared with lean men is accompanied by insulin resistance, impaired adipose tissue capillarization, and inflammation. *Circulation* 124: 67–76, 2011. doi:10.1161/CIRCULATIONAHA.111.027813.

188. Goossens GH, Blaak EE. Adipose tissue dysfunction and impaired metabolic health in human obesity: a matter of oxygen? *Front Endocrinol (Lausanne)* 6: 55, 2015.

189. Grahl N, Puttikamonkul S, Macdonald JM, Gamcsik MP, Ngo LY, Hohl TM, Cramer RA. In vivo hypoxia and a fungal alcohol dehydrogenase influence the pathogenesis of invasive pulmonary aspergillosis. *PLoS Pathog* 7: e1002145, 2011. doi:10.1371/journal.ppat.1002145.

190. Grainger CI, Greenwell LL, Lockley DJ, Martin GP, Forbes B. Culture of Calu-3 cells at the air interface provides a representative model of the airway epithelial barrier. *Pharm Res* 23: 1482–1490, 2006. doi:10.1007/s11095-006-0255-0.

191. Granger DN, Kvietys PR, Korthuis RJ, Premen AJ. Microcirculation of the intestinal mucosa. *Compr Physiol*, 2011. doi:10.1002/cphy.cp060139.

192. Grant JL, Smith B. Bone marrow gas tensions, bone marrow blood flow, and erythropoiesis in man. *Ann Intern Med* 58: 801–809, 1963. doi:10.7326/0003-4819-58-5-801.

193. Graven KK, Bellur D, Klahn BD, Lowrey SL, Amberger E. HIF-2alpha regulates glyceraldehyde-3-phosphate dehydrogenase expression in endothelial cells. *Biochim Biophys Acta* 1626: 10–18, 2003. doi:10.1016/S0167-4781(03)00049-6.

194. Gregory IC. The oxygen and carbon monoxide capacities of fetal and adult blood. *J Physiol* 236: 625–634, 1974. doi:10.1113/jphysiol.1974.sp010456.

195. Griffith OW, Meister A. Glutathione: interorgan translocation, turnover, and metabolism. *Proc Natl Acad Sci USA* 76: 5606–5610, 1979. doi:10.1073/pnas.76.11.5606.

196. Grimshaw MJ, Mason RM. Bovine articular chondrocyte function in vitro depends upon oxygen tension. *Osteoarthritis Cartilage* 8: 386–392, 2000. doi:10.1053/joca.1999.0314.

197. Grinnell F. Fibroblast biology in three-dimensional collagen matrices. *Trends Cell Biol* 13: 264–269, 2003. doi:10.1016/S0962-8924(03)00057-6.

198. Gruden G, Thomas S, Burt D, Lane S, Chusney G, Sacks S, Viberti G. Mechanical stretch induces vascular permeability factor in human mesangial cells: mechanisms of signal transduction. *Proc Natl Acad Sci USA* 94: 12112–12116, 1997. doi:10.1073/pnas.94.22.12112.

199. Guarino RD, Dike LE, Haq TA, Rowley JA, Pitner JB, Timmins MR. Method for determining oxygen consumption rates of static cultures from microplate measurements of pericellular dissolved oxygen concentration. *Biotechnol Bioeng* 86: 775–787, 2004. doi:10.1002/bit.20072.

201. Gullichsen E, Nelimarkka O, Halkola L, Niinikoski J. Renal oxygenation in endotoxin shock in dogs. *Crit Care Med* 17: 547–550, 1989. doi:10.1097/00003246-198906000-00013.

202. Gundry SR, Wang N, Sciolaro CM, Van Arsdell GS, Razzouk AJ, Hill AC, Bailey LL. Uniformity of perfusion in all regions of the human heart by warm continuous retrograde cardioplegia. *Ann Thorac Surg* 61: 33–35, 1996. doi:10.1016/0003-4975(95)00880-2.

203. Gunther H, Aumuller G, Kunke SVP, Thews G. Die Sauerstoffversorgung der Niere. 1. Verteilung der O2-Drucke in der Rattenniere unter Normbedingungen. *Resp Exp Med* 163: 251–264, 1974.

204. Guo R, Xu X, Lu Y, Xie X. Physiological oxygen tension reduces hepatocyte dedifferentiation in in vitro culture. *Sci Rep* 7: 5923, 2017. doi:10.1038/s41598-017-06433-3.

205. Gustafsson U, Persson JK, Suneson A, Kjellström BT. Microvascular lung tissue oxygenation--a methodological study in the pig. *Ann Acad Med Singapore* 28: 3–7, 1999.

206. Guzy RD, Hoyos B, Robin E, Chen H, Liu L, Mansfield KD, Simon MC, Hammerling U, Schumacker PT. Mitochondrial complex III is required for hypoxia-induced ROS production and cellular oxygen sensing. *Cell Metab* 1: 401–408, 2005. doi:10.1016/j.cmet.2005.05.001.

207. Guzy RD, Schumacker PT. Oxygen sensing by mitochondria at complex III: the paradox of increased reactive oxygen species during hypoxia. *Exp Physiol* 91: 807–819, 2006. doi:10.1113/expphysiol.2006.033506.

208. Haas B, Chrusciel S, Fayad-Kobeissi S, Dubois-Randé J-L, Azuaje F, Boczkowski J, Motterlini R, Foresti R. Permanent culture of macrophages at physiological oxygen attenuates the antioxidant and immunomodulatory properties of dimethyl fumarate. *J Cell Physiol* 230: 1128–1138, 2015. doi:10.1002/jcp.24844.

209. Haase VH. Hypoxia-inducible factors in the kidney. *Am J Physiol Renal Physiol* 291: F271–F281, 2006. doi:10.1152/ajprenal.00071.2006.

210. Haddad H, Windgassen D, Ramsborg CG, Paredes CJ, Papoutsakis ET. Molecular understanding of oxygen-tension and patient-variability effects on ex vivo expanded T cells. *Biotechnol Bioeng* 87: 437–450, 2004. doi:10.1002/bit.20166.

211. Hagen T, Taylor CT, Lam F, Moncada S. Redistribution of intracellular oxygen in hypoxia by nitric oxide: effect on HIF1alpha. *Science* 302: 1975–1978, 2003. doi:10.1126/science.1088805.

212. Haisjackl M, Germann R, Hasibeder W, Schwarz B, Salak N, Pajk W, Bonatti J, Nussbaumer W, Klima G, Kox W, Mutz N. Mucosal tissue oxygenation of the porcine jejunum during normothermic cardiopulmonary bypass. *Br J Anaesth* 82: 738–745, 1999. doi:10.1093/bja/82.5.738.

213. Haisjackl M, Luz G, Sparr H, Germann R, Salak N, Friesenecker B, Deusch E, Meusburger S, Hasibeder W. The effects of progressive anemia on jejunal mucosal and serosal tissue oxygenation in pigs. *Anesth Analg* 84: 538–544, 1997.

214. Hajjar DP, Farber IC, Smith SC. Oxygen tension within the arterial wall: relationship to altered bioenergetic metabolism and lipid accumulation. *Arch Biochem Biophys* 262: 375–380, 1988. doi:10.1016/0003-9861(88)90201-9.

215. Halliwell B. Oxidative stress in cell culture: an under-appreciated problem? *FEBS Lett* 540: 3–6, 2003. doi:10.1016/S0014-5793(03)00235-7.

216. Hamedani H, Kadlecek SJ, Ishii M, Emami K, Kuzma NN, Xin Y, Rossman M, Rizi RR. A variability study of regional alveolar oxygen tension measurement in humans using hyperpolarized (3) He MRI. *Magn Reson Med* 70: 1557–1566, 2013. doi:10.1002/mrm.24604.

217. Hamedani H, Shaghaghi H, Kadlecek SJ, Xin Y, Han B, Siddiqui S, Rajaei J, Ishii M, Rossman M, Rizi RR. Vertical gradients in regional alveolar oxygen tension in supine human lung imaged by hyperpolarized 3He MRI. *NMR Biomed* 27: 1439–1450, 2014. doi:10.1002/nbm.3227.

218. Hannah S, Mecklenburgh K, Rahman I, Bellingan GJ, Greening A, Haslett C, Chilvers ER. Hypoxia prolongs neutrophil survival in vitro. *FEBS Lett* 372: 233–237, 1995. doi:10.1016/0014-5793(95)00986-J.

219. Hara S, Hamada J, Kobayashi C, Kondo Y, Imura N. Expression and characterization of hypoxia-inducible factor (HIF)-3alpha in human kidney: suppression of HIF-mediated gene expression by HIF-3alpha. *Biochem Biophys Res Commun* 287: 808–813, 2001. doi:10.1006/bbrc.2001.5659.

220. Hardie DG, Hawley SA, Scott JW. AMP-activated protein kinase--development of the energy sensor concept. *J Physiol* 574: 7–15, 2006. doi:10.1113/jphysiol.2006.108944.

221. Hardie DG, Ross FA, Hawley SA. AMPK: a nutrient and energy sensor that maintains energy homeostasis. *Nat Rev Mol Cell Biol* 13: 251–262, 2012. doi:10.1038/nrm3311.

222. Harman D. Aging: a theory based on free radical and radiation chemistry. *J Gerontol* 11: 298–300, 1956. doi:10.1093/geronj/11.3.298.

223. Harms FA, Bodmer SIA, Raat NJH, Stolker RJ, Mik EG. Validation of the protoporphyrin IX-triplet state lifetime technique for mitochondrial oxygen measurements in the skin. *Opt Lett* 37: 2625–2627, 2012. doi:10.1364/OL.37.002625.

224. Harms FA, de Boon WM, Balestra GM, Bodmer SI, Johannes T, Stolker RJ, Mik EG. Oxygen-dependent delayed fluorescence measured in skin after topical application of 5-aminolevulinic acid. *J Biophotonics* 4: 731–739, 2011. doi:10.1002/jbio.201100040.

225. Harms FA, Voorbeijtel WJ, Bodmer SIA, Raat NJH, Mik EG. Cutaneous respirometry by dynamic measurement of mitochondrial oxygen tension for monitoring mitochondrial function in vivo. *Mitochondrion* 13: 507–514, 2013. doi:10.1016/j.mito.2012.10.005.

226. Harper SL, Pitts VH, Granger DN, Kvietys PR. Pancreatic tissue oxygenation during secretory stimulation. *Am J Physiol* 250: G316–G322, 1986.

227. Harrison JS, Rameshwar P, Chang V, Bandari P. Oxygen saturation in the bone marrow of healthy volunteers. *Blood* 99: 394, 2002. doi:10.1182/blood.V99.1.394.

228. He G, Shankar RA, Chzhan M, Samouilov A, Kuppusamy P, Zweier JL. Noninvasive measurement of anatomic structure and intraluminal oxygenation in the gastrointestinal tract of living mice with spatial and spectral EPR imaging. *Proc Natl Acad Sci USA* 96: 4586–4591, 1999. doi:10.1073/pnas.96.8.4586.

229. He L, Dinger B, Sanders K, Hoidal J, Obeso A, Stensaas L, Fidone S, Gonzalez C. Effect of p47phox gene deletion on ROS production and oxygen sensing in mouse carotid body chemoreceptor cells. *Am J Physiol Lung Cell Mol Physiol* 289: L916–L924, 2005. doi:10.1152/ajplung.00015.2005.

230. Heistad DD, Armstrong ML, Amundsen S. Blood flow through vasa vasorum in arteries and veins: effects of luminal Po_2. *Am J Physiol* 250: H434–H442, 1986.

231. Hellums JD. The resistance to oxygen transport in the capillaries relative to that in the surrounding tissue. *Microvasc Res* 13: 131–136, 1977. doi:10.1016/0026-2862(77)90122-4.

232. Hemann MT, Greider CW. Wild-derived inbred mouse strains have short telomeres. *Nucleic Acids Res* 28: 4474–4478, 2000. doi:10.1093/nar/28.22.4474.

233. Henderson JH, Ginley NM, Caplan AI, Niyibizi C, Dennis JE. Low oxygen tension during incubation periods of chondrocyte expansion is sufficient to enhance postexpansion chondrogenesis. *Tissue Eng Part A* 16: 1585–1593, 2010. doi:10.1089/ten.tea.2009.0411.

234. Hendgen-Cotta UB, Kelm M, Rassaf T. Myoglobin functions in the heart. *Free Radic Biol Med* 73: 252–259, 2014. doi:10.1016/j.freeradbiomed.2014.05.005.

235. Henry W. Experiments on the quantity of gases absorbed by water, at different temperatures, and under different pressures. *Philos Trans R Soc Lond* 93: 29–274, 1803. doi:10.1098/rstl.1803.0004.

236. Herold U, Jakob H, Kamler M, Thiele R, Tochtermann U, Weinmann J, Motsch J, Gebhard MM, Hagl S. Interruption of bronchial circulation leads to a severe decrease in peribronchial oxygen tension in standard lung transplantation technique. *Eur J Cardiothorac Surg* 13: 176–183, 1998. doi:10.1016/S1010-7940(97)00314-X.

237. Heughan C, Niinikoski J, Hunt TK. Oxygen tensions in lesions of experimental atherosclerosis of rabbits. *Atherosclerosis* 17: 361–367, 1973. doi:10.1016/0021-9150(73)90027-0.

238. Hewitson KS, McNeill LA, Riordan MV, Tian YM, Bullock AN, Welford RW, Elkins JM, Oldham NJ, Bhattacharya S, Gleadle JM, Ratcliffe PJ, Pugh CW, Schofield CJ. Hypoxia-inducible factor (HIF) asparagine hydroxylase is identical to factor inhibiting HIF (FIH) and is related to the cupin structural family. *J Biol Chem* 277: 26351–26355, 2002. doi:10.1074/jbc.C200273200.

239. Heywood HK, Lee DA. Bioenergetic reprogramming of articular chondrocytes by exposure to exogenous and endogenous reactive oxygen species and its role in the anabolic response to low oxygen. *J Tissue Eng Regen Med* 11: 2286–2294, 2017. doi:10.1002/term.2126.

240. Heywood HK, Lee DA. Low oxygen reduces the modulation to an oxidative phenotype in monolayer-expanded chondrocytes. *J Cell Physiol* 222: 248–253, 2010. doi:10.1002/jcp.21946.

241. Hirao M, Hashimoto J, Yamasaki N, Ando W, Tsuboi H, Myoui A, Yoshikawa H. Oxygen tension is an important mediator of the transformation of osteoblasts to osteocytes. *J Bone Miner Metab* 25: 266–276, 2007. doi:10.1007/s00774-007-0765-9.

242. Hirao M, Tamai N, Tsumaki N, Yoshikawa H, Myoui A. Oxygen tension regulates chondrocyte differentiation and function during endochondral ossification. *J Biol Chem* 281: 31079–31092, 2006. doi:10.1074/jbc.M602296200.

243. Hirsilä M, Koivunen P, Günzler V, Kivirikko KI, Myllyharju J. Characterization of the human prolyl 4-hydroxylases that modify the hypoxia-inducible factor. *J Biol Chem* 278: 30772–30780, 2003. doi:10.1074/jbc.M304982200.

244. Hirst DG, Denekamp J, Hobson B. Proliferation studies of the endothelial and smooth muscle cells of the mouse mesentery after irradiation. *Cell Tissue Kinet* 13: 91–104, 1980.

245. Hobbhahn J, Conzen PF, Goetz A, Seidl G, Gonschior P, Brendel W, Peter K. Myocardial surface Po_2--an indicator of myocardial tissue oxygenation? *Cardiovasc Res* 23: 529–540, 1989. doi:10.1093/cvr/23.6.529.

246. Hodson L. Adipose tissue oxygenation: Effects on metabolic function. *Adipocyte* 3: 75–80, 2014. doi:10.4161/adip.27114.

247. Hoffman WE, Charbel FT, Edelman G. Brain tissue oxygen, carbon dioxide, and pH in neurosurgical patients at risk for ischemia. *Anesth Analg* 82: 582–586, 1996.

248. Hoffman WE, Charbel FT, Edelman G, Ausman JI. Brain tissue oxygenation in patients with cerebral occlusive disease and arteriovenous malformations. *Br J Anaesth* 78: 169–171, 1997. doi:10.1093/bja/78.2.169.

249. Holmquist-Mengelbier L, Fredlund E, Löfstedt T, Noguera R, Navarro S, Nilsson H, Pietras A, Vallon-Christersson J, Borg A, Gradin K, Poellinger L, Påhlman S. Recruitment of HIF-1alpha and HIF-2alpha to common target genes is differentially regulated in neuroblastoma: HIF-2alpha promotes an aggressive phenotype. *Cancer Cell* 10: 413–423, 2006. doi:10.1016/j.ccr.2006.08.026.

250. Holzer C, Maier P. Maintenance of periportal and pericentral oxygen tensions in primary rat hepatocyte cultures: influence on cellular DNA and protein content monitored by flow cytometry. *J Cell Physiol* 133: 297–304, 1987. doi:10.1002/jcp.1041330213.

251. Holzwarth C, Vaegler M, Gieseke F, Pfister SM, Handgretinger R, Kerst G, Müller I. Low physiologic oxygen tensions reduce proliferation and differentiation of human multipotent mesenchymal stromal cells. *BMC Cell Biol* 11: 11, 2010. doi:10.1186/1471-2121-11-11.

252. Honig CR, Gayeski TE. Precapillary O2 loss and arteriovenous O2 diffusion shunt are below limit of detection in myocardium. *Adv Exp Med Biol* 248: 591–599, 1989. doi:10.1007/978-1-4684-5643-1_66.

253. Hoogsteen IJ, Lok J, Marres HAM, Takes RP, Rijken PFJW, van der Kogel AJ, Kaanders JHAM. Hypoxia in larynx carcinomas assessed by pimonidazole binding and the value of CA-IX and vascularity as surrogate markers of hypoxia. *Eur J Cancer* 45: 2906–2914, 2009. doi:10.1016/j.ejca.2009.07.012.

254. Horak P, Crawford AR, Vadysirisack DD, Nash ZM, DeYoung MP, Sgroi D, Ellisen LW. Negative feedback control of HIF-1 through REDD1-regulated ROS suppresses tumorigenesis. *Proc Natl Acad Sci USA* 107: 4675–4680, 2010. doi:10.1073/pnas.0907705107.

255. Horie N, So K, Moriya T, Kitagawa N, Tsutsumi K, Nagata I, Shinohara K. Effects of oxygen concentration on the proliferation and differentiation of mouse neural stem cells in vitro. *Cell Mol Neurobiol* 28: 833–845, 2008. doi:10.1007/s10571-007-9237-y.

256. Hosford PS, Millar J, Ramage AG, Marina N. Abnormal oxygen homeostasis in the nucleus tractus solitarii of the spontaneously hypertensive rat. *Exp Physiol* 102: 389–396, 2017. doi:10.1113/EP086023.

257. Hu C-J, Wang L-Y, Chodosh LA, Keith B, Simon MC. Differential roles of hypoxia-inducible factor 1α (HIF-1α) and HIF-2α in hypoxic gene regulation. *Mol Cell Biol* 23: 9361–9374, 2003. doi:10.1128/MCB.23.24.9361-9374.2003.

258. Huang Z, Fujiwara K, Minamide R, Hasegawa K, Yoshikawa K. Necdin controls proliferation and apoptosis of embryonic neural stem cells in an oxygen tension-dependent manner. *J Neurosci* 33: 10362–10373, 2013. doi:10.1523/JNEUROSCI.5682-12.2013.

259. Ikejiri A, Nagai S, Goda N, Kurebayashi Y, Osada-Oka M, Takubo K, Suda T, Koyasu S. Dynamic regulation of Th17 differentiation by oxygen concentrations. *Int Immunol* 24: 137–146, 2012. doi:10.1093/intimm/dxr111.

260. Intaglietta M, Johnson PC, Winslow RM. Microvascular and tissue oxygen distribution. *Cardiovasc Res* 32: 632–643, 1996. doi:10.1016/S0008-6363(96)00110-1.

261. Ishii T, Itoh K, Takahashi S, Sato H, Yanagawa T, Katoh Y, Bannai S, Yamamoto M. Transcription factor Nrf2 coordinately regulates a group of oxidative stress-inducible genes in macrophages. *J Biol Chem* 275: 16023–16029, 2000. doi:10.1074/jbc.275.21.16023.

262. Ishikawa Y, Ito T. Kinetics of hemopoietic stem cells in a hypoxic culture. *Eur J Haematol* 40: 126–129, 1988. doi:10.1111/j.1600-0609.1988.tb00808.x.

263. Ivanov KP, Derry AN, Vovenko EP, Samoilov MO, Semionov DG. Direct measurements of oxygen tension at the surface of arterioles, capillaries and venules of the cerebral cortex. *Pflugers Arch* 393: 118–120, 1982. doi:10.1007/BF00582403.

264. Jacobi CA, Zieren HU, Müller JM, Adili F, Pichlmaier H. Anastomotic tissue oxygen tension during esophagectomy in patients with esophageal carcinoma. *Eur Surg Res* 28: 26–31, 1996. doi:10.1159/000129436.

265. Jacobi CA, Zieren HU, Zieren J, Müller JM. Is tissue oxygen tension during esophagectomy a predictor of esophagogastric anastomotic healing? *J Surg Res* 74: 161–164, 1998. doi:10.1006/jsre.1997.5239.

266. Jamieson D, van den Brenk HAS. Electrode size and tissue pO2 measurement in rats exposed to air or high pressure oxygen. *J Appl Physiol* 20: 514–518, 1965. doi:10.1152/jappl.1965.20.3.514.

267. Janne d'Othée B, Rachmuth G, Munasinghe J, Lang EV. The effect of hyperoxygenation on T1 relaxation time in vitro. *Acad Radiol* 10: 854–860, 2003. doi:10.1016/S1076-6332(03)00004-7.

268. Jansson L, Barbu A, Bodin B, Drott CJ, Espes D, Gao X, Grapensparr L, Källskog Ö, Lau J, Liljebäck H, Palm F, Quach M, Sandberg M, Strömberg V, Ullsten S, Carlsson P-O. Pancreatic islet blood flow and its measurement. *Ups J Med Sci* 121: 81–95, 2016. doi:10.3109/03009734.2016.1164769.

269. Jaszczak P. Skin oxygen tension, skin oxygen consumption, and skin blood flow measured by a tc-pO2 electrode. *Acta Physiol Scand Suppl* 603: 53–57, 1991.

270. Jauniaux E, Gulbis B, Burton GJ. The human first trimester gestational sac limits rather than facilitates oxygen transfer to the foetus--a review. *Placenta* 24, Suppl A: S86–S93, 2003. doi:10.1053/plac.2002.0932.

271. Jauniaux E, Watson A, Burton G. Evaluation of respiratory gases and acid-base gradients in human fetal fluids and uteroplacental tissue between 7 and 16 weeks' gestation. *Am J Obstet Gynecol* 184: 998–1003, 2001. doi:10.1067/mob.2001.111935.

272. Jauniaux E, Watson AL, Hempstock J, Bao YP, Skepper JN, Burton GJ. Onset of maternal arterial blood flow and placental oxidative stress. A possible factor in human early pregnancy failure. *Am J Pathol* 157: 2111–2122, 2000. doi:10.1016/S0002-9440(10)64849-3.

273. Jayaraman S, Song Y, Vetrivel L, Shankar L, Verkman AS. Noninvasive in vivo fluorescence measurement of airway-surface liquid depth, salt concentration, and pH. *J Clin Invest* 107: 317–324, 2001. doi:10.1172/JCI11154.

274. Jensen MD, Wallach DF, Sherwood P. Diffusion in tissue cultures on gas-permeable and impermeable supports. *J Theor Biol* 56: 443–458, 1976. doi:10.1016/S0022-5193(76)80085-9.

275. Jiang J, Nakashima T, Liu KJ, Goda F, Shima T, Swartz HM. Measurement of Po_2 in liver using EPR oximetry. *J Appl Physiol (1985)* 80: 552–558, 1996. doi:10.1152/jappl.1996.80.2.552.

276. Jiang Y-Z, Wang K, Li Y, Dai C-F, Wang P, Kendziorski C, Chen D-B, Zheng J. Enhanced cellular responses and distinct gene profiles in human fetoplacental artery endothelial cells under chronic low oxygen. *Biol Reprod* 89: 133, 2013. doi:10.1095/biolreprod.113.110551.

277. Jiang Y-Z, Wang K, Li Y, Dai C-F, Wang P, Kendziorski C, Chen D-B, Zheng J. Transcriptional and functional adaptations of human endothelial cells to physiological chronic low oxygen. *Biol Reprod* 88: 114, 2013. doi:10.1095/biolreprod.113.108225.

278. Johnson LG, Dickman KG, Moore KL, Mandel LJ, Boucher RC. Enhanced Na+ transport in an air-liquid interface culture system. *Am J Physiol* 264: L560–L565, 1993.

279. Jurrus ER, Weiss HS. In vitro tissue oxygen tensions in the rabbit aortic arch. *Atherosclerosis* 28: 223–232, 1977. doi:10.1016/0021-9150(77)90172-1.

280. Kabon B, Nagele A, Reddy D, Eagon C, Fleshman JW, Sessler DI, Kurz A. Obesity decreases perioperative tissue oxygenation. *Anesthesiology* 100: 274–280, 2004. doi:10.1097/00000542-200402000-00015.

281. Kamga C, Krishnamurthy S, Shiva S. Myoglobin and mitochondria: a relationship bound by oxygen and nitric oxide. *Nitric Oxide* 26: 251–258, 2012. doi:10.1016/j.niox.2012.03.005.

282. Kamler M, Nowak K, Bock M, Herold U, Motsch J, Hagl S, Gebhard MM, Jakob H. Bronchial artery revascularization restores peribronchial tissue oxygenation after lung transplantation. *J Heart Lung Transplant* 23: 763–766, 2004. doi:10.1016/j.healun.2003.07.016.

283. Karanjawala ZE, Murphy N, Hinton DR, Hsieh CL, Lieber MR. Oxygen metabolism causes chromosome breaks and is associated with the neuronal apoptosis observed in DNA double-strand break repair mutants. *Curr Biol* 12: 397–402, 2002. doi:10.1016/S0960-9822(02)00684-X.

284. Karhausen J, Furuta GT, Tomaszewski JE, Johnson RS, Colgan SP, Haase VH. Epithelial hypoxia-inducible factor-1 is protective in murine experimental colitis. *J Clin Invest* 114: 1098–1106, 2004. doi:10.1172/JCI200421086.

285. Kaser DJ. On developing a thesis for Reproductive Endocrinology and Infertility fellowship: a case study of ultra-low (2%) oxygen tension for extended culture of human embryos. *J Assist Reprod Genet* 34: 303–308, 2017. doi:10.1007/s10815-017-0887-5.

286. Kaser DJ, Bogale B, Sarda V, Farland LV, Racowsky C. Randomized controlled trial of low (5%) vs. ultralow (2%) oxygen tension for in vitro development of human embryos. *Fertil Steril* 106: e4, 2016. doi:10.1016/j.fertnstert.2016.07.016.

287. Katopodi T, Tew SR, Clegg PD, Hardingham TE. The influence of donor and hypoxic conditions on the assembly of cartilage matrix by osteoarthritic human articular chondrocytes on Hyalograft matrices. *Biomaterials* 30: 535–540, 2009. doi:10.1016/j.biomaterials.2008.09.064.

288. Kaufman DL, Mitchell JA. Alterations in intrauterine oxygen tension during the estrous cycle in the rat and hamster and its regulation by ovarian steroid hormones: a comparative study. *Adv Exp Med Biol* 277: 745–750, 1990. doi:10.1007/978-1-4684-8181-5_85.

289. Kay AG, Dale TP, Akram KM, Mohan P, Hampson K, Maffulli N, Spiteri MA, El Haj AJ, Forsyth NR. BMP2 repression and optimized culture conditions promote human bone marrow-derived mesenchymal stem cell isolation. *Regen Med* 10: 109–125, 2015. doi:10.2217/rme.14.67.

290. Keeley TP, Siow RCM, Jacob R, Mann GEA. A PP2A-mediated feedback mechanism controls Ca^{2+}-dependent NO synthesis under physiological oxygen. *FASEB J* 31: 5172–5183, 2017. doi:10.1096/fj.201700211R.

291. Keeley TP, Siow RCM, Jacob R, Mann GE. Reduced SERCA activity underlies dysregulation of Ca^{2+} homeostasis under atmospheric O_2 levels. *FASEB J* 32: 2531–2538, 2018. doi:10.1096/fj.201700685RRR.

292. Kelly CJ, Colgan SP. Breathless in the Gut: Implications of Luminal O2 for Microbial Pathogenicity. *Cell Host Microbe* 19: 427–428, 2016. doi:10.1016/j.chom.2016.03.014.

293. Kelly CJ, Glover LE, Campbell EL, Kominsky DJ, Ehrentraut SF, Bowers BE, Bayless AJ, Saeedi BJ, Colgan SP. Fundamental role for HIF-1α in constitutive expression of human β defensin-1. *Mucosal Immunol* 6: 1110–1118, 2013. doi:10.1038/mi.2013.6.

294. Kelly CJ, Zheng L, Campbell EL, Saeedi B, Scholz CC, Bayless AJ, Wilson KE, Glover LE, Kominsky DJ, Magnuson A, Weir TL, Ehrentraut SF, Pickel C, Kuhn KA, Lanis JM, Nguyen V, Taylor CT, Colgan SP. Crosstalk between microbiota-derived short-chain fatty acids and intestinal epithelial HIF augments tissue barrier function. *Cell Host Microbe* 17: 662–671, 2015. doi:10.1016/j.chom.2015.03.005.

295. Kerger H, Torres Filho IP, Rivas M, Winslow RM, Intaglietta M. Systemic and subcutaneous microvascular oxygen tension in conscious Syrian golden hamsters. *Am J Physiol* 268: H802–H810, 1995.

296. Kessler M, Lubbers DW. Aufbau und Anwendungsmoglichkeit verschiedener Po_2-Elektroden. *Pflugers Arch Gesamte Physiol* 291: R82, 1966.

297. Khan M, Kutala VK, Wisel S, Chacko SM, Kuppusamy ML, Kwiatkowski P, Kuppusamy P (editors). *Oxygen Transport to Tissue XXIX*. New York: Springer, 2008, p. 45–52. doi:10.1007/978-0-387-74911-2_6

298. Khaw KS, Wang CC, Ngan Kee WD, Pang CP, Rogers MS. Effects of high inspired oxygen fraction during elective caesarean section under spinal anaesthesia on maternal and fetal oxygenation and lipid peroxidation. *Br J Anaesth* 88: 18–23, 2002. doi:10.1093/bja/88.1.18.

299. Kietzmann T, Hirsch-Ernst KI, Kahl GF, Jungermann K. Mimicry in primary rat hepatocyte cultures of the in vivo perivenous induction by phenobarbital of cytochrome P-450 2B1 mRNA: role of epidermal growth factor and perivenous oxygen tension. *Mol Pharmacol* 56: 46–53, 1999. doi:10.1124/mol.56.1.46.

300. Kim T-S, Misumi S, Jung C-G, Masuda T, Isobe Y, Furuyama F, Nishino H, Hida H. Increase in dopaminergic neurons from mouse embryonic stem cell-derived neural progenitor/stem cells is mediated by hypoxia inducible factor-1alpha. *J Neurosci Res* 86: 2353–2362, 2008. doi:10.1002/jnr.21687.

301. Kimberger O, Fleischmann E, Brandt S, Kugener A, Kabon B, Hiltebrand L, Krejci V, Kurz A. Supplemental oxygen, but not supplemental crystalloid fluid, increases tissue oxygen tension in healthy and anastomotic colon in pigs. *Anesth Analg* 105: 773–779, 2007. doi:10.1213/01.ane.0000277490.90387.96.

302. Kinnala PJ, Kuttila KT, Grönroos JM, Havia TV, Nevalainen TJ, Niinikoski JH. Pancreatic tissue perfusion in experimental acute pancreatitis. *Eur J Surg* 167: 689–694, 2001. doi:10.1080/11024150152619345.

303. Kinnala PJ, Kuttila KT, Grönroos JM, Havia TV, Nevalainen TJ, Niinikoski JHA. Splanchnic and pancreatic tissue perfusion in experimental acute pancreatitis. *Scand J Gastroenterol* 37: 845–849, 2002. doi:10.1080/gas.37.7.845.849.

304. Kitzmann JP, Pepper AR, Gala-Lopez B, Pawlick R, Kin T, O'Gorman D, Mueller KR, Gruessner AC, Avgoustiniatos ES, Karatzas T, Szot GL, Posselt AM, Stock PG, Wilson JR, Shapiro AM, Papas KK. Human islet viability and function is maintained during high-density shipment in silicone rubber membrane vessels. *Transplant Proc* 46: 1989–1991, 2014. doi:10.1016/j.transproceed.2014.06.002.

305. Knotzer H, Pajk W, Maier S, Ladurner R, Kleinsasser A, Wenzel V, Dünser MW, Ulmer H, Hasibeder WR. Arginine vasopressin reduces intestinal oxygen supply and mucosal tissue oxygen tension. *Am J Physiol Heart Circ Physiol* 289: H168–H173, 2005. doi:10.1152/ajpheart.01235.2004.

306. Knowles HJ, Mole DR, Ratcliffe PJ, Harris AL. Normoxic stabilization of hypoxia-inducible factor-1alpha by modulation of the labile iron pool in differentiating U937 macrophages: effect of natural resistance-associated macrophage protein 1. *Cancer Res* 66: 2600–2607, 2006. doi:10.1158/0008-5472.CAN-05-2351.

307. Koay EJ, Athanasiou KA. Hypoxic chondrogenic differentiation of human embryonic stem cells enhances cartilage protein synthesis and biomechanical functionality. *Osteoarthritis Cartilage* 16: 1450–1456, 2008. doi:10.1016/j.joca.2008.04.007.

308. Kofoed H, Sjøntoft E, Siemssen SO, Olesen HP. Bone marrow circulation after osteotomy. Blood flow, pO2, pCO2, and pressure studied in dogs. *Acta Orthop Scand* 56: 400–403, 1985. doi:10.3109/17453678508994357.

309. Komatsu H, Barriga A, Medrano L, Omori K, Kandeel F, Mullen Y. Oxygenated thawing and rewarming alleviate rewarming injury of cryopreserved pancreatic islets. *Biochem Biophys Res Commun* 486: 817–823, 2017. doi:10.1016/j.bbrc.2017.03.134.

310. Komatsu H, Cook C, Wang C-H, Medrano L, Lin H, Kandeel F, Tai Y-C, Mullen Y. Oxygen environment and islet size are the primary limiting factors of isolated pancreatic islet survival. *PLoS One* 12: e0183780, 2017. doi:10.1371/journal.pone.0183780.

311. Koros WJ, Wang J, Felder RM. Oxygen permeation through FEP Teflon and Kapton polyimide. *J Appl Polym Sci* 26: 2805–2809, 1981. doi:10.1002/app.1981.070260832.

312. Korsbäck C, Höckerstedt K. Small bowel and liver pO2 during vasopressin infusion into the superior mesenteric artery. *Ann Chir Gynaecol* 73: 50–53, 1984.

313. Kotaska K, Urinovska R, Klapkova E, Prusa R, Rob L, Binder T. Re-evaluation of cord blood arterial and venous reference ranges for pH, pO(2), pCO(2), according to spontaneous or cesarean delivery. *J Clin Lab Anal* 24: 300–304, 2010. doi:10.1002/jcla.20405.

314. Kovačič B. Culture systems: low-oxygen culture. *Methods Mol Biol* 912: 249–272, 2012.

315. Krieger JA, Landsiedel JC, Lawrence DA. Differential in vitro effects of physiological and atmospheric oxygen tension on normal human peripheral blood mononuclear cell proliferation, cytokine and immunoglobulin production. *Int J Immunopharmacol* 18: 545–552, 1996. doi:10.1016/S0192-0561(96)00057-4.

316. Krogh A. The number and distribution of capillaries in muscles with calculations of the oxygen pressure head necessary for supplying the tissue. *J Physiol* 52: 409–415, 1919. doi:10.1113/jphysiol.1919.sp001839.

317. Kumar A, Dailey LA, Swedrowska M, Siow R, Mann GE, Vizcay-Barrena G, Arno M, Mudway IS, Forbes B. Quantifying the magnitude of the oxygen artefact inherent in culturing airway cells under atmospheric oxygen versus physiological levels. *FEBS Lett* 590: 258–269, 2016. doi:10.1002/1873-3468.12026.

318. Kunath U, Uckmann C. Der Sauerstoffpartialdruck in der Magenfunduswand in Abhängigkeit von der arteriellen Blutzufuhr. *Langenbecks Arch Surg* 348: 191–199, 1979. doi:10.1007/BF01239447.

319. Kunisaki Y, Bruns I, Scheiermann C, Ahmed J, Pinho S, Zhang D, Mizoguchi T, Wei Q, Lucas D, Ito K, Mar JC, Bergman A, Frenette PS. Arteriolar niches maintain haematopoietic stem cell quiescence. *Nature* 502: 637–643, 2013. doi:10.1038/nature12612.

320. Kusuma S, Peijnenburg E, Patel P, Gerecht S. Low oxygen tension enhances endothelial fate of human pluripotent stem cells. *Arterioscler Thromb Vasc Biol* 34: 913–920, 2014. doi:10.1161/ATVBAHA.114.303274.

321. Laderoute KR. The interaction between HIF-1 and AP-1 transcription factors in response to low oxygen. *Semin Cell Dev Biol* 16: 502–513, 2005. doi:10.1016/j.semcdb.2005.03.005.

322. Lando D, Peet DJ, Gorman JJ, Whelan DA, Whitelaw ML, Bruick RK. FIH-1 is an asparaginyl hydroxylase enzyme that regulates the transcriptional activity of hypoxia-inducible factor. *Genes Dev* 16: 1466–1471, 2002. doi:10.1101/gad.991402.

323. Lando D, Peet DJ, Whelan DA, Gorman JJ, Whitelaw ML. Asparagine hydroxylation of the HIF transactivation domain a hypoxic switch. *Science* 295: 858–861, 2002. doi:10.1126/science.1068592.

324. Lane N. *Oxygen: the Molecule That Made the World*. Oxford, UK: OUP Oxford, 2002.

325. Lash JM, Bohlen HG. Perivascular and tissue P_{O_2} in contracting rat spinotrapezius muscle. *Am J Physiol* 252: H1192–H1202, 1987.

326. Le Q-T, Chen E, Salim A, Cao H, Kong CS, Whyte R, Donington J, Cannon W, Wakelee H, Tibshirani R, Mitchell JD, Richardson D, O'Byrne KJ, Koong AC, Giaccia AJ. An evaluation of tumor oxygenation and gene expression in patients with early stage non-small cell lung cancers. *Clin Cancer Res* 12: 1507–1514, 2006. doi:10.1158/1078-0432.CCR-05-2049.

327. Leary TS, Klinck JR, Hayman G, Friend P, Jamieson NV, Gupta AK. Measurement of liver tissue oxygenation after orthotopic liver transplantation using a multiparameter sensor. A pilot study. *Anaesthesia* 57: 1128–1133, 2002. doi:10.1046/j.1365-2044.2002.02782_5.x.

328. Lecoq J, Parpaleix A, Roussakis E, Ducros M, Goulam Houssen Y, Vinogradov SA, Charpak S. Simultaneous two-photon imaging of oxygen and blood flow in deep cerebral vessels. *Nat Med* 17: 893–898, 2011. doi:10.1038/nm.2394.

329. Lee CM, Genetos DC, You Z, Yellowley CE. Hypoxia regulates PGE(2) release and EP1 receptor expression in osteoblastic cells. *J Cell Physiol* 212: 182–188, 2007. doi:10.1002/jcp.21017.

330. Lee ES, Bauer GE, Caldwell MP, Santilli SM. Association of artery wall hypoxia and cellular proliferation at a vascular anastomosis. *J Surg Res* 91: 32–37, 2000. doi:10.1006/jsre.2000.5891.

331. Lee Y-A, Kim JY, Hong S-J, Lee S-H, Yoo MC, Kim KS, Yang H-I. Synovial proliferation differentially affects hypoxia in the joint cavities of rheumatoid arthritis and osteoarthritis patients. *Clin Rheumatol* 26: 2023–2029, 2007. doi:10.1007/s10067-007-0605-2.

333. Lei XG, Zhu J-H, Cheng W-H, Bao Y, Ho Y-S, Reddi AR, Holmgren A, Arnér ESJ. Paradoxical Roles of Antioxidant Enzymes: Basic Mechanisms and Health Implications. *Physiol Rev* 96: 307–364, 2016. doi:10.1152/physrev.00010.2014.

334. Leichtweiss H-P, Lübbers DW, Weiss C, Baumgärtl H, Reschke W. The oxygen supply of the rat kidney: measurements of int4arenal pO2. *Pflugers Arch* 309: 328–349, 1969. doi:10.1007/BF00587756.

335. Lengner CJ, Gimelbrant AA, Erwin JA, Cheng AW, Guenther MG, Welstead GG, Alagappan R, Frampton GM, Xu P, Muffat J, Santagata S, Powers D, Barrett CB, Young RA, Lee JT, Jaenisch R, Mitalipova M. Derivation of pre-X inactivation human embryonic stem cells under physiological oxygen concentrations. *Cell* 141: 872–883, 2010. doi:10.1016/j.cell.2010.04.010.

336. Lennon DP, Edmison JM, Caplan AI. Cultivation of rat marrow-derived mesenchymal stem cells in reduced oxygen tension: effects on in vitro and in vivo osteochondrogenesis. *J Cell Physiol* 187: 345–355, 2001. doi:10.1002/jcp.1081.

337. Leonard MO, Cottell DC, Godson C, Brady HR, Taylor CT. The role of HIF-1 alpha in transcriptional regulation of the proximal tubular epithelial cell response to hypoxia. *J Biol Chem* 278: 40296–40304, 2003. doi:10.1074/jbc.M302560200.

338. Levy MN, Imperial ES. Oxygen shunting in renal cortical and medullary capillaries. *Am J Physiol* 200: 159–162, 1961.

339. Li H, Hou H, Sucheta A, Williams BB, Lariviere JP, Khan MN, Lesniewski PN, Gallez B, Swartz HM. Implantable resonators--a technique for repeated measurement of oxygen at multiple deep sites with in vivo EPR. *Adv Exp Med Biol* 662: 265–272, 2010. doi:10.1007/978-1-4419-1241-1_38.

340. Li Q, Sun B, Wang X, Jin Z, Zhou Y, Dong L, Jiang L-H, Rong W. A crucial role for hydrogen sulfide in oxygen sensing via modulating large conductance calcium-activated potassium channels. *Antioxid Redox Signal* 12: 1179–1189, 2010. doi:10.1089/ars.2009.2926.

341. Li S, Oreffo ROC, Sengers BG, Tare RS. The effect of oxygen tension on human articular chondrocyte matrix synthesis: integration of experimental and computational approaches. *Biotechnol Bioeng* 111: 1876–1885, 2014. doi:10.1002/bit.25241.

342. Li T-S, Cheng K, Malliaras K, Matsushita N, Sun B, Marbán L, Zhang Y, Marbán E. Expansion of human cardiac stem cells in physiological oxygen improves cell production efficiency and potency for myocardial repair. *Cardiovasc Res* 89: 157–165, 2011. doi:10.1093/cvr/cvq251.

343. Li T-S, Marbán E. Physiological levels of reactive oxygen species are required to maintain genomic stability in stem cells. *Stem Cells* 28: 1178–1185, 2010.

344. Li W-C, Ruan X-Z, Zhang H-M, Zeng Y-J. Biomechanical properties of different segments of human umbilical cord vein and its value for clinical application. *J Biomed Mater Res B Appl Biomater* 76: 93–97, 2006. doi:10.1002/jbm.b.30339.

345. Lillegard JB, Fisher JE, Nedredal G, Luebke-Wheeler J, Bao J, Wang W, Amoit B, Nyberg SL. Normal atmospheric oxygen tension and the use of antioxidants improve hepatocyte spheroid viability and function. *J Cell Physiol* 226: 2987–2996, 2011. doi:10.1002/jcp.22651.

346. Lind Due V, Bonde J, Kann T, Perner A. Extremely low oxygen tension in the rectal lumen of human subjects. *Acta Anaesthesiol Scand* 47: 372, 2003. doi:10.1034/j.1399-6576.2003.00542.x.

347. Link G, Clark KE, Lang U. Umbilical blood flow during pregnancy: evidence for decreasing placental perfusion. *Am J Obstet Gynecol* 196: 489.e12987–489.e7, 2007. doi:10.1016/j.ajog.2006.11.017.

348. Lippitsch ME, Pusterhofer J, Leiner MJ, Wolfbeis OS. Fibre-optic oxygen sensor with the fluorescence decay time as the information carrier. *Anal Chim Acta* 205: 1–6, 1988. doi:10.1016/S0003-2670(00)82310-7.

349. Liss P, Nygren A, Revsbech NP, Ulfendahl HR. Intrarenal oxygen tension measured by a modified clark electrode at normal and low blood pressure and after injection of x-ray contrast media. *Pflugers Arch* 434: 705–711, 1997. doi:10.1007/s004240050455.

350. Liu KJ, Bacic G, Hoopes PJ, Jiang J, Du H, Ou LC, Dunn JF, Swartz HM. Assessment of cerebral pO2 by EPR oximetry in rodents: effects of anesthesia, ischemia, and breathing gas. *Brain Res* 685: 91–98, 1995. doi:10.1016/0006-8993(95)00413-K.

351. Liu Y, Cox SR, Morita T, Kourembanas S. Hypoxia regulates vascular endothelial growth factor gene expression in endothelial cells. Identification of a 5′ enhancer. *Circ Res* 77: 638–643, 1995. doi:10.1161/01.RES.77.3.638.

352. Lloyd BB, Cunningham DJC, Goode RC. Depression of hypoxic hyperventilation in man by sudden inspiration of carbon monoxide. In: *Arterial Chemoreceptors*, edited by Torrance RW. Oxford, UK: Blackwell, 1968, p. 145–148.

353. Locke R, Hauser CJ, Shoemaker WC. The use of surface oximetry to assess bowel viability. *Arch Surg* 119: 1252–1256, 1984. doi:10.1001/archsurg.1984.01390230024005.

354. Lodge KM, Thompson AA, Chilvers ER, Condliffe AM. Hypoxic regulation of neutrophil function and consequences for Staphylococcus aureus infection. *Microbes Infect* 19: 166–176, 2017. doi:10.1016/j.micinf.2016.10.005.

355. Löfstedt T, Fredlund E, Holmquist-Mengelbier L, Pietras A, Ovenberger M, Poellinger L, Påhlman S. Hypoxia inducible factor-2α in cancer. *Cell Cycle* 6: 919–926, 2007. doi:10.4161/cc.6.8.4133.

356. Lopci E, Grassi I, Chiti A, Nanni C, Cicoria G, Toschi L, Fonti C, Lodi F, Mattioli S, Fanti S. PET radiopharmaceuticals for imaging of tumor hypoxia: a review of the evidence. *Am J Nucl Med Mol Imaging* 4: 365–384, 2014.

357. Lord EM, Harwell L, Koch CJ. Detection of hypoxic cells by monoclonal antibody recognizing 2-nitroimidazole adducts. *Cancer Res* 53: 5721–5726, 1993.

358. Lösse B, Schuchhardt S, Niederle N. The oxygen pressure histogram in the left ventricular myocardium of the dog. *Pflugers Arch* 356: 121–132, 1975. doi:10.1007/BF00584292.

359. Louis NA, Hamilton KE, Canny G, Shekels LL, Ho SB, Colgan SP. Selective induction of mucin-3 by hypoxia in intestinal epithelia. *J Cell Biochem* 99: 1616–1627, 2006. doi:10.1002/jcb.20947.

360. Lu C, Rollins M, Hou H, Swartz HM, Hopf H, Miclau T, Marcucio RS. Tibial fracture decreases oxygen levels at the site of injury. *Iowa Orthop J* 28: 14–21, 2008.

361. Lu C, Saless N, Wang X, Sinha A, Decker S, Kazakia G, Hou H, Williams B, Swartz HM, Hunt TK, Miclau T, Marcucio RS. The role of oxygen during fracture healing. *Bone* 52: 220–229, 2013. doi:10.1016/j.bone.2012.09.037.

362. Lübbers DW, Baumgärtl H. Heterogeneities and profiles of oxygen pressure in brain and kidney as examples of the pO2 distribution in the living tissue. *Kidney Int* 51: 372–380, 1997. doi:10.1038/ki.1997.49.

363. Lund-Olesen K. Oxygen tension in synovial fluids. *Arthritis Rheum* 13: 769–776, 1970. doi:10.1002/art.1780130606.

364. Lyons DG, Parpaleix A, Roche M, Charpak S. Mapping oxygen concentration in the awake mouse brain. *eLife* 5: e12024, 2016. doi:10.7554/eLife.12024.

365. Maas DH, Storey BT, Mastroianni L Jr. Oxygen tension in the oviduct of the rhesus monkey (Macaca mulatta). *Fertil Steril* 27: 1312–1317, 1976. doi:10.1016/S0015-0282(16)42201-6.

366. MacCraith BD, McDonagh CM, O'Keeffe G, Keyes ET, Vos JG, O'Kelly B, McGilp JF. Fibre optic oxygen sensor based on fluorescence quenching of evanescent-wave excited ruthenium complexes in sol–gel derived porous coatings. *Analyst (Lond)* 118: 385–388, 1993. doi:10.1039/AN9931800385.

367. Mahnke A, Meier RJ, Schatz V, Hofmann J, Castiglione K, Schleicher U, Wolfbeis OS, Bogdan C, Jantsch J. Hypoxia in Leishmania major skin lesions impairs the NO-dependent leishmanicidal activity of macrophages. *J Invest Dermatol* 134: 2339–2346, 2014. doi:10.1038/jid.2014.121.

368. Maier P, Saad B, Schawalder HP. Effect of periportal- and centrilobular-equivalent oxygen tension on liver specific functions in long-term rat hepatocyte cultures. *Toxicol In Vitro* 8: 423–435, 1994. doi:10.1016/0887-2333(94)90164-3.

369. Maines MD. The heme oxygenase system: a regulator of second messenger gases. *Annu Rev Pharmacol Toxicol* 37: 517–554, 1997. doi:10.1146/annurev.pharmtox.37.1.517.

370. Malek AM, Alper SL, Izumo S. Hemodynamic shear stress and its role in atherosclerosis. *JAMA* 282: 2035–2042, 1999. doi:10.1001/jama.282.21.2035.

371. Mamchaoui K, Saumon G. A method for measuring the oxygen consumption of intact cell monolayers. *Am J Physiol Lung Cell Mol Physiol* 278: L858–L863, 2000. doi:10.1152/ajplung.2000.278.4.L858.

372. Manalo DJ, Rowan A, Lavoie T, Natarajan L, Kelly BD, Ye SQ, Garcia JGN, Semenza GL. Transcriptional regulation of vascular endothelial cell responses to hypoxia by HIF-1. *Blood* 105: 659–669, 2005. doi:10.1182/blood-2004-07-2958.

373. Mansfield KD, Simon MC, Keith B. Hypoxic reduction in cellular glutathione levels requires mitochondrial reactive oxygen species. *J Appl Physiol (1985)* 97: 1358–1366, 2004. doi:10.1152/japplphysiol.00449.2004.

374. Markway BD, Tan G-K, Brooke G, Hudson JE, Cooper-White JJ, Doran MR. Enhanced chondrogenic differentiation of human bone marrow-derived mesenchymal stem cells in low oxygen environment micropellet cultures. *Cell Transplant* 19: 29–42, 2010. doi:10.3727/096368909X478560.

375. Marshall C, Mamary AJ, Verhoeven AJ, Marshall BE. Pulmonary artery NADPH-oxidase is activated in hypoxic pulmonary vasoconstriction. *Am J Respir Cell Mol Biol* 15: 633–644, 1996. doi:10.1165/ajrcmb.15.5.8918370.

376. Martin GC, Green RS, Holzman IR. Acidosis in newborns with nuchal cords and normal Apgar scores. *J Perinatol* 25: 162–165, 2005. doi:10.1038/sj.jp.7211238.

377. Martinez I, Nedredal GI, Øie CI, Warren A, Johansen O, Le Couteur DG, Smedsrød B. The influence of oxygen tension on the structure and function of isolated liver sinusoidal endothelial cells. *Comp Hepatol* 7: 4, 2008. doi:10.1186/1476-5926-7-4.

378. Masson N, Singleton RS, Sekirnik R, Trudgian DC, Ambrose LJ, Miranda MX, Tian Y-M, Kessler BM, Schofield CJ, Ratcliffe PJ. The FIH hydroxylase is a cellular peroxide sensor that modulates HIF transcriptional activity. *EMBO Rep* 13: 251–257, 2012. doi:10.1038/embor.2012.9.

379. Mastrogiannaki M, Matak P, Keith B, Simon MC, Vaulont S, Peyssonnaux C. HIF-2α, but not HIF-1α, promotes iron absorption in mice. *J Clin Invest* 119: 1159–1166, 2009. doi:10.1172/JCI38499.

380. Mastroianni L Jr, Jones R. OXYGEN TENSION WITHIN THE RABBIT FALLOPIAN TUBE. *J Reprod Fertil* 9: 99–102, 1965. doi:10.1530/jrf.0.0090099.

381. Mathis C, Poussin C, Weisensee D, Gebel S, Hengstermann A, Sewer A, Belcastro V, Xiang Y, Ansari S, Wagner S, Hoeng J, Peitsch MC. Human bronchial epithelial cells exposed in vitro to cigarette smoke at the air-liquid interface resemble bronchial epithelium from human smokers. *Am J Physiol Lung Cell Mol Physiol* 304: L489–L503, 2013. doi:10.1152/ajplung.00181.2012.

382. McCallum WD, McAreavey RM. Human umbilical vessel diameters and bloodgas tensions in the first two minutes after delivery. *Gynecol Invest* 7: 201–212, 1976. doi:10.1159/000301383.

383. McGovern NN, Cowburn AS, Porter L, Walmsley SR, Summers C, Thompson AAR, Anwar S, Willcocks LC, Whyte MKB, Condliffe AM, Chilvers ER. Hypoxia selectively inhibits respiratory burst activity and killing of Staphylococcus aureus in human neutrophils. *J Immunol* 186: 453–463, 2011. doi:10.4049/jimmunol.1002213.

384. McLimans WF, Blumenson LE, Tunnah KV. Kinetics of gas diffusion in mammalian cell culture systems. II. Theory. *Biotechnol Bioeng* 10: 741–763, 1968. doi:10.1002/bit.260100604.

385. McNulty PH, King N, Scott S, Hartman G, McCann J, Kozak M, Chambers CE, Demers LM, Sinoway LI. Effects of supplemental oxygen administration on coronary blood flow in patients undergoing cardiac catheterization. *Am J Physiol Heart Circ Physiol* 288: H1057–H1062, 2005. doi:10.1152/ajpheart.00625.2004.

386. Meier J, Pape A, Kleen M, Hutter J, Kemming G, Habler O. Regional blood flow during hyperoxic haemodilution. *Clin Physiol Funct Imaging* 25: 158–165, 2005. doi:10.1111/j.1475-097X.2005.00603.x.

387. Meister A, Anderson ME. Glutathione. *Annu Rev Biochem* 52: 711–760, 1983. doi:10.1146/annurev.bi.52.070183.003431.

388. Mellstrom A, Månsson P, Jonsson K, Hartmann M. Measurements of subcutaneous tissue Po_2 reflect oxygen metabolism of the small intestinal mucosa during hemorrhage and resuscitation. An experimental study in pigs. *Eur Surg Res* 42: 122–129, 2009. doi:10.1159/000193295.

389. Metzen E, Wolff M, Fandrey J, Jelkmann W. Pericellular Po_2 and O2 consumption in monolayer cell cultures. *Respir Physiol* 100: 101–106, 1995. doi:10.1016/0034-5687(94)00125-J.

390. Metzger H, Heuber S. Local oxygen tension and spike activity of the cerebral grey matter of the rat and its response to short intervals of O2 deficiency or CO2 excess. *Pflugers Arch* 370: 201–209, 1977. doi:10.1007/BF00581695.

391. Meyer EG, Buckley CT, Thorpe SD, Kelly DJ. Low oxygen tension is a more potent promoter of chondrogenic differentiation than dynamic compression. *J Biomech* 43: 2516–2523, 2010. doi:10.1016/j.jbiomech.2010.05.020.

392. Michelakis ED, Hampl V, Nsair A, Wu X, Harry G, Haromy A, Gurtu R, Archer SL. Diversity in mitochondrial function explains differences in vascular oxygen sensing. *Circ Res* 90: 1307–1315, 2002. doi:10.1161/01.RES.0000024689.07590.C2.

393. Michiels C, Arnould T, Remacle J. Endothelial cell responses to hypoxia: initiation of a cascade of cellular interactions. *Biochim Biophys Acta* 1497: 1–10, 2000. doi:10.1016/S0167-4889(00)00041-0.

394. Mignon C, Uzunbajakava NE, Raafs B, Botchkareva NV, Tobin DJ. Photobiomodulation of human dermal fibroblasts in vitro: decisive role of cell culture conditions and treatment protocols on experimental outcome. *Sci Rep* 7: 2797, 2017. doi:10.1038/s41598-017-02802-0.

395. Mik EG, Johannes T, Ince C. Monitoring of renal venous Po_2 and kidney oxygen consumption in rats by a near-infrared phosphorescence lifetime technique. *Am J Physiol Renal Physiol* 294: F676–F681, 2008. doi:10.1152/ajprenal.00569.2007.

396. Miller GW, Mugler JP III, Altes TA, Cai J, Mata JF, de Lange EE, Tobias WA, Cates GD, Brookeman JR. A short-breath-hold technique for lung pO2 mapping with 3He MRI. *Magn Reson Med* 63: 127–136, 2010.

397. Millman JR, Tan JH, Colton CK. The effects of low oxygen on self-renewal and differentiation of embryonic stem cells. *Curr Opin Organ Transplant* 14: 694–700, 2009. doi:10.1097/MOT.0b013e3283329d53.

398. Mimura I, Nangaku M. The suffocating kidney: tubulointerstitial hypoxia in end-stage renal disease. *Nat Rev Nephrol* 6: 667–678, 2010. doi:10.1038/nrneph.2010.124.

399. Ming G, Zhenhao D. Prediction of oxygen solubility in pure water and brines up to high temperatures and pressures. *Geochim Cosmochim Acta* 74: 5631–5640, 2010. doi:10.1016/j.gca.2010.06.034.

400. Mitchell JA, Yochim JM. Intrauterine oxygen tension during the estrous cycle in the rat: its relation to uterine respiration and vascular activity. *Endocrinology* 83: 701–705, 1968. doi:10.1210/endo-83-4-701.

401. Mitchell JA, Yochim JM. Measurement of intrauterine oxygen tension in the rat and its regulation by ovarian steroid hormones. *Endocrinology* 83: 691–700, 1968. doi:10.1210/endo-83-4-691.

402. Mohyeldin A, Garzón-Muvdi T, Quiñones-Hinojosa A. Oxygen in stem cell biology: a critical component of the stem cell niche. *Cell Stem Cell* 7: 150–161, 2010. doi:10.1016/j.stem.2010.07.007.

403. Mondragon-Teran P, Baboo JZ, Mason C, Lye GJ, Veraitch FS. The full spectrum of physiological oxygen tensions and step-changes in oxygen tension affects the neural differentiation of mouse embryonic stem cells. *Biotechnol Prog* 27: 1700–1708, 2011. doi:10.1002/btpr.675.

404. Mondragon-Teran P, Lye GJ, Veraitch FS. Lowering oxygen tension enhances the differentiation of mouse embryonic stem cells into neuronal cells. *Biotechnol Prog* 25: 1480–1488, 2009. doi:10.1002/btpr.248.

405. Moore JA, Ethier CR. Oxygen mass transfer calculations in large arteries. *J Biomech Eng* 119: 469–475, 1997. doi:10.1115/1.2798295.

406. Morin SJ. Oxygen tension in embryo culture: does a shift to 2% O_2 in extended culture represent the most physiologic system? *J Assist Reprod Genet* 34: 309–314, 2017. doi:10.1007/s10815-017-0880-z.

407. Morosin M, Vignati C, Novi A, Salvioni E, Veglia F, Alimento M, Merli G, Sciomer S, Sinagra G, Agostoni P. The alveolar to arterial oxygen partial pressure difference is associated with pulmonary diffusing capacity in heart failure patients. *Respir Physiol Neurobiol* 233: 1–6, 2016. doi:10.1016/j.resp.2016.06.004.

408. Morote-Garcia JC, Rosenberger P, Nivillac NMI, Coe IR, Eltzschig HK. Hypoxia-inducible factor-dependent repression of equilibrative nucleoside transporter 2 attenuates mucosal inflammation during intestinal hypoxia. *Gastroenterology* 136: 607–618, 2009. doi:10.1053/j.gastro.2008.10.037.

409. Morrison SJ, Csete M, Groves AK, Melega W, Wold B, Anderson DJ. Culture in reduced levels of oxygen promotes clonogenic sympathoadrenal differentiation by isolated neural crest stem cells. *J Neurosci* 20: 7370–7376, 2000. doi:10.1523/JNEUROSCI.20-19-07370.2000.

410. Moss AJ, Samuelson P, Angell C, Minken SL. Polarographic evaluation of transmural oxygen availabitlity in intact muscular arteries. *J Atheroscler Res* 8: 803–810, 1968. doi:10.1016/S0368-1319(68)80042-0.

411. Müller M, Padberg W, Schindler E, Sticher J, Osmer C, Friemann S, Hempelmann G. Renocortical tissue oxygen pressure measurements in patients undergoing living donor kidney transplantation. *Anesth Analg* 87: 474–476, 1998.

412. Müller M, Schück R, Erkens U, Sticher J, Haase C, Hempelmann G. [Effects of lumbar peridural anesthesia on tissue pO2 of the large intestine in man]]. *Anasthesiol Intensivmed Notfallmed Schmerzther* 30: 108–110, 1995.

413. Mulligan-Kehoe MJ, Simons M. Vasa vasorum in normal and diseased arteries. *Circulation* 129: 2557–2566, 2014. doi:10.1161/CIRCULATIONAHA.113.007189.

414. Murphy CL, Polak JM. Control of human articular chondrocyte differentiation by reduced oxygen tension. *J Cell Physiol* 199: 451–459, 2004. doi:10.1002/jcp.10481.

415. Murphy CL, Sambanis A. Effect of oxygen tension and alginate encapsulation on restoration of the differentiated phenotype of passaged chondrocytes. *Tissue Eng* 7: 791–803, 2001. doi:10.1089/107632701753337735.

416. Najafipour H, Ferrell WR. Comparison of synovial Po_2 and sympathetic vasoconstrictor responses in normal and acutely inflamed rabbit knee joints. *Exp Physiol* 80: 209–220, 1995. doi:10.1113/expphysiol.1995.sp003841.

417. Nakamura M, Yamabe H, Osawa H, Nakamura N, Shimada M, Kumasaka R, Murakami R, Fujita T, Osanai T, Okumura K. Hypoxic conditions stimulate the production of angiogenin and vascular endothelial growth factor by human renal proximal tubular epithelial cells in culture. *Nephrol Dial Transplant* 21: 1489–1495, 2006. doi:10.1093/ndt/gfl041.

418. Nastri CO, Nóbrega BN, Teixeira DM, Amorim J, Diniz LMM, Barbosa MWP, Giorgi VSI, Pileggi VN, Martins WP. Low versus atmospheric oxygen tension for embryo culture in assisted reproduction: a systematic review and meta-analysis. *Fertil Steril* 106: 95–104.e17, 2016. doi:10.1016/j.fertnstert.2016.02.037.

419. Neumann HP, Bender BU, Berger DP, Laubenberger J, Schultze-Seemann W, Wetterauer U, Ferstl FJ, Herbst EW, Schwarzkopf G, Hes FJ, Lips CJ, Lamiell JM, Masek O, Riegler P, Mueller B, Glavac D, Brauch H. Prevalence, morphology and biology of

renal cell carcinoma in von Hippel-Lindau disease compared to sporadic renal cell carcinoma. *J Urol* 160: 1248–1254, 1998. doi:10.1016/S0022-5347(01)62509-6.

420. Newby D, Marks L, Lyall F. Dissolved oxygen concentration in culture medium: assumptions and pitfalls. *Placenta* 26: 353–357, 2005. doi:10.1016/j.placenta.2004.07.002.

421. Ng S, March S, Galstian A, Hanson K, Carvalho T, Mota MM, Bhatia SN. Hypoxia promotes liver-stage malaria infection in primary human hepatocytes in vitro. *Dis Model Mech* 7: 215–224, 2014. doi:10.1242/dmm.013490.

422. Ngo JP, Kar S, Kett MM, Gardiner BS, Pearson JT, Smith DW, Ludbrook J, Bertram JF, Evans RG. Vascular geometry and oxygen diffusion in the vicinity of artery-vein pairs in the kidney. *Am J Physiol Renal Physiol* 307: F1111–F1122, 2014. doi:10.1152/ajprenal.00382.2014.

423. Nicolaije C, Koedam M, van Leeuwen JPTM. Decreased oxygen tension lowers reactive oxygen species and apoptosis and inhibits osteoblast matrix mineralization through changes in early osteoblast differentiation. *J Cell Physiol* 227: 1309–1318, 2012. doi:10.1002/jcp.22841.

424. Nicolaije C, van de Peppel J, van Leeuwen JPTM. Oxygen-induced transcriptional dynamics in human osteoblasts are most prominent at the onset of mineralization. *J Cell Physiol* 228: 1863–1872, 2013. doi:10.1002/jcp.24348.

425. Nicolls MR, Zamora MR. Bronchial blood supply after lung transplantation without bronchial artery revascularization. *Curr Opin Organ Transplant* 15: 563–567, 2010. doi:10.1097/MOT.0b013e32833deca9.

426. Nie X, Laforest R, Elvington A, Randolph GJ, Zheng J, Voller T, Abendschein DR, Lapi SE, Woodard PK. PET/MRI of Hypoxic Atherosclerosis Using 64Cu-ATSM in a Rabbit Model. *J Nucl Med* 57: 2006–2011, 2016. doi:10.2967/jnumed.116.172544.

427. Nie X, Randolph GJ, Elvington A, Bandara N, Zheleznyak A, Gropler RJ, Woodard PK, Lapi SE. Imaging of hypoxia in mouse atherosclerotic plaques with (64)Cu-ATSM. *Nucl Med Biol* 43: 534–542, 2016. doi:10.1016/j.nucmedbio.2016.05.011.

428. Niinikoski J, Heughan C, Hunt TK. Oxygen tensions in the aortic wall of normal rabbits. *Atherosclerosis* 17: 353–359, 1973. doi:10.1016/0021-9150(73)90026-9.

429. Nöldge-Schomburg GF, Priebe HJ, Armbruster K, Pannen B, Haberstroh J, Geiger K. Different effects of early endotoxaemia on hepatic and small intestinal oxygenation in pigs. *Intensive Care Med* 22: 795–804, 1996. doi:10.1007/BF01709523.

430. Nombela-Arrieta C, Pivarnik G, Winkel B, Canty KJ, Harley B, Mahoney JE, Park S-Y, Lu J, Protopopov A, Silberstein LE. Quantitative imaging of haematopoietic stem and progenitor cell localization and hypoxic status in the bone marrow microenvironment. *Nat Cell Biol* 15: 533–543, 2013. doi:10.1038/ncb2730.. Erratum for this article available at http://dx.doi.org/10.1038/ncb2813.

431. Nowak K, Kamler M, Bock M, Motsch J, Hagl S, Jakob H, Gebhard MM. Bronchial artery revascularization affects graft recovery after lung transplantation. *Am J Respir Crit Care Med* 165: 216–220, 2002. doi:10.1164/ajrccm.165.2.2012101.

432. O'Connor JPB, Jackson A, Buonaccorsi GA, Buckley DL, Roberts C, Watson Y, Cheung S, McGrath DM, Naish JH, Rose CJ, Dark PM, Jayson GC, Parker GJM. Organ-specific effects of oxygen and carbogen gas inhalation on tissue longitudinal relaxation times. *Magn Reson Med* 58: 490–496, 2007. doi:10.1002/mrm.21357.

433. O'Connor PM, Anderson WP, Kett MM, Evans RG. Renal preglomerular arterial-venous O2 shunting is a structural anti-oxidant defence mechanism of the renal cortex. *Clin Exp Pharmacol Physiol* 33: 637–641, 2006. doi:10.1111/j.1440-1681.2006.04391.x.

434. O'Connor PM, Anderson WP, Kett MM, Evans RG. Simultaneous measurement of pO2 and perfusion in the rabbit kidney in vivo. *Adv Exp Med Biol* 599: 93–99, 2007. doi:10.1007/978-0-387-71764-7_13.

435. O'Driscoll SW, Fitzsimmons JS, Commisso CN. Role of oxygen tension during cartilage formation by periosteum. *J Orthop Res* 15: 682–687, 1997. doi:10.1002/jor.1100150509.

436. Ogawa S, Lee TM, Kay AR, Tank DW. Brain magnetic resonance imaging with contrast dependent on blood oxygenation. *Proc Natl Acad Sci USA* 87: 9868–9872, 1990. doi:10.1073/pnas.87.24.9868.

437. Olbryt M, Habryka A, Student S, Jarząb M, Tyszkiewicz T, Lisowska KM. Global gene expression profiling in three tumor cell lines subjected to experimental cycling and chronic hypoxia. *PLoS One* 9: e105104, 2014. doi:10.1371/journal.pone.0105104.

438. Olsson R, Carlsson P-O (editors). *Oxygen Transport to Tissue XXVII*. New York: Springer, 2006, p. 263–268. doi:10.1007/0-387-29540-2_42

439. Ortiz-Prado E, Natah S, Srinivasan S, Dunn JF. A method for measuring brain partial pressure of oxygen in unanesthetized unrestrained subjects: the effect of acute and chronic hypoxia on brain tissue PO(2). *J Neurosci Methods* 193: 217–225, 2010. doi:10.1016/j.jneumeth.2010.08.019.

440. Ottosen LDM, Hindkaer J, Husth M, Petersen DE, Kirk J, Ingerslev HJ. Observations on intrauterine oxygen tension measured by fibre-optic microsensors. *Reprod Biomed Online* 13: 380–385, 2006. doi:10.1016/S1472-6483(10)61443-5.

441. Palacios-Callender M, Hollis V, Mitchison M, Frakich N, Unitt D, Moncada S. Cytochrome c oxidase regulates endogenous nitric oxide availability in respiring cells: a possible explanation for hypoxic vasodilation. *Proc Natl Acad Sci USA* 104: 18508–18513, 2007. doi:10.1073/pnas.0709440104.

442. Pandian RP, Parinandi NL, Ilangovan G, Zweier JL, Kuppusamy P. Novel particulate spin probe for targeted determination of oxygen in cells and tissues. *Free Radic Biol Med* 35: 1138–1148, 2003. doi:10.1016/S0891-5849(03)00496-9.

443. Papandreou I, Cairns RA, Fontana L, Lim AL, Denko NC. HIF-1 mediates adaptation to hypoxia by actively downregulating mitochondrial oxygen consumption. *Cell Metab* 3: 187–197, 2006. doi:10.1016/j.cmet.2006.01.012.

444. Park S-K, Dadak AM, Haase VH, Fontana L, Giaccia AJ, Johnson RS. Hypoxia-induced gene expression occurs solely through the action of hypoxia-inducible factor 1alpha (HIF-1alpha): role of cytoplasmic trapping of HIF-2alpha. *Mol Cell Biol* 23: 4959–4971, 2003. doi:10.1128/MCB.23.14.4959-4971.2003.

445. Parpaleix A, Goulam Houssen Y, Charpak S. Imaging local neuronal activity by monitoring Po_2 transients in capillaries. *Nat Med* 19: 241–246, 2013. doi:10.1038/nm.3059.

446. Parrinello S, Samper E, Krtolica A, Goldstein J, Melov S, Campisi J. Oxygen sensitivity severely limits the replicative lifespan of murine fibroblasts. *Nat Cell Biol* 5: 741–747, 2003. doi:10.1038/ncb1024.. Erratum for this article at http://dx.doi.org/10.1038/ncb1043.

447. Pasarica M, Sereda OR, Redman LM, Albarado DC, Hymel DT, Roan LE, Rood JC, Burk DH, Smith SR. Reduced adipose tissue oxygenation in human obesity: evidence for rarefaction, macrophage chemotaxis, and inflammation without an angiogenic response. *Diabetes* 58: 718–725, 2009. doi:10.2337/db08-1098.

448. Patrick A, Seluanov M, Hwang C, Tam J, Khan T, Morgenstern A, Wiener L, Vazquez JM, Zafar H, Wen R, Muratkalyeva M, Doerig K, Zagorulya M, Cole L, Catalano S, Lobo Ladd AA, Coppi AA, Coşkun Y, Tian X, Ablaeva J, Nevo E, Gladyshev VN, Zhang ZD, Vijg J, Seluanov A, Gorbunova V. Sensitivity of primary fibroblasts in culture to atmospheric oxygen does not correlate with species lifespan. *Aging (Albany NY)* 8: 841–847, 2016. doi:10.18632/aging.100958.

449. Pattappa G, Thorpe SD, Jegard NC, Heywood HK, de Bruijn JD, Lee DA. Continuous and uninterrupted oxygen tension influences the colony formation and oxidative metabolism of human mesenchymal stem cells. *Tissue Eng Part C Methods* 19: 68–79, 2013. doi:10.1089/ten.tec.2011.0734.

450. Pearlstein DP, Ali MH, Mungai PT, Hynes KL, Gewertz BL, Schumacker PT. Role of mitochondrial oxidant generation in endothelial cell responses to hypoxia. *Arterioscler Thromb Vasc Biol* 22: 566–573, 2002. doi:10.1161/01.ATV.0000012262.76205.6A.

451. Pedersen M, Dissing TH, Mørkenborg J, Stødkilde-Jørgensen H, Hansen LH, Pedersen LB, Grenier N, Frøkiaer J. Validation of quantitative BOLD MRI measurements in kidney: application to unilateral ureteral obstruction. *Kidney Int* 67: 2305–2312, 2005. doi:10.1111/j.1523-1755.2005.00334.x.

452. Persson PB, Ehmke H, Kirchheim HR, Janssen B, Baumann JE, Just A, Nafz B. Autoregulation and non-homeostatic behaviour of renal blood flow in conscious dogs. *J Physiol* 462: 261–273, 1993. doi:10.1113/jphysiol.1993.sp019554.

453. Pettersen EO, Larsen LH, Ramsing NB, Ebbesen P. Pericellular oxygen depletion during ordinary tissue culturing, measured with oxygen microsensors. *Cell Prolif* 38: 257–267, 2005. doi:10.1111/j.1365-2184.2005.00345.x.

454. Pezzulo AA, Starner TD, Scheetz TE, Traver GL, Tilley AE, Harvey B-G, Crystal RG, McCray PB Jr, Zabner J. The air-liquid interface and use of primary cell cultures are important to recapitulate the transcriptional profile of in vivo airway epithelia. *Am J Physiol Lung Cell Mol Physiol* 300: L25–L31, 2011. doi:10.1152/ajplung.00256.2010.

455. Pinder AG, James PE. When does low oxygen become hypoxia? Implications for nitrite reduction. *Circ Res* 104: e25–e26, 2009. doi:10.1161/CIRCRESAHA.108.191569.

456. Pittman RN. Oxygen gradients in the microcirculation. *Acta Physiol (Oxf)* 202: 311–322, 2011. doi:10.1111/j.1748-1716.2010.02232.x.

457. Pittman RN. Oxygen transport and exchange in the microcirculation. *Microcirculation* 12: 59–70, 2005. doi:10.1080/10739680590895064.

458. Pittman RN. *Regulation of Tissue Oxygenation*. San Rafael, CA: Morgan & Claypool Life Sciences, 2011.

459. Pittman RN, Duling BR. Effects of altered carbon dioxide tension on hemoglobin oxygenation in hamster cheek pouch microvessels. *Microvasc Res* 13: 211–224, 1977. doi:10.1016/0026-2862(77)90086-3.

460. Pittman RN, Duling BR. Measurement of percent oxyhemoglobin in the microvasculature. *J Appl Physiol* 38: 321–327, 1975. doi:10.1152/jappl.1975.38.2.321.

461. Pittman RN, Duling BR. A new method for the measurement of percent oxyhemoglobin. *J Appl Physiol* 38: 315–320, 1975. doi:10.1152/jappl.1975.38.2.315.

462. Place TL, Domann FE, Case AJ. Limitations of oxygen delivery to cells in culture: An underappreciated problem in basic and translational research. *Free Radic Biol Med* 113: 311–322, 2017. doi:10.1016/j.freeradbiomed.2017.10.003.

463. Pohlmann A, Arakelyan K, Hentschel J, Cantow K, Flemming B, Ladwig M, Waiczies S, Seeliger E, Niendorf T. Detailing the relation between renal T2* and renal tissue pO2 using an integrated approach of parametric magnetic resonance imaging and invasive physiological measurements. *Invest Radiol* 49: 547–560, 2014. doi:10.1097/RLI.0000000000000054.

464. Portron S, Merceron C, Gauthier O, Lesoeur J, Sourice S, Masson M, Fellah BH, Geffroy O, Lallemand E, Weiss P, Guicheux J, Vinatier C. Effects of in vitro low oxygen tension preconditioning of adipose stromal cells on their in vivo chondrogenic potential: application in cartilage tissue repair. *PLoS One* 8: e62368, 2013. doi:10.1371/journal.pone.0062368.

465. Postigo L, Heredia G, Illsley NP, Torricos T, Dolan C, Echalar L, Tellez W, Maldonado I, Brimacombe M, Balanza E, Vargas E, Zamudio S. Where the O2 goes to: preservation of human fetal oxygen delivery and consumption at high altitude. *J Physiol* 587: 693–708, 2009. doi:10.1113/jphysiol.2008.163634.

466. Powers DE, Millman JR, Bonner-Weir S, Rappel MJ, Colton CK. Accurate control of oxygen level in cells during culture on silicone rubber membranes with application to stem cell differentiation. *Biotechnol Prog* 26: 805–818, 2010. doi:10.1002/btpr.359.

467. Powers DE, Millman JR, Huang RB, Colton CK. Effects of oxygen on mouse embryonic stem cell growth, phenotype retention, and cellular energetics. *Biotechnol Bioeng* 101: 241–254, 2008. doi:10.1002/bit.21986.

468. Prabhakar NR, Semenza GL. Oxygen sensing and homeostasis. *Physiology (Bethesda)* 30: 340–348, 2015.

469. Prasad SM, Czepiel M, Cetinkaya C, Smigielska K, Weli SC, Lysdahl H, Gabrielsen A, Petersen K, Ehlers N, Fink T, Minger SL, Zachar V. Continuous hypoxic culturing maintains activation of Notch and allows long-term propagation of human embryonic stem cells without spontaneous differentiation. *Cell Prolif* 42: 63–74, 2009. doi:10.1111/j.1365-2184.2008.00571.x.

470. Prytherch Z, Job C, Marshall H, Oreffo V, Foster M, BéruBé K. Tissue-Specific stem cell differentiation in an in vitro airway model. *Macromol Biosci* 11: 1467–1477, 2011.

471. Puente BN, Kimura W, Muralidhar SA, Moon J, Amatruda JF, Phelps KL, Grinsfelder D, Rothermel BA, Chen R, Garcia JA, Santos CX, Thet S, Mori E, Kinter MT, Rindler PM, Zacchigna S, Mukherjee S, Chen DJ, Mahmoud AI, Giacca M, Rabinovitch PS, Aroumougame A, Shah AM, Szweda LI, Sadek HA. The oxygen-rich postnatal environment induces cardiomyocyte cell-cycle arrest through DNA damage response. *Cell* 157: 565–579, 2014. doi:10.1016/j.cell.2014.03.032.. Erratum for this article available at http://dx.doi.org/10.1016/j.cell.2014.05.008.

472. Pugh CW, Ratcliffe PJ. Regulation of angiogenesis by hypoxia: role of the HIF system. *Nat Med* 9: 677–684, 2003. doi:10.1038/nm0603-677.

473. Purpura KA, George SH, Dang SM, Choi K, Nagy A, Zandstra PW. Soluble Flt-1 regulates Flk-1 activation to control hematopoietic and endothelial development in an oxygen-responsive manner. *Stem Cells* 26: 2832–2842, 2008. doi:10.1634/stemcells.2008-0237.

474. Raleigh JA, Chou SC, Arteel GE, Horsman MR. Comparisons among pimonidazole binding, oxygen electrode measurements, and radiation response in C3H mouse tumors. *Radiat Res* 151: 580–589, 1999. doi:10.2307/3580034.

475. Ramírez MÁ, Pericuesta E, Yáñez-Mó M, Palasz A, Gutiérrez-Adán A. Effect of long-term culture of mouse embryonic stem cells under low oxygen concentration as well as on glycosaminoglycan hyaluronan on cell proliferation and differentiation. *Cell Prolif* 44: 75–85, 2011. doi:10.1111/j.1365-2184.2010.00732.x.

476. Ratcliffe PJ. Oxygen sensing and hypoxia signalling pathways in animals: the implications of physiology for cancer. *J Physiol* 591: 2027–2042, 2013. doi:10.1113/jphysiol.2013.251470.

477. Rausch ME, Weisberg S, Vardhana P, Tortoriello DV. Obesity in C57BL/6J mice is characterized by adipose tissue hypoxia and cytotoxic T-cell infiltration. *Int J Obes* 32: 451–463, 2008. doi:10.1038/sj.ijo.0803744.

478. Readnower RD, Brainard RE, Hill BG, Jones SP. Standardized bioenergetic profiling of adult mouse cardiomyocytes. *Physiol Genomics* 44: 1208–1213, 2012. doi:10.1152/physiolgenomics.00129.2012.

479. Redfors B, Bragadottir G, Sellgren J, Swärd K, Ricksten S-E. Acute renal failure is NOT an "acute renal success"--a clinical study on the renal oxygen supply/demand relationship in acute kidney injury. *Crit Care Med* 38: 1695–1701, 2010. doi:10.1097/CCM.0b013e3181e61911.

480. Reeve HL, Michelakis E, Nelson DP, Weir EK, Archer SL. Alterations in a redox oxygen sensing mechanism in chronic hypoxia. *J Appl Physiol (1985)* 90: 2249–2256, 2001. doi:10.1152/jappl.2001.90.6.2249.

481. Reusch P, Wagdy H, Reusch R, Wilson E, Ives HE. Mechanical strain increases smooth muscle and decreases nonmuscle myosin expression in rat vascular smooth muscle cells. *Circ Res* 79: 1046–1053, 1996. doi:10.1161/01.RES.79.5.1046.

482. Reuther MS, Briggs KK, Schumacher BL, Masuda K, Sah RL, Watson D. In vivo oxygen tension in human septal cartilage increases with age. *Laryngoscope* 122: 2407–2410, 2012. doi:10.1002/lary.23478.

483. Reykdal S, Abboud C, Liesveld J. Effect of nitric oxide production and oxygen tension on progenitor preservation in ex vivo culture. *Exp Hematol* 27: 441–450, 1999. doi:10.1016/S0301-472X(98)00030-7.

484. Richman AI, Su EY, Ho G Jr. Reciprocal relationship of synovial fluid volume and oxygen tension. *Arthritis Rheum* 24: 701–705, 1981. doi:10.1002/art.1780240512.

485. Ricksten S-E, Bragadottir G, Redfors B. Renal oxygenation in clinical acute kidney injury. *Crit Care* 17: 221, 2013. doi:10.1186/cc12530.

486. Riley RJ, Johnson JW. Collecting and analyzing cord blood gases. *Clin Obstet Gynecol* 36: 13–23, 1993. doi:10.1097/00003081-199303000-00005.

487. Rivera BK, Naidu SK, Subramanian K, Joseph M, Hou H, Khan N, Swartz HM, Kuppusamy P. Real-time, in vivo determination of dynamic changes in lung and heart tissue oxygenation using EPR oximetry. *Adv Exp Med Biol* 812: 81–86, 2014. doi:10.1007/978-1-4939-0620-8_11.

488. Rodesch F, Simon P, Donner C, Jauniaux E. Oxygen measurements in endometrial and trophoblastic tissues during early pregnancy. *Obstet Gynecol* 80: 283–285, 1992.

489. Römers LH, Bakker C, Dollée N, Hoeks SE, Lima A, Raat NJ, Johannes T, Stolker RJ, Mik EG. Cutaneous mitochondrial P_{O_2}, but not tissue oxygen saturation, is an early indicator of the physiologic limit of hemodilution in the pig. *Anesthesiology* 125: 124–132, 2016. doi:10.1097/ALN.0000000000001156.

490. Rosen P, Boulton M, Moriarty P, Khaliq A, McLeod D. Effect of varying oxygen concentrations on the proliferation of retinal microvascular cells in vitro. *Exp Eye Res* 53: 597–601, 1991. doi:10.1016/0014-4835(91)90218-4.

491. Rosenberger C, Mandriota S, Jürgensen JS, Wiesener MS, Hörstrup JH, Frei U, Ratcliffe PJ, Maxwell PH, Bachmann S, Eckardt K-U. Expression of hypoxia-inducible factor-1α and -2α in hypoxic and ischemic rat kidneys. *J Am Soc Nephrol* 13: 1721–1732, 2002. doi:10.1097/01.ASN.0000017223.49823.2A.

492. Rosenberger P, Schwab JM, Mirakaj V, Masekowsky E, Mager A, Morote-Garcia JC, Unertl K, Eltzschig HK. Hypoxia-inducible factor-dependent induction of netrin-1 dampens inflammation caused by hypoxia. *Nat Immunol* 10: 195–202, 2009. doi:10.1038/ni.1683.

493. Ross C, Alston M, Bickenbach JR, Aykin-Burns N. Oxygen tension changes the rate of migration of human skin keratinocytes in an age-related manner. *Exp Dermatol* 20: 58–63, 2011. doi:10.1111/j.1600-0625.2010.01190.x.

494. Roy S, Khanna S, Bickerstaff AA, Subramanian SV, Atalay M, Bierl M, Pendyala S, Levy D, Sharma N, Venojarvi M, Strauch A, Orosz CG, Sen CK. Oxygen sensing by primary cardiac fibroblasts: a key role of p21(Waf1/Cip1/Sdi1). *Circ Res* 92: 264–271, 2003. doi:10.1161/01.RES.0000056770.30922.E6.

495. Roy S, Tripathy M, Mathur N, Jain A, Mukhopadhyay A. Hypoxia improves expansion potential of human cord blood-derived hematopoietic stem cells and marrow repopulation efficiency. *Eur J Haematol* 88: 396–405, 2012. doi:10.1111/j.1600-0609.2012.01759.x.

496. Rumsey WL, Pawlowski M, Lejavardi N, Wilson DF. Oxygen pressure distribution in the heart in vivo and evaluation of the ischemic "border zone". *Am J Physiol* 266: H1676–H1680, 1994.

497. Rumsey WL, Vanderkooi JM, Wilson DF. Imaging of phosphorescence: a novel method for measuring oxygen distribution in perfused tissue. *Science* 241: 1649–1651, 1988. doi:10.1126/science.3420417.

498. Saeedi BJ, Kao DJ, Kitzenberg DA, Dobrinskikh E, Schwisow KD, Masterson JC, Kendrick AA, Kelly CJ, Bayless AJ, Kominsky DJ, Campbell EL, Kuhn KA, Furuta GT, Colgan SP, Glover LE. HIF-dependent regulation of claudin-1 is central to intestinal epithelial tight junction integrity. *Mol Biol Cell* 26: 2252–2262, 2015. doi:10.1091/mbc.e14-07-1194.

499. Sahaf B, Atkuri K, Heydari K, Malipatlolla M, Rappaport J, Regulier E, Herzenberg LA, Herzenberg LA. Culturing of human peripheral blood cells reveals unsuspected lymphocyte responses relevant to HIV disease. *Proc Natl Acad Sci USA* 105: 5111–5116, 2008. doi:10.1073/pnas.0712363105.

500. Sakadžić S, Mandeville ET, Gagnon L, Musacchia JJ, Yaseen MA, Yucel MA, Lefebvre J, Lesage F, Dale AM, Eikermann-Haerter K, Ayata C, Srinivasan VJ, Lo EH, Devor A, Boas DA. Large arteriolar component of oxygen delivery implies a safe margin of oxygen supply to cerebral tissue. *Nat Commun* 5: 5734, 2014. doi:10.1038/ncomms6734.

501. Sakadzić S, Roussakis E, Yaseen MA, Mandeville ET, Srinivasan VJ, Arai K, Ruvinskaya S, Devor A, Lo EH, Vinogradov SA, Boas DA. Two-photon high-resolution measurement of partial pressure of oxygen in cerebral vasculature and tissue. *Nat Methods* 7: 755–759, 2010. doi:10.1038/nmeth.1490.

502. Sakadžić S, Roussakis E, Yaseen MA, Mandeville ET, Srinivasan VJ, Arai K, Ruvinskaya S, Wu W, Devor A, Lo EH, Vinogradov SA, Boas DA. Cerebral blood oxygenation measurement based on oxygen-dependent quenching of phosphorescence. *J Vis Exp* 4: 1694, 2011.

503. Salama R, Masson N, Simpson P, Sciesielski LK, Sun M, Tian Y-M, Ratcliffe PJ, Mole DR. Heterogeneous Effects of Direct Hypoxia Pathway Activation in Kidney Cancer. *PLoS One* 10: e0134645, 2015. doi:10.1371/journal.pone.0134645.

504. Samanta D, Semenza GL. Maintenance of redox homeostasis by hypoxia-inducible factors. *Redox Biol* 13: 331–335, 2017. doi:10.1016/j.redox.2017.05.022.

505. Santilli SM, Fiegel VD, Knighton DR. Alloxan diabetes alters the rabbit transarterial wall oxygen gradient. *J Vasc Surg* 18: 227–233, 1993. doi:10.1016/0741-5214(93)90602-I.

506. Santilli SM, Fiegel VD, Knighton DR. Changes in the aortic wall oxygen tensions of hypertensive rabbits. Hypertension and aortic wall oxygen. *Hypertension* 19: 33–39, 1992. doi:10.1161/01.HYP.19.1.33.

507. Santilli SM, Stevens RB, Anderson JG, Payne WD, Caldwell MD. Transarterial wall oxygen gradients at the dog carotid bifurcation. *Am J Physiol* 268: H155–H161, 1995.

508. Santilli SM, Tretinyak AS, Lee ES. Transarterial wall oxygen gradients at the deployment site of an intra-arterial stent in the rabbit. *Am J Physiol Heart Circ Physiol* 279: H1518–H1525, 2000. doi:10.1152/ajpheart.2000.279.4.H1518.

509. Santilli SM, Wernsing SE, Lee ES. Transarterial wall oxygen gradients at a prosthetic vascular graft to artery anastomosis in the rabbit. *J Vasc Surg* 31: 1229–1239, 2000. doi:10.1067/mva.2000.104590.

510. Santolucito JA, Whitcomb E. Effect of paraoxon on erythrocyte metabolism as measured by oxygen uptake in vitro. *Br J Pharmacol* 42: 298–302, 1971. doi:10.1111/j.1476-5381.1971.tb07111.x.

511. Sato Y, Endo H, Okuyama H, Takeda T, Iwahashi H, Imagawa A, Yamagata K, Shimomura I, Inoue M. Cellular hypoxia of pancreatic beta-cells due to high levels of oxygen consumption for insulin secretion in vitro. *J Biol Chem* 286: 12524–12532, 2011. doi:10.1074/jbc.M110.194738.

512. Schiller ZA, Schiele NR, Sims JK, Lee K, Kuo CK. Adipogenesis of adipose-derived stem cells may be regulated via the cytoskeleton at physiological oxygen levels in vitro. *Stem Cell Res Ther* 4: 79, 2013. doi:10.1186/scrt230.

513. Schipani E, Ryan HE, Didrickson S, Kobayashi T, Knight M, Johnson RS. Hypoxia in cartilage: HIF-1alpha is essential for chondrocyte growth arrest and survival. *Genes Dev* 15: 2865–2876, 2001.

514. Schödel J, Mole DR, Ratcliffe PJ. Pan-genomic binding of hypoxia-inducible transcription factors. *Biol Chem* 394: 507–517, 2013. doi:10.1515/hsz-2012-0351.

515. Schödel J, Oikonomopoulos S, Ragoussis J, Pugh CW, Ratcliffe PJ, Mole DR. High-resolution genome-wide mapping of HIF-binding sites by ChIP-seq. *Blood* 117: e207–e217, 2011. doi:10.1182/blood-2010-10-314427.

516. Schofield CJ, Ratcliffe PJ. Oxygen sensing by HIF hydroxylases. *Nat Rev Mol Cell Biol* 5: 343–354, 2004. doi:10.1038/nrm1366.

517. Schofield CJ, Ratcliffe PJ. Signalling hypoxia by HIF hydroxylases. *Biochem Biophys Res Commun* 338: 617–626, 2005. doi:10.1016/j.bbrc.2005.08.111.

518. Schrobback K, Klein TJ, Crawford R, Upton Z, Malda J, Leavesley DI. Effects of oxygen and culture system on in vitro propagation and redifferentiation of osteoarthritic human articular chondrocytes. *Cell Tissue Res* 347: 649–663, 2012. doi:10.1007/s00441-011-1193-7.

519. Schurek HJ, Jost U, Baumgärtl H, Bertram H, Heckmann U. Evidence for a preglomerular oxygen diffusion shunt in rat renal cortex. *Am J Physiol Renal Physiol* 259: F910–F915, 1990.

520. Schwanhäusser B, Busse D, Li N, Dittmar G, Schuchhardt J, Wolf J, Chen W, Selbach M. Global quantification of mammalian gene expression control. *Nature* 473: 337–342, 2011. doi:10.1038/nature10098.. Erratum for this article available at http://dx-.doi.org/10.1038/nature11848.

521. Sekine K, Kagawa Y, Maeyama E, Ota H, Haraguchi Y, Matsuura K, Shimizu T. Oxygen consumption of human heart cells in monolayer culture. *Biochem Biophys Res Commun* 452: 834–839, 2014. doi:10.1016/j.bbrc.2014.09.018.

522. Semenza GL. Oxygen sensing, hypoxia-inducible factors, and disease pathophysiology. *Annu Rev Pathol* 9: 47–71, 2014. doi:10.1146/annurev-pathol-012513-104720.

523. Semenza GL. Regulation of hypoxia-induced angiogenesis: a chaperone escorts VEGF to the dance. *J Clin Invest* 108: 39–40, 2001. doi:10.1172/JCI13374.

524. Setschenow J. Über die konstitution der salzlösungen auf grund ihres verhaltens zu kohlensäure. *Z Phys Chem* 4: 117–125, 1889. doi:10.1515/zpch-1889-0109.

525. Seylaz J, Pinard E. Continuous measurement of gas partial pressures in intracerebral tissue. *J Appl Physiol Respir Environ Exerc Physiol* 44: 528–533, 1978.

526. Sezai S, Sakurabayashi S, Yamamoto Y, Morita T, Hirano M, Oka H. Hepatic arterial and portal venous oxygen content and extraction in liver cirrhosis. *Liver* 13: 31–35, 1993. doi:10.1111/j.1600-0676.1993.tb00602.x.

527. Sharan M, Vovenko EP, Vadapalli A, Popel AS, Pittman RN. Experimental and theoretical studies of oxygen gradients in rat pial microvessels. *J Cereb Blood Flow Metab* 28: 1597–1604, 2008. doi:10.1038/jcbfm.2008.51.

528. Sheehy EJ, Buckley CT, Kelly DJ. Oxygen tension regulates the osteogenic, chondrogenic and endochondral phenotype of bone marrow derived mesenchymal stem cells. *Biochem Biophys Res Commun* 417: 305–310, 2012. doi:10.1016/j.bbrc.2011.11.105.

529. Sheridan WG, Lowndes RH, Young HL. Intraoperative tissue oximetry in the human gastrointestinal tract. *Am J Surg* 159: 314–319, 1990. doi:10.1016/S0002-9610(05)81226-7.

530. Sheridan WG, Lowndes RH, Young HL. Tissue oxygen tension as a predictor of colonic anastomotic healing. *Dis Colon Rectum* 30: 867–871, 1987. doi:10.1007/BF02555426.

531. Shibata M, Ichioka S, Ando J, Kamiya A. Microvascular and interstitial PO(2) measurements in rat skeletal muscle by phosphorescence quenching. *J Appl Physiol (1985)* 91: 321–327, 2001. doi:10.1152/jappl.2001.91.1.321.

532. Shibata M, and Kamiya A. Microvascular and interstitial pO 2 measurements in the skeletal muscle by phosphorescence quenching technique. *Proceedings of the First Joint BMES/EMBS Conference* 2: 806-vol, 1999.

533. Shimada H, Hashimoto Y, Nakada A, Shigeno K, Nakamura T. Accelerated generation of human induced pluripotent stem cells with retroviral transduction and chemical inhibitors under physiological hypoxia. *Biochem Biophys Res Commun* 417: 659–664, 2012. doi:10.1016/j.bbrc.2011.11.111.

534. Shonat RD, Johnson PC. Oxygen tension gradients and heterogeneity in venous microcirculation: a phosphorescence quenching study. *Am J Physiol Heart Circ Physiol* 272: H2233–H2240, 1997.

535. Shonat RD, Wilson DF, Riva CE, Pawlowski M. Oxygen distribution in the retinal and choroidal vessels of the cat as measured by a new phosphorescence imaging method. *Appl Opt* 31: 3711–3718, 1992. doi:10.1364/AO.31.003711.

536. Shweiki D, Itin A, Soffer D, Keshet E. Vascular endothelial growth factor induced by hypoxia may mediate hypoxia-initiated angiogenesis. *Nature* 359: 843–845, 1992. doi:10.1038/359843a0.

537. Silvola JM, Saraste A, Forsback S, Laine VJO, Saukko P, Heinonen SE, Ylä-Herttuala S, Roivainen A, Knuuti J. Detection of hypoxia by [18F]EF5 in atherosclerotic plaques in mice. *Arterioscler Thromb Vasc Biol* 31: 1011–1015, 2011. doi:10.1161/ATVBAHA.110.221440.

538. Simmen HP, Blaser J. Analysis of pH and pO2 in abscesses, peritoneal fluid, and drainage fluid in the presence or absence of bacterial infection during and after abdominal surgery. *Am J Surg* 166: 24–27, 1993. doi:10.1016/S0002-9610(05)80576-8.

539. Simon MC, Keith B. The role of oxygen availability in embryonic development and stem cell function. *Nat Rev Mol Cell Biol* 9: 285–296, 2008. doi:10.1038/nrm2354.

540. Sinaasappel M, van Iterson M, Ince C. Microvascular oxygen pressure in the pig intestine during haemorrhagic shock and resuscitation. *J Physiol* 514: 245–253, 1999. doi:10.1111/j.1469-7793.1999.245af.x.

541. Sinagowitz E, Golsong M, Wilms H, Halbfass HJ. [In vivo determination of local tissue Po_2 in renal cortex in kidney transplantation]. *Chir Forum Exp Klin Forsch* 1978: 299–302, 1978.

542. Siow RC, Sato H, Mann GE. Heme oxygenase-carbon monoxide signalling pathway in atherosclerosis: anti-atherogenic actions of bilirubin and carbon monoxide? *Cardiovasc Res* 41: 385–394, 1999. doi:10.1016/S0008-6363(98)00278-8.

543. Skolasinska K, Harbig K, Lübbers DW, Wodick R. Po_2 and microflow histograms of the beating heart in response to changes in arterial pO2. *Basic Res Cardiol* 73: 307–319, 1978. doi:10.1007/BF01906736.

544. Smith RH, Guilbeau EJ, Reneau DD. The oxygen tension field within a discrete volume of cerebral cortex. *Microvasc Res* 13: 233–240, 1977. doi:10.1016/0026-2862(77)90088-7.

545. Sobhanifar S, Aquino-Parsons C, Stanbridge EJ, Olive P. Reduced expression of hypoxia-inducible factor-1alpha in perinecrotic regions of solid tumors. *Cancer Res* 65: 7259–7266, 2005. doi:10.1158/0008-5472.CAN-04-4480.

546. Soini HO, Takala J, Nordin AJ, Mäkisalo HJ, Höckerstedt KA. Peripheral and liver tissue oxygen tensions in hemorrhagic shock. *Crit Care Med* 20: 1330–1334, 1992. doi:10.1097/00003246-199209000-00022.

547. Solodushko V, Parker JC, Fouty B. Pulmonary microvascular endothelial cells form a tighter monolayer when grown in chronic hypoxia. *Am J Respir Cell Mol Biol* 38: 491–497, 2008. doi:10.1165/rcmb.2007-0127OC.

548. Soothill PW, Nicolaides KH, Rodeck CH, Campbell S. Effect of gestational age on fetal and intervillous blood gas and acid-base values in human pregnancy. *Fetal Ther* 1: 168–175, 1986. doi:10.1159/000262264.

549. Sowter HM, Raval RR, Moore JW, Ratcliffe PJ, Harris AL. Predominant role of hypoxia-inducible transcription factor (Hif)-1alpha versus Hif-2alpha in regulation of the transcriptional response to hypoxia. *Cancer Res* 63: 6130–6134, 2003.

550. Spence VA, Beck JS. Transcutaneous measurement of Po_2 and PCO2 in the dermis at the site of the tuberculin reaction in healthy human subjects. *J Pathol* 155: 289–293, 1988. doi:10.1002/path.1711550403.

551. Spence VA, Walker WF. Measurement of oxygen tension in human skin. *Med Biol Eng* 14: 159–165, 1976. doi:10.1007/BF02478742.

552. Spencer JA, Ferraro F, Roussakis E, Klein A, Wu J, Runnels JM, Zaher W, Mortensen LJ, Alt C, Turcotte R, Yusuf R, Côté D, Vinogradov SA, Scadden DT, Lin CP. Direct measurement of local oxygen concentration in the bone marrow of live animals. *Nature* 508: 269–273, 2014. doi:10.1038/nature13034.

553. Stacpoole SR, Webber DJ, Bilican B, Compston A, Chandran S, Franklin RJ. Neural precursor cells cultured at physiologically relevant oxygen tensions have a survival advantage following transplantation. *Stem Cells Transl Med* 2: 464–472, 2013. doi:10.5966/sctm.2012-0144.

554. Stacpoole SRL, Bilican B, Webber DJ, Luzhynskaya A, He XL, Compston A, Karadottir R, Franklin RJM, Chandran S. Derivation of neural precursor cells from human ES cells at 3% O(2) is efficient, enhances survival and presents no barrier to regional specification and functional differentiation. *Cell Death Differ* 18: 1016–1023, 2011. doi:10.1038/cdd.2010.171.

556. Steinberg GR, Kemp BE. AMPK in health and disease. *Physiol Rev* 89: 1025–1078, 2009. doi:10.1152/physrev.00011.2008.

557. Steptoe PC, Edwards RG, Purdy JM. Human blastocysts grown in culture. *Nature* 229: 132–133, 1971. doi:10.1038/229132a0.

558. Stevens ED. Use of plastic materials in oxygen-measuring systems. *J Appl Physiol (1985)* 72: 801–804, 1992. doi:10.1152/jappl.1992.72.2.801.

559. Stevens KM. Oxygen requirements for liver cells in vitro. *Nature* 206: 199, 1965. doi:10.1038/206199a0.

560. Stücker M, Struk PA, Hoffmann K, Schulze L, Röchling A, Lübbers DW. The transepidermal oxygen flux from the environment is in balance with the capillary oxygen supply. *J Invest Dermatol* 114: 533–540, 2000. doi:10.1046/j.1523-1747.2000.00911.x.

561. Studer L, Csete M, Lee SH, Kabbani N, Walikonis J, Wold B, McKay R. Enhanced proliferation, survival, and dopaminergic differentiation of CNS precursors in lowered oxygen. *J Neurosci* 20: 7377–7383, 2000. doi:10.1523/JNEUROSCI.20-19-07377.2000.

562. Subczynski WK, Hopwood LE, Hyde JS. Is the mammalian cell plasma membrane a barrier to oxygen transport? *J Gen Physiol* 100: 69–87, 1992. doi:10.1085/jgp.100.1.69.

563. Sun X, Volobouéva LA, Stary CM, Giffard RG. Physiologically normal 5% O2 supports neuronal differentiation and resistance to inflammatory injury in neural stem cell cultures. *J Neurosci Res* 93: 1703–1712, 2015. doi:10.1002/jnr.23615.

564. Swirski FK, Nahrendorf M, Etzrodt M, Wildgruber M, Cortez-Retamozo V, Panizzi P, Figueiredo J-L, Kohler RH, Chudnovskiy A, Waterman P, Aikawa E, Mempel TR, Libby P, Weissleder R, Pittet MJ. Identification of splenic reservoir monocytes and their deployment to inflammatory sites. *Science* 325: 612–616, 2009. doi:10.1126/science.1175202.

565. Sylvester JT, Shimoda LA, Aaronson PI, Ward JPT. Hypoxic pulmonary vasoconstriction. *Physiol Rev* 92: 367–520, 2012. doi:10.1152/physrev.00041.2010.

566. Synnestvedt K, Furuta GT, Comerford KM, Louis N, Karhausen J, Eltzschig HK, Hansen KR, Thompson LF, Colgan SP. Ecto-5′-nucleotidase (CD73) regulation by hypoxia-inducible factor-1 mediates permeability changes in intestinal epithelia. *J Clin Invest* 110: 993–1002, 2002. doi:10.1172/JCI0215337.

567. Takahashi E, Endoh H, Doi K. Intracellular gradients of O2 supply to mitochondria in actively respiring single cardiomyocyte of rats. *Am J Physiol* 276: H718–H724, 1999.

568. Takahashi E, Endoh H, Doi K. Visualization of myoglobin-facilitated mitochondrial O(2) delivery in a single isolated cardiomyocyte. *Biophys J* 78: 3252–3259, 2000. doi:10.1016/S0006-3495(00)76861-5.

569. Takahashi R, Kobayashi C, Kondo Y, Nakatani Y, Kudo I, Kunimoto M, Imura N, Hara S. Subcellular localization and regulation of hypoxia-inducible factor-2alpha in vascular endothelial cells. *Biochem Biophys Res Commun* 317: 84–91, 2004. doi:10.1016/j.bbrc.2004.03.010.

570. Thermann M, Jostarndt L, Eberhard F, Richter H, Sass W. [Oxygen supply of the human small intestine in mechanical ileus]. *Langenbecks Arch Chir* 363: 179–184, 1985. doi:10.1007/BF01261291.

571. Thomas DD, Liu X, Kantrow SP, Lancaster JR Jr. The biological lifetime of nitric oxide: implications for the perivascular dynamics of NO and O2. *Proc Natl Acad Sci USA* 98: 355–360, 2001. doi:10.1073/pnas.98.1.355.

572. Thomas SR. The biomedical applications of fluorine-19 NMR. In: *Magnetic Resonance Imaging*, edited by Partain CL, Price RR, Patton JA, Kulkarni MV, James AE. Philadelphia, PA: Saunders, 1988, p. 1536–1552.

573. Thomas SR, Pratt RG, Millard RW, Samaratunga RC, Shiferaw Y, McGoron AJ, Tan KK. In vivo Po_2 imaging in the porcine model with perfluorocarbon F-19 NMR at low field. *Magn Reson Imaging* 14: 103–114, 1996. doi:10.1016/0730-725X(95)02046-V.

574. Thompson AA, Binham J, Plant T, Whyte MK, Walmsley SR. Hypoxia, the HIF pathway and neutrophilic inflammatory responses. *Biol Chem* 394: 471–477, 2013. doi:10.1515/hsz-2012-0335.

575. Thompson CB. Into Thin Air: How We Sense and Respond to Hypoxia. *Cell* 167: 9–11, 2016. doi:10.1016/j.cell.2016.08.036.

576. Thorp JA, Trobough T, Evans R, Hedrick J, Yeast JD. The effect of maternal oxygen administration during the second stage of labor on umbilical cord blood gas values: a randomized controlled prospective trial. *Am J Obstet Gynecol* 172: 465–474, 1995. doi:10.1016/0002-9378(95)90558-8.

577. Thulborn KR, Waterton JC, Matthews PM, Radda GK. Oxygenation dependence of the transverse relaxation time of water protons in whole blood at high field. *Biochim Biophys Acta* 714: 265–270, 1982. doi:10.1016/0304-4165(82)90333-6.

578. Tiede LM, Cook EA, Morsey B, Fox HS. Oxygen matters: tissue culture oxygen levels affect mitochondrial function and structure as well as responses to HIV viroproteins. *Cell Death Dis* 2: e246, 2011. doi:10.1038/cddis.2011.128.. An erratum for this article has been published at http://dx.doi.org/10.1038/cddis.2012.11.

579. Tilles AW, Berthiaume F, Yarmush ML, Tompkins RG, Toner M. Bioengineering of liver assist devices. *J Hepatobiliary Pancreat Surg* 9: 686–696, 2002. doi:10.1007/s005340200095.

580. Timpson CJ, Carter CC, Olmsted J III. Mechanism of quenching of electronically excited ruthenium complexes by oxygen. *J Phys Chem* 93: 4116–4120, 1989. doi:10.1021/j100347a048.

581. Tokuda Y, Crane S, Yamaguchi Y, Zhou L, Falanga V. The levels and kinetics of oxygen tension detectable at the surface of human dermal fibroblast cultures. *J Cell Physiol* 182: 414–420, 2000. doi:10.1002/(SICI)1097-4652(200003)182:3<414::AID-JCP12>3.0.CO;2-5.

582. Tordjman J (editor). *Physiology and Physiopathology of Adipose Tissue*. New York: Springer, 2013, p. 67–75. doi:10.1007/978-2-8178-0343-2_6

583. Torres Filho IP, Intaglietta M. Microvessel Po_2 measurements by phosphorescence decay method. *Am J Physiol* 265: H1434–H1438, 1993.

584. Torres Filho IP, Kerger H, Intaglietta M. pO2 measurements in arteriolar networks. *Microvasc Res* 51: 202–212, 1996. doi:10.1006/mvre.1996.0021.

585. Torres Filho IP, Leunig M, Yuan F, Intaglietta M, Jain RK. Noninvasive measurement of microvascular and interstitial oxygen profiles in a human tumor in SCID mice. *Proc Natl Acad Sci USA* 91: 2081–2085, 1994. doi:10.1073/pnas.91.6.2081.

586. Trayhurn P. Hypoxia and adipose tissue function and dysfunction in obesity. *Physiol Rev* 93: 1–21, 2013. doi:10.1152/physrev.00017.2012.

587. Trepiana J, Meijide S, Navarro R, Hernández ML, Ruiz-Sanz JI, Ruiz-Larrea MB. Influence of oxygen partial pressure on the characteristics of human hepatocarcinoma cells. *Redox Biol* 12: 103–113, 2017. doi:10.1016/j.redox.2017.02.004.

588. Treuhaft PS, MCCarty DJ. Synovial fluid pH, lactate, oxygen and carbon dioxide partial pressure in various joint diseases. *Arthritis Rheum* 14: 475–484, 1971. doi:10.1002/art.1780140407.

590. Tripathi A, Bydder GM, Hughes JM, Pennock JM, Goatcher A, Orr JS, Steiner RE, Greenspan RH. Effect of oxygen tension on NMR spin-lattice relaxation rate of blood in vivo. *Invest Radiol* 19: 174–178, 1984. doi:10.1097/00004424-198419030-00004.

591. Tsai AG, Friesenecker B, Mazzoni MC, Kerger H, Buerk DG, Johnson PC, Intaglietta M. Microvascular and tissue oxygen gradients in the rat mesentery. *Proc Natl Acad Sci USA* 95: 6590–6595, 1998. doi:10.1073/pnas.95.12.6590.

593. Tsai AG, Johnson PC, Intaglietta M. Is the distribution of tissue pO(2) homogeneous? *Antioxid Redox Signal* 9: 979–984, 2007. doi:10.1089/ars.2007.1633.

594. Tsai AG, Johnson PC, Intaglietta M. Oxygen gradients in the microcirculation. *Physiol Rev* 83: 933–963, 2003. doi:10.1152/physrev.00034.2002.

595. Tuncay OC, Ho D, Barker MK. Oxygen tension regulates osteoblast function. *Am J Orthod Dentofacial Orthop* 105: 457–463, 1994. doi:10.1016/S0889-5406(94)70006-0.

596. Turner J, Quek L-E, Titmarsh D, Krömer JO, Kao L-P, Nielsen L, Wolvetang E, Cooper-White J. Metabolic profiling and flux analysis of MEL-2 human embryonic stem cells during exponential growth at physiological and atmospheric oxygen concentrations. *PLoS One* 9: e112757, 2014. doi:10.1371/journal.pone.0112757.

597. Tuuli MG, Longtine MS, Nelson DM. Review: Oxygen and trophoblast biology–a source of controversy. *Placenta* 32, Suppl 2: S109–S118, 2011. doi:10.1016/j.placenta.2010.12.013.

598. Tygstrup N, Winkler K, Mellemgaard K, Andreassen M. Determination of the hepatic arterial blood flow and oxygen supply in man by clamping the hepatic artery during surgery. *J Clin Invest* 41: 447–454, 1962. doi:10.1172/JCI104497.

599. Uchida T, Rossignol F, Matthay MA, Mounier R, Couette S, Clottes E, Clerici C. Prolonged hypoxia differentially regulates hypoxia-inducible factor (HIF)-1alpha and HIF-2alpha expression in lung epithelial cells: implication of natural antisense HIF-1alpha. *J Biol Chem* 279: 14871–14878, 2004. doi:10.1074/jbc.M400461200.

600. Ugolini GS, Pavesi A, Rasponi M, Fiore GB, Kamm R, Soncini M. Human cardiac fibroblasts adaptive responses to controlled combined mechanical strain and oxygen changes in vitro. *eLife* 6: e22847, 2017. doi:10.7554/eLife.22847.

601. Utting JC, Robins SP, Brandao-Burch A, Orriss IR, Behar J, Arnett TR. Hypoxia inhibits the growth, differentiation and bone-forming capacity of rat osteoblasts. *Exp Cell Res* 312: 1693–1702, 2006. doi:10.1016/j.yexcr.2006.02.007.

602. Vāvere AL, Lewis JS. Cu-ATSM: a radiopharmaceutical for the PET imaging of hypoxia. *Dalton Trans* (43): 4893–4902, 2007. doi:10.1039/b705989b.

603. Vadapalli A, Pittman RN, Popel AS. Estimating oxygen transport resistance of the microvascular wall. *Am J Physiol Heart Circ Physiol* 279: H657–H671, 2000. doi:10.1152/ajpheart.2000.279.2.H657.

604. Vajpayee N, Graham SS, and Bem S. Basic examination of blood and bone marrow. *Henrys clinical diagnosis and management by laboratory methods* 22: 509–535, 2011.

605. Valenzuela P, Guijarro R. The effects of time on pH and gas values in the blood contained in the umbilical cord. *Acta Obstet Gynecol Scand* 85: 1307–1309, 2006. doi:10.1080/00016340600697488.

606. Valorani MG, Montelatici E, Germani A, Biddle A, D'Alessandro D, Strollo R, Patrizi MP, Lazzari L, Nye E, Otto WR, Pozzilli P, Alison MR. Pre-culturing human adipose tissue mesenchymal stem cells under hypoxia increases their adipogenic and osteogenic differentiation potentials. *Cell Prolif* 45: 225–238, 2012. doi:10.1111/j.1365-2184.2012.00817.x.

607. van Uden P, Kenneth NS, Rocha S. Regulation of hypoxia-inducible factor-1alpha by NF-kappaB. *Biochem J* 412: 477–484, 2008. doi:10.1042/BJ20080476.

608. van Wagensveld BA, van Gulik TM, Gabeler EE, van der Kleij AJ, Obertop H, Gouma DJ. Intrahepatic tissue pO2 during continuous or intermittent vascular inflow occlusion in a pig liver resection model. *Eur Surg Res* 30: 13–25, 1998. doi:10.1159/000008553.

609. Vanden Hoek TL, Becker LB, Shao Z, Li C, Schumacker PT. Reactive oxygen species released from mitochondria during brief hypoxia induce preconditioning in cardiomyocytes. *J Biol Chem* 273: 18092–18098, 1998. doi:10.1074/jbc.273.29.18092.

610. Vanderkooi JM, Maniara G, Green TJ, Wilson DF. An optical method for measurement of dioxygen concentration based upon quenching of phosphorescence. *J Biol Chem* 262: 5476–5482, 1987.

611. VanderMeer TJ, Wang H, Fink MP. Endotoxemia causes ileal mucosal acidosis in the absence of mucosal hypoxia in a normodynamic porcine model of septic shock. *Crit Care Med* 23: 1217–1226, 1995. doi:10.1097/00003246-199507000-00011.

612. Vassilaki N, Kalliampakou KI, Kotta-Loizou I, Befani C, Liakos P, Simos G, Mentis AF, Kalliaropoulos A, Doumba PP, Smirlis D, Foka P, Bauhofer O, Poenisch M, Windisch MP, Lee ME, Koskinas J, Bartenschlager R, Mavromara P. Low oxygen tension enhances hepatitis C virus replication. *J Virol* 87: 2935–2948, 2013. doi:10.1128/JVI.02534-12.

613. Vaupel P, Braunbeck W, Thews G. Respiratory gas exchange and pO2-distribution in splenic tissue. *Adv Exp Med Biol* 37A: 401–406, 1973. doi:10.1007/978-1-4684-3288-6_50.

614. Vaupel P, Frinak S, Müller-Klieser W, Manz R. The end of a postulate: There are no hostile metabolic conditions within the normal spleen. *Bibl Anat* 20: 403–406, 1981.

615. Victor VM, Nuñez C, D'Ocón P, Taylor CT, Esplugues JV, Moncada S. Regulation of oxygen distribution in tissues by endothelial nitric oxide. *Circ Res* 104: 1178–1183, 2009. doi:10.1161/CIRCRESAHA.109.197228.

616. Villarruel SM, Boehm CA, Pennington M, Bryan JA, Powell KA, Muschler GF. The effect of oxygen tension on the in vitro assay of human osteoblastic connective tissue progenitor cells. *J Orthop Res* 26: 1390–1397, 2008. doi:10.1002/jor.20666.

617. Villeneuve L, Tiede LM, Morsey B, Fox HS. Quantitative proteomics reveals oxygen-dependent changes in neuronal mitochondria affecting function and sensitivity to rotenone. *J Proteome Res* 12: 4599–4606, 2013. doi:10.1021/pr400758d.

618. Vink RG, Roumans NJ, Čajlaković M, Cleutjens JPM, Boekschoten MV, Fazelzadeh P, Vogel MAA, Blaak EE, Mariman EC, van Baak MA, Goossens GH. Diet-induced weight loss decreases adipose tissue oxygen tension with parallel changes in adipose tissue phenotype and insulin sensitivity in overweight humans. *Int J Obes* 41: 722–728, 2017. doi:10.1038/ijo.2017.38.

619. Viticchiè G, Agostini M, Lena AM, Mancini M, Zhou H, Zolla L, Dinsdale D, Saintigny G, Melino G, Candi E. p63 supports aerobic respiration through hexokinase II. *Proc Natl Acad Sci USA* 112: 11577–11582, 2015. doi:10.1073/pnas.1508871112.

620. Vorp DA, Lee PC, Wang DH, Makaroun MS, Nemoto EM, Ogawa S, Webster MW. Association of intraluminal thrombus in abdominal aortic aneurysm with local hypoxia and wall weakening. *J Vasc Surg* 34: 291–299, 2001. doi:10.1067/mva.2001.114813.

621. Vorp DA, Wang DH, Webster MW, Federspiel WJ. Effect of intraluminal thrombus thickness and bulge diameter on the oxygen diffusion in abdominal aortic aneurysm. *J Biomech Eng* 120: 579–583, 1998. doi:10.1115/1.2834747.

622. Vovenko E. Distribution of oxygen tension on the surface of arterioles, capillaries and venules of brain cortex and in tissue in normoxia: an experimental study on rats. *Pflugers Arch* 437: 617–623, 1999. doi:10.1007/s004240050825.

623. Vovenko EP. Transmural oxygen tension gradients in rat cerebral cortex arterioles. *Neurosci Behav Physiol* 39: 363–370, 2009. doi:10.1007/s11055-009-9142-6.

624. Vretzakis G, Ferdi E, Papaziogas B, Dragoumanis C, Pneumatikos J, Tsangaris I, Tsakiridis K, Konstantinou F. Coronary sinus venoarterial CO2 difference in different hemodynamic states. *Acta Anaesthesiol Belg* 55: 221–227, 2004.

625. Wagenführ L, Meyer AK, Braunschweig L, Marrone L, Storch A. Brain oxygen tension controls the expansion of outer subventricular zone-like basal progenitors in the developing mouse brain. *Development* 142: 2904–2915, 2015. doi:10.1242/dev.121939.

626. Walker A, Maddern L, Day E, Renou P, Talbot J, Wood C. Fetal scalp tissue oxygen tension measurements in relation to maternal dermal oxygen tension and fetal heart rate. *J Obstet Gynaecol Br Commonw* 78: 1–12, 1971. doi:10.1111/j.1471-0528.1971.tb00184.x.

627. Walmsley SR, Cowburn AS, Clatworthy MR, Morrell NW, Roper EC, Singleton V, Maxwell P, Whyte MK, Chilvers ER. Neutrophils from patients with heterozygous germline mutations in the von Hippel Lindau protein (pVHL) display delayed apoptosis and enhanced bacterial phagocytosis. *Blood* 108: 3176–3178, 2006. doi:10.1182/blood-2006-04-018796.

628. Walmsley SR, Print C, Farahi N, Peyssonnaux C, Johnson RS, Cramer T, Sobolewski A, Condliffe AM, Cowburn AS, Johnson N, Chilvers ER. Hypoxia-induced neutrophil survival is mediated by HIF-1alpha-dependent NF-kappaB activity. *J Exp Med* 201: 105–115, 2005. doi:10.1084/jem.20040624.

629. Wang F, Thirumangalathu S, Loeken MR. Establishment of new mouse embryonic stem cell lines is improved by physiological glucose and oxygen. *Cloning Stem Cells* 8: 108–116, 2006. doi:10.1089/clo.2006.8.108.

630. Wang GL, Jiang BH, Rue EA, Semenza GL. Hypoxia-inducible factor 1 is a basic-helix-loop-helix-PAS heterodimer regulated by cellular O2 tension. *Proc Natl Acad Sci USA* 92: 5510–5514, 1995. doi:10.1073/pnas.92.12.5510.

631. Wang H, Flach H, Onizawa M, Wei L, McManus MT, Weiss A. Negative regulation of Hif1a expression and TH17 differentiation by the hypoxia-regulated microRNA miR-210. *Nat Immunol* 15: 393–401, 2014. doi:10.1038/ni.2846.

632. Wang W, Winlove CP, Michel CC. Oxygen partial pressure in outer layers of skin of human finger nail folds. *J Physiol* 549: 855–863, 2003. doi:10.1113/jphysiol.2002.037994.

633. Ward J. Oxygen sensors in context. *Bioenergetics* 1777: 1–14, 2008. doi:10.1016/j.bbabio.2007.10.010.

634. Warnecke C, Zaborowska Z, Kurreck J, Erdmann VA, Frei U, Wiesener M, Eckardt K-U. Differentiating the functional role of hypoxia-inducible factor (HIF)-1alpha and HIF-2alpha (EPAS-1) by the use of RNA interference: erythropoietin is a HIF-2alpha target gene in Hep3B and Kelly cells. *FASEB J* 18: 1462–1464, 2004. doi:10.1096/fj.04-1640fje.

635. Waypa GB, Chandel NS, Schumacker PT. Model for hypoxic pulmonary vasoconstriction involving mitochondrial oxygen sensing. *Circ Res* 88: 1259–1266, 2001. doi:10.1161/hh1201.091960.

636. Waypa GB, Guzy R, Mungai PT, Mack MM, Marks JD, Roe MW, Schumacker PT. Increases in mitochondrial reactive oxygen species trigger hypoxia-induced calcium responses in pulmonary artery smooth muscle cells. *Circ Res* 99: 970–978, 2006. doi:10.1161/01.RES.0000247068.75808.3f.

637. Weidling J, Sameni S, Lakey JRT, Botvinick E. Method measuring oxygen tension and transport within subcutaneous devices. *J Biomed Opt* 19: 087006, 2014. doi:10.1117/1.JBO.19.8.087006.

638. Weinberg F, Hamanaka R, Wheaton WW, Weinberg S, Joseph J, Lopez M, Kalyanaraman B, Mutlu GM, Budinger GRS, Chandel NS. Mitochondrial metabolism and ROS generation are essential for Kras-mediated tumorigenicity. *Proc Natl Acad Sci USA* 107: 8788–8793, 2010. doi:10.1073/pnas.1003428107.

639. Weiner CP, Sipes SL, Wenstrom K. The effect of fetal age upon normal fetal laboratory values and venous pressure. *Obstet Gynecol* 79: 713–718, 1992.

640. Weinmann M, Jendrossek V, Güner D, Goecke B, Belka C. Cyclic exposure to hypoxia and reoxygenation selects for tumor cells with defects in mitochondrial apoptotic pathways. *FASEB J* 18: 1906–1908, 2004. doi:10.1096/fj.04-1918fje.

641. Weir EK, Archer SL. The mechanism of acute hypoxic pulmonary vasoconstriction: the tale of two channels. *FASEB J* 9: 183–189, 1995. doi:10.1096/fasebj.9.2.7781921.

642. Welch WJ, Baumgärtl H, Lübbers D, Wilcox CS. Nephron pO2 and renal oxygen usage in the hypertensive rat kidney. *Kidney Int* 59: 230–237, 2001. doi:10.1046/j.1523-1755.2001.00483.x.

643. Westfall SD, Sachdev S, Das P, Hearne LB, Hannink M, Roberts RM, Ezashi T. Identification of oxygen-sensitive transcriptional programs in human embryonic stem cells. *Stem Cells Dev* 17: 869–881, 2008. doi:10.1089/scd.2007.0240.

644. Whalen WJ, Nair P, Ganfield RA. Measurements of oxygen tension in tissues with a micro oxygen electrode. *Microvasc Res* 5: 254–262, 1973. doi:10.1016/0026-2862(73)90035-6.

645. Whitcutt MJ, Adler KB, Wu R. A biphasic chamber system for maintaining polarity of differentiation of cultured respiratory tract epithelial cells. *In Vitro Cell Dev Biol* 24: 420–428, 1988. doi:10.1007/BF02628493.

646. White M, Rouleau JL, Ruddy TD, De Marco T, Moher D, Chatterjee K. Decreased coronary sinus oxygen content: a predictor of adverse prognosis in patients with severe congestive heart failure. *J Am Coll Cardiol* 18: 1631–1637, 1991. doi:10.1016/0735-1097(91)90495-U.

647. White RA, Nolan L, Harley D, Long J, Klein S, Tremper K, Nelson R, Tabrisky J, Shoemaker W. Noninvasive evaluation of peripheral vascular disease using transcutaneous oxygen tension. *Am J Surg* 144: 68–75, 1982. doi:10.1016/0002-9610(82)90604-3.

648. Wiener L, Santamore WP, Venkataswamy A, Plzak L, Templeton J. Postoperative monitoring of myocardial oxygen tension: experience in 51 coronary artery bypass patients. *Clin Cardiol* 5: 431–435, 1982. doi:10.1002/clc.4960050802.

649. Wild JM, Fichele S, Woodhouse N, Paley MNJ, Kasuboski L, van Beek EJR. 3D volume-localized pO2 measurement in the human lung with 3He MRI. *Magn Reson Med* 53: 1055–1064, 2005. doi:10.1002/mrm.20423.

650. Wilkening RB, Meschia G. Current topic: comparative physiology of placental oxygen transport. *Placenta* 13: 1–15, 1992. doi:10.1016/0143-4004(92)90002-B.

651. Wilkinson PL, Graham BH, Moyers JR, Hamilton WK, Ports TA, Ullyot DJ, Chatterjee K. Changes in mixed venous and coronary sinus P50 secondary to anesthesia and

cardiac disease. *Anesth Analg* 59: 751–758, 1980. doi:10.1213/00000539-198010000-00006.

652. Williams SEJ, Wootton P, Mason HS, Bould J, Iles DE, Riccardi D, Peers C, Kemp PJ. Hemoxygenase-2 is an oxygen sensor for a calcium-sensitive potassium channel. *Science* 306: 2093–2097, 2004. doi:10.1126/science.1105010.

653. Wilson DF, Erecińska M, Drown C, Silver IA. The oxygen dependence of cellular energy metabolism. *Arch Biochem Biophys* 195: 485–493, 1979. doi:10.1016/0003-9861(79)90375-8.

654. Winbury MM, Howe BB, Weiss JR. Effect of nitroglycerin and dipyridamole on epicardial and endocardial oxygen tension–further evidence for redistribution of myocardial blood flow. *J Pharmacol Exp Ther* 176: 184–199, 1971.

655. Winegrad S, Henrion D, Rappaport L, Samuel JL. Self-protection by cardiac myocytes against hypoxia and hyperoxia. *Circ Res* 85: 690–698, 1999. doi:10.1161/01.RES.85.8.690.

656. Winter JD, Estrada M, Cheng H-LM. Normal tissue quantitative T1 and T2* MRI relaxation time responses to hypercapnic and hyperoxic gases. *Acad Radiol* 18: 1159–1167, 2011. doi:10.1016/j.acra.2011.04.016.

657. Wittenberg JB. Myoglobin-facilitated oxygen diffusion: role of myoglobin in oxygen entry into muscle. *Physiol Rev* 50: 559–636, 1970. doi:10.1152/physrev.1970.50.4.559.

658. Wittenberg JB. On optima: the case of myoglobin-facilitated oxygen diffusion. *Gene* 398: 156–161, 2007. doi:10.1016/j.gene.2007.02.040.

659. Wolff M, Fandrey J, Jelkmann W. Microelectrode measurements of pericellular P_{O_2} in erythropoietin-producing human hepatoma cell cultures. *Am J Physiol* 265: C1266–C1270, 1993. doi:10.1152/ajpcell.1993.265.5.C1266.

660. Wölfle D, Schmidt H, Jungermann K. Short-term modulation of glycogen metabolism, glycolysis and gluconeogenesis by physiological oxygen concentrations in hepatocyte cultures. *Eur J Biochem* 135: 405–412, 1983. doi:10.1111/j.1432-1033.1983.tb07667.x.

661. Wolinsky H, Glagov S. Nature of species differences in the medial distribution of aortic vasa vasorum in mammals. *Circ Res* 20: 409–421, 1967. doi:10.1161/01.RES.20.4.409.

662. Wong AP, Bear CE, Chin S, Pasceri P, Thompson TO, Huan L-J, Ratjen F, Ellis J, Rossant J. Directed differentiation of human pluripotent stem cells into mature airway epithelia expressing functional CFTR protein. *Nat Biotechnol* 30: 876–882, 2012. doi:10.1038/nbt.2328.

663. Wood IS, Stezhka T, Trayhurn P. Modulation of adipokine production, glucose uptake and lactate release in human adipocytes by small changes in oxygen tension. *Pflugers Arch* 462: 469–477, 2011. doi:10.1007/s00424-011-0985-7.

664. Worlitzsch D, Tarran R, Ulrich M, Schwab U, Cekici A, Meyer KC, Birrer P, Bellon G, Berger J, Weiss T, Botzenhart K, Yankaskas JR, Randell S, Boucher RC, Döring G. Effects of reduced mucus oxygen concentration in airway Pseudomonas infections of cystic fibrosis patients. *J Clin Invest* 109: 317–325, 2002. doi:10.1172/JCI0213870.

665. Xie P, Sun Y, Ouyang Q, Hu L, Tan Y, Zhou X, Xiong B, Zhang Q, Yuan D, Pan Y, Liu T, Liang P, Lu G, Lin G. Physiological oxygen prevents frequent silencing of the DLK1-DIO3 cluster during human embryonic stem cells culture. *Stem Cells* 32: 391–401, 2014. doi:10.1002/stem.1558.

666. Xie Y, Zhang J, Lin Y, Gaeta X, Meng X, Wisidagama DRR, Cinkornpumin J, Koehler CM, Malone CS, Teitell MA, Lowry WE. Defining the role of oxygen tension in human neural progenitor fate. *Stem Cell Reports* 3: 743–757, 2014. doi:10.1016/j.stemcr.2014.09.021.

667. Yamakawa M, Liu LX, Date T, Belanger AJ, Vincent KA, Akita GY, Kuriyama T, Cheng SH, Gregory RJ, Jiang C. Hypoxia-inducible factor-1 mediates activation of cultured vascular endothelial cells by inducing multiple angiogenic factors. *Circ Res* 93: 664–673, 2003. doi:10.1161/01.RES.0000093984.48643.D7.

668. Yan H-M, Ramachandran A, Bajt ML, Lemasters JJ, Jaeschke H. The oxygen tension modulates acetaminophen-induced mitochondrial oxidant stress and cell injury in cultured hepatocytes. *Toxicol Sci* 117: 515–523, 2010. doi:10.1093/toxsci/kfq208.

669. Yanagi K, Miyoshi H, Ohshima N. Improvement of metabolic performance of hepatocytes cultured in vitro in a packed-bed reactor for use as a bioartificial liver. *ASAIO J* 44: M436–M440, 1998. doi:10.1097/00002480-199809000-00022.

670. Yang Y, Xu Y, Ding C, Khoudja RY, Lin M, Awonuga AO, Dai J, Puscheck EE, Rappolee DA, Zhou C. Comparison of 2, 5, and 20 % O2 on the development of post-thaw human embryos. *J Assist Reprod Genet* 33: 919–927, 2016. doi:10.1007/s10815-016-0693-5.

671. Yarmush ML, Toner M, Dunn JC, Rotem A, Hubel A, Tompkins RG. Hepatic tissue engineering. Development of critical technologies. *Ann N Y Acad Sci* 665, 1 Biochemical E: 238–252, 1992. doi:10.1111/j.1749-6632.1992.tb42588.x.

673. Ye J, Gao Z, Yin J, He Q. Hypoxia is a potential risk factor for chronic inflammation and adiponectin reduction in adipose tissue of ob/ob and dietary obese mice. *Am J Physiol Endocrinol Metab* 293: E1118–E1128, 2007. doi:10.1152/ajpendo.00435.2007.

674. Yedwab GA, Paz G, Homonnai TZ, David MP, Kraicer PF. The temperature, pH, and partial pressure of oxygen in the cervix and uterus of women and uterus of rats during the cycle. *Fertil Steril* 27: 304–309, 1976. doi:10.1016/S0015-0282(16)41722-X.

675. Yeomans ER, Hauth JC, Gilstrap LC III, Strickland DM. Umbilical cord pH, PCO2, and bicarbonate following uncomplicated term vaginal deliveries. *Am J Obstet Gynecol* 151: 798–800, 1985. doi:10.1016/0002-9378(85)90523-X.

676. Yin J, Gao Z, He Q, Zhou D, Guo Z, Ye J. Role of hypoxia in obesity-induced disorders of glucose and lipid metabolism in adipose tissue. *Am J Physiol Endocrinol Metab* 296: E333–E342, 2009. doi:10.1152/ajpendo.90760.2008.

677. Yochim JM, Mitchell JA. Intrauterine oxygen tension in the rat during progestation: its possible relation to carbohydrate metabolism and the regulation of nidation. *Endocrinology* 83: 706–713, 1968. doi:10.1210/endo-83-4-706.

678. Yoshida Y, Takahashi K, Okita K, Ichisaka T, Yamanaka S. Hypoxia enhances the generation of induced pluripotent stem cells. *Cell Stem Cell* 5: 237–241, 2009. doi:10.1016/j.stem.2009.08.001.

679. Yu BP. Cellular defenses against damage from reactive oxygen species. *Physiol Rev* 74: 139–162, 1994. doi:10.1152/physrev.1994.74.1.139.

680. Yu JX, Kodibagkar VD, Cui W, Mason RP. 19F: a versatile reporter for non-invasive physiology and pharmacology using magnetic resonance. *Curr Med Chem* 12: 819–848, 2005. doi:10.2174/0929867053507342.

681. Yu J, Ishii M, Law M, Woodburn JM, Emami K, Kadlecek S, Vahdat V, Guyer RA, Rizi RR. Optimization of scan parameters in pulmonary partial pressure oxygen measurement by hyperpolarized 3He MRI. *Magn Reson Med* 59: 124–131, 2008. doi:10.1002/mrm.21416.

682. Yu J, Rajaei S, Ishii M, Law M, Emami K, Woodburn JM, Kadlecek S, Vahdat V, Rizi RR. Measurement of pulmonary partial pressure of oxygen and oxygen depletion rate with hyperpolarized helium-3 MRI: a preliminary reproducibility study on pig model. *Acad Radiol* 15: 702–712, 2008. doi:10.1016/j.acra.2008.01.024.

683. Yuan G, Vasavda C, Peng Y-J, Makarenko VV, Raghuraman G, Nanduri J, Gadalla MM, Semenza GL, Kumar GK, Snyder SH, Prabhakar NR. Protein kinase G-regulated production of H2S governs oxygen sensing. *Sci Signal* 8: ra37, 2015. doi:10.1126/scisignal.2005846.

684. Zagórski Z, Gossler B, Naumann GO. Effect of low oxygen tension on the growth of bovine corneal endothelial cells in vitro. *Ophthalmic Res* 21: 440–442, 1989. doi:10.1159/000266935.

685. Zahm AM, Bucaro MA, Ayyaswamy PS, Srinivas V, Shapiro IM, Adams CS, Mukundakrishnan K. Numerical modeling of oxygen distributions in cortical and cancellous bone: oxygen availability governs osteonal and trabecular dimensions. *Am J Physiol Cell Physiol* 299: C922–C929, 2010. doi:10.1152/ajpcell.00465.2009.

686. Zahm AM, Bucaro MA, Srinivas V, Shapiro IM, Adams CS. Oxygen tension regulates preosteocyte maturation and mineralization. *Bone* 43: 25–31, 2008. doi:10.1016/j.bone.2008.03.010.

687. Zäll S, Milocco I, Ricksten SE. Effects of adenosine on myocardial blood flow and metabolism after coronary artery bypass surgery. *Anesth Analg* 73: 689–695, 1991.

688. Zauner A, Bullock R, Di X, Young HF. Brain oxygen, CO2, pH, and temperature monitoring: evaluation in the feline brain. *Neurosurgery* 37: 1168–1177, 1995. doi:10.1227/00006123-199512000-00017.

689. Zeitouni NE, Dersch P, Naim HY, von Köckritz-Blickwede M. Hypoxia Decreases Invasin-Mediated Yersinia enterocolitica Internalization into Caco-2 Cells. *PLoS One* 11: e0146103, 2016. doi:10.1371/journal.pone.0146103.

690. Zeitouni NE, Fandrey J, Naim HY, von Köckritz-Blickwede M. Measuring oxygen levels in Caco-2 cultures. *Hypoxia (Auckl)* 3: 53–66, 2015.

691. Zemplenyi T, Crawford DW, Cole MA. Adaptation to arterial wall hypoxia demonstrated in vivo with oxygen microcathodes. *Atherosclerosis* 76: 173–179, 1989. doi: 10.1016/0021-9150(89)90101-9.

692. Zhang C, Bélanger S, Pouliot P, Lesage F. Measurement of Local Partial Pressure of Oxygen in the Brain Tissue under Normoxia and Epilepsy with Phosphorescence Lifetime Microscopy. *PLoS One* 10: e0135536, 2015. doi:10.1371/journal.pone.0135536.

693. Zhang JL, Morrell G, Rusinek H, Warner L, Vivier P-H, Cheung AK, Lerman LO, Lee VS. Measurement of renal tissue oxygenation with blood oxygen level-dependent MRI and oxygen transit modeling. *Am J Physiol Renal Physiol* 306: F579–F587, 2014. doi: 10.1152/ajprenal.00575.2013.

694. Zhang Y, Xie C, Wang H, Foss RM, Clare M, George EV, Li S, Katz A, Cheng H, Ding Y, Tang D, Reeves WH, Yang L-J. Irisin exerts dual effects on browning and adipogenesis of human white adipocytes. *Am J Physiol Endocrinol Metab* 311: E530–E541, 2016. doi:10.1152/ajpendo.00094.2016.

695. Zhao F, Sellgren K, Ma T. Low-oxygen pretreatment enhances endothelial cell growth and retention under shear stress. *Tissue Eng Part C Methods* 15: 135–146, 2009. doi:10.1089/ten.tec.2008.0321.

696. Zheng L, Kelly CJ, Colgan SP. Physiologic hypoxia and oxygen homeostasis in the healthy intestine. A Review in the Theme: Cellular Responses to Hypoxia. *Am J Physiol Cell Physiol* 309: C350–C360, 2015. doi:10.1152/ajpcell.00191.2015.

697. Zhou L, Dosanjh A, Chen H, Karasek M. Divergent effects of extracellular oxygen on the growth, morphology, and function of human skin microvascular endothelial cells. *J Cell Physiol* 182: 134–140, 2000. doi:10.1002/(SICI)1097-4652(200001)182:1<134::AID-JCP15>3.0.CO;2-Y.

698. Zhu J, Aja S, Kim E-K, Park MJ, Ramamurthy S, Jia J, Hu X, Geng P, Ronnett GV. Physiological oxygen level is critical for modeling neuronal metabolism in vitro. *J Neurosci Res* 90: 422–434, 2012. doi:10.1002/jnr.22765.

699. Zorov DB, Juhaszova M, Sollott SJ. Mitochondrial reactive oxygen species (ROS) and ROS-induced ROS release. *Physiol Rev* 94: 909–950, 2014. doi:10.1152/physrev.00026.2013.

700. Zscharnack M, Poesel C, Galle J, Bader A. Low oxygen expansion improves subsequent chondrogenesis of ovine bone-marrow-derived mesenchymal stem cells in collagen type I hydrogel. *Cells Tissues Organs* 190: 81–93, 2009. doi:10.1159/000178024.